Cranfield UNIVERSITY

Guido Servetti

Modelling and Predicting Fatigue Crack Growth Behaviour in Weld Induced Residual Stress Fields

SCHOOL OF ENGINEERING

PhD THESIS

CRANFIELD UNIVERSITY

SCHOOL OF ENGINEERING

PhD THESIS

Academic Year 2010-11

Guido Servetti

Modelling and Predicting Fatigue Crack Growth Behaviour in Weld Induced Residual Stress Fields

Supervisor: Dr Xiang Zhang

January 2011

Abstract

In the last few decades, new design concepts and manufacture processes have been developed in order to reduce the maintenance and manufacturing costs, and structural weight of aircraft components. The integral metallic structure with welding processes is one of the most promising solutions. The exclusion of fasteners and overlapping joints in the airframe reduces the costs, the weight, and eliminates stress concentrations near the holes. The research and development of welding processes for large civil aircraft is in the early stages, thus assessment of their impact on damage tolerance (DT) design must be carried out before the technology can be applied for large civil aircraft.

Fatigue crack growth rate is a key factor in DT assessment hence the aim of this study is to investigate the influence of weld residual stress fields on fatigue crack growth (FCG) behaviour in aerospace aluminium alloys. The objectives are to provide a prediction methodology and a better understanding of the plasticity effects on the FCG in welded Al-Li alloy structures.

The prediction methodology is based on two different approaches: superposition approach and effective stress intensity factor range ΔK_{eff}. Finite element methods have been used to calculate the stress intensity factor, thus the effective ratio, by using the modified virtual crack closure technique to calculate K_{res}. FCG rate was predicted by using the linear elastic fracture mechanics (LEFM) with existing empirical prediction laws modified for the weld case. The latter is a superposition based approach which is limited to tensile residual stress field and it is not valid for crack growing into compressive residual stress field. Therefore a second approach was developed by considering ΔK_{eff} both with LEFM via effective ratio and a novel approach with plasticity induced crack closure combined with residual stress field. Both methodologies were validated for different

experimental test cases published in the literature.

Cyclic plasticity induced crack closure analysis of a crack growing into a residual stress field require a great computational effort. Those novel analyses are achievable nowadays because of high performance computer grids. The plasticity effects on the FCG, have been investigated in order to define its importance in terms of prediction accuracy and its behaviour. Recognising the importance of material non-linearity behaviour at crack tip and in the plastic wake, crack closure induced by cyclic plasticity have been accounted in welded structures. A better understanding on the effects of the residual stresses on the crack closure has been provided in terms of plastic wake, crack opening displacement and strain level. Two opposite effects have been recognised to have a direct influence on the opening stress, and a quantification of the σ_{op} is provided. First some analyses without residual stresses were developed in order to validate the model with previous cases found in literature. Then the case with residual stresses was investigated. The evolution of the entire residual stress field, for elastic and plastic material, was investigated and the behaviour of the stress field during crack propagation is provided.

Fatigue crack growth behaviour in a realistic test article simulating the fuselage panel structure was investigated by both experimental and numerical modelling.

In conclusion, a novel investigation on plasticity induced crack closure combined with weld residual stress fields, is investigated in terms of FCG behaviour, while their effects on the prediction methodology are assessed by comparing the superposition and ΔK_{eff} approach.

Acknowledgements

First and foremost I would like to thank my supervisor Dr. Xiang Zhang for the great and untiring support and for the guidance during my PhD. I would like also to thank the members of the COINS project, Pr. Phil Irving, Dr. Yu-E Ma, Pr. Stewart Williams, Eng. Marco Pacchione.

I want to thanks also Dr. Les Oswald for the help with the grid computers.

I would like also to give a special thank to all my colleagues and friends: Marco B., David, Mattia, Andrea, Matteo, Jeremy, Giuliano, Neveed, Erminio, Guido M., Francesco, Michele, Ade, Christian, Cinzia, Marco N., Ryoko, Natalia, Da Qing, Vasilis, Melanie.

Last but not least, a very special thank to my family: my parents, my sister, my brother and my grandmother. Thanks to support me in many ways.

Contents

Abstract i

Acknowledgements iii

Contents iv

List of figures x

List of tables xix

List of acronyms, nomenclature and symbols xx

1 Introduction 1

1.1 Background 1

1.1.1 Welded integral metallic structures 2

1.1.2 Design philosophy against fatigue: damage tolerance . . . 4

1.1.3 Definition of Residual Stress 5

1.2 Scope, aim and objectives 6

1.3 Research methods 7

1.3.1 Project background 7

1.3.2 Computational approach 7

1.4 Thesis structure 9

2 Literature review and theoretical framework 11

2.1 Linear elastic fracture mechanics principles 12

2.1.1 Stress intensity factor 12
2.1.2 Derivation of main LEFM parameters 15
2.1.3 Crack tip plastic zone 18
2.2 Fatigue crack growth prediction methods 22
2.2.1 Paris equation 22
2.2.2 Influence of the mean stress and the ΔK_{eff} 22
2.2.3 Harter-T method 23
2.2.4 Crack closure based laws and two parameter laws 24
2.2.5 Constant and variable amplitude load 27
2.3 FE numerical analysis: LEFM & plasticity induced crack closure 28
2.3.1 FE in linear elastic fracture mechanics 28
2.3.2 Finite element formulation for plasticity 30
2.3.3 Plasticity induced fatigue crack closure 33
2.3.4 Element type and mesh size 38
2.3.5 Material models 39
2.3.6 Determination of crack opening level 44
2.4 Welds in integral metallic structures 46
2.4.1 Welding processes for aerospace aluminium alloys 46
2.4.2 Effects of weld on fatigue crack growth rate 49
2.4.3 Residual stresses in welded joints 49
2.4.4 Residual stresses measurement techniques 52
2.4.5 Modelling & inputting residual stresses 53
2.4.6 Residual stress intensity factor: K_{res} 56
2.4.7 RS influence on fatigue crack propagation 57
2.5 Summary of the chapter 62

3 Methodology 64

3.1 LEFM analysis 64
3.1.1 Calculation of the stress intensity factors 64

3.1.2 Residual stress intensity factor: K_{res} 68
3.1.3 Total stress intensity factor 71
3.2 Modelling plasticity induced crack closure 77
3.2.1 Mesh refinement 77
3.2.2 Crack surface contact modelling 79
3.2.3 Crack advance scheme 80
3.2.4 Crack opening criterion 81
3.2.5 Material model 82
3.3 Prediction methods for FCG life 83
3.3.1 LEFM superposition 83
3.3.2 Crack closure approach 86
3.4 Summary of the chapter 89

4 Plasticity induced crack closure with weld residual stress 90
4.1 Crack closure analysis without residual stress 91
4.2 Crack propagation effects 96
4.2.1 Residual stresses redistribution 96
4.2.2 Stress and strain history 101
4.3 Key parameters of plasticity induced crack closure 106
4.3.1 Plastic zone size 106
4.3.2 Plastic wake due to permanent plastic strain 110
4.3.3 Crack opening displacement 114
4.3.4 Crack tip stress distribution 116
4.4 Effect of residual stress on opening stress 117
4.4.1 Two opposite effects 117
4.4.2 Opening stress level in assumed constant residual stresses field 119
4.5 Plasticity induced crack closure with compressive RS 124
4.5.1 Crack closure model 125

4.5.2 Crack opening displacement and longitudinal stresses . . . 129
4.6 Summary of the chapter . . . 134

5 Predicting fatigue crack growth in weld residual stress fields 137
5.1 Crack growing from the weld . . . 138
5.1.1 Problem statement: M(T) specimen . . . 138
5.1.2 Evaluation of the K_{res} and R_{eff} . . . 139
5.1.3 Constant amplitude load . . . 141
5.1.4 Constant stress intensity factor range . . . 144
5.2 Crack growing towards the weld . . . 149
5.2.1 Problem statement: ESE(T) specimen . . . 149
5.2.2 Evaluation of R_{eff} and ΔK_{eff} . . . 153
5.2.3 Comparison of predictions with experimental results . . . 158
5.3 Discussion of the superposition and closure approach . . . 159
5.4 Summary of the chapter . . . 162

6 FSW fuselage longitudinal joints 165
6.1 Problem statement: fuselage panel with FSW joints and stringer features . . . 166
6.2 FE analysis . . . 168
6.2.1 Modelling technique . . . 168
6.2.2 Stress analysis: secondary bending . . . 169
6.2.3 Weld residual stress effect . . . 172
6.2.4 Stress intensity factor solutions . . . 177
6.3 Experimental tests . . . 181
6.3.1 Test sample preparation and test process . . . 183
6.3.2 Fatigue crack growth test results . . . 186
6.4 Comparison of modelling with experimental tests . . . 191
6.4.1 Strains . . . 191
6.4.2 FCG lives . . . 194

6.5 Summary of the chapter 196

7 Conclusions **197**

7.1 Summary of the research 197

7.2 Conclusive remarks 200

7.3 Contribution to the knowledge 200

7.4 Limitations 201

7.5 Suggested work 201

References **203**

A Dissemination of the results **219**

B Fuselage panel: technical drawings and modelling approaches **220**

List of Figures

1.1 Integral metallic structure: FS welded wing panel [Courtesy AIRBUS UK]. 2

1.2 Damage tolerance design concept. 5

2.1 The three modes of loading a cracked solid. 12

2.2 Infinite element and polar coordinate system. 13

2.3 Effects of specimen thickness on fracture toughness 15

2.4 Crack opening displacement definition. 17

2.5 First approximation of the plastic zone size. 19

2.6 Irwin plastic zone size correction. 19

2.7 Crack closure parameter at minimum load. 20

2.8 Effects of different R Ratio. 23

2.9 Effective stress intensity factor. 24

2.10 Normalised opening stress level for different empirical rule. 25

2.11 Typical stress strain curve. 40

2.12 Isotropic hardening. 41

2.13 Kinematic hardening. 43

2.14 Friction stir welding process. 47

2.15 Microstructure classification of friction stir welds: A) Unaffected material (Parent plate). B) Heat affected zone (HAZ). C) Thermo-mechanically affected zone (TMAZ). D) Weld nugget 48

2.16 Residual stress distribution for different welding processes. 50

2.17 Biaxial RS distribution of FSW (Al-Li 2098). 51

2.18 Distribution of residual stresses and global tensioning effects. . . . 51

2.19 Tensile residual stress effect on cyclic loading. 58

2.20 Compressive residual stress effect on cyclic loading. 58

3.1 Modified virtual crack closure technique. 65

3.2 Modelling of the M(T) specimen. 66

3.3 Mesh sensitivity study: β solution. 67

3.4 Mesh sensitivity study: errors. 67

3.5 Balance of residual stresses. 68

3.6 Distribution of residual stresses with no crack. 70

3.7 Redistribution of residual stresses with crack propagation. 70

3.8 Validation of the K_{res} with weight function method (WFM). . . . 71

3.9 Superposition approach. 72

3.10 MVCCT with for an applied stress. 73

3.11 MVCCT for a residual stress field. 73

3.12 SIF superposition. 74

3.13 SERR and mutual work. 75

3.14 Mesh refinement study. 78

3.15 Mesh of the crack closure model. 79

3.16 Crack surface contact modelling. 79

3.17 Node release scheme. 80

3.18 Flowchart of the LEFM method to calculate the FCG life. 84

3.19 Material curve 2024-T351 from AFGROW. 87

3.20 Prediction method by using the ΔK_{eff} approach. 88

4.1 Crack opening displacement without RS. 92

4.2 Crack opening displacement. 93

4.3 Stresses distribution. 94

4.4 Strain distribution. 94

4.5 Opening stress level obtain with FE and the respective lower and upper band: respectively Newman and Ibrahim. 95

4.6 Line where the stresses have been calculated. 96

4.7 Redistribution of RS on the crack line: elastic analysis, unload conditions. 98

4.8 Redistribution of RS on the crack line: quai-static plastic analysis, unload conditions. 98

4.9 Redistribution of RS at 5 mm above the crack line: elastic analysis, unload conditions. 99

4.10 Redistribution of RS at 5 mm above the crack line: plastic analysis, unload conditions. 99

4.11 Redistribution of RS at 35 mm from the crack line: elastic analysis, unload conditions. 100

4.12 Redistribution of RS at 35 mm from the crack line: plastic analysis, unload conditions. 100

4.13 Element used for the evaluation of stress and strain history. 102

4.14 Stress history. 103

4.15 Strain history. 104

4.16 Stress strain history. 105

4.17 Iso-stress line for 2024 T-351 without RS. 107

4.18 Iso-stress line for 2198 without RS. 107

4.19 Initial RS distribution for different material and weld process. . . 108

4.20 Iso-stress line for 2024 with RS. 109

4.21 Iso-stress line for 2198 RS. 109

4.22 Plastic zone size and plastic wake definition. 110

4.23 Plastic wake (dimension mm). 111

4.24 Plastic wake due to VPPA welding RS (dimension mm). 112

4.25 Plastic wake and plastic zone size in presence of residual stress field. 113

4.26 Crack opening displacement. 115

4.27 Stress at the crack tip. 116

4.28 Plasticity induced crack closure. 117

4.29 Two opposite effects of residual stresses on crack opening stress. . 118

4.30 Opening stress level with and without RS. 119

4.31 Distribution of constant balanced residual stress fields. 120

4.32 Comparison of displacement and stresses for different constant balance RS field at unload condition. 121

4.33 Comparison of displacement and stresses for different constant balanced RS field at load condition. 122

4.34 Opening stress level for different constant balanced RS field. . . . 123

4.35 RS field effect on the plastic wake and plastic zone size. 123

4.36 FSW ESE(T) distribution. 125

4.37 Mesh used for the elasto-plastic model. 126

4.38 Iso-stress contour map at crack length 16 mm without RS (unit = MPa, mm). 127

4.39 Iso-stress contour map at crack length 16 with RS (unit = MPa, mm). 127

4.40 Comparison of the y-axis strains with and without residual stresses at crack length 16 mm at unload conditions. 128

4.41 Comparison of the normalised COD with and without RS at maximum load. 129

4.42 Comparison of the normalised COD with and without RS at minimum load. 130

4.43 Normalised COD at maximum load at different crack length with RS. 131

4.44 Normalised COD at minimum load at different crack length with RS. 131

4.45 Normalised COD at different percentage of the load at crack length 12 mm. 132

4.46 Different percentage of the longitudinal stresses at a crack length 12 mm. 132

4.47 Different percentage of the normalised COD at a crack length 16 mm. 133

4.48 Different percentage of the longitudinal stresses at a crack length 16 mm. 133

4.49 Opening stress with and without RS. 134

5.1 Sketch of the M(T) test sample. 138

5.2 Redistribution of RS on the crack line. 140

5.3 Calculated K_{res} for the VPPA residual stress distribution. 140

5.4 R_{eff} for the constant amplitude load. 141

5.5 Comparison of predicted and measured FCG rates under constant amplitude load: nominal $R = 0.1$. 142

5.6 Comparison of predicted and measured FCG rates under constant amplitude load: nominal $R = 0.6$. 143

5.7 Comparison of predicted and measured FCG life under constant amplitude load: nominal $R = 0.1$ with VPPA RS field. 143

5.8 Comparison between prediction by Walker and Nasgro equation for ΔK=4,6 MPa$\sqrt{m}$ 146

5.9 Comparison between prediction by Walker and Nasgro equation for ΔK=11,15 MPa$\sqrt{m}$. 147

5.10 R_{eff} for the constant stress intensity factor range. 148

5.11 Geometry and mesh of the 1/2 FE model used for an elastic analysis. 149

5.12 Beta solution for the ESE(T). 150

5.13 Measured residual stress field and FE input [courtesy GKSS]. . . . 151

5.14 Longitudinal residual stresses in the FE model. 152

5.15 Effective ratio and K_{res} for the ESE(T) specimen. 153

5.16 Comparison of the opening factor determined with the two methods. 155

5.17 Effective stress intensity factor range. 155

5.18 Normalised load ratio parameter. 156

5.19 Two prediction methods for the crack closure approach with the superposition approach. 158

5.20 Fatigue crack life prediction. 159

5.21 Comparison of the superposition method with the crack closure model for the M(T) specimen. 160

5.22 Comparison of the crack closure and superposition for the ESE(T) specimen. 161

5.23 Analysis procedure of the two prediction methods. 161

6.1 Application of friction stir welding in the fuselage structure. . . . 166

6.2 CAD drawing of the stringer panel test sample geometry. 167

6.3 2D FE model of the stringer panel. 168

6.4 Contour map for the displacement (unit=mm). 170

6.5 Optional caption for list of figures 171

6.6 Out of plane displacement. 172

6.7 Longitudinal stress in clamped conditions. 173

6.8 Mean and bending stress a the symmetry line. 173

6.9 Inputted biaxial residual stress distribution. 174

6.10 Biaxial residual stress distribution after balance on the symmetry line. 175

6.11 Biaxial residual stress distribution after balance on the free edge. 175

6.12 Biaxial stress distribution along the crack propagation line after balance. 176

6.13 MVCCT with secondary bending effects. 177

6.14 SIF calculated for the stringer panel and equivalent M(T) geometry. 179

6.15 Strain energy release rate and K_{res}. 180

6.16 Superposition by using the MVCCT. 180

6.17 Stress intensity factor range. 181

6.18 Effective R ratio. 182

6.19 Fatigue test machine. 182

6.20 Large friction stir welded sheet with FSW direction. 183

6.21 Photo of the test sample cut off from stringer panel. 183

6.22 Preparation of the specimen. 184

6.23 Strain gauges wire for measurement. 185

6.24 Stresses on the top surface. 186

6.25 Definition of the crack propagation observation points. 187

6.26 Comparison of the left side of the crack on top and bottom surface. 187

6.27 Comparison of the right side of the crack on the top and bottom surface. 188

6.28 Comparison of the left and right side of the crack for sample 1, bottom surface. 188

6.29 Comparison of the left and right side of the crack for sample 2, bottom surface. 189

6.30 Comparison of the left and right side of the crack for sample 1, top surface. 189

6.31 Comparison of the left and right side of the crack for sample 2, top surface. 190

6.32 Comparison of the overall average of the two samples. 190

6.33 Strain gauges position (Dimension mm). 191

6.34 Calculated and measured strains. 192

6.35 Calculated and measured mean strains. 192

6.36 Calculated and measured bending strains 193

6.37 Material curve for 2198 FSW. 194

6.38 Comparison of the prediction with the experimental data. 195

B.1 Section of the hybrid concept: FSW and rivetted stringer. 220

B.2 Strain energy release rate from RS field. 221

B.3 Comparison of the residual SIF. 221

B.4 Comparison of the total and applied SIF. 222

B.5 Superposition by using the J-integral. 223

B.6 Superposition by using the MVCCT. 223

B.7 Stress intensity factor range. 224

B.8 Effective R ratio. 224

List of Tables

1.1 Pros and cons of welding process with integral metallic structures. 3

2.1 Comparison of methods in the recent literature and current work. 33

2.2 Several applications of plasticity induced crack closure. 36

2.3 Pros and cons of the friction stir welding process. 48

2.4 Residual stresses measurements techniques. 52

2.5 Methods for predicting fatigue crack growth rates in presence of welding residual stresses. 59

3.1 Material properties for Al 2024 T-351. 83

3.2 Material constants used in the crack growth laws for 2024-T351. . 85

4.1 Sample cases to investigate the plastic zone size: M(T) with 100 MPa and R=0.1. 106

4.2 Percentage difference between forward plastic zone size and plastic wake. 124

6.1 Material properties of Aluminium 2198. 167

6.2 Parameters used in the strain gauges measurement. 186

List of abbreviations, nomenclature and symbols

Abbreviations

2D	Two dimensional
3D	Three dimensional
COD	Crack opening displacement
DT	Damage tolerance
ESE(T)	Eccentrically-Loaded Single Edge Crack Tension Specimen
FCG	Fatigue crack growth
FEM	Finite element method
FSW	Friction stir welding
HAZ	Heat affected zone
HTM	Harter-T method
IMS	Integral metallic structure
LBW	Laser beam welding
LEFM	Linear elastic fracture mechanics
MIG	Metal inert gas
M(T)	Middle crack tension
MVCCT	Modified virtual crack closure technique
RS	Residual stress
SERR	Strain energy release rate
SIF	Stress intensity factor
TMAZ	Thermo-mechanical affected zone
TWI	The Welding Institute
VPPA	Variable polarity plasma arc
WF	Weight function

Nomenclature

a	Crack length
b	Specimen width
C, n, m, p, q	Material crack growth rate constants
E	Elastic modulus
F	Force, Yield surface function
G	Strain energy release rate
J	J-integral
K	Stress intensity factor
l	Length
N	Number of cycles
Q	Isotropic hardening coefficient
R	R ratio
S	Stress
t	Thickness
u, v, w	Displacements
U	Elastic energy, Normalised load ratio parameter
w	Width
x, y, z	Axes, coordinates

Super and Subscripts

I, II, III	Opening, sliding, tearing modes
$1, 2, 3$	Principal stresses
σ_α	back stress
app	Applied
bot	Bottom
c	Toughness
cri	Critical
dev	Deviatoric tensor
eff	Effective
i	i^{th} index
max	Maximum
min	Minimum
op	Opening
p	Potential

vm	von Mises
th	Threshold
top	Top
tot	Total
x, y, z	Directions
ys	Yield strength
∞	Remote

Symbols

β	Dimensionless stress intensity factor
ε	Strain
ν	Poisson's ratio
σ	Stress
γ	Kinematic hardening coefficient

Notation

{}	Tensor second order
[]	Tensor first order

Chapter 1

Introduction

1.1 Background

The new design concepts for aircraft structures are driven by the pursuit of the reduction of maintenance and manufacture costs and weight saving. The latter has brought aircraft industry to face the challenge of new materials. Aluminium alloys have been the most reliable material due to their good mechanical properties and their lightness. Their recent development is a third generation of Al-Li alloys with enhanced mechanical and fatigue properties [1, 2]. Nevertheless, in the last few decades, metals have been challenged by composite materials [3] because they offer a higher directional strength with a lower weight. However new failure modes occur [4–7], therefore more research is needed, to increase their capabilities and to satisfy the aviation regulations.

Nonetheless the potentiality of metals is not totally exploited yet: the manufacturing processes with metals have been further explored and the outcome produced innovative costs and weight saving solutions [8–10]. One of them is the integral metallic structures together with a new joint technique such as welding [11]. Among the welding processes friction stir welding (FSW) is one of the most appealing and efficient [12] that can be used with Al-Li alloys of third generation. However residual stress fields introduced after the welding and change of material properties need to be assessed. Moreover the use of this process is novel for large civil aircraft, therefore more research and investigations are needed to assure a safe use of this technology for large production.

1.1.1 Welded integral metallic structures

One of the main advantage of the integral metallic structure by welding process is the exclusion of fasteners and overlapping joints in the airframe which reduces the manufacture and maintenance costs together with structural weight of fuselage and wing panels (see figure 1.1).

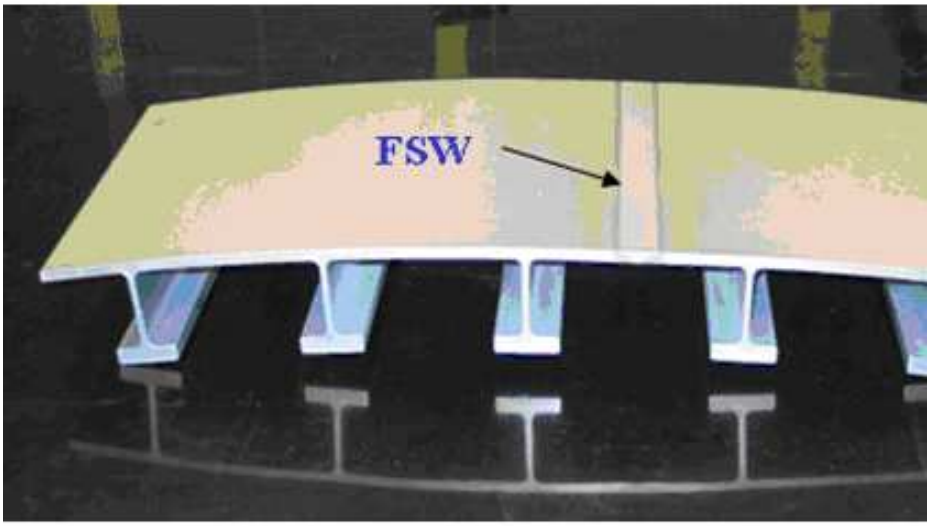

Figure 1.1: Integral metallic structure: FS welded wing panel [Courtesy AIRBUS UK].

The absence of fastener holes will also remove the crack initiation sources resulting in much better fatigue endurance and simplification in inspection. Several works have demonstrated that the technology is mature and that advantages in terms of cost and weight saving of the structure is significant [11–14] and it can be exploited for wing and fuselage applications (see figure 1.1). A welded IMS gets rid of hundreds of fasteners, which can reduce the weight by 20% with respect to a same model built by the traditional joining technique. In the case of the Eclipse, 263 welds replaced 7000 fasteners. Therefore a weld integral structure will preclude initial crack due to holes of the rivets thus the maintenance will benefit in terms of time and costs. The Eclipse Aviation claimed that the costs of their aircraft had been reduced by 25% due to the use of the friction stir welding (FSW) process [14, 15]. Several welding processes are applicable to airframe aluminium alloys for aircraft structure, among them there are FSW,

laser beam welding (LBW), and fusion welding, e.g. the variable polarity plasma arc (VPPA) and metal inert gas (MIG) welding. Friction stir welding and integral metallic structures are relatively new but there have been a few examples in aeronautical industrial applications [13,16]. The passage of this technology from a small business jet to civil commercial aircraft requires more effort in terms of design and manufacturing research in order to satisfy the regulations authorities. Welding processes have an old history in aeronautics even though the use of such process has not been frequently used for fuselage or wing structures [16,17]. Mechanical fastening has been preferred as an established technology.

Table 1.1: Pros and cons of welding process with integral metallic structures.

Advantages	Disadvantages
- Reduction of manufacturing and maintenance costs.	- Residual stresses field introduced in the structure.
- Reduction of structural weight.	- Absence of crack stopper.
- Reduction of manufacturing time by using a single step operation i.e. easier to be automated.	- Distortion of large components.
- Reduce the number of part i.e. decrease of complexity.	- Material properties degradation.
- Avoid high density rivets.	- Material softening.
- Potentially leakage free structure i.e. avoid sealant.	- Reparability of welded structures.
- No overlap region i.e. no fretting.	- Defects due to lack of penetration.
- Continuous load path.	- Difficulty to join dissimilar alloys.
- Increase of stiffness due to the absence of the holes.	- New technology for large aircraft.
- No crack initiation starting from holes.	

Table 1.1 resumes the pros and cons of weld processes in aeronautical structure application. One of the main problems is the small range of alloys that can be welded and to join dissimilar alloys [18] but FSW is more weldable thus a more variety of alloys can be joined, such the series 2xxx and 7xxx that have always encountered problems in the previous welding [19]. Another disadvantage is the distortion in the welded plates but in friction stir welding the shrinkage is very low. The residual stresses that have a high influence on the damage tolerance design, can be controlled by applying a preload which for certain crack geometries

can be a benefit [20]. The final surface is very smooth and because no additional material is needed, the probability of defects in FSW is much lower than in the previous welding processes. The microstructure must be considered too: the hardness changes and it affects the stiffness of the material which changes also the response to an external load in terms of stresses and displacement and in term of natural frequency that could affect the aeroelastic response of the overall structure. Three main aspects need to be investigated for design: hardness, microstructure changes and residual stresses which have a great influence on damage tolerance aspects [21, 22]. The use of welded structure has been assessed as well as their impact on integral metallic structures but the technology needs more research to fully understand the issues on damage tolerance design [11].

This work attempts to contribute and to advance the damage tolerance design issues by proposing prediction approaches for fatigue crack growth rate and to understand the effects of weld by including residual stresses in the methodology in order to establish their influence and behaviour on crack propagation.

1.1.2 Design philosophy against fatigue: damage tolerance

The structure design against fatigue has been driven by three main design philosophies that aim to guarantee safety: safe life, fail safe and damage tolerance.

The first design philosophy adopted for metal structures in the 1950's was the safe life approach. This concept assumed that the structure must be free of defects and it must be changed after a determined life. The life is determined by tests and calculation by using a safety factor and implying no defect within this period. This also requires that a structure with an initial defect can not be used in service. The component will be withdraw at the end of its life even if in good conditions. The major drawback is that if failure occurs it may be catastrophic: fatigue is a safety problem. Moreover the costs are increased first because a component with an initial defect can not be installed and secondly the direct operating costs are increased due to the regular substitution of the component that could last much longer.

Due to the mentioned problems later in the 1970's the fail-safe philosophy emerged. It entails that if a defect occur in the component this will not affect the safety of

the operation. In this case fatigue becomes a maintenance problem. A crack for example can occur in service operation but the design need to guarantee that it will grow slow enough to safely carry its load to the next expected inspection, after which it will be changed. The main advantage with this approach is that fatigue is not a safety problem but a maintenance problem. However a component with an initial defect will be still rejected and the failed component may have be used for a longer period.

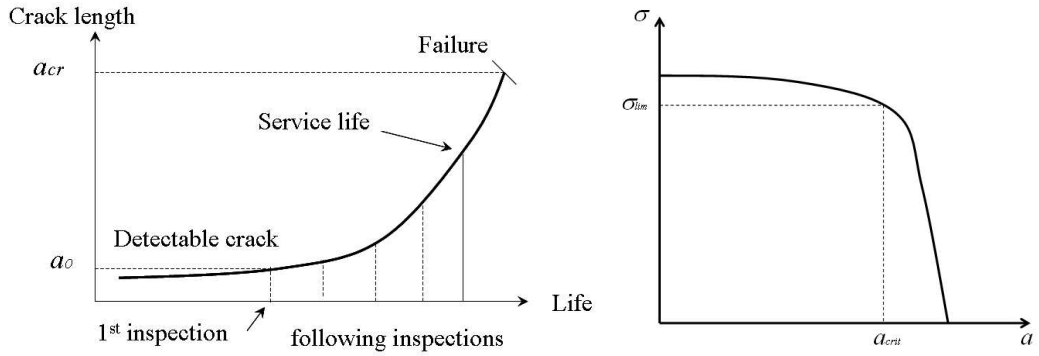

(a) Crack growth curve. (b) Strength curve.

Figure 1.2: Damage tolerance design concept.

Damage tolerance is the current design philosophy. It assumes pre-existing defects in the structure and it allows slow crack growth will guarantee a safe operation service. The design requirements are the secondary load path, slow crack propagation properties, damage detectability and tolerant of small initial damage. As the previous concept fatigue is a maintenance problems but the service life of the component is increased. This design concept is presented in figure 1.2. Three main critical aspects for the analysis need to be assessed: inspection period, crack growth life and residual strength. Fatigue crack growth rate is the most important which needs to be assessed for damage tolerance design of structural components that can be used in large civil aircraft.

1.1.3 Definition of Residual Stress

The definition of "Residual Stress" is generally used to define the internal balanced stresses that remain in the structure even if no external load is applied. The majority of the published papers [22–24], indicate with this definition, the stresses caused by machining, surface treatment (i.e. cold working, shot peening)

or welding processes [25–27]. However some authors called residual stresses, the stresses due to plasticity induced crack closure, which remain behind the crack tip when the crack grows [28, 29]. Because the arguments were treated separately there was no confusions between the type of residual stresses, therefore no further specification was necessary. Nevertheless throughout this thesis, the word "Residual Stress" is referred as the weld induced residual stresses unless specified. The reason to maintain the general definition is because of consistency with the vast literature that concern the weld residual stresses [22–27].

1.2 Scope, aim and objectives

The damage tolerance assessment of this research will deal mainly on predictive models of fatigue crack growth propagation. The crack will propagate in welded butt joint for different configurations, i.e. crack growing from the welding, towards the welding or parallel to the welding. Non-linearity aspects will be taken into account in the prediction of the fatigue crack growth rate and life, giving a good practice on the several methods that can be used in order to deliver a final guidance on how predict the fatigue crack growth life. The methodology encompasses also material plasticity and its potentiality is assessed by comparing numerical results with experimental and analytical results. The aim of this work is to investigate the influence of the welding residual stresses on the fatigue crack growth behaviour in aluminium alloys in order to explore the impact of FSW in IMS for damage tolerance design. The main objectives for the overall research project are:

- To predict fatigue crack growth rate, using the linear elastic fracture mechanics and taking into account the effect of welding residual stresses.
- To develop numerical modelling technique by taking account of any non-linear effects such as residual stress re-distribution, plastic material and crack closure behaviour.
- To establish a good practice and guidance to apply the above methodologies for predicting fatigue crack growth life; i.e combine linear elastic with non linear effect.

- To model and test crack propagation of demonstrative hybrid structural joint i.e. fuselage skin-stringer sections, fabricated by welding and riveting.

The results will be validated by experimental tests from the open literature, or test results by partners in the same project as well as tests conducted by the author.

1.3 Research methods

1.3.1 Project background

The COINS (COst effective INtegral metallic Structures) is a large research project led by a consortium of 14 European partners. The aim is: "Extending the application of integral metallic structure utilising friction stir welding by: advancing the state of the art of FSW technology, developing new geometries for FSW and through innovation in design". The constitution of the partners shows this project is interesting, from the knowledge point of view with three research organizations and two Universities, its applicability and its use in aeronautical industry: there are eight end-users. BAE System acts as the coordinator. ALCAN provides material and contributes to the project. The end users are Airbus Germany, Alenia Aeronautica, Dassault, SABCA, SHORTS, Piaggio Aereo, Fatronik, Airbus UK. The three research organizations are: EADS F, EADS G, GKSS and the two Universities are University of Patras and Cranfield University. The role of Cranfield University was to work on the FSW Standards, mechanical testing prediction of fatigue crack growth and model of structures behaviour. The integral metallic structure with the use of welding process will find application in fuselage and wing structures.

1.3.2 Computational approach

One of the most important aspects of weld which influences the FCGR is due to the presence of thermal residual stresses. In order to assess the crack growth in a plate through a residual stress field the stress intensity factor (SIF) must be evaluated as it is the most important parameters in linear elastic fracture

mechanics based life prediction. Nevertheless the first step of this work has been the implementation of residual stresses in the FE model. Previous researches show that the thermal analysis and the mechanical analysis can be done separately [20, 30, 31] and this work focuses on the mechanical analysis using a given RS field. Two main approaches have been considered. The first is based on the superposition of two stress intensity factor solutions due to the weld residual stresses and the applied load. Life prediction is made by using three empirical methods modified for the welded case: the Walker equation, NASGRO equation and Harter-T method. The residual stress intensity factor K_{res} is the main parameter which has been evaluated by the finite element analysis. The validation has been done with results found in the literature. However some limitations have been found and therefore the effective stress intensity factor range ΔK_{eff} together with plasticity induced closure effects have been introduced. The plastic analysis requires more effort in terms of modelling and computational time but it entails to have a better understanding of the mechanisms which act on the crack propagation through a residual stress field. The use of ΔK_{eff} together with FASTRAN method for crack growth prediction encompasses the non-linearity that can arise when plasticity induced crack closure occur. Only few researches have been found on the assessment of the crack closure level in presence of residual stresses by using finite element analysis with elastic plastic material and cyclic load. The model was set for a case without residual stresses and validated by previous results, then the case with residual stresses has been assessed. A comparison of the numerical results via FE with empirical and analytical methods has been done. Models have been carried out with commercial FE code ABAQUS in order to evaluate stress intensity factor. FORTRAN and MATLAB have also been used as subroutine to evaluate the FCGR. FORTRAN and ABAQUS interface together to apply residual stress field and to run several analysis. Python has been also used to help post process the results of the finite element analysis. The analyses have been run on a cluster computer high performance facility at Cranfield University.

1.4 Thesis structure

Chapter 2 presents the theoretical background, principles, the fundamental equations and the laws used in fracture mechanics and fatigue life prediction. A literature review on the problem of residual stresses in fracture mechanics and on the crack propagation has been given. Material non-linearity that has been largely discussed in terms of crack closure is herein presented to give a general picture of the actual scenario of the numerical methods and the modelling issues to calculate the opening stress level. A general discussion introduces several kinds of welds (in particular the friction stir weld) and their possible impact on fatigue crack growth by assessing the influence of residual stresses on the prediction methods found in the literature.

Chapter 3 explains the methodology used in this thesis. The prediction methods to calculate the fatigue crack growth are presented together with the modelling features that are assessed and validated. Two main prediction approaches are presented: the superposition by using the R_{eff} and the effective stress intensity factor range by using ΔK_{eff}. Also the modelling features for the computational analyses for the crack propagation are shown since they are fundamental parameters for the opening stress evaluation.

Chapter 4 discusses the plasticity induced crack closure with weld residual stresses. A case without residual stresses was assessed first in order to validate the model, which is followed by a qualitative and a quantitative analysis on the influence of the residual stress field on the plastic zone size, crack opening displacement, plastic strain, plastic wake and opening stress. A better understanding of the closure mechanism is provided and its evolution when the crack propagates through the residual stress field.

Chapter 5 presents the main results of the predictions made by the two approaches i.e. the superposition and the effective stress intensity factor. Those two methods are used for two scenarios: a crack growing from the weld and a crack growing into the weld. Also the plastic non-linearity has been considered in the predictions and compared with previous results. A constant amplitude load is generally applied but also the validation for a constant stress intensity factor range has been made.

Chapter 6 presents the study of a FSW joint for fuselage application with

rivetted stringer features. A riveted stringer and a friction stir weld skin joint with a crack growing parallel to the weld line has been modelled and tested. Because of the secondary bending introduced by the pad-up strains have been also measured and calculated. The predicted lifes have been compared with the test results.

Chapter 7 resumes the influence of residual stresses and a direction for further research in this field is discussed by proposing future works.

Appendix A lists the findings of the present work and the forum where they have been published or presented.

Appendix B shows the technical drawings for the stringer panel and a comparison of different approach to calculate the stress intensity factor.

Chapter 2

Literature review and theoretical framework

This chapter provides the basic knowledge that will be discussed and largely used throughout this thesis and it resumes the literature by reviewing the linear elastic fracture mechanics principles and the current modelling issues in plasticity induced crack closure. The effects of the welded structures, i.e. residual stresses on fatigue crack growth, are discussed and the main findings of the literature are presented herein.

Section 2.1 introduces the key parameters of linear elastic fracture mechanics (LEFM): stress intensity factor, strain energy release rate, and crack tip plasticity and their derivations. The following section 2.2 is about the fatigue principles and the laws to predict the fatigue crack growth with final comments on crack closure based laws and most recent two parameter laws.

The importance of numerical finite element modelling is examined in section 2.3. The classical numerical methods used in LEFM are provided as well as a discussion on the plasticity induced crack closure. In some cases residual stresses (RS) change the crack closure hence the effective stress intensity factor range ΔK_{eff}. Therefore it is important to discuss the cause that induces the crack closure in non-welded specimen: material plasticity. The state of the art of the modelling is presented in section 2.3 where the main aspects are highlighted. A lot of research has been carried on in this field but there are few attempts that consider the effect of RS with plasticity induced crack closure. One of the

objectives of this research is to explore this field and to expand the knowledge of the non-linear effect on the opening stress level in presence of weld residual stress field.

The last section 2.4 focuses on the weld processes and their influence on the fatigue crack growth propagation in terms of residual stresses. A detailed discussion on their effects on the predictive methods is given, and an insight of the current state of the art on how predict the fatigue life in welded structures is provided.

2.1 Linear elastic fracture mechanics principles

This section aims to review the basic knowledge of fracture mechanics and fatigue crack growth modelling. There will be a description of the most important formulations used throughout this work in order to better understand the mathematical tools and the physical principles used.

2.1.1 Stress intensity factor

The stress intensity factor is one of the most important parameters in linear elastic fracture mechanics (LEFM).

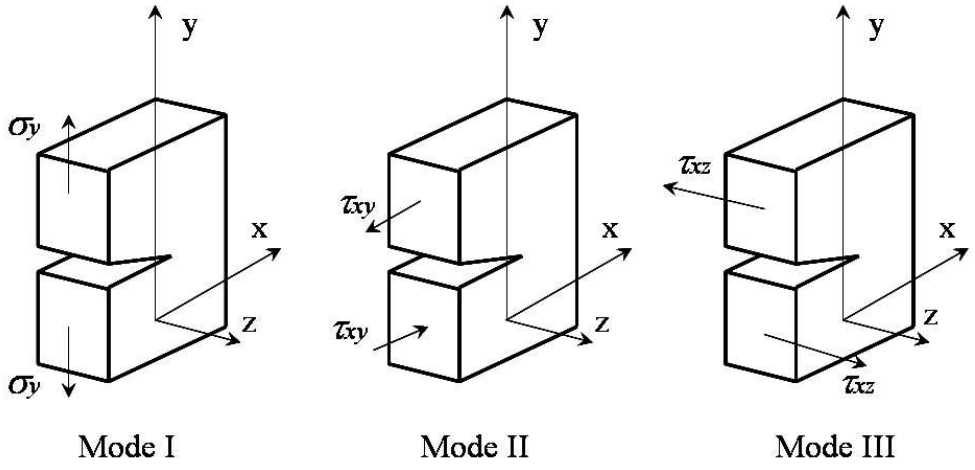

Figure 2.1: The three modes of loading a cracked solid.

A cracked plate can be loaded differently and three modes can be distinguished

depending on how the load act on the crack (see figure 2.1). They are generally referred as mode I, II, and III that are opening, sliding and tearing mode respectively. In order to obtain the crack tip stress field for the mode I the following equation can be used:

$$\sigma_{ij} = \frac{K_I}{\sqrt{2\pi r}} f_{ij}(\theta) \tag{2.1}$$

Where σ_{ij} represents the stress tensor acting on an infinite element dx-dy and its distance from the crack tip is defined by the polar coordinate r and θ (see Figure 2.2).

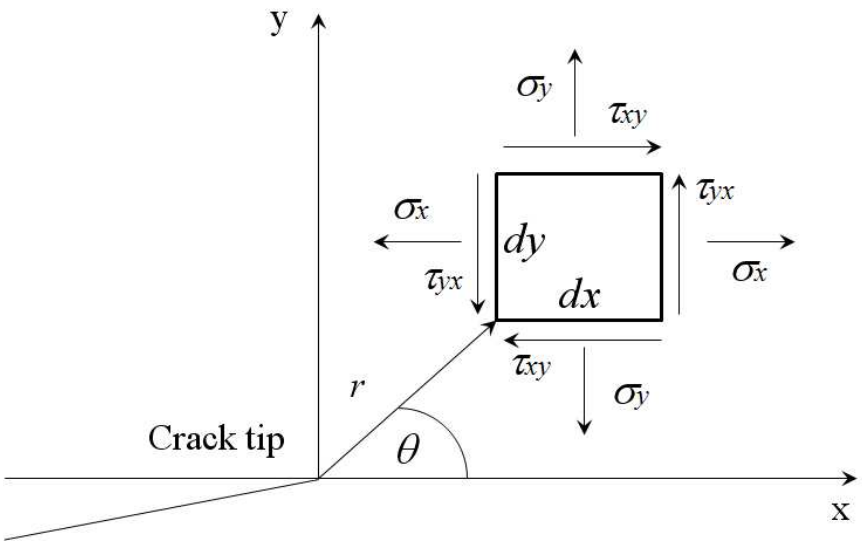

Figure 2.2: Infinite element and polar coordinate system.

The functions $f_{ij}(\theta)$ are non-dimensional and they are different for the three modes. K_I is defined as stress intensity factor (SIF) which characterizes the crack tip stress field for the mode I. K_{II} and K_{III} will define the stress field for the modes II and III respectively at the crack tip, hence if different cracks have the same K then they will have the same distribution of stresses around the crack tip. The mode that include the loading in different directions is called "mixed mode". In general for a certain geometry and load configuration:

$$K_I = \beta \sigma_\infty \sqrt{\pi a} \tag{2.2}$$

β is the non-dimensional SIF that is a geometric factor which relates the SIF

for a plate with a particular geometry to the SIF of an infinite plate. It could be considered as a geometric correction to the SIF of the centre-cracked infinite plate. Once the K is known, the stress field around the crack tip can be found as:

$$\begin{aligned}\sigma_x &= \frac{K_I}{\sqrt{2\pi r}} cos\frac{\theta}{2}\left(1 - sin\frac{\theta}{3}sin\frac{3\theta}{2}\right)\\ \sigma_y &= \frac{K_I}{\sqrt{2\pi r}} cos\frac{\theta}{2}\left(1 + sin\frac{\theta}{3}sin\frac{3\theta}{2}\right)\\ \tau_{xy} &= \frac{K_I}{\sqrt{2\pi r}} sin\frac{\theta}{2}cos\frac{\theta}{2}cos\frac{3\theta}{2}\end{aligned} \tag{2.3}$$

and the displacements can be found as:

$$\begin{aligned}u &= \frac{K_I}{4\mu}\sqrt{\frac{r}{2\pi}}\left((2\kappa - 1)cos\frac{\theta}{2} - cos\frac{3\theta}{2}\right)\\ v &= \frac{K_I}{4\mu}\sqrt{\frac{r}{2\pi}}\left((2\kappa + 1)sin\frac{\theta}{2} - sin\frac{3\theta}{2}\right)\end{aligned} \tag{2.4}$$

Where $\mu = \frac{E}{2(1+\nu)}$ is the shear modulus and κ:

$$\kappa = \begin{cases} 3 - 4\nu & \text{plane strain } (\varepsilon_{zz}{=}0)\\ (3-\nu)/(1+\nu) & \text{plane stress } (\sigma_{zz}{=}0)\end{cases} \tag{2.5}$$

The SIF is an important parameter also because it can establish when the fracture occur by using the following criterion:

$$K_I \geq K_{Ic} \tag{2.6}$$

where K_{Ic} is the fracture toughness and it depends on the material but also the thickness has an important role on this parameter:

$$t \geq 2.5\left(\frac{K_{Ic}}{\sigma_{ys}}\right)^2 \tag{2.7}$$

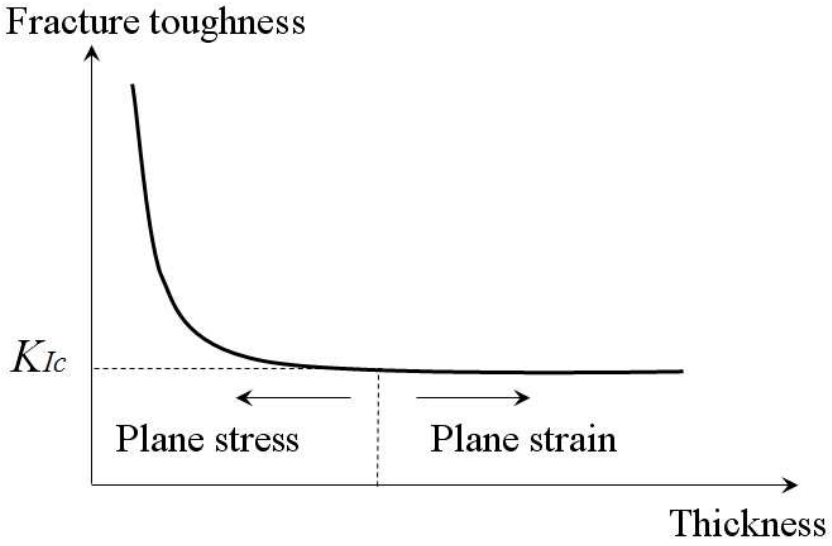

Figure 2.3: Effects of specimen thickness on fracture toughness

where σ_{ys} is the yield stress of the material. The fatigue toughness K_{Ic} can be found only in plane strain condition. In the case of plane stress condition the critical SIF K_{Icrit} must be computed using an empirical fitting law of the graph sketched in figure (2.3). More information concerning this subject can be found in Broek, Anderson, Janssen [32–34].

2.1.2 Derivation of main LEFM parameters

The stress intensity factor above described is the most important parameter in LEFM, however to assess the fracture of a solid, also energy principles are often used. This section aims to provide the derivation and the links of the energy terms with other LEFM parameters such fracture toughness, SIF, and crack opening displacement (COD).

In the early 1920's Griffith established that a balance occurs between the potential energy, which is the mechanical energy, and the surface energy. Consider a cracked solid plate, the balanced energy terms can be written as:

$$\frac{d}{da}(F - U) = \frac{dU_c}{da} \tag{2.8}$$

where U is the elastic energy, F the work performed by the external force, and U_c the energy for crack formation. The right side of equation (2.8) is called strain

energy release rate (SERR) G, and, the left side is called crack resistance R.

It can be demonstrated that G is always equal to the derivative of the elastic energy [32]:

$$G = \left(\frac{dU_p}{da}\right) = -\left(\frac{d(F-U)}{da}\right) = \frac{dU_c}{da} \tag{2.9}$$

Where U_p is the potential energy. It can be demonstrated [34] that the energy release rate is equal to:

$$\begin{aligned} G &= \frac{\pi\sigma^2 a}{E} && \text{plane stress} \\ G &= (1-\nu^2)\frac{\pi\sigma^2 a}{E} && \text{plane strain} \end{aligned} \tag{2.10}$$

The SERR can be connected to the SIF by using the crack closure integral [33]:

$$\begin{aligned} K_I &= \sqrt{G_I\, E} && \text{plane stress} \\ K_I &= \sqrt{\frac{G_I\, E}{1-\nu^2}} && \text{plane strain} \end{aligned} \tag{2.11}$$

The energy around the crack tip can be also defined with the so called J-integral. Rice [32,35] has defined the J-integral as a contour integral around the crack tip which is the change in potential energy for a virtual crack extension da:

$$J = -\frac{\partial V}{\partial a} \tag{2.12}$$

where V is the potential energy. For linear elastic material $-\partial V/\partial a = G$ therefore $J = G$.

Also of importance is the displacement of the crack as presented in figure 2.4. The following equation, can be applied to determine the crack opening displacement

COD:

$$COD = 2v = \frac{4\sigma}{E}\sqrt{a^2 - x^2} \tag{2.13}$$

Which can be related by the SIF with the following equation:

$$v = \frac{2K_I}{E}\sqrt{\frac{a - x^2/a}{\pi}} \tag{2.14}$$

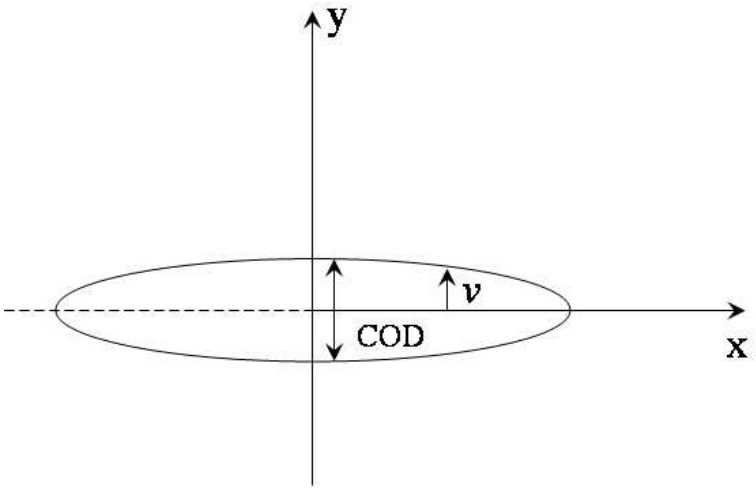

Figure 2.4: Crack opening displacement definition.

Similarly to SIF fracture criterion (equation 2.6) a failure criterion based on the SERR can be written:

$$G_I \geq G_{Ic} \tag{2.15}$$

where G_{Ic} is the critical energy release rate for mode I. Another common criterion is the material fracture toughness K_{Ic}. When the maximum applied stress reaches this value the specimen is broken:

$$K_{max} = \beta\sigma_{max}\sqrt{\pi a} \geq K_{Ic} \tag{2.16}$$

The main difference of the two criteria is that the net section yield depends, on the material because of the yielding stress, but mostly on its geometry. K_{crit} is

the critical SIF for cracking which is a characteristic of the material even if can vary with the thickness of the specimen and its assumption i.e. it depends on plane stress conditions or plane strain conditions.

It is important to know which is the failure criterion, hence when the crack reaches its critical length in order to calculate the final crack length. The critical crack length a_{crit} can be found with the following equation:

$$a_{crit} = W\left(1 - \frac{\sigma_{max}}{\sigma_{ys}}\right) \tag{2.17}$$

where W is half or total width for specimen with a middle crack or edge crack respectively while σ_{ys} and σ_{max} are the yielding and the maximum applied stress. This criterion is also known as the net section yield criterion because this is the critical length at which the net section yield reaches and overcomes the value of the yielding stress:

$$\sigma_{net} \geq \sigma_{ys} \tag{2.18}$$

The net section yielding σ_{net} is defined as the stress at the cross section which is the section of the total width diminished by the crack section. It can be expressed with the following equation:

$$\sigma_{net} = \frac{\sigma_{max} W}{W - a} \tag{2.19}$$

2.1.3 Crack tip plastic zone

The elastic crack tip stress field is characterised by a singularity due to the fact that the material is completely elastic hence does not have yielding stress. In case of plastic material an important parameter related to the stress field close to the crack tip is the plastic zone size. A first estimation of the plastic zone size for plane stress can be given by:

$$r_p^* = \frac{1}{2\pi}(\frac{K_I}{\sigma_{ys}})^2 \tag{2.20}$$

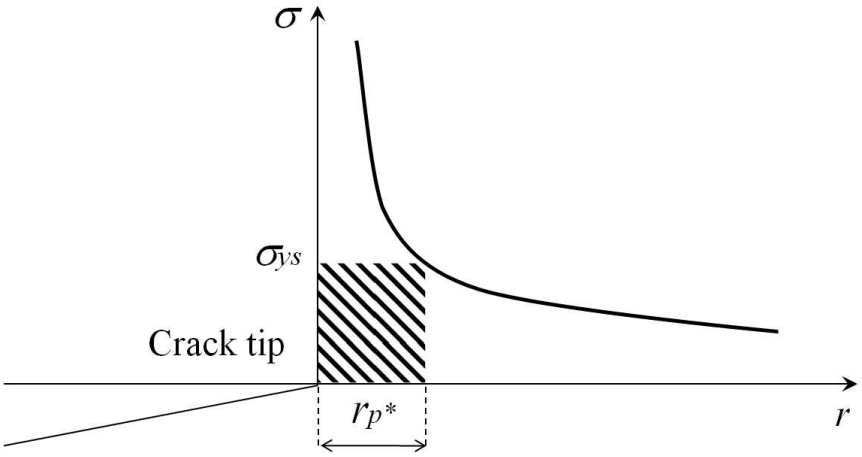

Figure 2.5: First approximation of the plastic zone size.

which is the plastic zone size shown in figure 2.5. Figure 2.6 shows the case of an elasto-plastic behaviour. In a plastic material the stress overcomes the yielding stress and the energy enclosed in the area A would be transferred in the area B. This means that the plastic zone size would be bigger than the previous case showed in figure 2.5.

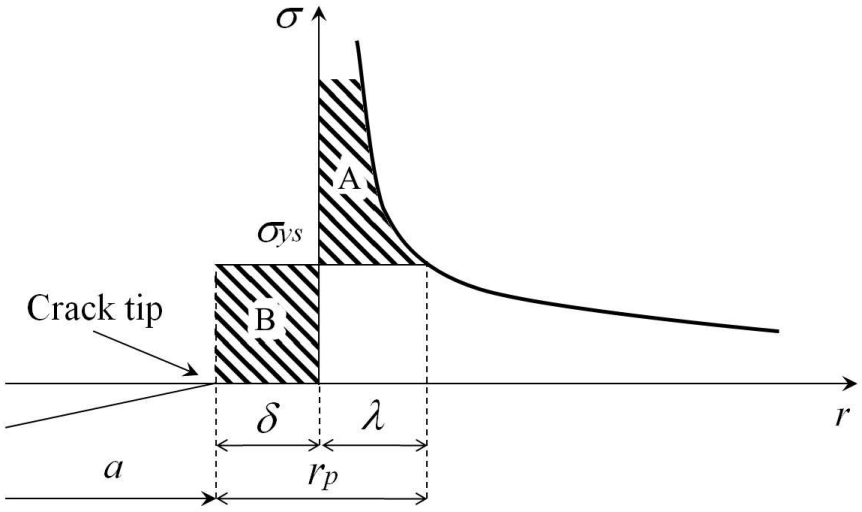

Figure 2.6: Irwin plastic zone size correction.

The correction is known as Irwin‘s plastic zone correction and it can be demonstrated that the actual plastic zone size, for plane stress, is the double of the first

estimation hence:

$$r_p = 2r_p^* = \frac{1}{\pi}(\frac{K_{max}}{\sigma_{ys}})^2 \tag{2.21}$$

The sketch in figure 2.7 shows the effect of plasticity and the cyclic load on the longitudinal stresses. This effect is not taken into account when using elastic material under static load therefore an elastic-plastic analysis needs to be carried on. In a plastic material, the forward plastic zone created under maximum load conditions, leaves permanent plastic strain that will form the so call revere plastic zone that can be observed at its minimum load condition. Those compressive stresses will also be the cause of the opening level changes at minimum load hence they are very important to determine the effective stress intensity factor range. This will have an influence on the fatigue crack propagation as it will shown in the following section.

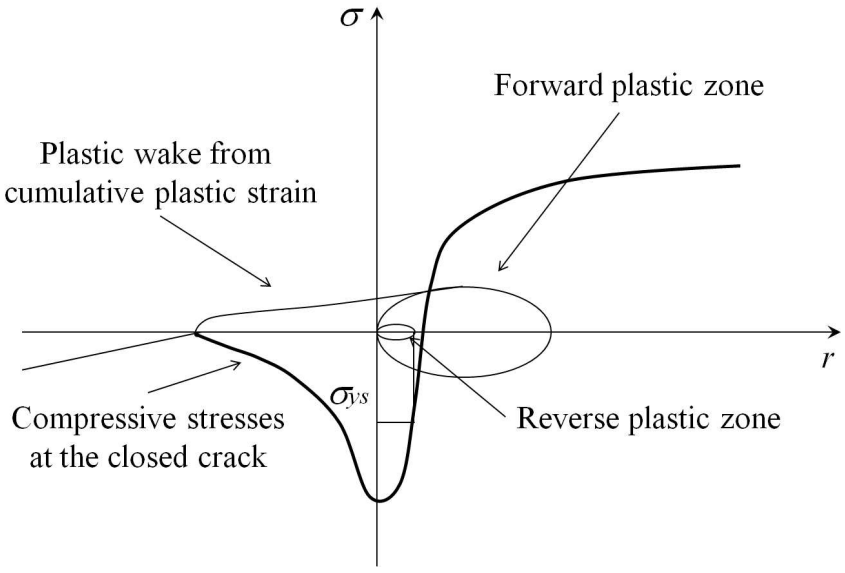

Figure 2.7: Crack closure parameter at minimum load.

It is important to notice that the evaluation of the plastic zone size is done with von Mises stresses because the biaxial stress field can be taken into account. However this will bring to have lower von Mises stresses along the crack propagation as it is demonstrated below. Starting from the definition of the von Mises

stress:

$$2\sigma_{vm}^2 = (\sigma_1 - \sigma_2)^2 + (\sigma_2 - \sigma_3)^2 + (\sigma_3 - \sigma_1)^2 \tag{2.22}$$

Where σ_1, σ_2, σ_3 are the principal stress that can be related with the stress intensity factor by the following:

$$\sigma_1 = \frac{K}{\sqrt{2\pi r}} cos\frac{\theta}{2}(1 + sin\frac{\theta}{2}) \tag{2.23}$$

$$\sigma_2 = \frac{K}{\sqrt{2\pi r}} cos\frac{\theta}{2}(1 - sin\frac{\theta}{2}) \tag{2.24}$$

By considering the plane stress condition with σ_3=0 and by substituting equations 2.23 and 2.24 into equation 2.22 it can be written:

$$r_p(\theta) = \frac{K^2}{4\pi\sigma_{vm}^2}[1 + 3/2sin^2\theta + cos\theta] \tag{2.25}$$

Where for θ=0 and considering the von Mises as the yielding stress σ_{vm}=σ_{ys} the equation becomes:

$$r_p = \frac{K^2}{2\pi\sigma_{ys}^2} \tag{2.26}$$

When assuming the Irwin plastic correction eq. 2.26 becomes:

$$r_p = \frac{K^2}{\pi\sigma_{ys}^2} \tag{2.27}$$

Which will be used to evaluate the plastic zone size.

2.2 Fatigue crack growth prediction methods

2.2.1 Paris equation

The first to notice a relationship between the fatigue crack growth rate and the stress intensity factor was Paris [36] who found an empirical correlation between them. This law took his name and it is very well known:

$$\frac{da}{dN} = C(\Delta K)^n \tag{2.28}$$

where C and n are material constants. This law is the fundamental of the actual modern fracture mechanics. Its great importance is due to the fact that once the stress intensity factor range ΔK is known, the fatigue crack growth rate can be calculated. Its limitation are the empirical constants that must be tuned for the different materials and different load conditions. At constant amplitude load the FCGR will be influenced only by the stress ratio R which cannot be taken into account by this law. The actual mean stress of the applied load will change hence it will change the crack propagation and the crack life.

2.2.2 Influence of the mean stress and the ΔK_{eff}

The effect of R on the fatigue crack propagation is shown in the sketch in figure 2.8. For positive ratio when the ratio is increasing also the fatigue crack growth rate is increasing which means that for higher R the crack propagates faster. This means that for a given stress intensity factor range it is possible to have different FCGR and this effect is clearly missing in the Paris law but it is important for more complex loading conditions different from a constant amplitude load. The mean stress will be an important factor that must be evaluated in the case of variable amplitude loading, residual stresses field or secondary bending influence.

The first law that took into account the R effect was the Walker law [37]:

$$\frac{da}{dN} = C(\Delta K_{app}(1-R)^{m-1})^n \tag{2.29}$$

Where C and n are the Paris law material constant and m controls the shift

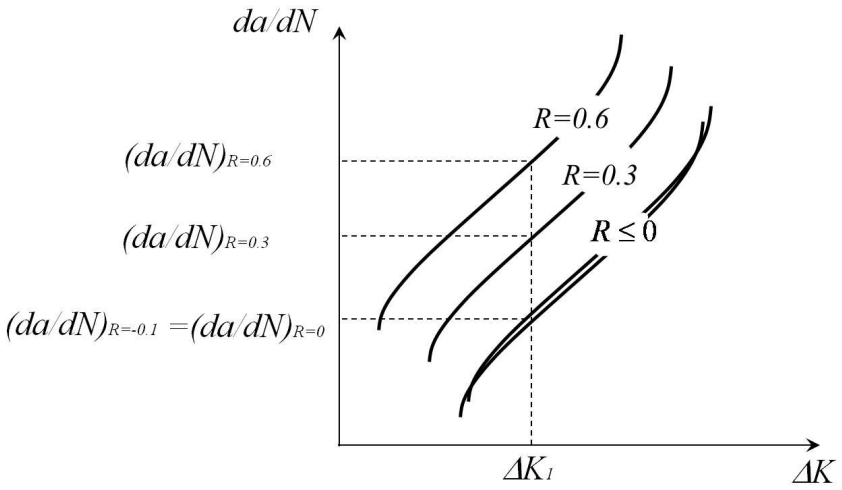

Figure 2.8: Effects of different R Ratio.

between two curves with two different stress ratio R. Another development of the Walker equation has been the Forman equation [37] that includes the effects of the threshold ΔK_{th} and the toughness K_c:

$$\frac{da}{dN} = C_F \frac{(\Delta K - \Delta K_{th})^{n_F}}{[(1-R)K_c - \Delta K]} \tag{2.30}$$

One of the most complete law is the NASGRO equation:

$$\frac{da}{dN} = C[(\frac{1-f}{1-R})\Delta K_{app}]^n \frac{(1-\frac{\Delta K_{th}}{\Delta K_{app}})^p}{(1-\frac{K_{max}}{K_{crit}})^q} \tag{2.31}$$

Where K_{crit} is the fracture toughness for a particular thickness and f determines the closure level. C and n are material constants different from the Paris material constant and p and q determine the slope in the threshold zone and in the failure region respectively. For further details on the Walker and NASGRO equation see the AFGROW manual [37].

2.2.3 Harter-T method

Another prediction method used in LEFM is the Harter-T method. This method permits to calculate the FCGR if the material coefficients of the NASGRO or Walker equation are unknown. This method needs at least two material curves

with two different stress ratio R. From the Walker equation for two different R the following relationship can be written:

$$\Delta K_1(1-R_1)^{m-1} = \Delta K_2(1-R_2)^{m-1} \tag{2.32}$$

It is possible to interpolate point by point the m coefficient by using:

$$m = 1 + [\log \frac{\Delta K_1}{\Delta K_2} / \log \frac{(1-R_2)}{(1-R_1)}] \tag{2.33}$$

By knowing m from equation 2.32 different ΔK can be achieved, for a defined R ratio that in the welded plate will be the R_{eff}. This procedure finds the material curve for that particular ratio and ΔK_{app} can be input in the same curve to find the crack growth rate. A more detailed description will be given in the methodology chapter.

2.2.4 Crack closure based laws and two parameter laws

Since Elber [38] introduced the concept of crack closure many attempts have been done to define the opening stress level. During a cyclic load tensile permanent plastic deformation have been left behind the crack tip [39]. The stress required to open the crack is called crack opening stress. Even if the concept is simple (see the sketch in figure 2.9) the opening stress is not easy to achieve.

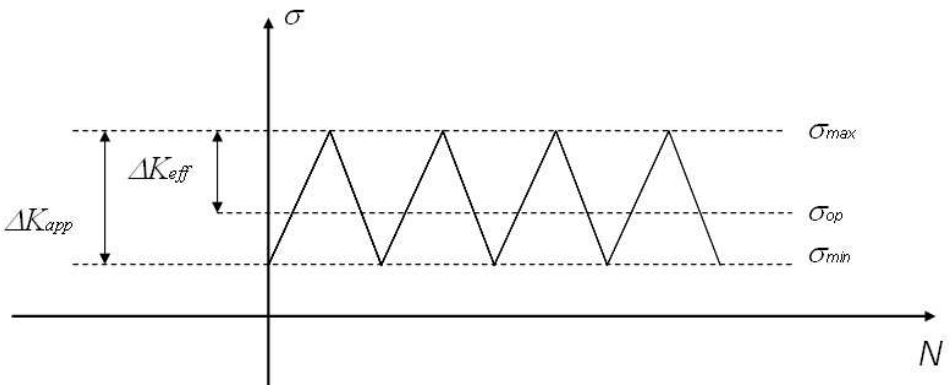

Figure 2.9: Effective stress intensity factor.

Measurements techniques aim to locate when the crack is fully open but they have an high cost and a lot of effort is needed because the deformations are not

uniform and it is difficult to define the location in order to consider the crack fully open [28]. Numerical simulations can be also performed but it has been found that many several modelling issues influence the value of opening stress [40, 41]. However it is generally accepted that the crack growth under a load with a low ratio leaves a plastic wake behind its tip and this will change the stress intensity factor range. The minimum applied load need to be modified because the crack will not be open at its minimum load but at a higher load which will be the opening stress σ_{op}. Hence a new stress intensity factor range must be considered in the prediction of the crack growth rate:

$$\Delta K_{eff} = (\sigma_{max} - \sigma_{op})\beta\sqrt{\pi a} \tag{2.34}$$

Elber first proposed an empirical rule to correlate the opening stress level with R for the the 2024-T3 material:

$$U = \frac{\Delta\sigma_{eff}}{\Delta\sigma} = \frac{\Delta K_{eff}}{\Delta K} = 0.5 + 0.4R \tag{2.35}$$

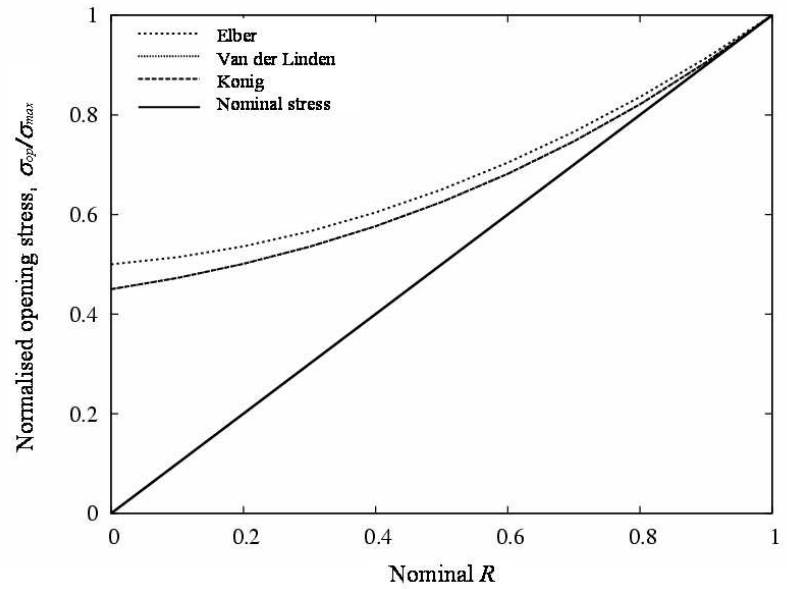

Figure 2.10: Normalised opening stress level for different empirical rule [42].

Figure 2.10 shows some other empirical rules based on the measurements. Even if there are some contradictions on the exact opening stress level it is possible to state that the closure effects is negligible for high nominal stress ratio while it is more important for low R level. In this debate an important novelty has been

introduced with this work: crack closure in presence of residual stresses.

In this case the stress intensity factor range will depend on the crack-opening load. The non-linearity of the crack closure is due to the fact that can vary depending on whether the crack is opened or not which essentially affects the K_{min} term while the K_{max} remains the same. For this reason another SIF parameter which defines the crack opening must be defined. Several authors [30] indicates this parameter as K_{op} which becomes the real lower boundary in the SIF range. Beghini and Bertini [31] considered even the case in which the crack is partially closed and obtain the K_{op} by using an experimental curve of strain versus load applied. Elber [38] used an experimental relation between the nominal SIF range and the effective SIF range as:

$$\Delta K_{eff} = U \Delta K_{app} \tag{2.36}$$

Where U is an empirical coefficient which depends on the material properties and one way to obtain it is by doing several tests. In this case the approach depends on the experimental results and experimental calibrations and it is not always systematic [43]. The definition of the crack-opening load depends on the measurement location with respect to the crack tip and the technique that is employed. Recent works have been done in order to develop a new method by assuming a two parameter driving force, which are the ΔK_{app} and the $K_{max,app}$ combined, proposed by Noroozi and al. [44, 45]. Even if the formulation at the earlier stages tended to be suitable for high stress ratio the latest researches show good results also for plasticity residual stresses [44]. The idea of this method is different from the closure concept because in this case the driving force is changing due to the residual stresses near the crack tip because of the cyclic plasticity. It is generally accepted that the crack growth is influenced by the stress and the strain field near the crack tip field by argument of the stress intensity factor. The unified two parameter model take into account not only the stress intensity factor but also the loading mean stresses by knowing their stress-strain history near the tip. In the other methods the loading stress had a great influence to the crack tip from the geometric factor β. In this case the residual SIF due to cyclic plasticity has been considered in order to calculate $K_{max,tot}$. A study on the effects of the nominal R ratio was found in the unified two parameter formulation [44] and it confirms that for high ratio the compressive stresses are

not sufficient to influence the range of the SIF while for lower positive nominal R ratio the effects of the compressive residuals stresses must be considered. The prediction of the fatigue crack growth is different from the classical methods and it is in the form:

$$\frac{da}{dN} = C(\Delta\kappa)^{\gamma} \tag{2.37}$$

Where C is fatigue crack growth constant and γ is the fatigue crack growth equation exponent which depend on the material. The new SIF range is:

$$\Delta\kappa = K_{max,tot}^{p} \Delta K_{tot}^{1-p} \tag{2.38}$$

Where p is the driving force coefficient. Therefore the effects of the compressive applied load have been taken into account by the stress intensity factor that considers the distribution near the crack tip. Other works have followed regarding the two parameter driving force [46–48].

2.2.5 Constant and variable amplitude load

The prediction laws presented above in the previous section concern constant amplitude load cases which are mainly used in experimental tests. To simulate the flight load conditions several spectrum cases are stored [37] and can be applied to perform a fatigue and damage tolerance analysis. The load sequence is then reordered to calculate the life of the component. To determine the fatigue life the cumulative damage law is often used [49], which is based on the $S-N$ curve and is expressed by:

$$\sum_{i=1}^{k} \frac{n_i}{N_i} = C \tag{2.39}$$

Where n_i is the number of cycles for a particular applied stress while N is the number of cycles to failure. This law is better known as Miner rule and for design purposes is taken $C = 1$ even if experimentally the value has found to be between 0.27 and 2.2. Another common method is the rainflow technique which can also

be used to reorder the load spectrum and to calculate the crack propagation by applying the new sequence in the crack propagation laws described in the previous. Throughout this thesis mainly constant amplitude load cases were assumed because of the necessity of comparing experimental tests and prediction results in order to validate the latter.

2.3 FE numerical analysis: LEFM & plasticity induced crack closure

This section focuses on the numerical analysis with the finite element method that are normally applicable in fracture mechanics. First it is presented an insight of the classical numerical approaches to calculate the stress intensity fracture in linear elastic fracture mechanics. Then the plasticity induced modelling issues are discussed in order to have a clear view on the criteria to obtain the opening stress i.e. the stress intensity factor range ΔK_{eff}. Plasticity models have been largely used in the past to explain non-linear behaviour of the metals. This section introduces the behaviour of the material close to the crack tip and the mechanism involved in the plasticity induced crack closure.

2.3.1 FE in linear elastic fracture mechanics

The use of the finite element method in fracture mechanics started in the 1970s and it has become more and more popular. The increased computational power of the computers makes the FEM the main tool to solve problems in many field of engineering. In fracture mechanics the main objective is to find the stress intensity factor near the crack tip. The SIF for certain geometries can be evaluated from standard solutions from reference books [50, 51] but they are not exhaustive for all geometries. There are two principal numerical methods to evaluate the SIF: the direct methods and the indirect methods. The direct methods are strongly mesh dependent and an accurate choice of the mesh and the elements must be done. The problem in modelling the area near the crack tip is caused by the singularity present in the SIF formulation. Near the crack the mesh must be very fine and it can be coarse far from it to save computational time by using a transitional mesh. The first elements developed were triangular [52], then

four nodes and eight nodes were developed later on but the main feature remain the shape functions that are changing with the number of nodes. In order to take into account the singularity, special singular elements were developed: the mid node has been moved closer to the crack tip, normally a quarter of the edge of the element [53]. The most promising approach is to use a quadratic 8 nodes isoparametric elements and manipulating the mid side node moving it near the crack tip. Those solutions are more effective on the direct methods like the displacement extrapolation and the stress substitution method. The first method uses the displacements equations 2.4: a value of K can be found for a certain coordinate value of r and θ hence a linear extrapolation can be done in order to evaluate K at the crack tip (r=0). The stress distribution method uses equations 2.3 to evaluate the SIF. Such approach is more mesh dependent and less accurate than the previous one, because a really accurate stress distribution near the crack tip is required. The indirect methods are less mesh dependent because they are energy methods and a relative coarse mesh can be used. Isoparametric elements with four nodes are good to predict the SIF in indirect technique. There are several approaches based on the energy principle:

- Strain energy release rate: calculate the strain energy release rate from which it is possible to calculate the SIF. Two FE analyses are required.
- Virtual crack extension technique: it is a variant of the previous method which uses just one FE analysis to evaluate the strain energy release rate and then the SIF.
- J-integral method: the computation of J-integral calculated and for LEFM are equal to G value and after that the evaluation of K.
- Virtual crack closure technique: it is based on the principle that the energy required to close the crack is equal to the energy to open it. SIF is calculated from the computation of the energy release rate.
- Modified virtual crack closure technique: it is a variant of the previous method but it requires only one FE analysis.

The modified virtual crack closure technique (MVCCT) is mainly used in this work due to the advantage of being less mesh dependent and because it is a robust and efficient method; the only limitation is that it can be used only in the

LEFM. Irwin stated that if a crack extends for a small amount Δa , the energy absorbed in the process is equal to the work required to close the crack to its previous length [54, 55]. In order to calculate the strain energy release rate G due to crack extension the following equation is used:

$$G = \frac{1}{2\Delta a} F_{yy,i}(v_j - v_j^*) \tag{2.40}$$

where $F_{yy,i}$, i is the nodal reaction force perpendicular to the crack growth path at the crack tip node i, and v_j and v_j^* the crack opening displacements. Δa is the crack extension length that equals to the crack tip mesh size, and t the thickness. Stress intensity factor can be found by:

$$\begin{aligned} K &= \sqrt{G\,E} && \text{plane stress } (\sigma_{zz}{=}0) \\ K &= \sqrt{\frac{G\,E}{1-\nu^2}} && \text{plane strain } (\varepsilon_{zz}{=}0) \end{aligned} \tag{2.41}$$

The relation between the SIF and the strain energy release rate holds only for the linear elastic conditions.

2.3.2 Finite element formulation for plasticity

A brief summary on how the plasticity can be implemented in the FE method is presented in this section. From the principle of virtual work the following equation can be written [56–58] by neglecting the inertia terms and assuming quasi-static conditions:

$$\delta\{W\} = \int_\Omega \delta\{D\}^T\{\sigma\}dV - \int_{\partial\Omega} \{t\} \cdot \delta\{v\}dA \tag{2.42}$$

With the discretization of the FE the 2.42 become:

$$\delta\{W\} = \int_\Omega \Big(\sum_{i=1}^{Nnode} \{B\}_i d\{v\}_i \Big)^T \{\sigma\}dV - \int_{\partial\Omega} \{t\} \cdot \Big(\sum_{i=1}^{Nnode} [N]_i \delta\{v_i\} \Big) dA \tag{2.43}$$

Where $\{B\}$ is the tensor of the derivative of the shape functions and $\{N\}$ is the tensor of the shape function. For an elasto-plastic material the constitutive equation is:

$$\{\sigma\} = \{C\}\{\epsilon\}^e = \{C\}(\epsilon - \epsilon^p) \tag{2.44}$$

so that:

$$\delta\{W\} = \delta\{v\}_i^T\Big(\sum_{i,j=1}^{Nnode}\int_\Omega \{B\}_i^T\{C\}\{B\}_j dV\Big)\{u\}_j - \delta\{v\}_i^T\sum_{i,j=1}^{Nnode}\int_\Omega \{B\}_i^T\{C\}\{\epsilon\}^p dV -$$

$$-\delta\{v\}_i^T\sum_{i=1}^{Nnode}\int_{\partial\Omega}[N]_i\{t\}dA \tag{2.45}$$

Hence one can write as well:

$$\{k\}\Delta\{u\} - \Delta\{f^p\} = \Delta\{f\} \tag{2.46}$$

or in a shorter form:

$$\{k\}\Delta\{u\} = \Delta\{f'\} \tag{2.47}$$

The main different from the FE formulation of an elastic material is that the constitutive equation are different because of the the term ϵ^p and for this reason the stiffness matrix will change and a new part of the stiffness matrix need to be added that can be written as:

$$\Delta\{f^p\} = \sum_{i,j=1}^{Nnode}\int_\Omega \{B\}_i^T\{C\}\{\epsilon\}^p dV \tag{2.48}$$

that will account of the plastic strain. The implicit integration scheme that are more used in the commercial finite element are the tangential stiffness method, the initial tangential stiffness method and the Newton-Raphson method [57].

They are often preferred to the explicit method which are more suitable for dynamic or response problem [56, 57]. The implicit or explicit FE methods are, respectively, those that use implicit or explicit integration scheme to integrate the momentum and the equilibrium equation. The implicit method minimise the residual force at each step in order to calculate the residual force which is within the specified tolerance. By calling the residual force Ψ the following equation explain the objectives of the method:

$$\Psi = \{k([u])\}[u] - [f] = 0 \tag{2.49}$$

By using the Taylor expansion it can be written:

$$\{\Psi(u)\} + \frac{\partial\{\Psi(u)\}}{\partial[u]}\Delta[u]O(\Delta[u]^2) = 0 \tag{2.50}$$

by defining the effective tangent stiffness matrix:

$$\{J\} = \partial\{\Psi\}/\partial[u] \tag{2.51}$$

hence neglecting the terms of high order the 2.50 may be written as:

$$\{\Psi\} + \{J\}\Delta[u] = 0 \tag{2.52}$$

so that:

$$\{J(u_n)\}\Delta u_n = -\{\Psi(u_n)\} \tag{2.53}$$

At each iteration the displacement is updated:

$$[u]_{n+1} = [u]_n + \Delta[u]_n \tag{2.54}$$

When one implements plasticity models the set of constitutive equation need to be changed as it has been shown previously.

2.3.3 Plasticity induced fatigue crack closure

Crack closure has been investigated by many researchers both by empirical approaches and finite element methods [23, 28, 29, 40–42, 59–78]. The empirical approaches are based on measuring the crack opening displacement or the changes of compliance. These methods need very accurate measurements and they are time consuming. The second approach is numerical and is based on the concept that closure is induced by plasticity. The closure induced by plasticity causes a plastic wake which is left behind the crack tip and it is caused by permanent plastic deformations which closes the crack earlier then the actual minimum load. This closure will produce compressive stresses that will influence the stress intensity factor hence the fatigue crack growth rate.

Table 2.1: Comparison of methods in the recent literature and current work.

	Present work	Literature
Specimen type.	Centre crack tension.	Centre crack tension [41, 68]. Compact tension [41, 70, 71, 74].
Element type.	Quadrilateral 2D elements. Plane stress.	2D elements. Triangular, quadrilateral. Plane stress, plane strain.
Mesh refinement.	Mesh size 25 and 12.5 μm	de Matos and Nowell [71] 10 μm . Herrera et al. [68] 12.5 μm. Zapatero [74] et al. 19 μm.
Contact modelling.	Contact elements	Spring elements. Nodal constrain. Truss elements. Contact elements.
Node release scheme.	At max load every load cycle.	At the max load every load cycle [41, 68, 69]. At the min load every load cycle [69]. At the min load every two cycles [72].
Crack opening criteria.	Stress method.	Stress method [69]. Displacement at the first node [68]. Displacement at the second node [41].
Material model effect.	Mixed kinematic isotropic.	Elastic perfect plastic [71, 72]. Mixed kinematic isotropic [68, 69].

Some authors employed the finite difference method [61] achieving good agreement with experimental measurements. Recently the boundary element method has been adopted also showing good results [61]. However this method is not fully developed also because the application are in general restricted. Finite ele-

ment method has been widely used because it is more robust, and it can be used in many other applications. However this approach depends on many modelling parameters [40]: element type, mesh size, determination of crack opening level, crack advance scheme, constitutive relationship. Table 2.1 shows different modelling aspects that need to be taken into account and it compares the published results with those used in this work. One of the first choice are the material type and dimension but also the material model is important. It can influence the choice of the crack advance scheme when more cycles have been applied before the crack propagates. The most common way of modelling crack propagation is extending crack length after one cycle at the minimum load [28, 40]. However some other authors advance the crack tip at the maximum or at the minimum load after two load cycles.

Other issues to take into account are the type of the specimens used M(T) or C(T), the nominal stress ratio and the maximum load applied which can give some differences on the final crack opening stress value σ_{op} . Several numerical simulation of plasticity-induced fatigue crack closure with finite element method have been performed in the past to calculate σ_{op} . In order to have an optimum construction of the numerical model different parameters must be take into account as shown in table 2.1 which presents a comparison of some methods and issues in the recent literature with the current work.

The width and the shape of the plastic wake are directly influenced by the load condition hence a bigger tensile applied stress will bring to a bigger plastic wake i.e. an higher permanent plastic wake deformations. However in the case of initial residual stresses another parameter to assess will be the redistribution of residual stresses behind the crack tip at different positions respect to the crack propagation line. The plasticity induced crack closure covers multiple studies and several applications can be addressed with it (see table 2.2).

One of the first application was to determine the opening stress level for a constant amplitude load. It was observed that σ_{op} changes for different R, yielding stress σ_{ys} and σ_{max} [28, 40]. Elber, Schijve and Newman found some correlations between the nominal stress ratio R and the opening stress level [38, 42, 79]. Those works also established that a major difference arise when conditions of plane stress or plane strain are assumed.

This debate is still on going and several works [28, 40, 60, 63, 80–82] attempt

to define both the value of σ_{op} via FE and the understanding of the closure mechanism and the effects of the thickness. Some researchers doubt on the existence of closure in plane strain conditions [40]. For thick plate, the plastic zone size is smaller because of the constraint of the thickness at the crack tip. For thin sheet, the closure is more evident and it is explained as plastic material flows from the through the thickness direction to the axial in-plane direction. The results is a bigger plastic zone size and during unloading the contraction creates the plastic wake. To verify the plane strain condition a 3D analysis comparison can be used to understand the effect of the thickness. Several attempts have been done in this directions among them more recently de Matos and Nowell [71] and Alizadeh [70] performs some 3D analyses. Alizadeh found that the 3D opening stress level is similar to the case of 2D plane stress. The opening value has been also compared with a strip yield model similar to that one used by Newman. The results for the three cases were close. The values of normalised opening stress σ_{op}/σ_{max} go from 0.4 for the 2D analysis to 0.5 for the strip yield model. The 3D analysis when the stress is calculated at the free surface is 0.45 which is between the two previous values. When the opening stress is calculated in the middle of the thickness, the 3D analysis deliver a value which is slightly bigger than 0.3 that is a typical value for plane strain conditions. Although there are some differences in values, the 3D FE analysis confirms the mechanism of plane stress and plane strain conditions.

de Matos and Nowell [71] also found that another crack closure parameter that will change the opening stress value is the crack advance scheme. There are different crack release scheme that can be adopted in modelling plasticity induced crack closure. Some author release the node at the maximum applied load some other at the minimum load applied. They also investigated on the influence of the number of cycles applied to the crack tip before the node release. They found that for 2D analysis in plane stress condition the influence is small while more difference occur in 2D plane strain and 3D plane strain condition. Although the "optimum" number of cycles has not been found it has been shown that after 8 cycles the opening stress level do not change much. They also recognise that the changing in opening stress level is due to the rachetting phenomenon near the crack tip. This is an important issue because further research should aim to discover a model where the crack could growth following physical criteria by considering strain hardening and softening. Few attempts have been made in this direction, one of this considers the accumulated plastic strain as a propagation

criteria. Nowell compared experimental measuring with the strip yield model for constant amplitude load and overload condition [82,83]. The technique employed was moire interferometry that despite other techniques like photoelasticity can be suitable for all materials. The most common technique used are the compliance measurements which is based on the load and displacement, the strain gauges combined with contour method or hole drilling method, the electric resistance and the laser speckle interferometry. All those experimental methods can be expensive and time consuming moreover the opening stress value is sensitive to the position where it is measured.

Table 2.2: Several applications of plasticity induced crack closure.

Application	Description	Author
Basic constant amplitude behaviour.	Crack opening level characterization for different load condition i.e. σ_{max} and R.	Newman [84], Solanki [59], Zapatero [74], Gonzalez [68], Daniewicz [85].
Plane stress v.s. plane strain	Debate on crack tip constrain, on the existence of crack closure in plain strain. Influence of the thickness on the opening stress.	McClung [63], de Matos and Nowell [71,82], Alizadeh [70] Fleck [60], Gonzalez [68], Codrington [86].
Load Hystory Effects	Single overload or underload, high-low block loading.	Zhang [87], McClung [28], Nowell [83], Zapatero [74], Pommier [88].
Time-dependent effects	Investigation on time dependent and temperature dependent effects on closure by using sophisticated constitutive relationship.	Chaboche [89], Sehitoglu and Sun [80], Pommier [90].
Microstructural effects	Study of microstructural effects by alternating the material properties: different material properties for the same specimen.	McClung [28], Pommier [90].
Short cracks	The closure behaviour of short crack has been studied, with the differences were due to the notch effects.	Palazotto [81], Daniewicz [78]
Weld residual stress effects	Study of the discontinuity closure induced by the initial residual stress field.	Choi and Song [91]
Path-Independent Integrals	Investigation related to the plastic fracture mechanics in order to establish the path-independence.	Wang et al [92].
Numerical-Experimental investigations	The aim was to address the opening stress and compare it with the experimental data.	McClung [93], de Matos [82], Newman [79], Nowell [83], Zapatero [74].
FE-Strip Yield model Studies	The FE are compared with the classical Newman equation based on the strip yield modelling.	Newman [79], Hou [94], Alizadeh [70].
Three dimensional analysis	2D and 3D FE analysis are compared.	de Matos and Nowell [71], Alizadeh [70].

Only few attempts assess the FE plasticity induced crack closure with an initial

residual stress field. Choi and Song [91] modelled crack growth behaviour in both tensile and compressive residual stress fields using the finite element method with elastic-plastic material behaviour. They found that cracks were partially closed due to the influence of welding residual stresses and calculated the effective stress intensity factor range ΔK_{eff} for this kind of crack profiles. They calculated the crack opening stress based on the crack mouth closure behaviour. Hence the crack was fully open when all the node were detached from the crack surface. They found the calculated σ_{op} is sensitive to the crack tip position. However they study the opening stress for a small portion of the crack propagation with a relative long crack length i.e. 22 to 24 mm. For this reason they used a relative coarse mesh for smallest element size: 0.25 mm. The increased computational power allows the FE to perform plasticity induced crack closure analysis with a longer propagation of crack length in order to have the value of the opening stress for the whole crack propagation and to have a better understanding on the mechanism of the phenomenon. By knowing the mechanism of closure it is possible to assess the main parameters involved in a plasticity induced closure model in a residual stress. Many authors focus on the crack opening displacement to show the profile of the plastic wake due to permanent plastic deformation. This is useful to compare the COD with elastic case but it is not a significant parameter in terms of opening stress level. However the plastic wake has a big indirect influence on the opening stress because it influences the compressive stresses due to the closed crack. Compressive stresses which are influenced by the crack opening displacement are also a criterion to establish the crack opening stress level that si the stress at which the crack is completely open. However few authors have investigated the plastic wake left behind the crack tip in terms of plastic strain and visualised it.

Due to the increased computational power of the computers nowadays, it was possible to conduct pioneering analysis of plasticity induced crack closure with residual stress field by using FE. The aim of those analyses is to fulfill the gap of knowledge that was not covered by the previous works, in terms of qualitative behaviour of the crack, quantitative value of opening stress in a long crack propagation under cyclic plastic load, and understanding of the closure mechanism that interact with the initial weld residual stress field. The results are presented and discussed in chapter 4.

2.3.4 Element type and mesh size

Elements are one of the first choice in setting up the model. The early researchers used constant strain triangular (CST) elements and quadrilater elements [95]. Quadrilater elements are mainly used and good agreement can be found by different works [28, 40, 68, 70, 74]. Some others used eight node elements to better capture the stress field around the crack tip. The main drawbacks is to have a lot of computational time that need to be invested. Dougherty at al. also found that the high gradient stresses induced in the 8 node elements creates an accurate opening displacement which may give inaccurate results of opening stress [96]. Other authors investigated the opening stress by using singular elements [87] to have a better description of the stress field. Both closure phenomena and overload were succesfully investigated. Some other claim the singular elements are inappropriate because the stress field near the crack tip is changed by the plasticity induced crack closure [28]. Nowadays the most used and reliable type of elements are the quadrilateral four node with the Kirchoff or Reisner Mindlin theory [40]. The real ongoing debate is on the tip constrain assumption hence on the use of plane stress and plane strain conditions which will bring the discussion on the use of 3D and 2D elements. It is accepted by the all community that the opening stress is much lower for the plane strain conditions, because the formation of the plastic zone is constrained by the thickness of the plate [32]. Some recent works have been done on the 3D v.s. 2D approach [40, 70, 71]. It has been shown that the 3D approach gives an opening stress level which depends on thickness of the specimen and some more investigations are needed because of the shape evolution: closure level gradient along the crack front will alter the shape of the crack front during the crack propagation i.e. the shape of the free surface edge will also change the opening stress [40]. Plane stress and plane strain conditions have always give different opening stress level lower for plane strain and higher for plan stress [28, 40]. In plane strain condition the material can not be transferred from the thickness direction to the axial direction because of the constrains of the out of plane deformations as can happen in plane stress conditions, for this reason some researchers debate on the existence of closure in plane strain conditions [40, 63, 70]. When choosing the elements also the mesh need to be evaluated. The mesh size must be very fine to capture the reverse plastic zone size produced when unloading. It has been found that for applied cyclic load the reversed plastic zone size is ten times smaller then the forward

plastic zone size formed during the loading [40]. Thus a common parameter which defines the mesh size is the ratio between the element size and the forward plastic zone size $\Delta a/r_p$. For plane stress condition for a nominal applied stress ratio R=0 this parameter is 0.10 [28, 40].

2.3.5 Material models

The constitutive equations of the material have another role on the assessment of the opening stress level. Several laws have been considered, with isotropic hardening kinematic hardening or a mixed between the two hardening rates. Small differences have been found in the type of hardening model but some variations can be found when the ratio H/E is changing [40].

Elastic-perfectly plastic model has been extensively used for modelling plasticity induced crack closure [28]. Both the kinematic hardening and isotropic hardening models have been used. The plastic model is within continuum plasticity, assuming the time independency, incompressibility, consistency and isotropic conditions. By considering the uniaxial field, the simplest way to represent the behaviour of stress strain curve is the perfect plastic model which does not deem the hardening. Once the applied stress overcome the yielding the stress remain at the same level without changing. If one wants to consider the linear hardening then the stress will linearly increase with a small slope respect to the elastic regime. This is called linear strain hardening as is shown in figure 2.11.

In multi-axial field one of the best known and used criterion is the von Mises criterion. The yield boundary is defined by a function f in the principal stress field that lead to the following definition:

$f < 0$ Elastic regime.

$f = 0$ Plastic regime.

The function f can not be greater than 0 because of the consistency condition which requires that the loading point must be on the f curve during the plastic deformation. The von Mises yield function is symmetric because of isotropic conditions, it is independent on the hydrostatic stress hence can be written in

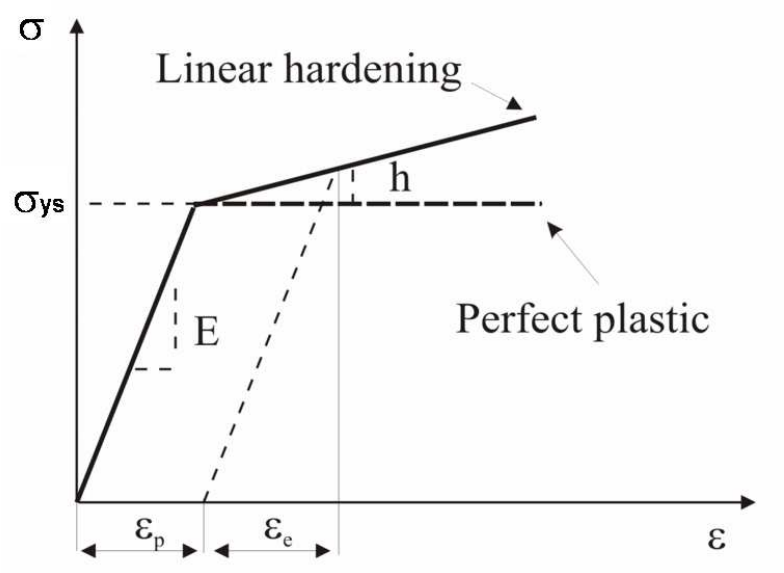

Figure 2.11: Typical stress strain curve.

terms of deviatoric tensor $[\sigma']$

$$f = \sigma_e - \sigma_y = (\frac{3}{2}[\sigma'] : [\sigma'])^{1/2} - \sigma_y \tag{2.55}$$

by developing the double product ":" in terms of stresses and principle stresses respectively:

$$\sigma_e = [\frac{3}{2}(\sigma_{11}^2 + \sigma_{22}^2 + \sigma_{33}^2 + 2\sigma_{12}^2 + 2\sigma_{23}^2 + 2\sigma_{31}^2)]^{1/2} \tag{2.56}$$

$$\sigma_e = \frac{1}{\sqrt{2}}[(\sigma_1 - \sigma_2)^2 + (\sigma_2 - \sigma_3)^2 + (\sigma_3 - \sigma_1)^2]^{1/2} \tag{2.57}$$

The last equation confirms that the hydrostatic pressure does not have any influence on the plastic deformation because also at very high but equal $\sigma_1, \sigma_2, \sigma_3$ the function f will be less than zero hence in elastic regime ($\sigma_e = 0$). The function in the triaxial space correspond geometrically to a cylinder with the axes along the lines of the principal stresses. By supposing plane stress conditions i.e. $\sigma_3 = 0$ f will be defined on the plane $\sigma_1 \div \sigma_2$ as the intersection curve of the cylinder with the plane itself that is an ellipse as shown in figure 2.12.

Once the criterion of plasticity is defined it is now important to know how the

deformed plastic deformation evolve in the plastic regime hence (because of consistency condition) how the yield von Mises function evolves during the deformation. The problem becomes to express the rate of the strain that can be seen as the gradient of the function in the direction perpendicular to the tangent of the ellipse:

$$d\epsilon^p = d\lambda \frac{\partial f}{\partial \{\sigma\}} \tag{2.58}$$

It can be demonstrated that an equivalent form to write this equation is:

$$d\epsilon^p = \frac{3}{2} dp \frac{[\sigma']}{\sigma_e} \tag{2.59}$$

where dp is the increment in effective plastic strain. The von Mises yield function can be written also as:

$$f([\sigma'], p) = \sigma_e - \sigma_y(p) = 0 \tag{2.60}$$

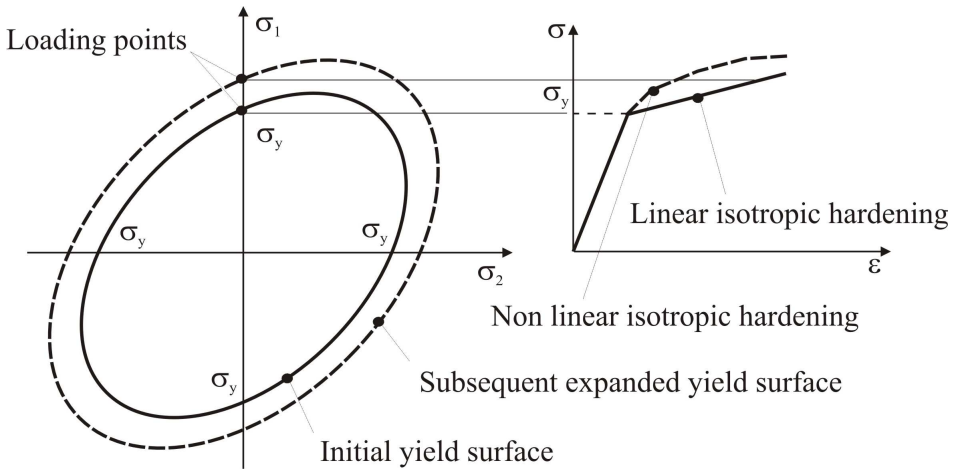

Figure 2.12: Isotropic hardening.

The increment of effective plastic strain dp needs to be evaluated in order to model the behaviour of the function in plastic regime in order to see how the metal hardens. When the functions f expands equally in all the directions then the hardening is referred to as isotropic (see figure 2.12). Because of the consistency condition the loading point needs to be on the curve of the function f hence when the loading overcomes the yielding stress the ellipse must expand

i.e. the $\sigma_y(p)$ must increase. Assuming σ_{y0} as the constant value of the yielding stress one can write:

$$\sigma_y(p) = \sigma_{y0} + r(p) \tag{2.61}$$

where $r(p)$ is the isotropic hardening function. One of the most common function which is implemented in ABAQUS [97] and used in this work is:

$$dr(p) = b(Q - r)dp \tag{2.62}$$

where Q and b are material parameter, b determines the rate at which the saturation point is reached. The saturation point is defined by Q because when dp is very high the exponential term tends to zero hence:

$$\sigma_y(p) = \sigma_{y0} + Q \tag{2.63}$$

Another type of hardening is the so called kinematic hardening. As shown in picture 2.13 this time the ellipse can be shifted of a particular value σ_α that is called back stress tensor. Because it moves in the principal stresses axes it is formally a stress. The yield von Mises function to deem the kinematic hardening will change as:

$$f = (\frac{3}{2}([\sigma'] - [\sigma_\alpha]') : ([\sigma'] - [\sigma_\alpha]'))^{1/2} - \sigma_y \tag{2.64}$$

It is important to notice that the kinematic hardening does not have any effects when only positive load have been applied but only in reverse loading its effect can be appreciated (see figure 2.13). The yielding stress occur earlier than when loading, this effect is referred to as Bauschinger effect. In this work the backstress evolution is taken into account by the Ziegler hardening law plus a non-linear kinematic component:

$$d\sigma_\alpha = C\frac{1}{\sigma_{y0}}(\sigma - \sigma_\alpha)d\epsilon_p - \gamma\sigma_\alpha d\epsilon_p \tag{2.65}$$

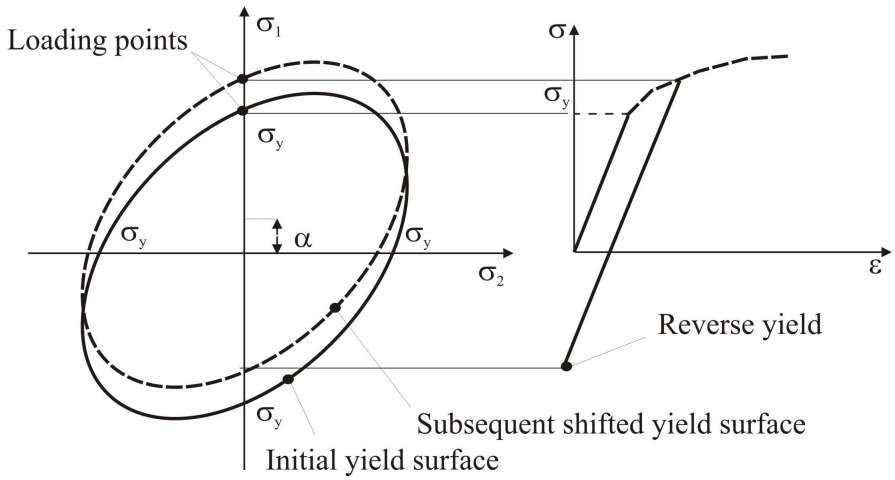

Figure 2.13: Kinematic hardening.

Which takes into account the kinematic hardening where $\gamma\sigma_\alpha d\epsilon_p$ represents the non linear component of the kinematic hardening. C/γ is the saturation component of plasticity hence the maximum stress that can be reached is:

$$\sigma = \sigma_{y0} + C/\gamma \tag{2.66}$$

The material models is an elastic-plastic with non linear kinematic isotropic hardening model was used. Such model, that considers both type of hardening, is a mixed isotropic and kinematic hardening model. The yield surface function is defined by:

$$F = f(\sigma - \sigma_\alpha) - \sigma^0 \tag{2.67}$$

Where σ^0 is the yield stress and $f(\sigma - \sigma_\alpha)$ is the equivalent Von Mises stress which in tensors can be expressed by:

$$f(\sigma - \sigma_\alpha) = \sqrt{\frac{3}{2}(S - \sigma_\alpha^{dev}) : (S - \sigma_\alpha^{dev})} \tag{2.68}$$

Where S is the deviatoric tensor and σ_α^{dev} is the deviatoric part of the backstress tensor which will take into account the effects of kinematic hardening. The

plastic flow will vary following the equation:

$$\dot{\epsilon}^{pl} = \dot{\bar{\epsilon}}\frac{\partial F}{\partial \sigma} \tag{2.69}$$

that relates the plastic flow with the equivalent plastic strain rate which can be obtained by the expression:

$$\sigma^0 \dot{\bar{\epsilon}} = \sigma : \dot{\epsilon}^{pl} \tag{2.70}$$

The backstress evolution is taken into account by the Ziegler hardening law [89]:

$$\dot{\sigma_\alpha} = C\frac{1}{\sigma^0}(\sigma - \sigma_\alpha)\dot{\epsilon}^{pl} - \gamma\sigma_\alpha\dot{\epsilon}^{pl} \tag{2.71}$$

Which takes into account the kinematic hardening where $\gamma\sigma_\alpha\dot{\epsilon}^{pl}$ represents the non linear component of the kinematic hardening. The isotropic hardening is considered with an exponential law:

$$\sigma^0 = \sigma_{ys} + Q_\infty(1 - e^{-b\bar{\epsilon}^{pl}}) \tag{2.72}$$

Where Q_∞ and b are material parameters. To define the material parameters a material curve $\sigma - \epsilon$ is needed [97].

2.3.6 Determination of crack opening level

The determination of crack opening and closing level has been debated by many researchers [59, 69, 72, 80]. The most popular approach is by considering the node displacement i.e. when the displacement at the node is different from zero the crack is considered open. However within this method a dispute is ongoing. Some researchers used the first node behind the crack tip while other the second node behind the crack tip. The first node behind the crack tip is physically the last detached node, however the reason of using the second node is to avoid the high stress gradient which can influence the first node in FE. Another drawback of this method is the long computational effort in order to find

the exact percentage of the applied load at which the crack can be considered fully open. The increment of the load must be very small hence a high computational cost. This approach is robust and simple but it can be not accurate enough, moreover does not take into account the whole residual stress field at the crack tip. Since initial weld residual stress occur another method based on the stresses ahead at the crack tip was preferred.

The contact stress method proposed by Sehitoglu and Sun [80] where the crack is considered open when all the compressive stresses behind the crack tip become zero. Wu and Ellyin [69], followed by other researchers, re-defined the opening stress as the remote applied stress necessary to change the stresses perpendicular to the crack tip from negative to positive, which is related to the meaning of the stress intensity factor. This is the concept of Elber himself that the crack is open when has the potential to growth. The approach has been widely accepted in the scientific community but it has been erroneous in evaluating the closing stress. Gonzalez-Herrera and Zapatero reported that the closing stress by using this method can be erroneous [68, 74]. de Matos and Nowell [72] showed that this is due to the fact that during the unloading stage the longitudinal stresses are always compressive. In the same work they have also compared different approaches of evaluating the opening stress level by considering the previous cited methods with weight function and analytical model proposed by Nowell himself. The methods give similar predictions in terms of opening stress level and in particular the weight function method seems to be the best balance between accuracy and computational costs. Moreover WF are simple and do not require to be very close to the crack tip or rely on the single node, is not particular mesh dependent and it can be used by knowing the distribution of the longitudinal stresses in unload condition. Another method is by determining the residual stress intensity factor by the compressive stresses along crack surface behind the crack tip by considering a linear distribution of stresses [59, 72]. Solanki et al. [59] proposed a evisitation of the contact stress method with a concept similar to the WF by using nodal force distribution on the crack surface behind the crack tip. The opening stress intensity factor can be calculated assuming a linear distribution of the forces. They achieved good results in plane strain condition for both M(T) and C(T) specimen.

2.4 Welds in integral metallic structures

Integral metallic structures (IMS) are a design solution which can enhance the aircraft structure by forestalling concentration of stresses close to the hole of conventional rivetted structures and by reducing the weight, because the rivets can be avoid by machining or welding. The manufacturing can be faster and simpler therefore a considerable amount of money can be saved. On the other hand the absence of crack stoppers makes the assembly a non fail safe structure without any secondary path hence several issues need to be address with the airworthiness and regulation authorities. In order to exploit the potentiality of IMS more research and understanding is needed.

One of the solutions proposed to introduce crack stopper or retarders is represented by bonded straps which can delay or stop the crack [98, 99]. The solution was found to be effective but the selection of the crack stopper is fundamental to give the advantage sought. Several works have been carried on in this direction [100] where the materials, dimensions and adhesive properties were assessed. In the last decades another valuable solution was investigated: IMS combined with welds [11]. The new material alloys developed [2], the weld type [22] and the control of residual stress [20] make this design solution extremely appealing and capable of challenging the other novel concept design.

According with the recent published literature, this section provides a description of the design impact of IMS with welding, by focussing on the residual stresses which are the main concern of this thesis.

2.4.1 Welding processes for aerospace aluminium alloys

Welding processes have been largely used in automotive and naval industry but for structure components in aircraft industry its use date back to some decades ago [14, 17, 101]. Several welding processes have been used and investigated with aluminium alloy such the Metal Inert Gas (MIG), Variable Polarity Plasma Arc (VPPA) and Friction Stir Welding (FSW), which is one of the most promising. The FSW process was invented by The Welding Institute (TWI) in 1991 [12] and it is autogenous which means that no additional material is required and it does not emit radiations, sparks, fumes, chips. The joint is affected to low

shrinkage. The process creates a solid state phase where the metal does not reach its melting temperature hence does not melt but the metal parts that have to be joined are plasticised [12]. At this point the separate components can be joined. The configuration of the process is shown in figure 2.14.

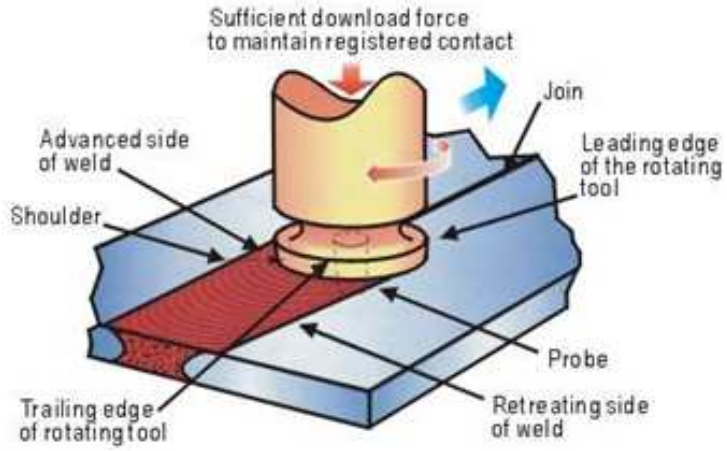

Figure 2.14: Friction stir welding process [12].

The tool which produces the heat is made by a rotating part that is the shoulder and a pin that moves the shoulder in the transverse direction. The pin must also give the right pressure at which the friction stir will occur. The material of the tool is nickel-cobalt base alloy which guarantees the performance at high temperatures. The temperature at which the sheets are heated is the most important parameter that is defined by the pressure of the pin, the transverse velocity and the rotational velocity of the tools. Typically it reaches 783 K [102]. Several studies have been conducted to optimise the process in terms of residual stresses, microstructure, Heat Affected Zone (HAZ) [103–106]. Therefore such parameters can not be suitable for every weld operation since they depend on the material of the plate and its geometry configuration. A good advantage in FSW is that it can be used for thicker plates and for a larger selection of alloys i.e.: it can be applied for dissimilar alloys. The process advantages result from the fact that the FSW process (as all friction welding of metals) takes place in the solid phase below the melting point of the materials to be joined. The ability to join materials, which are difficult to fusion weld, for example the 2000 and 7000 aluminium alloys series enlarge the perspective of design. Friction stir welding tools can use purpose-designed equipment or modified existing machine tool technology. The process is also suitable for automation and adaptable for

robot use. The advantages of this weld respect to the previous classical processes are resumed in table 2.3.

Table 2.3: Pros and cons of the friction stir welding process.

Advantages	Disadvantages
- Low distortion, even in long welds	- Work pieces must be rigidly clamped
- Low transverse residual stresses	- Backing bar required
- No fume and gas	- Keyhole at the end of each weld
- No porosity	- Cannot make joints which require metal deposition (e.g. fillet welds)
- No spatter	
- Tool re-usable for many welds	

The microstructure of the welding process can be seen in figure 2.15. There are several parts with different characteristic depending on the position and how the welding process affected such areas.

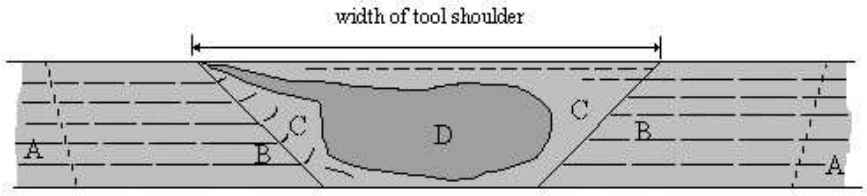

Figure 2.15: Microstructure classification of friction stir welds: A) Unaffected material (Parent plate). B) Heat affected zone (HAZ). C) Thermo-mechanically affected zone (TMAZ). D) Weld nugget [22].

A) Parent plate: This region has not been affected by the welding process thus the effects of the welding process are absent.

B) Heat affected zone (HAZ): In this region, the material has experienced a thermal cycle which has modified the microstructure and/or the mechanical properties. However, there is no plastic deformation occurring in this area.

C) Thermo-mechanically affected zone (TMAZ): In this region, the material has been plastically deformed by the friction stir welding tool, and the heat from the process will also have exerted some influence on the material. In the case of aluminium, it is possible to get significant plastic

strain without re-crystallisation in this region, and there is generally a distinct boundary between the re-crystallised zone and the deformed zones of the TMAZ. In the earlier classification, these two sub-zones were treated as distinct micro-structural regions.

D) Weld nugget: The re-crystallised area in the TMAZ in aluminium alloys has traditionally been called the nugget. It is suggested that this area is treated as a separate sub-zone of the TMAZ. It was proved that this area is characterized by circular concentric line.

2.4.2 Effects of weld on fatigue crack growth rate

The welding processes change the material properties of the structure and that affect the crack propagation. Microstructure and hardness changes are localized in the welded strip and they influence the crack propagation. A third effect that has a great influence on the FCGR is the residual stress field which has been found to be the main parameter affecting the life of the crack [22, 27, 107, 108]. For this reason this work will focus on residual stress and on their influence on FCGR.

2.4.3 Residual stresses in welded joints

The residual stresses are self-balanced stresses that exist in a structure where no external load is applied and they can be caused by surface treatments [109], manufacturing or welding processes [24, 26]. They are along the three directions and they are usually called longitudinal, transverse and through the thickness. The longitudinal stresses correspond to the stresses along the longitudinal axis which are parallel to the welding line, transverse stresses are perpendicular to the joint line and the stresses through the thickness are orthogonal to the plane of the plate. Because the residual stresses must be balanced there is a tensile residual stress field near the weld line and a compressive residual stress field away from the weld zone. It has been found that the longitudinal residual stresses are more relevant because the magnitude of the tensile stress is much higher [24, 26]. The highest value has normally been found in the HAZ where there is the highest difference of the temperature during the process [24, 25, 107]. For some welding process like the VPPA the magnitude can reach a peak which is around 150-180

MPa of the tensile stress, metal inert gas (MIG) has the higher stress tensile peak which is 300 MPa [24]. Friction stir welding (FSW) has a peak that is depending on the welding parameters i.e. dimension of the pin and rotational and transverse speed. Therefore the peak can vary from 140-150 MPa [24,110], to 300 MPa [111], some other find higher values which are near 200 MPa [22]. The values of transversal residual stresses are circa 20-30 MPa for different welding processes and the stresses are in the same order of magnitude or less. Considering that the measure error can be 10 MPa the transverse are usually negligible. Typically the tensile residual stress peak is between 40% and 70% of the σ_{ys}. The negative stress values is normally around -60 MPa [24, 26] but in same cases can go below to -150 MPa [27]. The initial distribution is tensile near the weld zone and it becomes compressive away from it. However along the weld line the trend curve remain the same hence the stresses remain constantly tensile moving along the weld line or constantly compressive in the zone far from the joint line. Just near the edge the stresses will change because of the free edges.

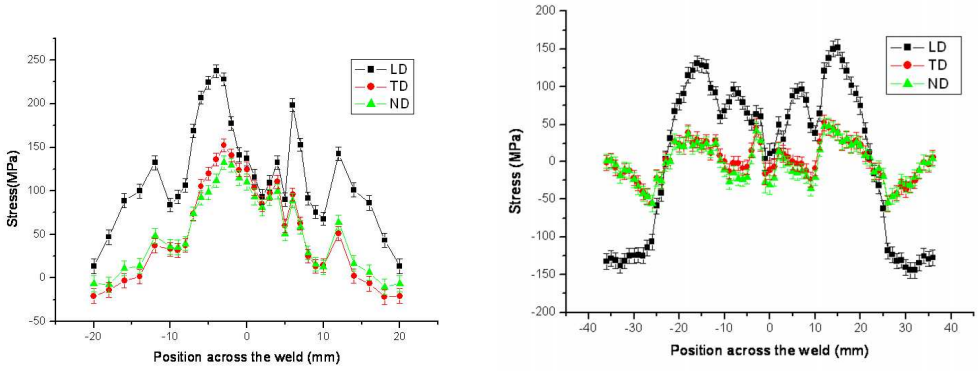

(a) Metal inert gas (MIG) welding process (Al 2024) [112].

(b) Variable polarity plasma arc (VPPA) welding process (Al 2024) [27].

Figure 2.16: Residual stress distribution for different welding processes.

Some typical distributions of residual stresses are shown in figures 2.16 respectively for the metal inert gas and the variable polarity plasma arc welding process. The longitudinal RS are the most important but also the transverse and through the thickness can be relevant. Figure 2.17 shows the measured distribution of a biaxial RS field for the friction stir welding. The transverse weld residual stresses are in the order of 30 MPa but there is also a lot of noise in the measurements. Some other measurements showed that the transverse residual stresses are negligible because they have a low order of magnitude (see figures 2.18).

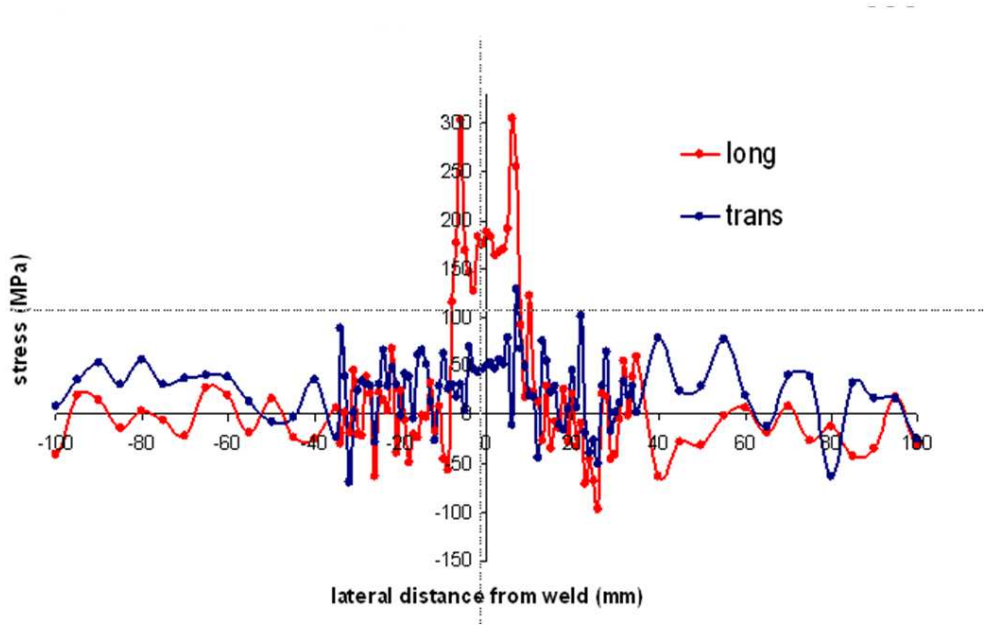

Figure 2.17: Biaxial RS distribution of FSW (Al-Li 2098) [111].

The residual stresses can be modified by applying pre tension load before the process as demonstrated in [113]. This technique is efficient to control the RS field and it can decrease the detrimental effects of tension RS (see figure 2.18).

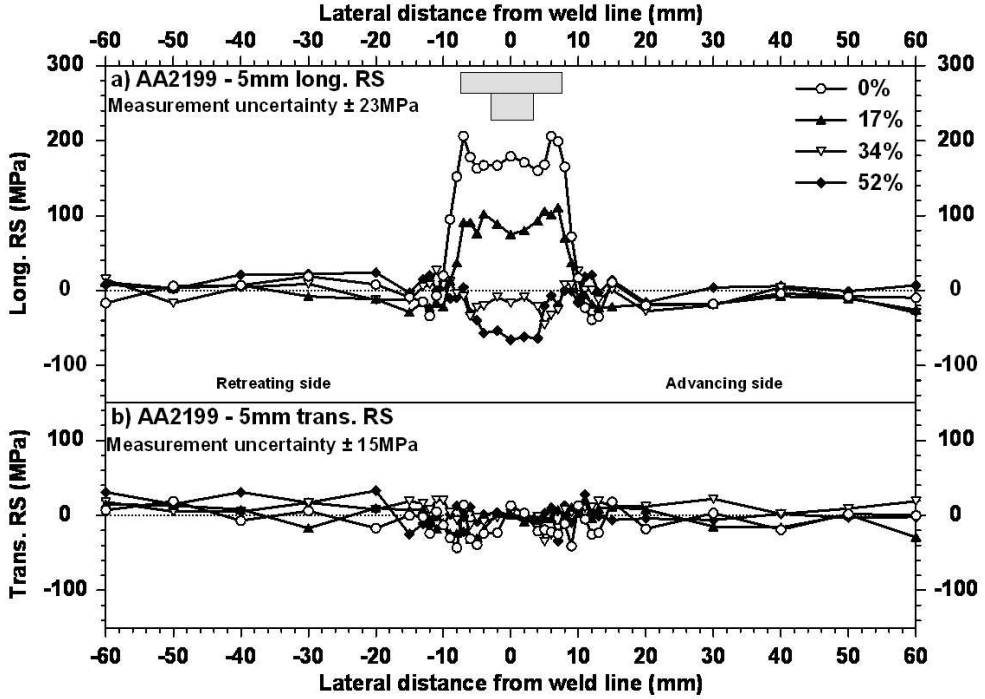

Figure 2.18: Distribution of residual stresses and global tensioning effects [113].

The initial distribution of stresses can influence the fatigue crack growth rate (FCGR). The VPPA for example has a distribution of the tensile stress which is wider compared to FSW where the tensile stress zone is narrow. The configuration of the crack and the specimen play also an important role. When the crack propagates in a compressive stress field the rate of the crack growth is lower than in the parent plate and vice versa the FCGR increases when the propagation occurs through a tensile stress field.

2.4.4 Residual stresses measurement techniques

Several methods for measuring welding residual stresses have been used in the past among them the principals can be separated in destructive and non-destructive techniques (see table 2.4).

Table 2.4: Residual stresses measurements techniques [114].

Destructive	Non-destructive
- Hole drilling	- X-ray Bragg diffraction
- Ring core	- X-ray diffraction by synchrotron
- Crack compliance	- Neutron diffraction
- Contour method	- Ultrasonic method
	- Magnetic method
	- Optical fluorescence

The destructive techniques are common because they can be done with a low economic costs but the specimens involved can not be used anymore. However they can guarantee a robust and reliable measurement and they provide a measurement through all the thickness of the test [114]. The hole drilling method is largely used when the measurement are limited to a small area of the surface of the specimen. The method consists in drilling a hole at a centre of a strain rosette [115,116]. The ring core method is a variation of the previous where also strain gauges are involved. Those two are more suitable for localised measurements than scan of the all specimen as in the case of welding residual stresses. Other methods are more suitable to cover a scan line of measurement such the compliance method which is also a destructive technique. It relies on several

consecutive cuts and measurements by using also analytical methods in order to achieve the residual stresses. The contour method is another technique that has been recently used showing good results compared with others and it provides a complete stress map of the specimen [117]. The only disadvantage is that is a destructive technique. Recently the electric strain gauges technique has been revised [115] and the method is accurate and it uses reasonable priced equipment. The most challenging task is to measure the residual stresses through the thickness of the plate and the strain gauges are not enough anymore.

Non-destructive technique can be more expensive and less accessible but they offer good measurements on structure that can be subsequently used for testing. Neutron diffraction, synchrotron X-ray scanning and neutron strain scanning are robust and good methods to measure even if a certain margin of error is possible which is around 10 MPa [27]. Some differences arise from one method to another, for example 9% between the contour method and the synchroton has been found but the last one is considered the most precise [110] and it has also a very large spatial resolution [118]. One of the main difference between the neutron diffraction and the X-ray diffraction is the limitation of the second method on the depth of measuring. X-ray can go at about 0.05 mm while neutron diffraction go up to 10 cm [115]. However the synchroton guarantee a higher energy which allow this technique to have a better penetration hence to have a deeper measurement [114,119]. Among non-destructive methods there is also the ultrasonic method which is based on the variation of the ultrasonic waves and the magnetic method which is applicable to ferromagnetic materials only [116]. Also those techniques rely on the distortion produced by the welding process from which is possible to achieve the strain distribution, by measuring the distortion of the crystalline structure of the materials [27].

2.4.5 Modelling & inputting residual stresses

In order to obtain the residual stress field either a measurements on the physical plate or a thermo-mechanical analysis can be done. Several works have been done in order to model the residual stresses [120–125]. To simulate the welding process a thermal analysis determines the temperature field history that will cause the residual stress state after the process. Thermal analysis of welding process depends on one main parameter that is the temperature field varying

with time [124, 125]. However during the welding process several other aspects affect the temperature. In FSW the transverse velocity of the shoulder and the rotational speed of the pin defines the temperature history. Some works modelled the entire welding process but they need to know thermal and mechanical properties, the friction behaviour between the two materials and the plastic flow rule which are not easy to determine with accuracy. A 3-D finite element analysis can be used in order to simulate the mechanical reaction of the tool by taking into account the heat transfer, the material flow and plastic flow [122]. The FE model gives good results but the problem is complex and it needs to be validated first with experimental measurements which was done with success. However the repeatability of the modelling features will be limited to an example with similar parameters. Colegrove et al [120] studied the process by focusing on the metal flow via computational fluid dynamic (CFD). The study gave a good interpretation of the flow field around the tool but it over predicts the temperature of the weld. The mismatching is explained by the different viscosity value during the process that can be different from the representative value and also the rotation speed has a great influence on the temperature value. The modelling approach is good and it can be used to predict the temperature but the aforementioned problems need to be addressed first. Another approach was to study the evaluation of the heat transfer process by using finite difference method which gives good agreements compared with the measured values of the temperature [121]. In general the CFD and the finite difference method are very good to understand and to model the temperature history and field while FE are more suitable to obtain the residual stress field [123]. Classical thermal analyses give good results in terms of stresses magnitude but they cannot predict for example the non-symmetry of the distributions of residual stress due to the different rotational speed of the pin. Rajesh et al. used in a thermal analysis a heat input based on the Williams's model that takes into account the non symmetry of the peak of residual stresses in friction stir weld [126]. The determination of residual stresses by FE can be done according to [124–126] but it depends on the temperature history that is not easy to obtain. The modelling of the heat transfer can be done by modelling the plastic flow via CFD or finite difference method. The modelling of the entire weld process gave good progress and a better understanding of the mechanism. The modelling is almost mature to have a good prediction method for residual stresses calculation but further investigations are needed to simulate the entire welding process.

Thermal analysis and mechanical analysis can be done separately [30, 126]. For this reason a residual stress field can be treated as given and then inputted in the model as other works already did [127, 128]. This is the approach of this research since the scope is to investigate the influence of residual stresses on the fatigue crack propagation [31, 129].

Without the presence of external loading the specimens is stress free and the condition of the principle of virtual work must be satisfied. The virtual principle work states that the external work is equal to the internal work that means:

$$\delta W_{ext}^{ab} = \delta W_{int}^{ab} \tag{2.73}$$

$$\int_V F^a \delta u^b = \int_V \sigma^a \delta \epsilon^b \tag{2.74}$$

Where W_{ext}^{ab} and W_{int}^{ab} are the external and the internal work respectively on the systems a and b. F^a is the force of the system a acting on the displacement u^b of the system b. The stress σ^a is the stress of the system a acting on the strain ϵ^b of the system b. The condition of the principle virtual work states that the integral of the internal work must be equal to the integral of the external work. When stresses or strain have been inputted in the model the FE code does not always guarantee such condition. Recently an attempt has been made in order to establish the influence of RS by using eigenstrain method [130,131]. This method permits to find a distribution of eigenstrain from a distribution of residual stresses or residual strain. It has a good agreement between the prediction made and the measured results and the advantage of not using an iterative procedure give benefits in terms of computational time. Moreover the method can evaluate the direct problem of finding the distribution of stresses from a distribution of strain and its inverse problem. However there are several disadvantages in using it. The direct problem can be solved if it is known a priori the weight function present in the model that is easy to achieve only for simple geometries. The inverse problem depends on the stresses distribution made during a thermo-elastic analysis which can have some disadvantage as discussed in the previously. As it has been discussed before the eigenstrain method is good but it depends on the distribution of stresses of a thermo-analysis and is not always easy to find the weight function that must be used. For the interpretation of the residual

stress field the residual displacement approach is suitable for the interpretation of the residual stress field and it gives a good agreement with the measured data but it is limited in the use of analytical weight function and it can not evaluate how the stresses are redistributed for different crack length. Another approach is by input measured residual stresses in the finite element model [27, 132]. This method became very common, it is robust and gives a good interpretation of the residual stress field. The condition of the principle virtual work is satisfied and the evaluation of the stresses for different crack length can be achieved [133]. Moreover it can be used in analytical and numerical analysis.

2.4.6 Residual stress intensity factor: K_{res}

To calculate stress intensity factor, FEA by MVCCT or J-integral can be used but several works proposed analytical methods by weight functions (WF) [134–145]. The numerical methods are often used in combination with a stress analysis in order to understand the redistribution of the initial residual stress and its evolution with the crack propagation. For this reason they offer a more comprehensive study case [27, 146]. Particularly this work will focus on the MVCCT used to calculate the K_{res} which is a robust and efficient method. More details can be found also in [133]. Even if is not comprehensive as the numerical methods, the analytical approach is good and reliable and it was often used in the past. The weight function is the mathematical Green function used in several scientific areas to solve differential equation subjected to boundary conditions. A classic weight function is used to perform an integral or a sum giving more "weight" to some variable better than others. In this case the stress is evaluated over a certain domain in order to give the stress intensity factor that characterises the stress field. It is been showed that those are appropriate tools to evaluate the stress intensity factor for residual stress [31, 135–139]. Glinka and Shen [139] proposed a general method to achieve analytical and numerical weight functions for cracks in mode I. This method depends on three unknown parameters that can be evaluated by knowing the reference stress intensity factor expression. The unique feature of the weight function is that once the function is determined for a specified body and geometry then the method can be applied for different load conditions as defined by Bueckner [134] and Rice [35]. However the method has not a universal application but it depends on the load reference and it can not be applied for high gradient reference stress field. In several works [137–139] it has

been shown that the crack opening displacement functions to derive the weight functions can have some limitations and it depends not only on the geometry but also on the reference stress intensity factor. The analytical weight function takes into account the redistribution of the stresses when the crack length is increasing and it has the following form:

$$K = \int_0^a h(x,a)\sigma_r(x)dx \tag{2.75}$$

Where $\sigma_r(x)$ is the initial distribution of the residual stresses and $h(x,a)$ is the weight function. The weight function $h(x,a)$ can be determined by the following relationship derived by Bueckner [134]:

$$h(x,a) = \frac{H}{K_{ref}}\frac{\partial u_r}{\partial a} \tag{2.76}$$

Where K_{ref} is the reference stress intensity factor and $u_r(x,a)$ is the crack opening displacement field and $H = E$ for plane stress and $H = E/(1-\nu)$. The universal features of weight function proposed by Glinka and Shen [139] reduce the derivations the WF to three parameters therefore the method proposed is a versatile and efficient.

2.4.7 RS influence on fatigue crack propagation

Whereas all of these affect the FCG rates, thermal residual stress has been identified as the most influential factor, and this was demonstrated in the friction stir welds [22, 138] and plasma welds [27, 146]. Efforts have been devoted to the investigation of residual stress effect on FCG rates (e.g. [27,127,129,141,147,148]). Two methods have been widely used to calculate FCG rates in residual stress fields. One employs the superposition rule to determine the effective stress ratio (R_{eff}) to account for the residual stress effect [149, 150]. The other is based on the crack closure concept originally proposed by Elber [38]. Residual stress will change the mean stress as well while the closure effects are changing the stress range. Tensile residual stress will increase the mean stress while the stress intensity factor range will be changed by the opening stresses. Figures 2.19 and 2.20 show respectively how tensile and compressive residual stresses can change the

stress range applied.

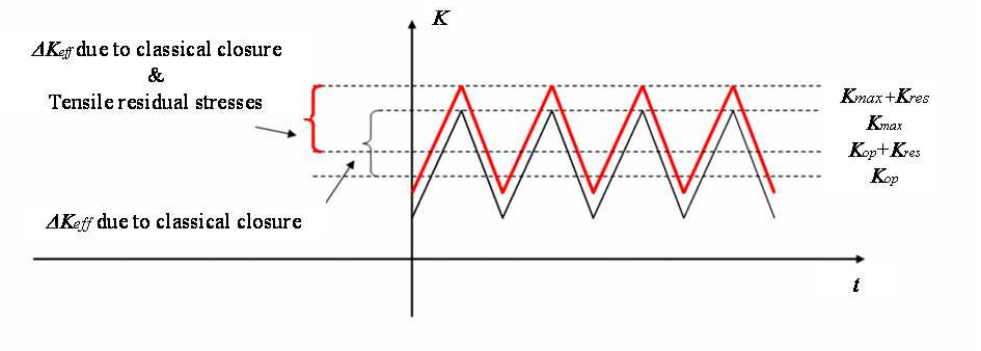

Figure 2.19: Tensile residual stress effect on cyclic loading.

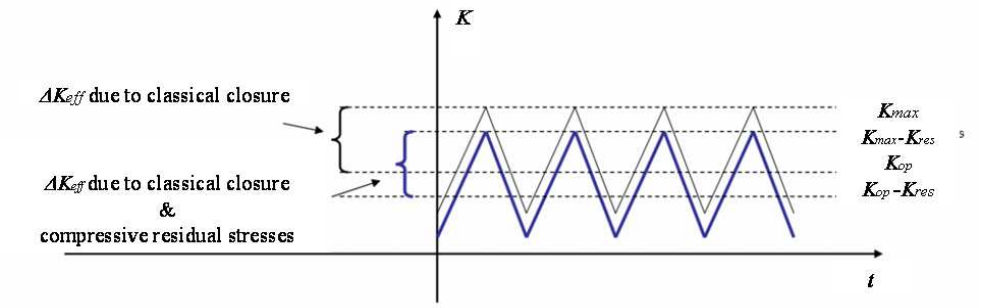

Figure 2.20: Compressive residual stress effect on cyclic loading.

In both cases the weld residual stresses change the mean stress which affects the stress intensity factor range ΔK_{eff} which becomes the final aim for the crack growth life prediction. It will be shown in the the following chapter how those factor will change the prediction approaches depending on the residual stress field encountered by the crack during its propagation. This chapter discusses how the opening stress σ_{op} is affected by the tensile or compressive residual stresses.

Crack propagation is influenced by the FSW due to the presence of the residual stresses, the change of the micro-hardness and microstructure and the heat affected zone properties. In the normal fusion weld as well as the friction stir weld, residual stresses are the most important parameter which influences the fatigue crack growth rate [22, 27, 30].

The configuration of the geometry of the crack and the specimens combined with the direction of the weld line is fundamental to assess the effects of the RS on the fatigue crack growth [22]. Beghini et al [127] used three different CT specimens and they utilised different prediction models to evaluate SIF. Tensile residual

stresses occur in the centre of the plate where the weld is located. In the zone near the edges the stresses are compressive and they bring benefits in term of crack life. The crack starting from the centre, perpendicular to the weld, is a critical scenario. Tensile stresses are produced after the cooling of the material which volume reduces when the metal returns to the room temperature. During the reduce of material volume the welded part is stretched by the non welded part producing tensile residual stresses.

Table 2.5: Methods for predicting fatigue crack growth rates in presence of welding residual stresses.

Author	Year	Method	Configuration
Glinka [151]	1979	Superposition	M(T) longitudinal weld
Parker [150]	1982	Superposition	M(T) longitudinal weld
Itoh [65]	1989	ΔK_{eff}	M(T) longitudinal
Beghini Bertini [31]	1990	Superposition and ΔK_{eff}	CT transversal weld
Beghini Bertini Vitale [141]	1994	Superposition and ΔK_{eff}	CT transversal weld
Galatolo [152]	1996	Empirical coefficients	CT longitudinal M(T) longitudinal weld
Pouget [129]	2007	Superposition and ΔK_{eff}	C(T) longitudinal weld
Liljedahl [146]	2009	Superposition	M(T) longitudinal
Servetti Zhang [133]	2009	Superposition	M(T) longitudinal weld
Ghidini Dalle Donne [148]	2009	Superposition and AFGROW	Transversal welding with hole

It was found that in welding structure the initial residual stress due to the weld process mainly affects the FCGR [22, 24, 27, 153]. Table 2.5 lists some of the works done in order to predict the FCGR in presence of welding residual stresses compared with experimental data. In order to find the FCGR by using empirical prediction law the stress intensity factor range and the effective ratio R_{eff} must be calculated. The residual stress field influences the FCGR mainly in terms of K_{res} which is the residual stress intensity factor. Glinka and Parker [150, 151]

first proposed the superposition of two stress intensity factor solutions:

$$\Delta K_{tot} = K_{tot,max} - K_{tot,min} = K_{app,max} + K_{res} - (K_{app,min} + K_{res}) \tag{2.77}$$

$$\Delta K_{tot} = K_{app,max} - K_{app,min} = \Delta K_{app} \tag{2.78}$$

The stress intensity factor range is not influenced by the residual stress field but the effective ratio is:

$$R_{eff} = \frac{K_{tot,min}}{K_{tot,max}} = \frac{K_{app,min} + K_{res}}{K_{app,max} + K_{res}} \tag{2.79}$$

After Glinka and Parker the superposition method has been used but in some cases also the effective stress intensity factor has been combined to it. Beghini and Bertini [31] made a distinction among three different status of the crack. Their crack growths from a compressive to a tensile RS field, hence it could have been: closed, partially closed or completely open. When compressive RS occur the crack can be partially closed. In this case contact non-linearity occur hence the superposition principle can not be applied but an effective stress intensity factor range must be used in order to deem the real low boundary of ΔK_{eff}. For crack open at minimum load the classic superposition method can be used. The case for a partially closed crack require the assessment of the real minimum SIF that is the K_{op}. The analysis of the SIF and the different status of the cracks has been clearly shown by using both analytical method with the weight functions and finite element to find the residual stress intensity factor. However is not clear how the life is predicted and how the ΔK_{eff} and the R_{eff} can be related with the FCGR.

The ΔK_{eff} has been later exploited to find FCGR. Itoh at al. [65] proposed a method base on measuring the opening stress hence ΔK_{eff}. They first performed a finite element analysis and calculated the effective stress intensity factor range ΔK_{eff} by using a stress extrapolation method. By using the superposition principle they could achieve R_{eff} as in the aforementioned method and relate it empirically with the U obtained experimentally. The final prediction has been

made by using the curve $da/dNv.s.\Delta K_{eff}$ and it matches with experimental data. This method can be interesting whether the relationship between U and R_{eff} can be extended for more cases. Moreover the necessity to have the material curve $da/dNv.s.\Delta K_{eff}$ require the measurement of the opening stress which can be time consuming and expensive for many cases.

Beghini et al. [141] approached again with the ΔK_{eff} method and the R_{eff} by also using an auxiliary function which depends on empirical parameters that can affect the repeatability of the predictions. Also Galatolo et al. [152] used empirical coefficients that give good results but do not have a large range of prediction cases. Recently some other works have been done with the superposition method that has been shown to be robust and reliable when the crack grows into a tensile residual stress field. Liljedahl et al. used the R_{eff} together with the NASGRO equation predicting the FCGR for constant amplitude stress intensity factor range which shows the bigger role of the R_{eff} in presence of welding tensile RS field. Servetti and Zhang [133] also used the superposition method by comparing different method i.e. Walker equation, NASGRO equation, Harter T-method by predicting the life for constant amplitude load and constant stress intensity factor range for cases where the crack grows mainly in the tensile RS field. Because in a compressive residual stress field non-linearity arise and the superposition holds only for linear cases. The residual stress intensity factor K_{res} was calculated with the modified virtual crack closure technique (MVCCT). Also interesting is a recent comparison of the two approaches done by Pouget [129] for a C(T) specimen in a case with longitudinal weld. The prediction has been made for constant stress intensity factor range applied constant and it shows that the superposition principle does not predict as well as the ΔK_{eff} approach. The crack grows from a compressive to a tensile residual stress field and for this case the second approach has been confirmed to be better. However in this case the opening load level from which has been calculated the K_{op} has been obtained from experimental tests with the opening method. This is still a lack in the prediction method because a measurement is needed. It is worth to notice that the cases where the crack propagates mainly within a tensile residual stress field the superposition method is more appropriate while the ΔK_{eff} method is more suitable for crack propagating through compressive residual stresses. As it will be also demonstrated in chapter 5.

2.5 Summary of the chapter

A review of the principles of fracture mechanics and fatigue prediction laws is herein provided together with some literature on the ΔK_{eff} based laws and the recent two parameters laws. It is also presented a description of the most common numerical FE methods in LEFM and a description of the FE implementation used in the plastic analysis of commercial code.

Particular attention is given to plasticity induced crack closure models and the broad literature which is provided in this chapter pointed out some gaps that can be further investigated: plasticity induced crack closure with weld initial residual stresses. A lot of effort of such analyses is spent in calculating the crack opening stress value which is shown to be dependent on different modelling parameters. Among them the element types, mesh refinement, node release scheme, contact and material model need to be assessed. A great difference arises whether plane stress and plane strain conditions are assumed and a comparison with 3D FE analysis confirms the different σ_{op} values of the two mentioned cases. Experimental measurements were also conducted in order to establish the exact value of the opening stress but they still have a margin of error that can be further improved. Other applications aim to study the load history effects, the time dependent effects, microstructural effects, short crack effects but only few attempt were done on weld residual stresses with plasticity induced crack closure made via FE. With an increased computational power it is possible to perform such analyses and to quantify the opening stress in a residual stress field by accounting for plasticity induced crack closure effects. The opening stress criterion has been found to be stress based or displacement based. When discussing the effects of plasticity with a residual stress field the displacement method is not appropriate because does not account for the stresses near the crack tip. For this reason the stress method is more appropriate to study the plasticity induced crack closure with residual stress field.

Residual stresses have a major influence on the fatigue crack growth rate. Numerical model to calculate residual stress are based on numerical methods such as FE, computational fluid dynamics (CFD), and finite difference method. Since the scope of this research concerns the effects of RS on the FCG initial residual stress are input in the FE model. The K_{res} is then calculated; numerical and analytical methods have been presented. Weight functions and J-integral method

were used in the past and the MVCCT is introduced in this work to calculate the K_{res}. The current FCG prediction laws, which account for RS field, are shown and presented. Based on this literature a methodology with the MVCCT is developed and presented in the next chapter.

Chapter 3

Methodology

This chapter explains the methodologies that were developed and the FE modelling aspects that were implemented. The methodology aims to predict the fatigue crack growth life since the focus of this research is to achieve the knowledge and the capability for life prediction in welded aeronautical structures. The first section 3.1 presents the FE models that calculate the fatigue crack growth driving forces for a crack propagating through a welding residual stress field. The second section 3.2 addresses FE modelling builded when performing a plasticity induced crack closure analysis. Those issues are very important to calculate the opening stress value hence the stress intensity factor range ΔK_{eff} by taking into account material non-linearity. The third section 3.3 shows the prediction laws that have been used throughout this work in order to understand how the driving forces will influence the final life of the crack.

3.1 LEFM analysis

3.1.1 Calculation of the stress intensity factors

To achieve a better knowledge on the influence of the residual stresses a preliminary study on a sample without residual stresses was performed first. The SIF was evaluated by the FEM and then compared with a theoretical solution that can be found in the literature for the case studied [32], [50]. The specimen assumed is an M(T) with a central crack under uniform tension load. The modified

virtual crack closure technique known as the MVCCT method [54] was used for calculating the strain energy release rate (SERR or G) due to crack extension:

$$G = \frac{1}{2t\Delta a} F_{yy,j}(v_j - v_j^*) \tag{3.1}$$

where $F_{yy,i}$ is the nodal reaction force perpendicular to the crack growth path at the crack tip node i, and v_j and v_j^* the crack opening displacements as shown in figure 3.1, a is the crack extension length which is the same as the crack tip element size, and t the thickness. Stress intensity factor (SIF or K) can be found by:

$$K = \sqrt{GE} \quad \text{(plane stress)} \tag{3.2}$$

$$K = \sqrt{\frac{GE}{1-\nu^2}} \quad \text{(plane strain)} \tag{3.3}$$

As an energy-based method the MVCCT is less dependent on the finite element mesh size. The relation between K and G only holds for the linear elastic material condition.

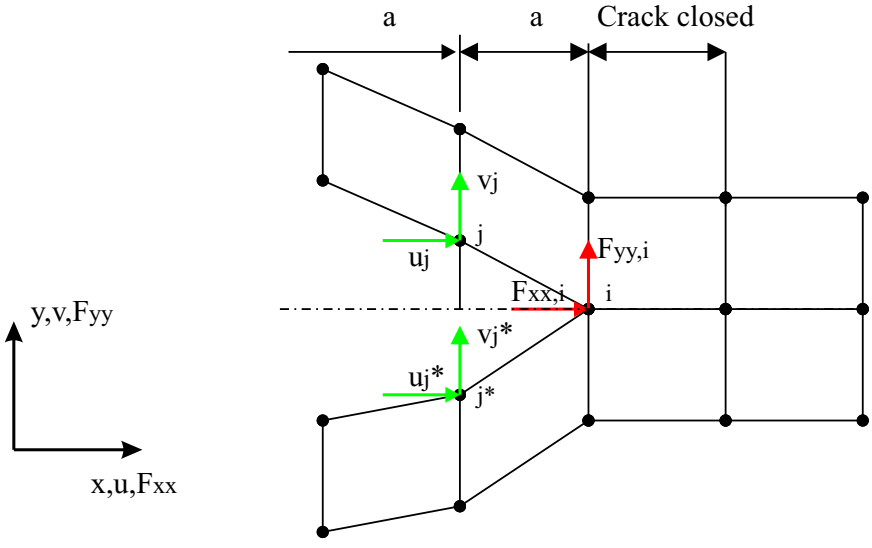

Figure 3.1: Modified virtual crack closure technique.

Herein is a mesh sensitivity analysis. An M(T) geometry is taken first by assuming half plate symmetry and then by assuming a quarter of plate symmetry

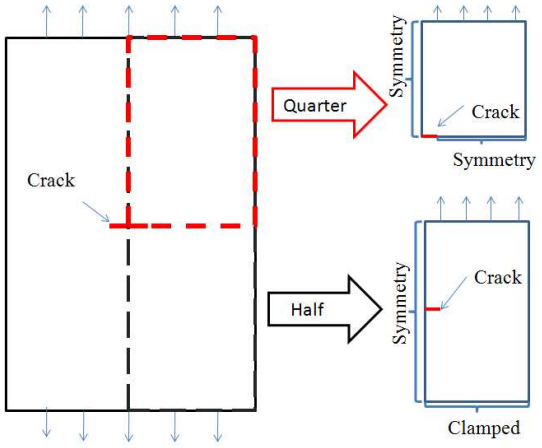

Figure 3.2: Modelling of the M(T) specimen.

(see figure 3.2). The MVCCT is validated with classical analytical solution by comparing the non-dimensional stress intensity factor β for different mesh size as depicted in figure 3.3. The percentage error is defined as:

$$\epsilon = \frac{\beta_{FE} - \beta_{theory}}{\beta_{theory}} \cdot 100 \tag{3.4}$$

where the β_{FE} is calculated as:

$$\beta_{FE} = \frac{K}{\sigma\sqrt{\pi a}} \tag{3.5}$$

with K is calculated as previously described with the MVCCT. The analytical β_{theory} solution for M(T) is given by:

$$\beta_{thoery} = \sqrt{1/cos(\frac{\pi a}{W})} \tag{3.6}$$

where W is the width of the specimen.

Figure 3.3 shows that elements smaller than 1 mm are in good agreement with the analytical solutions, the error is below 1%, for a mesh size of 2 mm there is a bigger difference in the solution with a percentage error of 4% (figure 3.4). Note that the error does not improve with increasing of the crack length because as it is expected from a direct method. The method used is based on energy and therefore less mesh dependent than the direct method where a longer crack

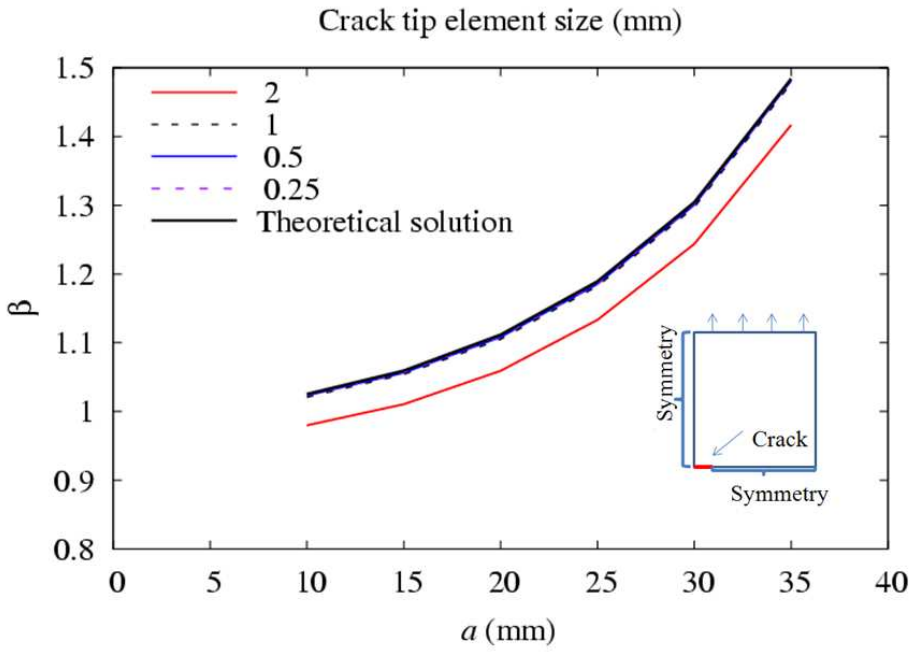

Figure 3.3: Mesh sensitivity study: β solution.

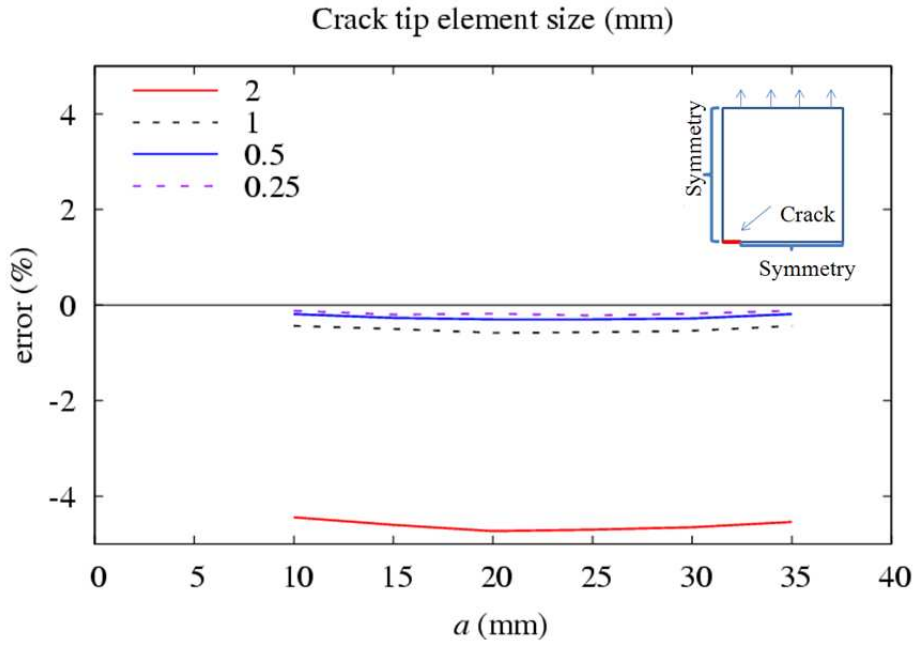

Figure 3.4: Mesh sensitivity study: errors.

would have improve the accuracy by assuming a constant mesh on the crack propagation line.

3.1.2 Residual stress intensity factor: K_{res}

After the welding process the plate is subjected to an initial residual stress field that will affect the crack tip SIF and therefore must be implemented and considered in the finite element model (FEM). In the measurements of residual stresses, using the diffraction methods, the deformation of the crystalline structure of the metal is measured first and then the stresses are back calculated assuming that the plate is elastic and isotropic [27,132]. Recently an attempt has been made in order to establish the influence of RS by using the eigenstrain method [130,131]. This method permits to find a distribution of eigenstrain from a set of distribution of residual stresses or residual strain which can be incomplete. The method is promising but it requires a precise knowledge of the elastic stiffness matrix coefficients of the welded plate. Moreover this is a pure analytical, by using a variational method, and it can not be implemented in commercial FE code for further analysis. For this reason it is a common practice to input stresses in the FEM [27].

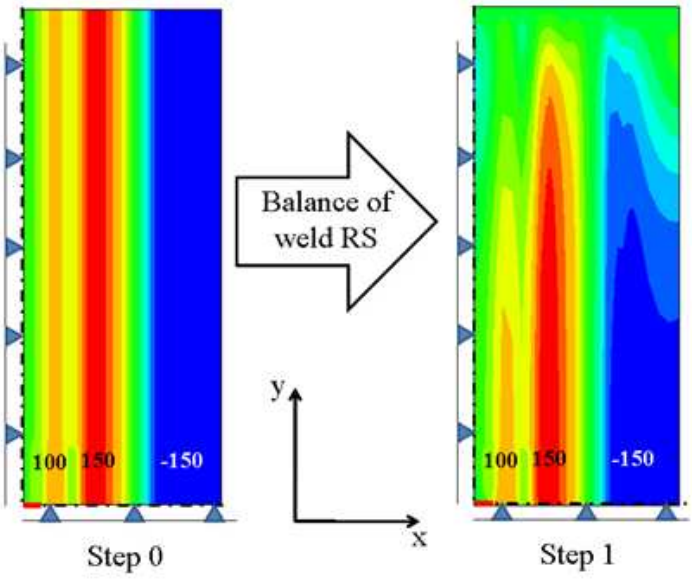

Figure 3.5: Balance of residual stresses.

Two approaches have been evaluated in this work: inputting of residual displacements and inputting of residual stresses. Initial residual displacement can be

input as boundary condition with a FORTRAN program which has been developed. For a known distribution of biaxial strain the corresponding displacement can be found and then input the biaxial residual displacement field in the model. Those become the initial conditions of the plate from which the distribution of stresses can be achieved. This method is good to make an interpretation of the initial stress state of the plate where no crack has been modelled. Nevertheless each node must be constrained and it can not predict the re-distribution of the stresses and their evolution during the crack growing. However analytical methods can be employed, for example the weight functions, where the initial distribution of the stress field is required to evaluate the residual SIF. To apply the residual stresses distribution an ABAQUS subroutine implemented called SIGINI has been used. In order to balance them to have the internal work equal to zero the command UNBALANCED STRESSES has been utilised. Without the presence of external loading the specimens is stress free and the equilibrium conditions must be satisfied. After input the stresses, one step is necessary to relax the RS in their equilibrium condition considering the stress free condition at the free edges. The prediction of the results is good in comparison with the measured data and the condition of principle virtual work is satisfied. The final results for no crack condition have good agreement with the measured values as shown in figure 3.6. Input residual stresses match the experimental data better than input residual displacements. The residual displacement approach is suitable to interpret and verify the residual stress field and it gives good agreement with the measured data but it is limited in the use of analytical weight function and it can not evaluate how the stresses are redistributed for different crack length. The stress inputting method is the best solution because the condition of the principle virtual work is satisfied and the evaluation of the stresses for different crack length can be achieved. Moreover it can be used in analytical and numerical analysis.

Figure 3.7 shows the redistribution of residual stresses for different crack lengths compared with measured data in [132]. Since the FE analysis was linear elastic, there is a peak in the calculated stress distribution near the crack tip position that is much higher than the measured value due to the stress singularity effect and such peak stress is dependent on the FE mesh size. In this very small crack tip zone comparison with the experimental data is poor. Also the experimental data can be inaccurate in this region because the deformation are measured first and after a linear elastic law the stresses have been calculated. However, away

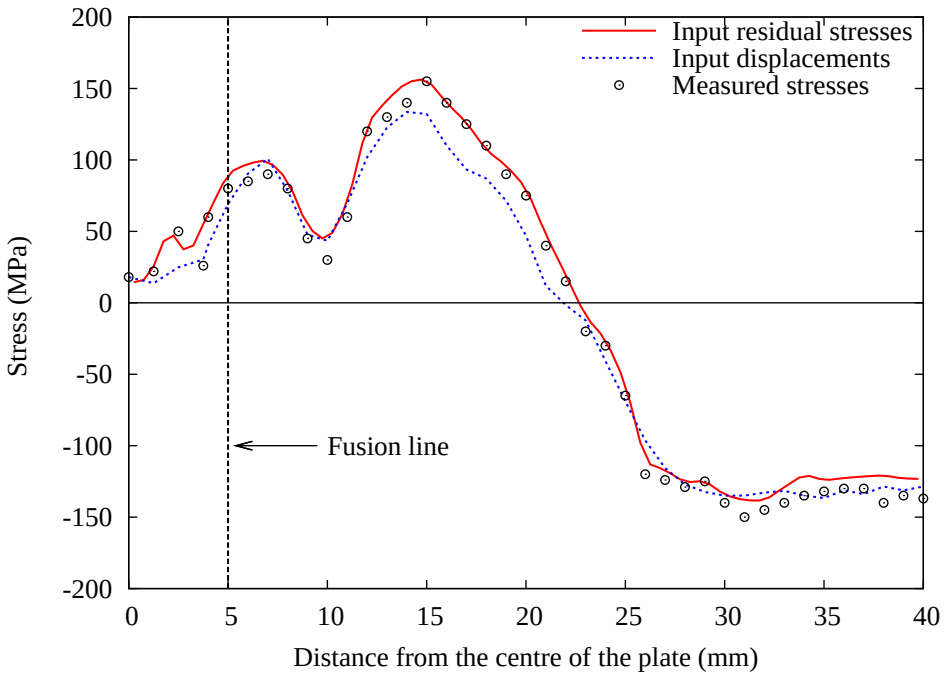

Figure 3.6: Distribution of residual stresses with no crack.

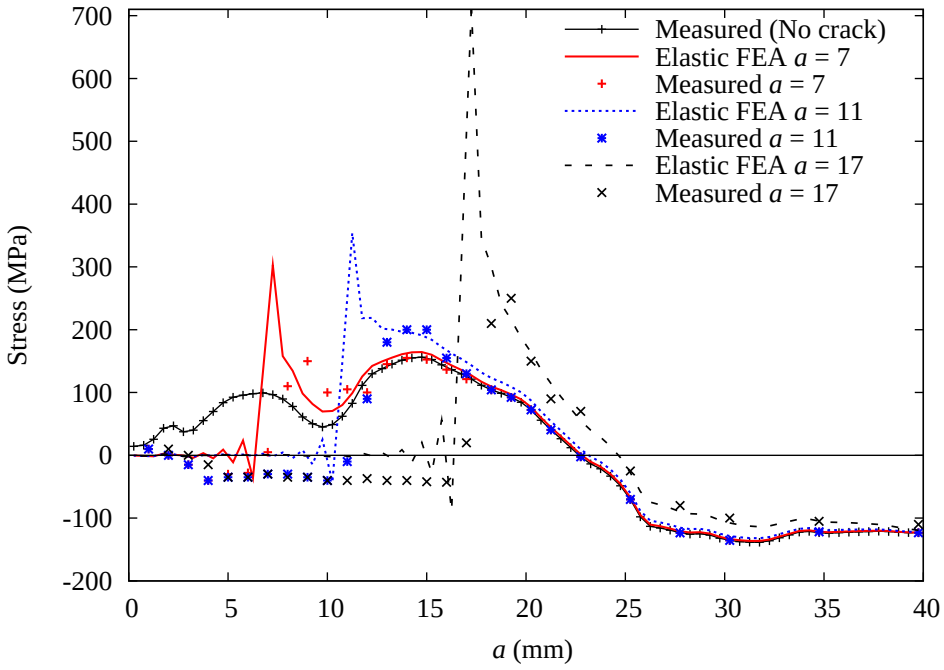

Figure 3.7: Redistribution of residual stresses with crack propagation.

from the crack tip region the calculated residual stress distribution due to crack extension agrees with the measured trend. The discrepancy in the crack-tip stress calculation will not affect the calculation of the SIF because it was calculated indirectly from the strain energy release rate.

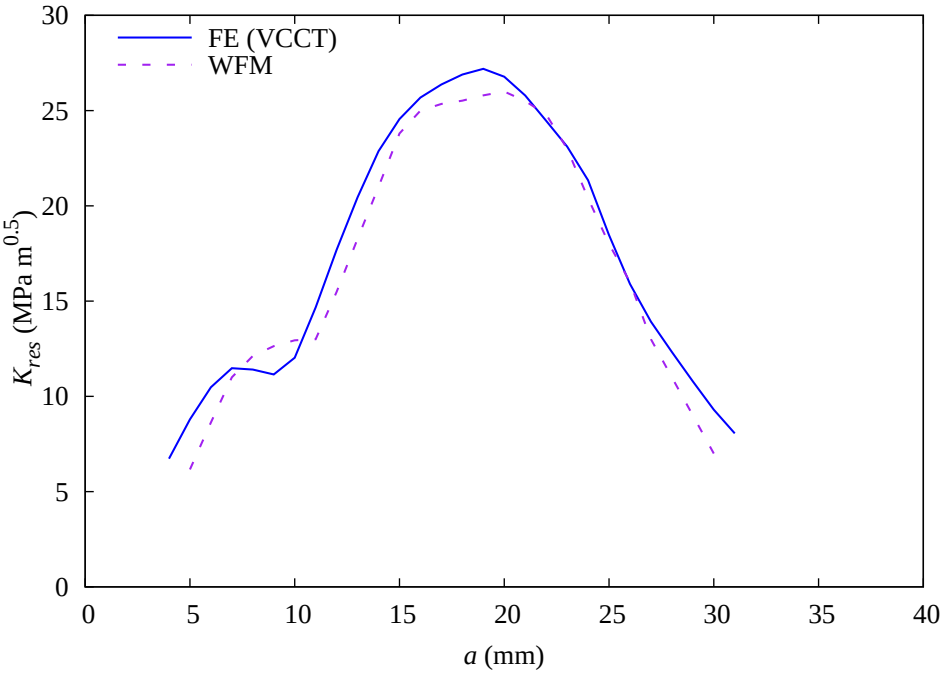

Figure 3.8: Validation of the K_{res} with weight function method (WFM) [143].

The K_{res} calculated with the MVCCT is compared with the weight function method [143] in order to validate the FE approach (see figure 3.8). The average error of the analytical solution is less than 5% which means that the MVCCT is a good and reliable approach compared with analytical methods such weight functions.

3.1.3 Total stress intensity factor

In LEFM conditions, the total SIF K_{tot} can be found by superposition of the two SIF solutions:

$$K_{tot} = K_{app} + K_{res} \tag{3.7}$$

where K_{app} and K_{res} are obtained separately by FEM for two different stress

field as shown in figure 3.9.

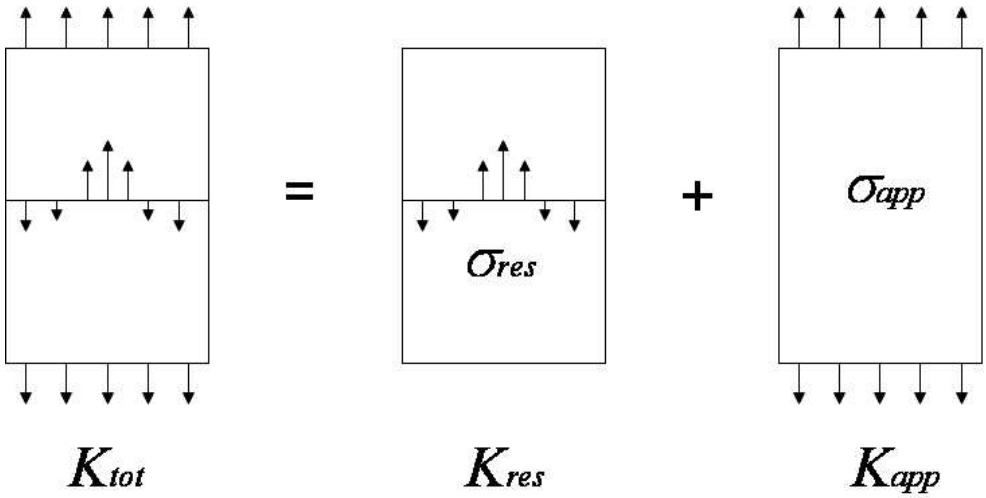

Figure 3.9: Superposition approach.

Superposition has been widely used in the framework of LEFM. The calculations of strain energy release rate and SIF described in eqs. 3.1 can be performed separately for both externally applied and internal residual stress fields. As illustrated in figure 3.10 and 3.11, by applying respective stress fields to the same FE model, G_{app} and G_{res} can be found with the following:

$$G_{app} = \frac{1}{2t\Delta a} F_{app} \Delta v_{app} \tag{3.8}$$

$$G_{res} = \frac{1}{2t\Delta a} F_{res} \Delta v_{res} \tag{3.9}$$

and then K_{app} and K_{res} can be calculated respectively:

$$K_{app} = \sqrt{G_{app} E} \tag{3.10}$$

$$K_{res} = \sqrt{G_{res} E} \tag{3.11}$$

It should be noted that the mechanical and thermal stress field depend one each other and a mutual work by the reaction forces due to the applied load F_{appl} over the displacements due to the residual stresses v_{res} should be considered and vice

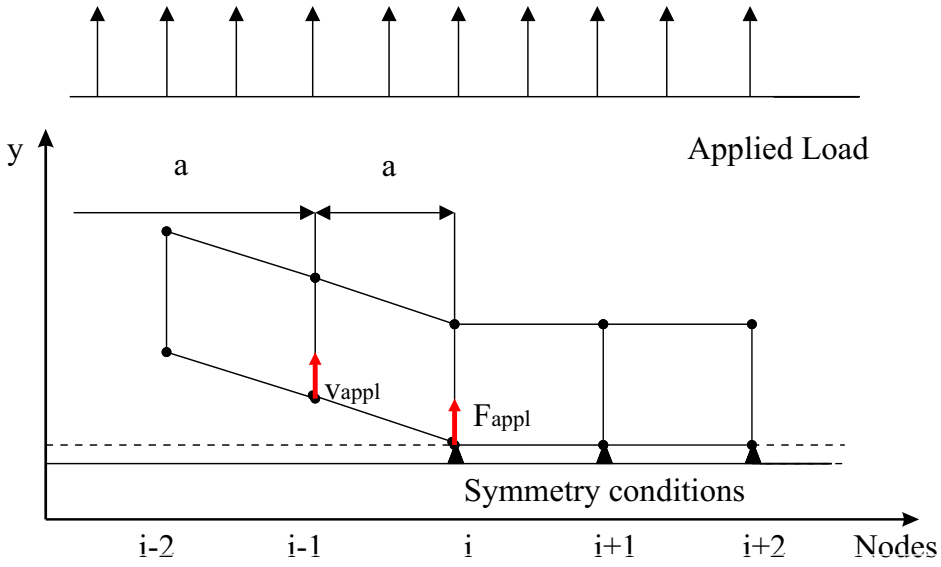

Figure 3.10: MVCCT with for an applied stress.

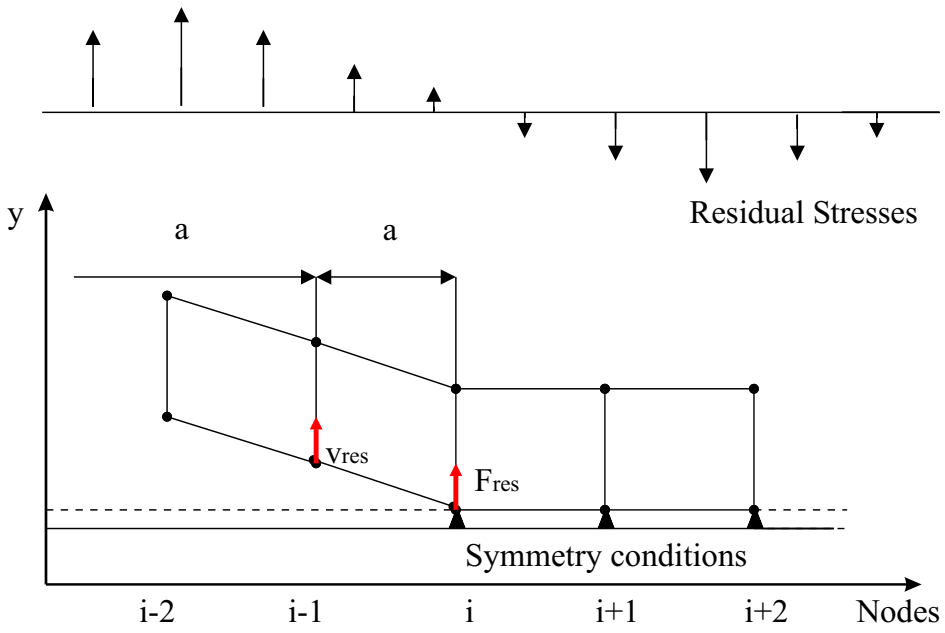

Figure 3.11: MVCCT for a residual stress field.

versa. From the VCCT formulation the value of the total energy release rate $G_{tot,mut}$, which considers also the mutual work can be obtained:

$$G_{tot,mut} = \frac{1}{2t\Delta a}(F_{app}v_{app} + F_{res}v_{res} + F_{res}v_{app} + F_{res}v_{app}) \tag{3.12}$$

which leads to:

$$G_{tot,mut} = G_{app} + G_{res} + G_{mut} \tag{3.13}$$

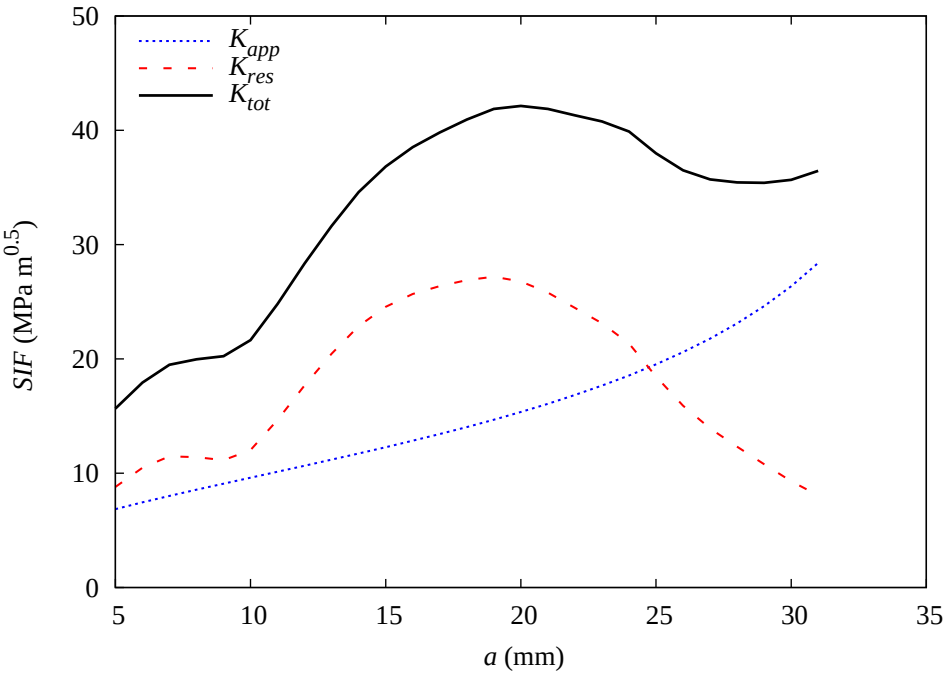

Figure 3.12: SIF superposition.

Where t is the thickness and Δa is the crack increment. Eq. 3.13 is verified below when both the applied load and the thermal residual stresses are applied in a FE analysis, the reaction force is the sum of the two effects:

$$F_{tot} = F_{app} + F_{res} \tag{3.14}$$

so for the displacements:

$$v_{tot} = v_{app} + v_{res} \tag{3.15}$$

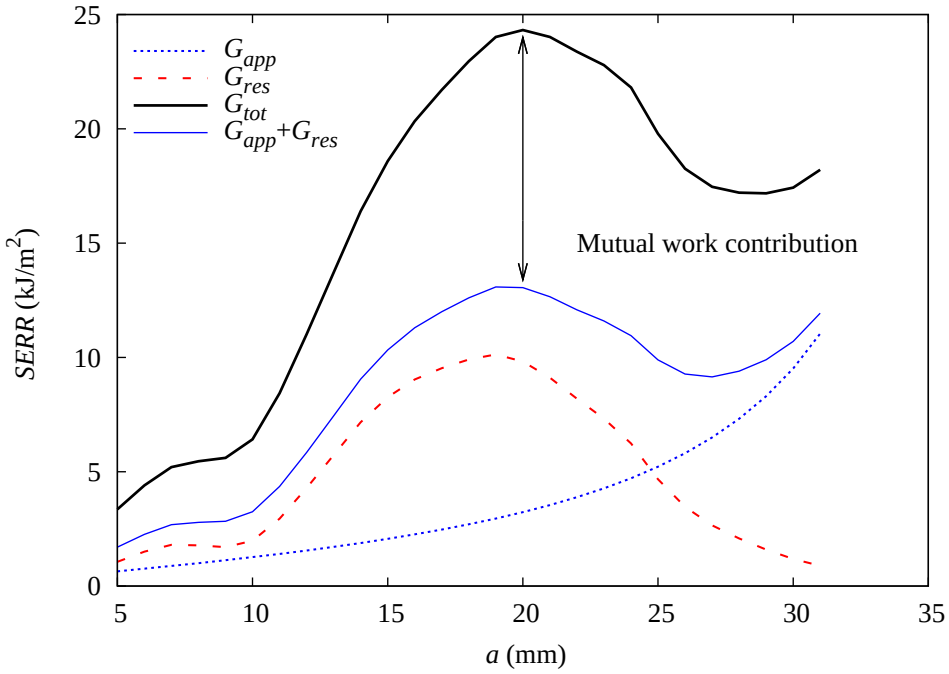

Figure 3.13: SERR and mutual work.

To demonstrate the validity of the equation 3.13 the starting point is the superposition of K:

$$K_{tot} = K_{res} + K_{app} \tag{3.16}$$

which can be also written as:

$$\sqrt{G_{tot}E} = \sqrt{G_{res}E} + \sqrt{G_{app}E} \tag{3.17}$$

where:

$$G_{tot} = \frac{1}{t\Delta a} F_{tot} v_{tot} \tag{3.18}$$

From equations 3.14 and 3.15:

$$G_{tot} = \frac{1}{t\Delta a}(F_{app} + F_{res})(v_{app} + v_{res}) \tag{3.19}$$

combining the 3.17 and 3.19:

$$\sqrt{\frac{1}{t\Delta a}(F_{app}+F_{res})(v_{res}+v_{app})} = \sqrt{\frac{1}{t\Delta a}F_{res}v_{res}} + \sqrt{\frac{1}{t\Delta a}F_{app}v_{app}} \tag{3.20}$$

Squaring the equation and simplifying:

$$F_{app}v_{app} + F_{res}v_{res} + F_{res}v_{app} + F_{app}v_{res} =$$

$$= F_{app}v_{app} + F_{res}v_{res} + 2\sqrt{F_{app}v_{res}F_{res}v_{app}} \tag{3.21}$$

$$F_{res}v_{app} + F_{app}v_{res} = 2\sqrt{F_{app}v_{res}F_{res}v_{app}} \tag{3.22}$$

Square again:

$$(F_{res}v_{app})^2 + (F_{app}v_{res})^2 + 2F_{app}v_{res}F_{res}v_{app} = 4F_{app}v_{res}F_{res}v_{app} \tag{3.23}$$

$$(F_{res}v_{app})^2 + (F_{app}v_{res})^2 - 2F_{app}v_{res}F_{res}v_{app} = 0 \tag{3.24}$$

That is:

$$(F_{res}v_{app} - F_{app}v_{res})^2 = 0 \tag{3.25}$$

This is the Betti Theorem [154] of the mutual work that can be applied also for the energy release rate in LEFM. It derives from the principle virtual work and it states that the force on a first system per the displacement of the second system is the same as the force of the second system on the displacement of the first system. In equations:

$$F_{res}v_{app} = F_{app}v_{res} \tag{3.26}$$

Hence the G can be written as:

$$G_{tot} = G_{tot,mut} = \frac{1}{2t\Delta a}(F_{app}v_{app} + F_{res}v_{res} + 2F_{appl}v_{res}) \tag{3.27}$$

Or indifferently:

$$G_{tot,mut} = \frac{1}{2t\Delta a}(F_{app}v_{app} + F_{res}v_{res} + 2F_{res}v_{app}) \tag{3.28}$$

Thus it can be stated that:

$$G_{tot,mut} = G_{res} + G_{app} + G_{mut} \neq G_{res} + G_{app} \tag{3.29}$$

where:

$$G_{mut} = F_{res}v_{app} + F_{appl}v_{res} \tag{3.30}$$

Figure 3.13 shows some numerical results that confirm the superposition of SIF while for the energy the mutual contribution must be taken into account.

3.2 Modelling plasticity induced crack closure

3.2.1 Mesh refinement

The mesh size to evaluate the crack closure effects depends on the crack tip plastic zone size. The crack tip elements must be small enough in order to take into account the effects of the plastic zone on the closure. When a tensile load is applied near the crack tip a forward plastic zone can be determined:

$$2r_p = \frac{1}{\alpha\pi}(\frac{K_{max}}{\sigma_{ys}})^2 \tag{3.31}$$

Where $\alpha = 1$ or 3 respectively for the plane stress and plane strain conditions. r_p is the plastic zone size. According to Solanki et al. 2004 [40], one needs at

least 3-4 elements in the reversed plastic zone which is $\Delta r_p = r_p/4$ for a static load, while is $\Delta r_p = r_p/10$ for the cyclic load.

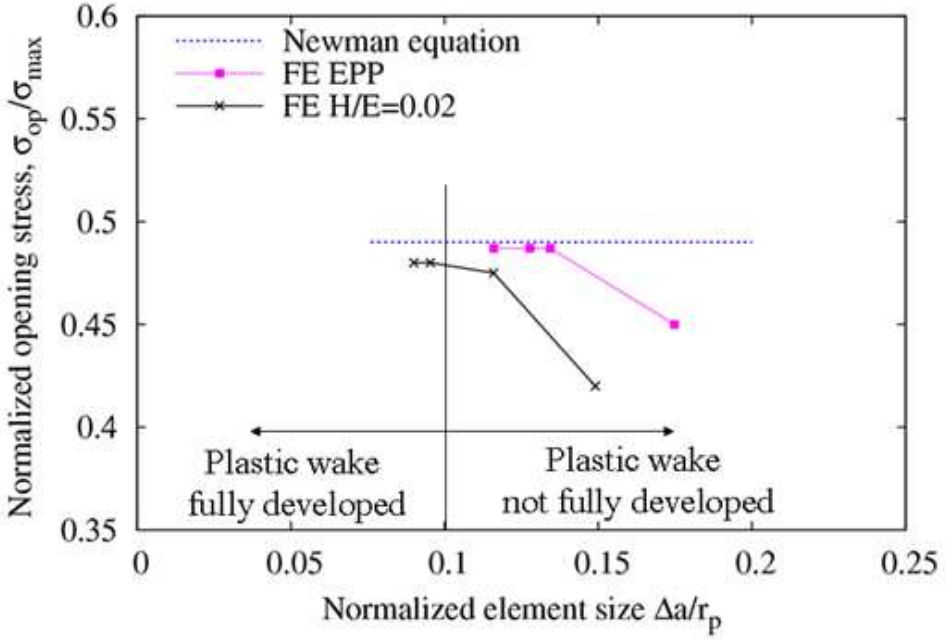

Figure 3.14: Mesh refinement study.

The finest mesh used is 0.025 mm. Supposing a crack of 3 mm and a maximum applied load of 100 MPa the plastic zone in plane stress condition $r_p \cong$0.24 mm. From figure 3.14 it is possible to see that for the mixed isotropic and kinematic hardening model used in this work the crack opening stress level is in agreement with the Newman solution. However for a ratio $\Delta a/r_p$ higher than 0.125 the opening stress level does not match, hence for a mesh size of 0.025 mm the forward plastic zone size r_p cannot be smaller than 0.2 mm.

Because the aim of this work is to find the influence of thermal residual stresses due to welding on the crack closure the mesh have to be fine all along the crack line as showed in figure 3.15, although other works analyze just a small portion of the crack closure. RS are changing along the direction of the crack propagation for this reason it is not enough to have a small portion of crack propagation to study.

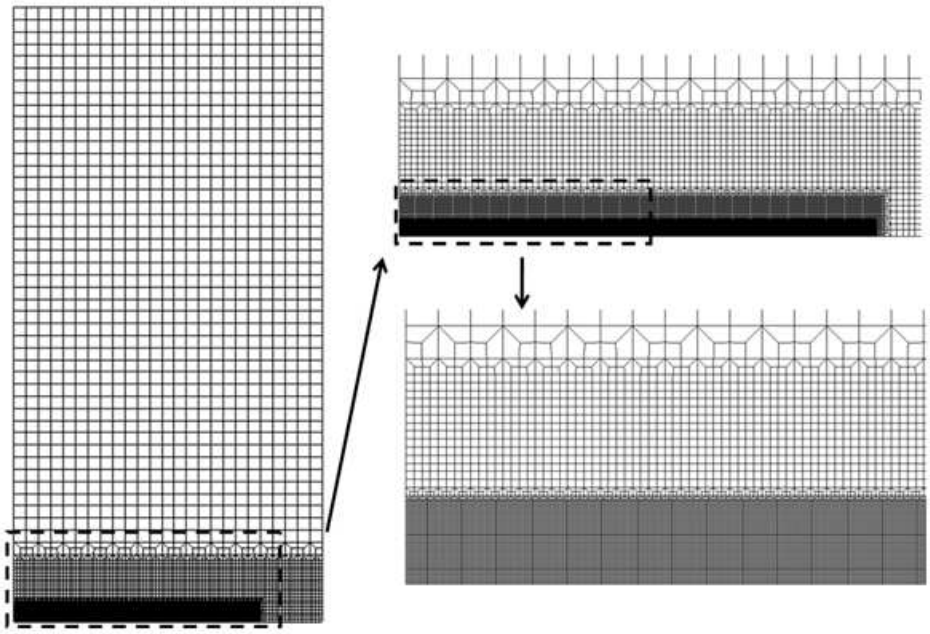

Figure 3.15: Mesh of the crack closure model.

3.2.2 Crack surface contact modelling

To prevent the crack surfaces from penetrating at the closure load, some mechanisms must be implemented into the FE model. According to Solanki et al. 2004 [40], there are four major modelling methods: a) changing the stiffness of spring elements; b) imposing crack surface nodal constraints; c) truss elements; d) contact elements.

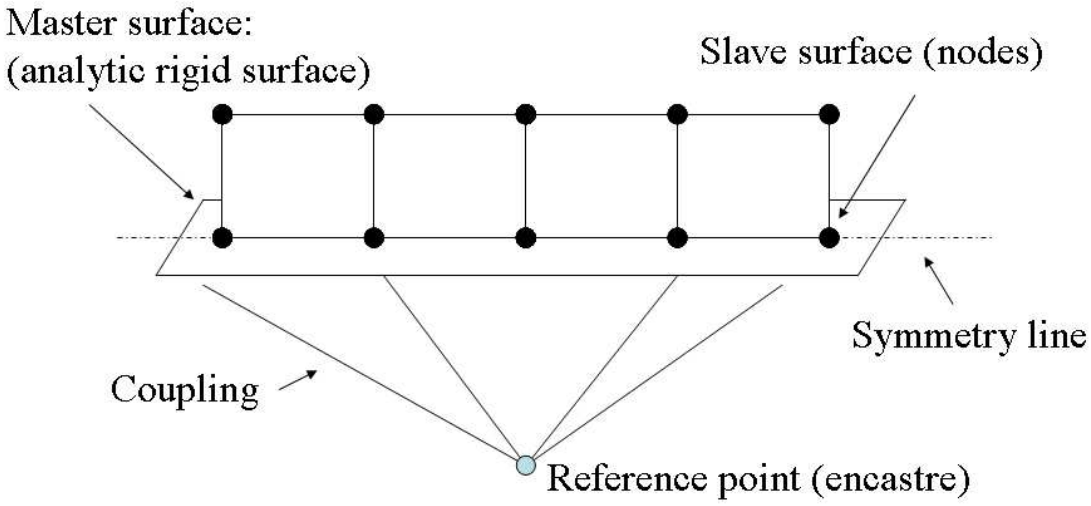

Figure 3.16: Crack surface contact modelling.

The contact model has been implemented by using ABAQUS which considers the interactions between a master surface and a slave surface (see figure 3.16). The master surface is the analytic surface made by rigid 2D shell elements while the row of the elements lying on the symmetry line is considered as the slave surface. The contact is defined as "hard contact": it allows the separation and minimizes the penetration of the slave surface into the master surface. Because of the use of rigid element the compressive stresses occur only for the elements of the slave surface which are deformed by previous tensile load and penetration into the master surface does not occur. The rigid analytic surface has been constrained by a reference point which has all the degrees of freedom blocked. The reference point is linked to the master surface by a coupling constrain, which means that all the degree of freedom of the reference point will be the same of the master surface which is encastred.

3.2.3 Crack advance scheme

Conventional node release techniques will disconnect the crack tip nodes and advance crack tip artificially, which will just model the crack closure phenomenon and calculate crack opening stress level due to cyclic plasticity effect.

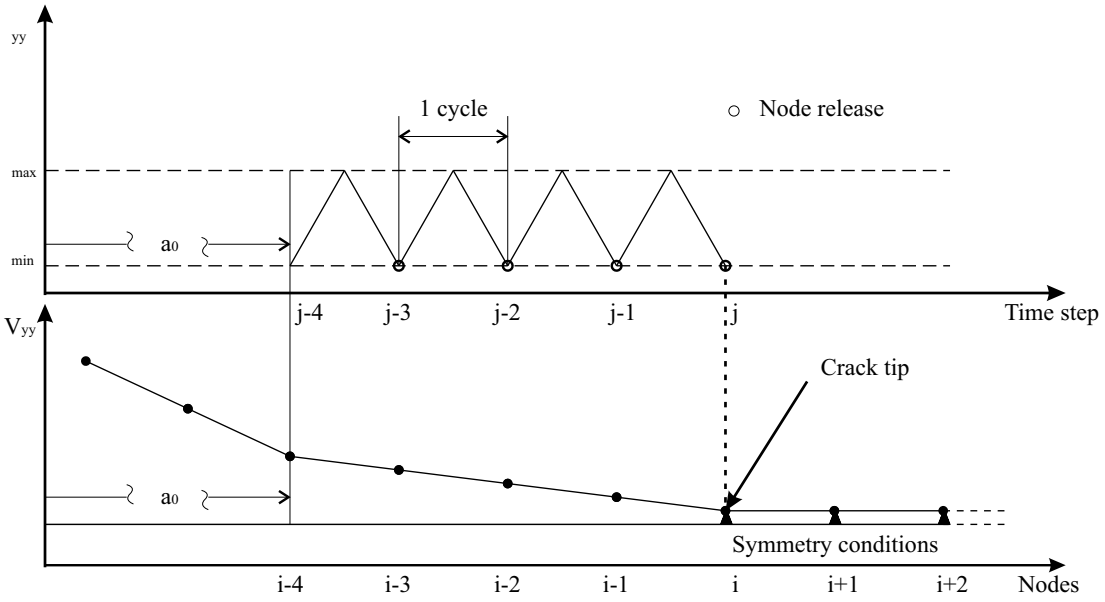

Figure 3.17: Node release scheme.

This is just like using the same method to produce the function due to crack

geometry change. However, this technique will not model the real physics of fatigue crack growth where a plastic wake occurs. The most popular advanced scheme is the release node method which is simple and reliable. In the literature it has never been found any influence of the crack propagation technique on the crack closure release but an on going debate is about the cyclic load. Some researcher use to release the node after one cycle at the minimum load, some others at the maximum load and some at different loading-unloading condition. Some studies found that the σ_{op} is independent on the method used, some others found that some differences occur but the reasons are still unclear according to Solanki et al. [40]. Some other works discuss on having different cycles before releasing the nodes but can be useless because the stress-strain curve stabilises after one cycle for elastic perfect plastic model. By releasing the node at the minimum load convergence more computational problems can be avoided. For this reasons the node will be released at the minimum load in order to assess the influence of a thermal residual stresses on the plastic wake and on the forward and plastic zone. The load has been incrementally applied at 10% of the total load at 10% of the step time which is not physically related to the physical time. Even if the first part of the loading is elastic is suggested to increase incrementally the load from the beginning in order to avoid convergence problems. It has been seen that the critically part is the final part of the loading condition and the initial part of the unloading condition thus a smaller unloading step is suggested in case convergence problems will arise. The STEP facilities in ABAQUS has been used and each step a loading and unloading condition has been done and then release the node in order to pass to the following step. The node release scheme is shown in figure 3.17.

3.2.4 Crack opening criterion

Conventional criteria for crack opening are:

- First node behind the crack tip becomes “open”
- Second node behind the crack tip
- Stress at crack tip node changes sign from compressive to tensile.

Solanki et al. 2004 [41] used the entire crack surface nodal force distribution under the minimum load - a method based on contact condition criterion. Many authors have used the displacement of the node near the crack tip to evaluate the opening stress. Some of the works have used the second node behind the crack tip and some others used the first node behind the crack tip. This debate is still on going but both node locations results strongly mesh dependent and the incremental load to find the opening displacement must be very accurate and it will influence the computation time. Moreover the displacement method will not account of the stress ahead the crack tip. Because in welded structure there is an initial residual stress field, it is important to monitor the stresses, particularly the area close to the crack tip. For this reason the stress method is used in evaluating the crack opening value. The current method is based on the assessment of the applied stress at which the compressive stresses ahead the crack tip pass from compressive to tensile.

3.2.5 Material model

Elastic-perfectly plastic model has been extensively used for modelling plasticity induced crack closure. In this work effects of material hardening have been considered by both kinematic hardening and isotropic hardening models. Although for each crack size it has been applied one cycle so the effect of kinematic and isotropic hardening is less relevant but an exhaustive plastic model has been implemented in order to see if this may influence the opening stress. It has been shown in the past that the hardening law does not have a great influence on the final value of the opening stress. The plastic model herein described is an elastic-plastic model with non linear kinematic-isotropic hardening model which is included in ABAQUS. Such model includes both type of hardening, it is a mixed isotropic and kinematic hardening model. The yield surface function, which governs the plastic behaviour, is defined by:

$$F = f(\sigma - \alpha) - \sigma_{ys} \tag{3.32}$$

Where σ_{ys} is the yielding stress, and α is the backstress which represents the shift of the yield surface function in terms of stress. α describes also the non

linear kinematic hardening component which equation is the following:

$$\dot{\alpha} = C\frac{1}{\sigma^0}(\sigma - \alpha)\dot{\epsilon}^{pl} - \gamma\alpha\dot{\epsilon}^{pl} \tag{3.33}$$

Table 3.1: Material properties for Al 2024 T-351 [97]

σ_{ys}	Q_∞ (MPa)	b	C (MPa)	γ
324	21	14	1531	14

Where C and γ are material parameters, $\dot{\epsilon}^{pl}$ is the rate of the equivalent plastic strain and σ^0 is the size of the yield surface and it determines its deformation hence its evolution is the isotropic hardening component which can be described as:

$$\sigma^0 = \sigma_{ys} + Q_\infty(1 - e^{-b\bar{\epsilon}^{pl}}) \tag{3.34}$$

where Q_∞ is the amount of cyclic hardening and b is the rate of cyclic hardening. They are both material constants shown in table 3.1. The material constants can be extrapolated from a test data set or stress-strain curve found in the literature [97].

3.3 Prediction methods for FCG life

3.3.1 LEFM superposition

Figure 3.18 shows the scheme adopted in order to calculate the FCG life within LEFM which involves stress analysis, fracture mechanics analysis and fatigue analysis which calculate the crack life. The most important parameter in this case is the K_{res} which is obtained from the fracture mechanics analysis. Then by knowing the material law for the material considered it is possible to calculate the FCGR and integrate it to find the crack growth life.

In order to find the FCGR by using empirical prediction law the stress intensity factor range and the effective ratio R_{eff} must be calculated. The residual stress field influences the FCGR mainly in terms of K_{res} which is the residual stress

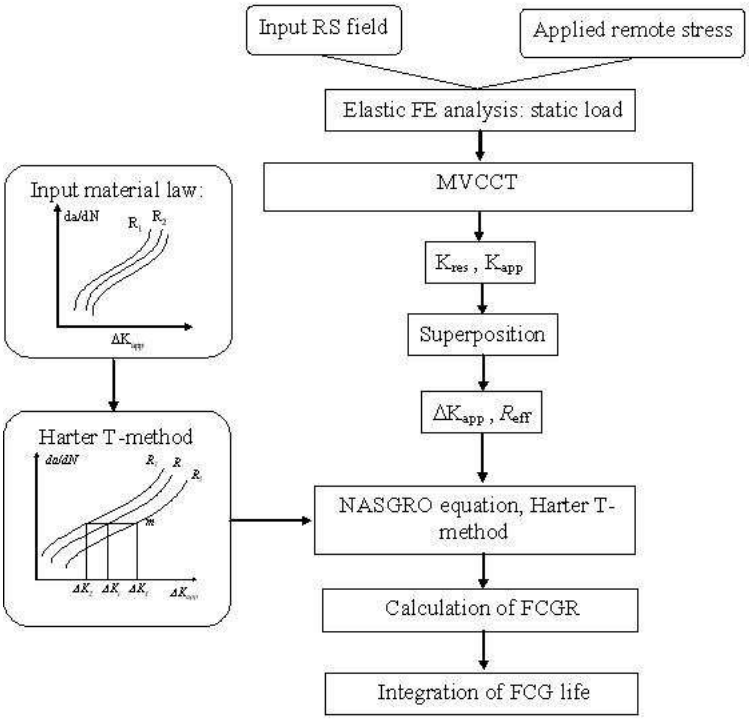

Figure 3.18: Flowchart of the LEFM method to calculate the FCG life.

intensity factor. Glinka and Parker [150, 151] first proposed the superposition of two stress intensity factor solutions:

$$\Delta K_{tot} = K_{tot,max} - K_{tot,min} = K_{app,max} + K_{res} - (K_{app,min} + K_{res}) \tag{3.35}$$

$$\Delta K_{tot} = K_{app,max} - K_{app,min} = \Delta K_{app} \tag{3.36}$$

The stress intensity factor range is not influenced by the residual stress field but the effective ratio is:

$$R_{eff} = \frac{K_{tot,min}}{K_{tot,max}} = \frac{K_{app,min} + K_{res}}{K_{app,max} + K_{res}} \tag{3.37}$$

In terms of fatigue crack growth rate this will influence the Walker and NASGRO equation that will be affected by R_{eff}. In particular the Walker equation will

be:

$$\frac{da}{dN} = C(\Delta K_{app}(1 - R_{eff})^{m-1})^n \tag{3.38}$$

Where C and n are the Paris law material constants and m controls the shift between two curves with two different stress ratio R. The NASGRO equation will change as well:

$$\frac{da}{dN} = C[(\frac{1-f}{1-R_{eff}})\Delta K_{app}]^n \frac{(1 - \frac{\Delta K_{th}}{\Delta K_{app}})^p}{(1 - \frac{K_{max}+K_{res}}{K_{crit}})^q} \tag{3.39}$$

Where ΔK_{th} is the threshold stress intensity factor range, K_{crit} is the fracture toughness for a particular thickness and f determines the closure level. C and n are material constants different from the Paris material constants and p and q determine the slope in the threshold zone and in the failure region respectively. The values of the constants used in this work are in table 3.2. For further detail on the Walker and NASGRO equation see the AFGROW manual [37].

Table 3.2: Material constants used in the crack growth laws for 2024-T351.[a]

Walker	$C = 4.80$ x 10^{-11}	$n = 3.2$	$m = 0.6937$	
NASGRO	$C = 1.71$ x 10^{-10}	$n = 3.353$	$p = 0.5$	$q = 1$

[a]Data source: NASGRO database on 2024-T351 (plate & sheet; L-T) from AFGROW software version 4.11.14.0 [37]. Units: da/dN and C in $m/cycle$, K in $MPa\sqrt{m}$.

Another prediction method used in this work is the Harter-T method. This method permits to calculate the FCGR if the material coefficients of the NASGRO or Walker equation are unknown. This method needs at least two material curves with two different stress ratio R. From the Walker equation for two different crack growth we can have the following relationship:

$$\Delta K_1(1 - R_1)^{m-1} = \Delta K_2(1 - R_2)^{m-1} \tag{3.40}$$

Where it is possible to interpolate point by point the m coefficient using:

$$m = 1 + [\log \frac{\Delta K_1}{\Delta K_2} / \log \frac{(1 - R_2)}{(1 - R_1)}] \tag{3.41}$$

By knowing m it is possible from equation 3.41 to achieve the different ΔK for a defined R ratio that in the welded plate will be the R_{eff}. This procedure find the material curve for that particular ratio and from that material curve it is possible to enter with an input ΔK_{app} in order to find the crack growth rate.

3.3.2 Crack closure approach

The prediction of fatigue crack growth by meaning of effective stress intensity factor range ΔK_{eff} has been applied to deem the closure effects in a constant amplitude load or overload condition. Some researchers used this approach in the past [31, 65, 141]. For this cases the effects of the plasticity have not been taken into account but only elastic FE analyses are considered. Figure 3.20 shows the procedure that has been used which correlates the ΔK_{eff} with the fatigue crack growth rate.

Stress intensity factor range is mainly influenced by crack closure hence the fatigue crack growth rate will be affected. From different material curves da/dN v.s. ΔK_{app} for different R ratio it is possible to achieve a single material curve da/dN v.s. ΔK_{eff}.

From this curve it is possible to make an interpolation thus enter with the ΔK_{eff} compute with the FEA and predict the crack growth rate value. In order to pass from the material curve with ΔK_{app} to the single curve with ΔK_{eff} the following equation must be used:

$$K_{op}/K_{max} = A_0 + A_1 R + A_2 R^2 + A_3 R^3, \quad \text{for } R \geq 0 \tag{3.42}$$

$$K_{op}/K_{max} = A_0 + A_1 R, \quad \text{for } R < 0 \tag{3.43}$$

$$K_{op} = K_{min}, \quad \text{if } \frac{K_{op}}{K_{max}} < R \tag{3.44}$$

$$K_{op}/K_{max} = 0, \quad \text{if } \frac{K_{op}}{K_{max}} < 0 \tag{3.45}$$

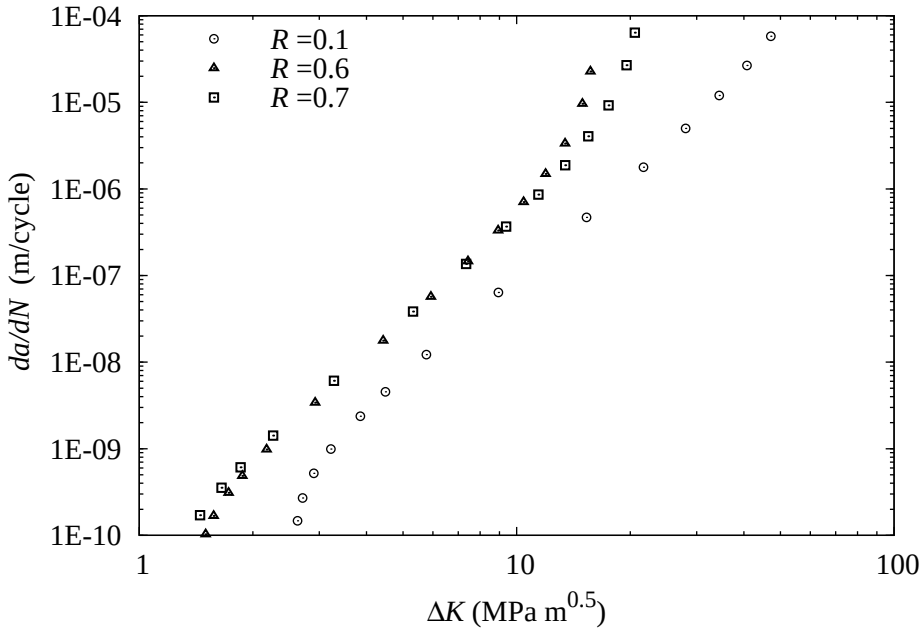

(a) Original material curves.

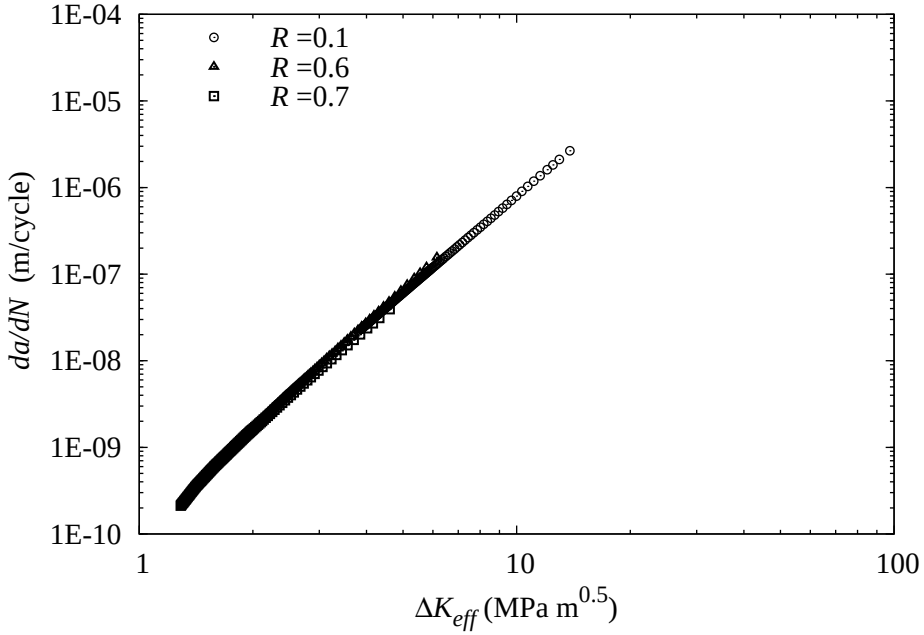

(b) Cluster of material curves.

Figure 3.19: Material curve 2024-T351 from AFGROW [37]

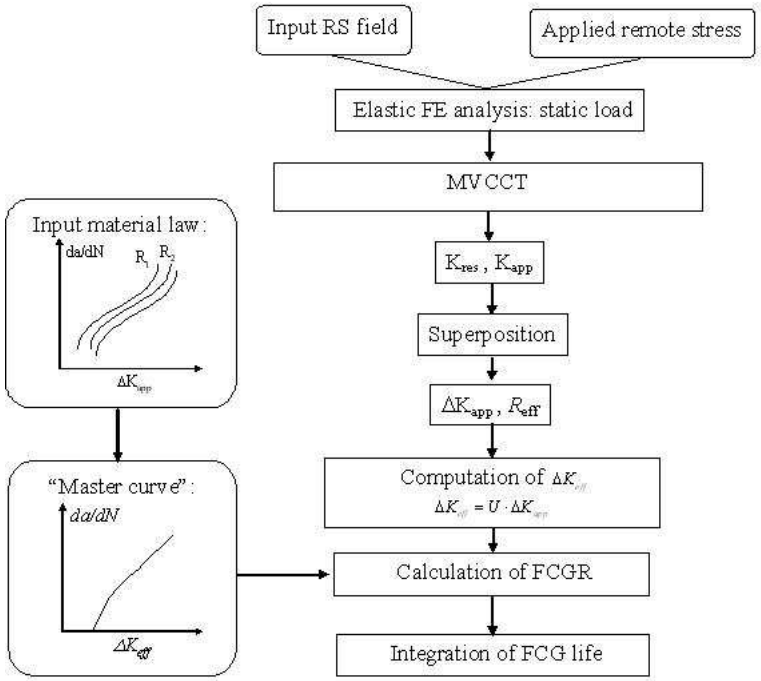

Figure 3.20: Prediction method by using the ΔK_{eff} approach.

with $R = K_{min}/K_{max}$. The coefficients are:

$$\begin{aligned} A_0 &= (0.825 - 0.34\alpha + 0.05\alpha^2)\left[cos\left(\frac{\pi}{2}\frac{S_{max}F_w}{\sigma_y s}\right)\right]^{\frac{1}{\alpha}} \\ A_1 &= (0.415 - 0.071\alpha)\frac{S_{max}F_w}{\sigma_y s} \\ A_2 &= 1 - A_0 - A_1 - A_3 \\ A_3 &= 2A_0 + A_1 - 1 \end{aligned} \tag{3.46}$$

The coefficient α can vary from 1 (plane stress) to 3 (plane strain). F_w is the width effect for a given specimen. The presented equations are valid only for a crack growth rate which is less then $0.8\sigma_{ys}$. This method was developed by Newman which is based on the Dugdale strip-yield model [79]. In order to achieve the ΔK_{eff} is by calculating the U parameter:

$$U = \frac{\Delta K_{eff}}{\Delta K_{app}} \tag{3.47}$$

Which can be achieved by using the following:

$$U = \frac{1 - \frac{K_{op}}{K_{max,tot}}}{1 - R_{eff}} \tag{3.48}$$

For welded samples use R_{eff} to replace R, and K_{op}/K_{max} can be found by using the Newman's [79] relation 3.42:

$$K_{op}/K_{max,tot} = A_0 + A_1 R_{eff} + A_2 R_{eff}^2 + A_3 R_{eff}^3, \quad \text{for } R_{eff} \geq 0 \tag{3.49}$$

$$K_{op}/K_{max,tot} = A_0 + A_1 R_{eff}, \quad \text{for } R_{eff} < 0 \tag{3.50}$$

The two equations calculate the ratio of opening stress in terms of SIF. The validity of this assumption is further discussed in chapter 5.

3.4 Summary of the chapter

A methodology to calculate the FCG by taking into account for the weld residual stress is presented in this chapter. The MVCCT was validated for simple classical cases by comparing FE with M(T) β solutions. The method of inputting RS and balance them is explained and their redistribution show a good comparison with measured residual stresses values at different crack length except the region close to ahead the crack tip. The K_{res} solution calculated with MVCCT is compared with analytical solution, i.e. weight function, by showing an average error of 5%. A description is provided on the modelling parameters used to build the plastic model. The mesh refinement is presented and establish the correct size that will be computationally efficient without loosing accuracy. The superposition and the crack closure approach have been described and the fatigue crack growth laws are provided.

Chapter 4

Plasticity induced crack closure with weld residual stress

This chapter discusses the effects of material non-linearity of welded specimens i.e. how the plasticity induced crack closure will be changed by a weld residual stress field. Numerical analyses via finite element method have been run in order to understand the crack closure mechanism and to obtain the crack opening stress value. It was found in the literature (see chapter 2) that σ_{op} is sensitive to the modelling aspects. Section 4.1 stems the results for the case without residual stresses, in order to validate the model by comparing the outcome with published opening stress values.

Section 4.2 concerns the plastic residual stresses redistribution under quasi static load conditions and it establishes how the effects of the propagation will influence the redistribution of RS field, how the stresses and strain will evolve during crack propagation and the synergism between them. The aim of this analysis is to provide the hystory of the material by meaning of $\sigma - \epsilon$ curve and the evolution of the initial RS field, in order to understand better the variables that affect the opening stress with and without RS.

Typical parameters involved in plasticity induced crack closure, which have been debated in the literature, are discussed and compared with the residual stresses case in section 4.3. Aspects of the closure mechanism such as plastic zone size, plastic strain, crack opening displacement (COD) and plastic wake are presented both with and without weld residual stresses. The objectives are to give a quali-

tative and a quantitative description in order to illustrate and to understand the mechanism of the key parameters involved. Those factors influence the opening stress value which is what is needed to calculate the effective stress intensity factor range ΔK_{eff}. The quantification of σ_{op} in weld RS field is given in section 4.4. Differently from the opening stress induced solely by cyclic plasticity, the welding RS changes σ_{op} with the crack propagation because of the redistribution of the initial RS field. The purely contribution of RS can be quantified by assuming a crack growing in a constant RS field. The latter study is presented in the same section.

Section 4.5 investigates the plasticity induced crack closure in a compressive residual stress field. The aim of this study is to assess the importance of the effect, of the plasticity and the RS that induce the crack closure, on the ΔK_{eff}.

To the author‘s knowledge the aforementioned material non-linearity effects in the presence of residual stress field are not investigated. For this reason more and novel aspects can be found in order to give a better understanding of the plasticity in welded structures. Those pioneering analyses aim to give a qualitative and quantitative results for pursuing a full understanding of the phenomenon and an accurate value of σ_{op} in presence of RS. Because there is a lot of computational effort involved in the numerical run, the efficiency needs to be improved for future applications. Therefore a better understanding needs to be addressed. Measurements of the crack opening stress can also be addressed in future works in order to compare them with numerical results.

4.1 Crack closure analysis without residual stress

It was shown in chapter 2 how the crack opening stress values can vary due to the modelling choices. A plasticity induced crack closure analysis without residual stresses is presented herein, in order to validate the modelling assumptions which have been done in chapter 3. The model represents an M(T) specimen made of Al 2024-T351 with 100 MPa of applied stress at R=0. The crack opening displacement (COD) obtained with the numerical solution was compared with theory. The COD has a classical analytical solution that takes into account for a correction of the plastic zone size. A comparison of the COD profiles is presented for a cyclic load case by using FEM and the analytical case with the

plastic zone size correction as explained below. The main difference between the two is the formation of the plastic wake in the finite element which is clearly shown in figure 4.1. Because of the elastic plastic material, the applied load leaves, behind the crack tip, tensile deformations which characterises the plastic wake. The analytical solution deems the plastic effect by using the so called Irwin‘s correction.

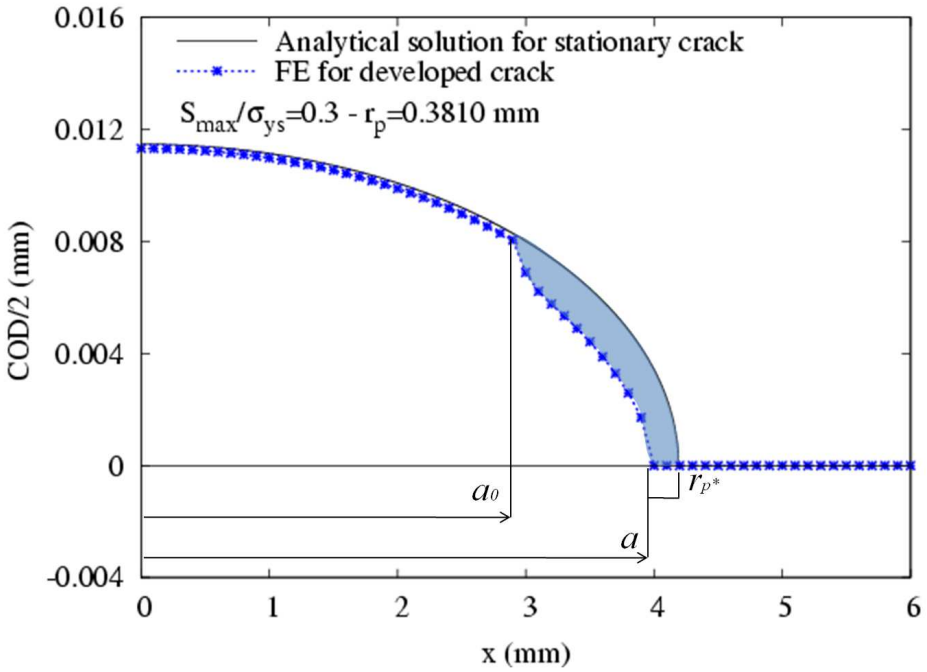

Figure 4.1: Crack opening displacement without RS.

The COD when assuming elastic material conditions is defined as:

$$COD = 2v = \frac{4\sigma}{E}\sqrt{a^2 - x^2} \tag{4.1}$$

the crack opening displacement with plastic zone correction is:

$$COD = 2v = \frac{4\sigma}{E}\sqrt{a_{eff}^2 - x^2} \tag{4.2}$$

where a_{eff} is the sum of the crack length and the plastic zone size:

$$a_{eff} = a + r_p \tag{4.3}$$

where a is half crack length whilst the forward plastic zone size r_p takes into account of the Irwin correction and it is defined as:

$$r_p = \frac{1}{\pi}(\frac{K_I}{\sigma_{ys}})^2 \tag{4.4}$$

with σ_{ys} be the yielding stress of the material. The COD in the centre of the crack calculated with FE is in very good agreement with the analytical result with an error around 1%.

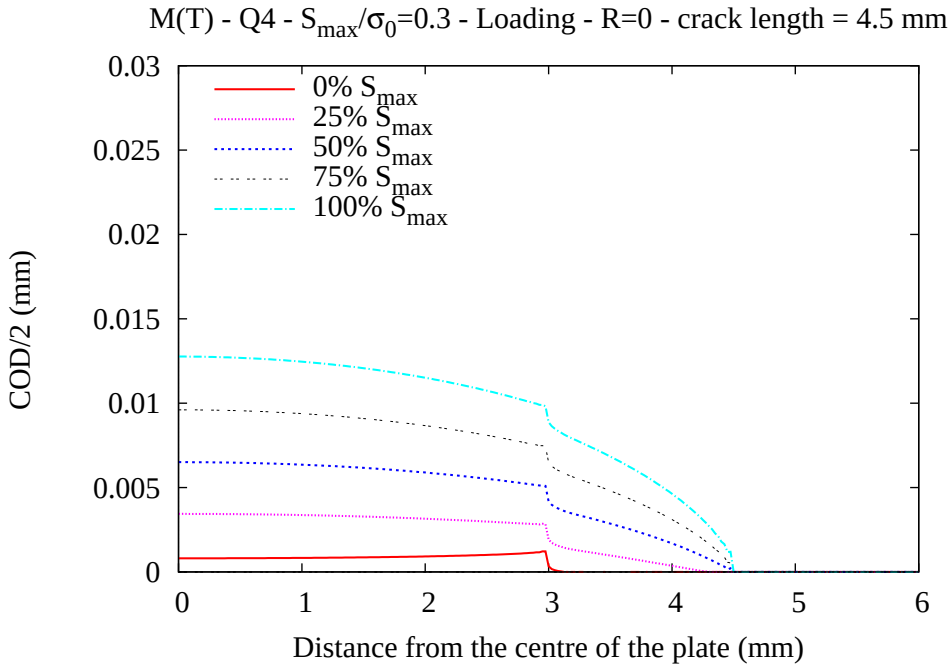

Figure 4.2: Crack opening displacement.

The crack opening displacement for the FEA and for the COD equation with the Irwin correction are the same except for the cycled part where there have been permanent plastic deformations. A preexistent crack of 3 mm in the model propagates for 2.5 mm and leaves behind the crack tip a plastic deformation which causes compressive residual stresses when the plate is unloaded. The compressive stresses are not permanent since they are produced only when the crack is closed because of the tensile deformation due to the plastic behaviour of the material. Figures 4.2, 4.3, 4.4 presents the distribution of COD, stresses and strains respectively. The displacement profile is clearly influenced by the plastic wake, when cyclic load has been applied the displacement is lower which causes a previous closure when the load is low.

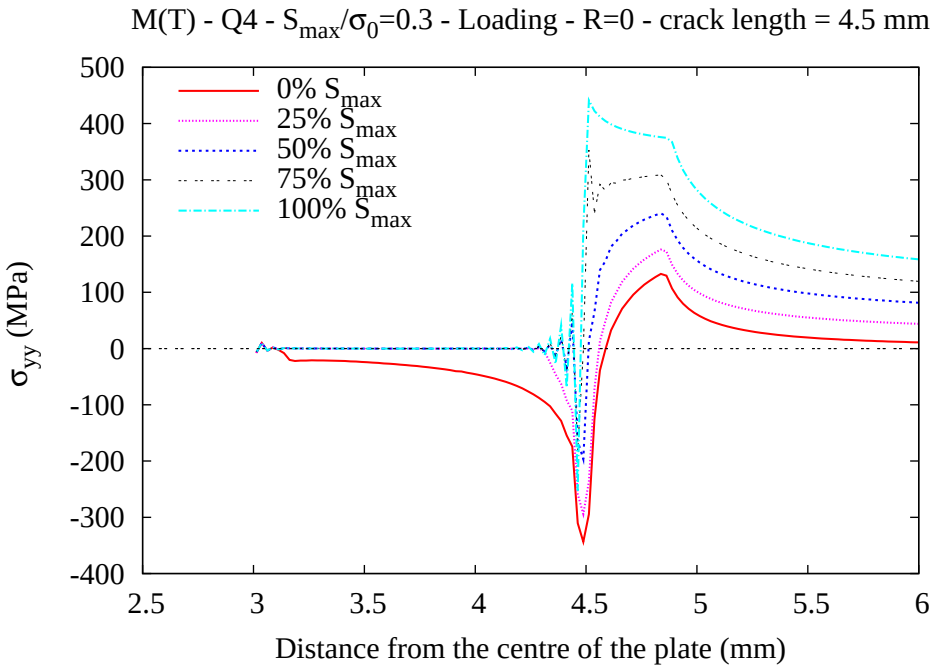

Figure 4.3: Stresses distribution.

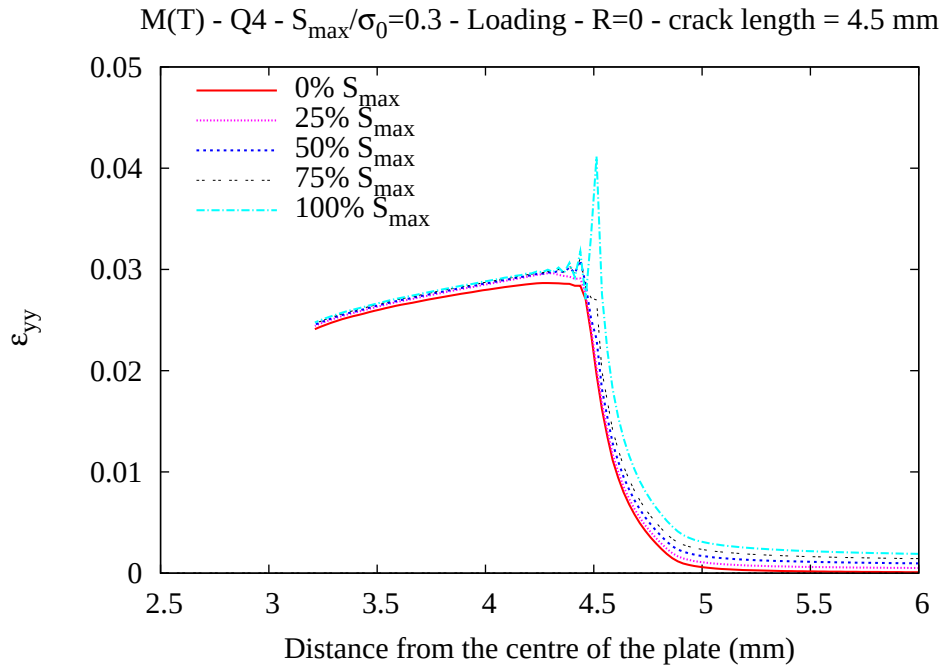

Figure 4.4: Strain distribution.

This behaviour is explained by the permanent plastic strains behind the crack tip that causes compressive stresses when the crack is closed or partially closed. By referring to figure 4.2 and 4.3 it is possible to see that for 0% of the load the crack is closed and hence compressive stresses arise, when the crack is loaded at 25% of the maximum load the compressive stresses are in the limited area behind the crack tip where the closure is present. Compressive stresses are higher close to the crack tip because of the reversed plastic zone. In order to consider the crack fully open the stresses in the first element ahead the crack tip must become positive from negative.

The value of the normalised opening stress for two different material models is shown in figure 4.5. The comparison is made with some previous results by Newman [155] and Ibrahim [156] which confirms the opening stress stabilises at a value which is close to 0.5 for $R = 0$.

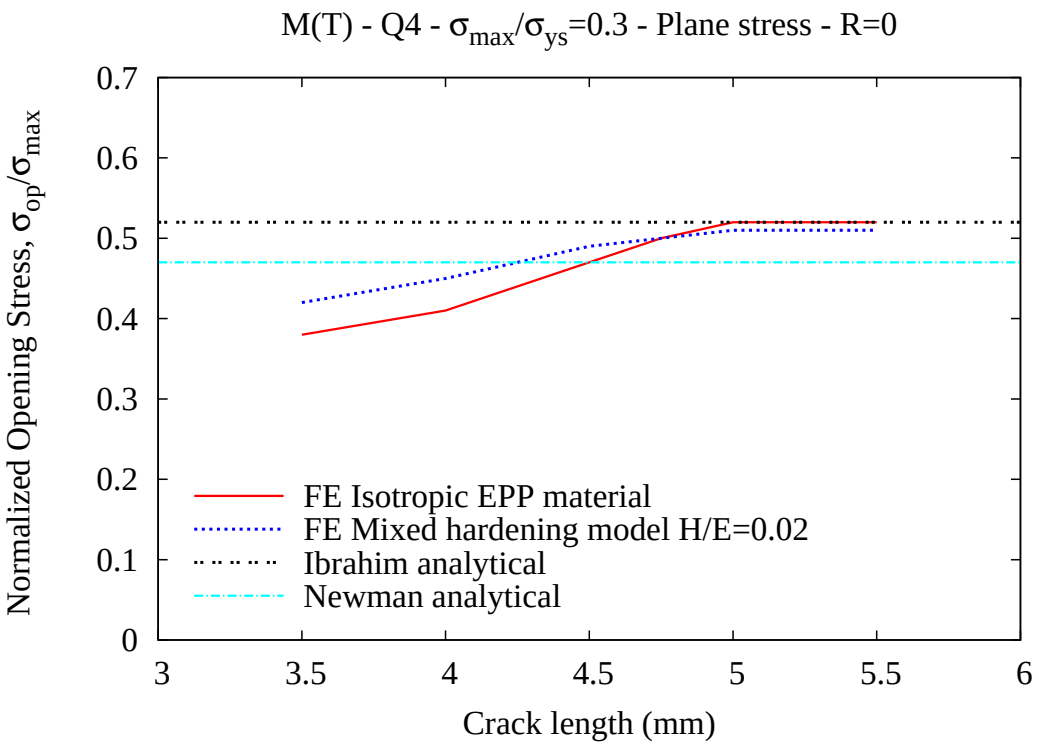

Figure 4.5: Opening stress level obtain with FE and the respective lower and upper band: respectively Newman [155] and Ibrahim [156].

4.2 Crack propagation effects

The σ_{op} depends whether the crack propagates in a negative or positive stress field, but also on the redistribution during the crack propagation, the loading and unloading condition and the stress and strain field history during crack propagation. Those aspects will be presented in this section in order to have a better insight of the phenomenon. The scope of this section is the evaluation of stress and strain during propagation, their evolution as a stress field and as a $\sigma - \epsilon$ material curve. The residual stress assumed in this section is a distribution of the VPPA welding already presented in chapter 3.

4.2.1 Residual stresses redistribution

The following graphs show the residual stresses redistribution with the crack propagation. From an initial residual stress field without crack, RS changes and redistributes when the crack grows. The FE analysis evaluates for different crack length the change of longitudinal residual stresses (σ_{yy}) that have been calculated along three lines: on the crack propagation line (CPL), 5 mm above CPL and 35 mm above CPL (figure 4.6). The redistribution of residual stresses is a matter of balance of stresses. When the crack propagates the stresses behind the crack, perpendicular to the surface of the crack becomes zero because there is a free edge condition. Therefore the rest of the residual changes in order to keep the field balanced. The stresses along the crack line can be compared with measured data taken from the literature [27] while there are no measurements data for the line above the CPL.

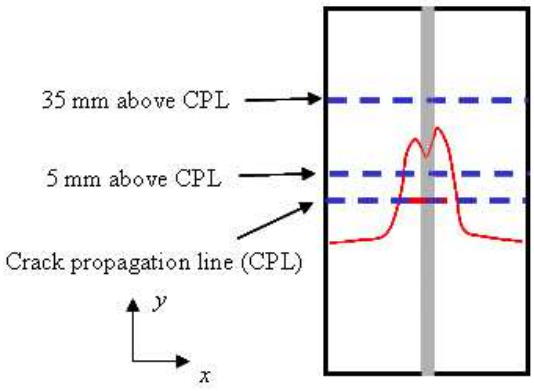

Figure 4.6: Line where the stresses have been calculated.

Two main factors are investigated in this analysis:

- RS redistribution in a distance from the CPL
- Elasto-plastic analysis and cyclic load on the redistribution of RS with crack extension and comparison with the elastic analysis.

Both the elastic and elastic-plastic material behaviour was modelled. For the elasto-plastic analysis a stress of 100 MPa at R=0 was applied. The redistribution on the crack line for the two models, in unload conditions, shows that elastic analysis has a peak near the crack tip while the elasto-plastic analysis is closer to the measured data near the crack tip. When the line of redistribution is far from the CPL for example 35 mm (figure 4.11) the crack propagation has a small influence on the redistribution of RS. When the redistribution is on 5 mm above the CPL (see figure 4.9 4.10) the peak of stresses for the elastic influences the redistribution on this line. The elasto-plastic analysis is influenced by the plastic strain and the residual stresses are changed also ahead the crack tip differently from the elastic analysis. Note that the plastic analysis produces higher residual stresses ahead the crack tip, due to the accumulated plastic strain which arise before the crack, as presented in the next section (figure 4.15). This results can be unprecise based on the fact that a similar behaviour occur also for the crack propagating along the crack propagation line (figure 4.8) where a smaller difference between the measured data and models arise.

At the second line above the crack propagation line, at 35 mm distance, the stresses are not influenced by the crack propagation. At 5 mm the crack propagation is still important in terms of stress re-distribution. The redistribution affects only the area close to the crack propagation line while away from it ($y >> 0$) the initial residual stresses are still there and their distribution is very similar to the initial one. At 5 mm This is an important effect that will be better discussed in section 4.4.1. The re-distribution is caused by the fact that during the propagation, the free surface of the crack increases hence the longitudinal stresses need to satisfy new boundary conditions. This is the first cause which re-distribute the residual stresses. The second cause occurs ahead the crack tip where the quasi-static load applied induces plastic strain and contributes to re-distribute the residual stresses as it is shown in the following section 4.2.2.

Note that for longer crack length there is a difference between the elastic and

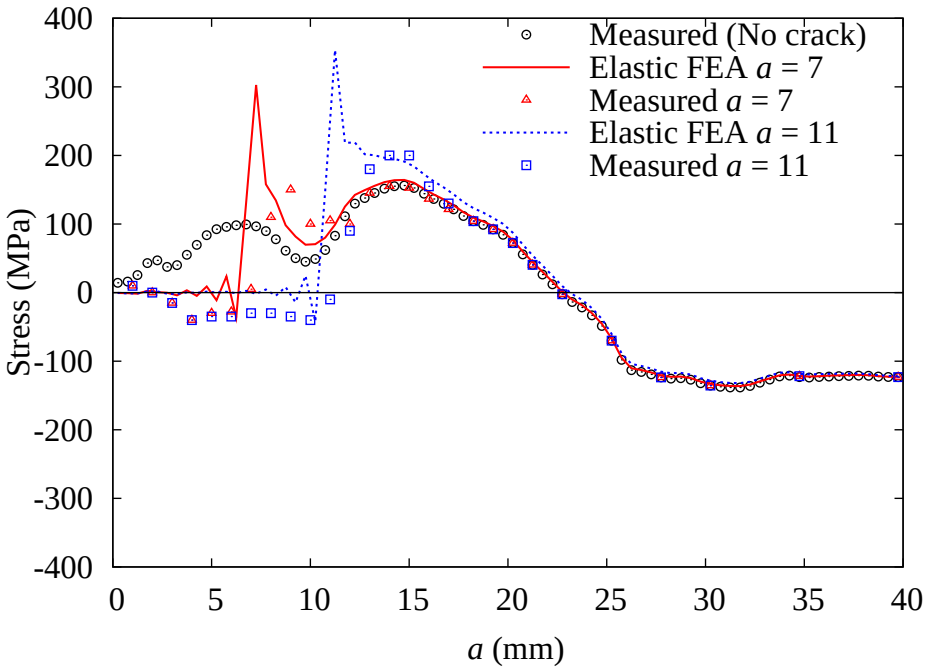

Figure 4.7: Redistribution of RS on the crack line: elastic analysis, unload conditions.

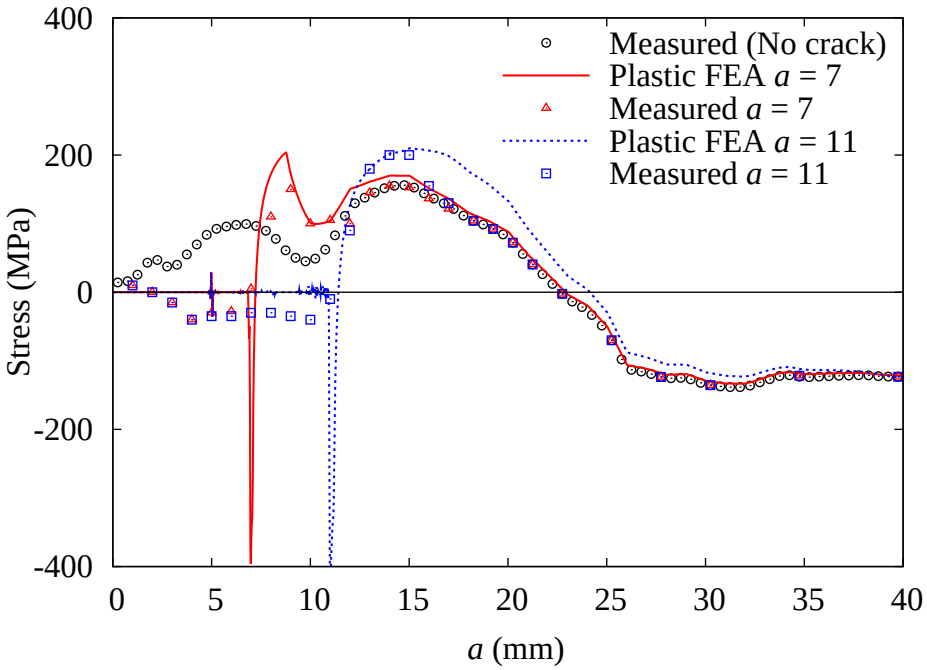

Figure 4.8: Redistribution of RS on the crack line: quai-static plastic analysis, unload conditions.

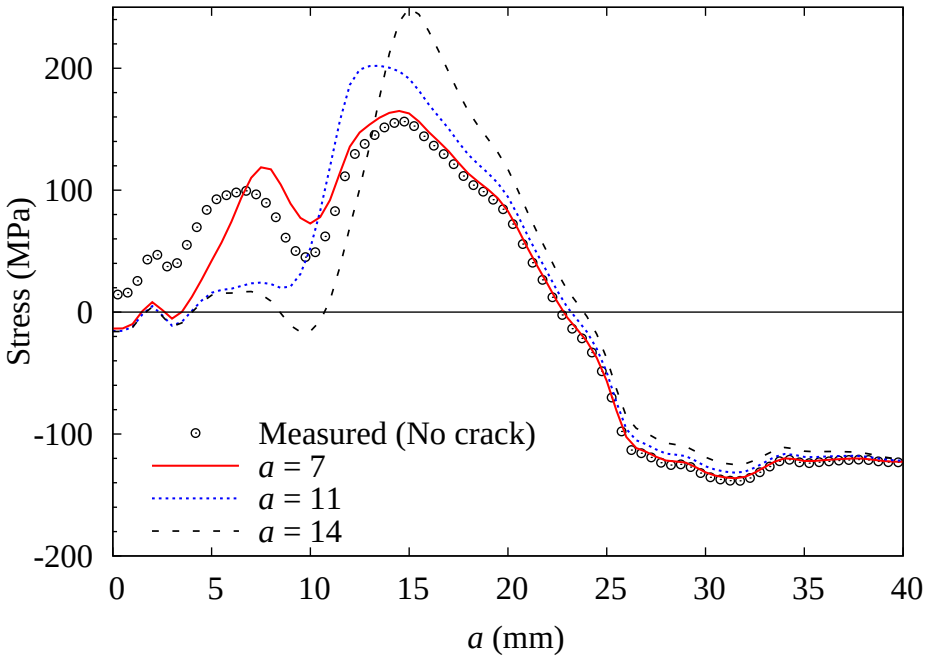

Figure 4.9: Redistribution of RS at 5 mm above the crack line: elastic analysis, unload conditions.

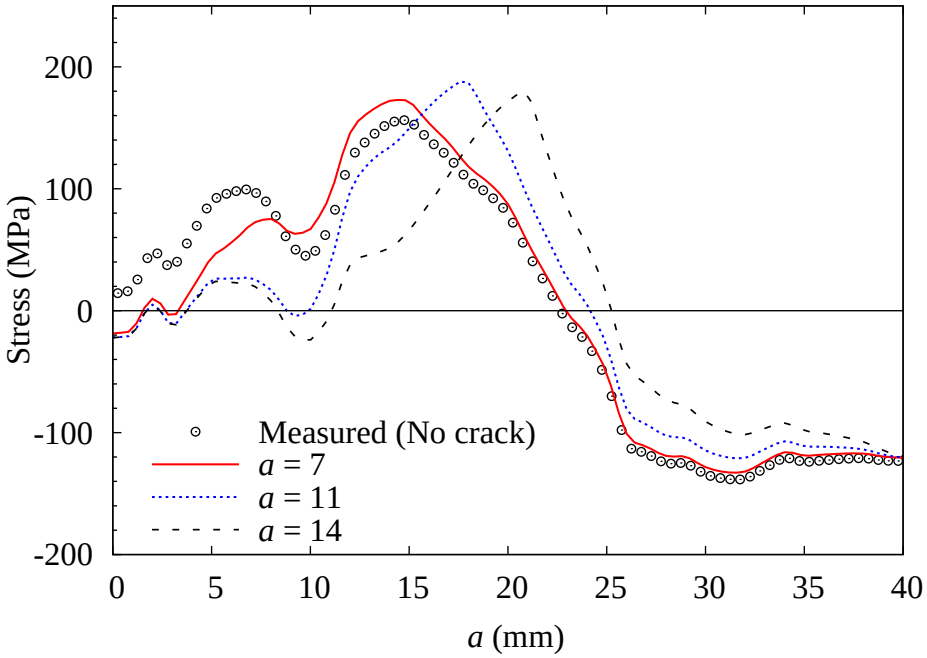

Figure 4.10: Redistribution of RS at 5 mm above the crack line: plastic analysis, unload conditions.

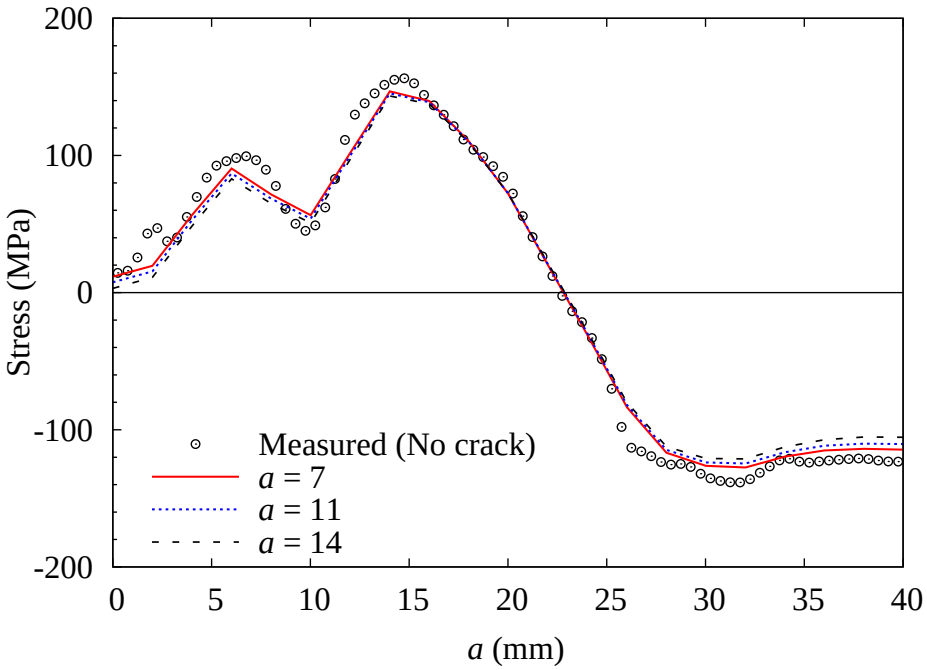

Figure 4.11: Redistribution of RS at 35 mm from the crack line: elastic analysis, unload conditions.

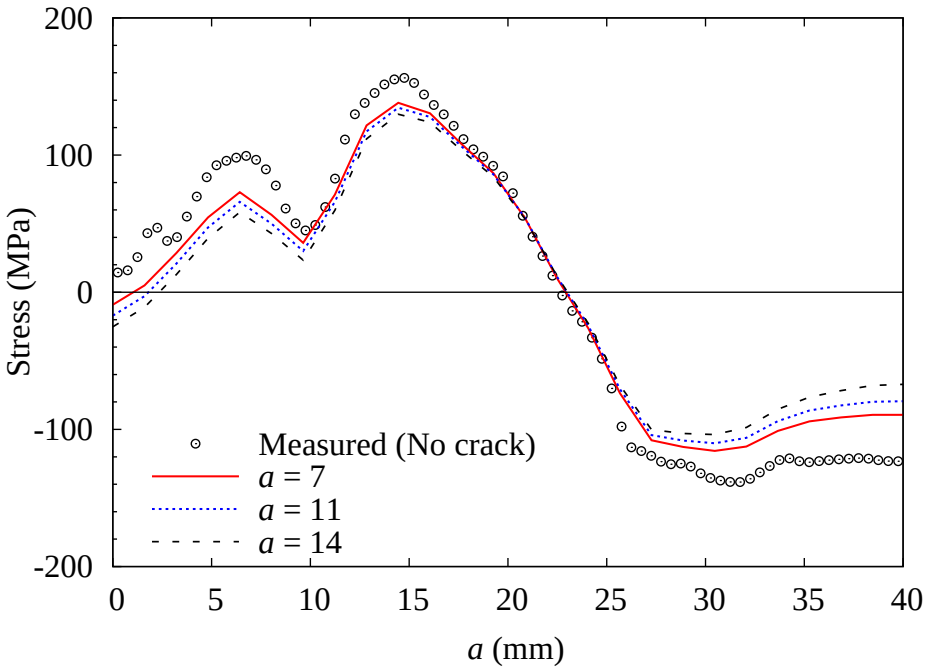

Figure 4.12: Redistribution of RS at 35 mm from the crack line: plastic analysis, unload conditions.

the elasto-plastic analysis. By comparing the weld residual stresses ahead the crack tip the value are generally higher than the measured data (see figure 4.8). The plastic model used has a great influence on the following redistribution of stresses and in particular on its history. The research on the mathematical plastic model which could represent the evolution of the strain and stress is still on going [28, 40] and it is difficult to achieve the behaviour of a cycled metal plate a priori. Moreover the welded plates have a further variable difficult to take into account i.e. weld residual stresses. The following section investigate the evolution of the stress and strain for the two cases: with and without residual stress.

4.2.2 Stress and strain history

In order to understand the formation of the plastic wake and the permanent deformations that occur in the elasto-plastic model the evolution time history of stresses and strain is presented. The stresses and strain are evaluated for a fixed position at 4.25 mm from the centre of the plate (figure 4.13). When the time step (which is related to the time history rather than the physical time) increases, the crack propagates and stresses and strains are calculated. Cases with and without residual stresses are evaluated with a maximum applied stress 100 MPa at R=0. The conditions are the same as before: M(T), 2024, VPPA weld and a crack propagating from 3 mm to 5.5 mm.

From the stress history of the case without RS after the crack tip behind the stresses are in compression when the crack is unloaded and go to zero when the load is applied (see figure 4.14(a)). When the crack is longer than 4.25 mm the compressive stresses arise only at minimum load. In the case with RS the longitudinal stresses go to zero after few cycles because the tensile RS field above the crack tip open the crack in unload conditions (see figure 4.14(b)). After 4.25 mm there are compressive stresses due to the reverse plastic zone size, but when the crack advance up to 4.5 the stresses tent to go to zero because the plastic wake effect are close the crack tip in a tensile residual stress field as it will be showed better in 4.4.1. The strain history (see figure 4.15) shows that the formation of the plastic wake starts ahead the crack tip because of the tensile stress field near the crack tip which influences the plastic strains deformations more and more when the crack is approaching to the element. After the unloading condition

there is the formation of the reverse plastic zone which is compressive and is due to the high stress concentration near the crack tip.

Note that the plastic strains which occur ahead the crack tip influence the re-distribution of the weld residual stresses. In particular higher stresses will occur compared with experimental measurements as presented in the previous section (see figure 4.8 at crack length 11 mm). For longer cycled crack length the development of the plastic strain is overrated respect to short cycled crack where it was shown a good agreement between the measured data and the FE results.

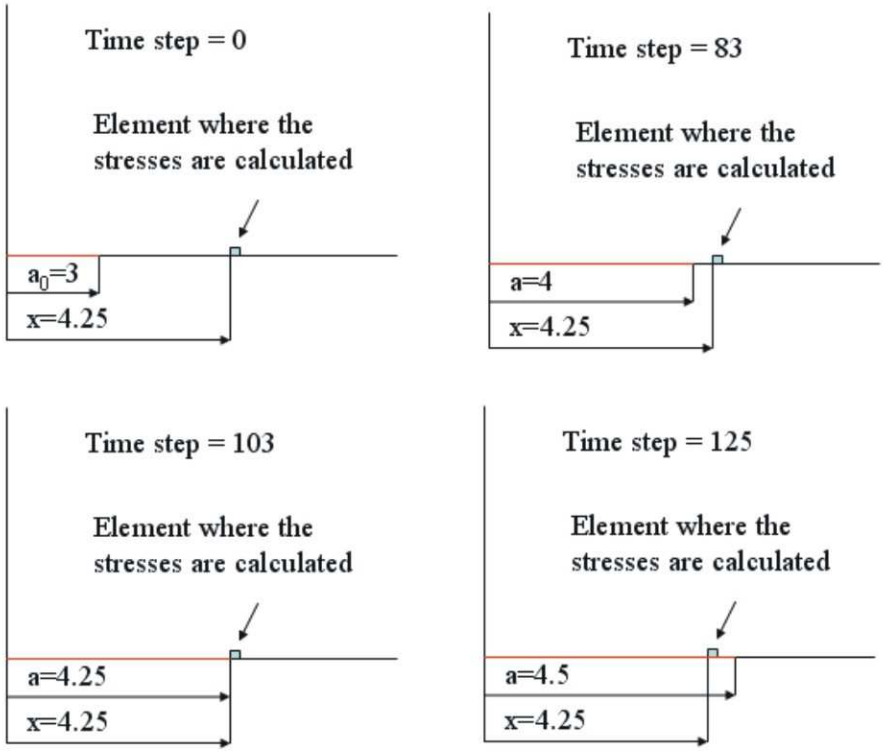

Figure 4.13: Element used for the evaluation of stress and strain history.

The history of the material law is shown in figure 4.16. When the crack tip is in position p1, before the reference element, the stress-strain curve has a small plastic behaviour and the unloading is completely elastic in both cases with and without RS. The only difference is the magnitude of the strain which is larger in the tensile RS field. At position p2 the crack tip is at the reference element. There is an entire cycle unload-load-unload in a-b-c points respectively with the high stress at that position. It is possible to observe the actual behaviour of the material i.e. different tensile and compressive plastic regime. This is the Baushinger effect which is caused by the choice of the mixed isotropic-kinematic

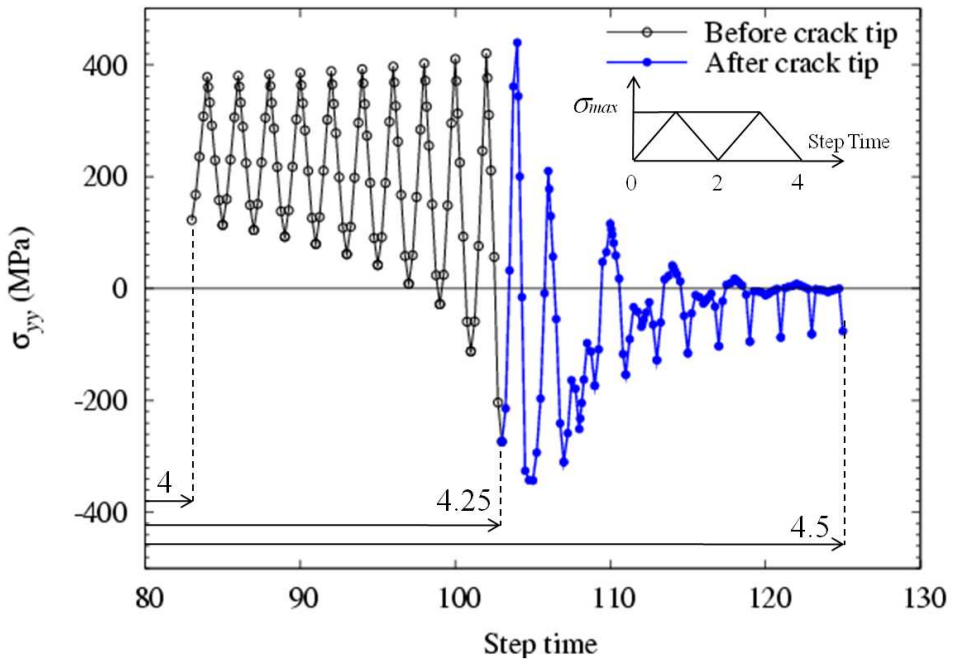

(a) History of the longitudinal stresses without residual stress field at different crack lengths (unit mm).

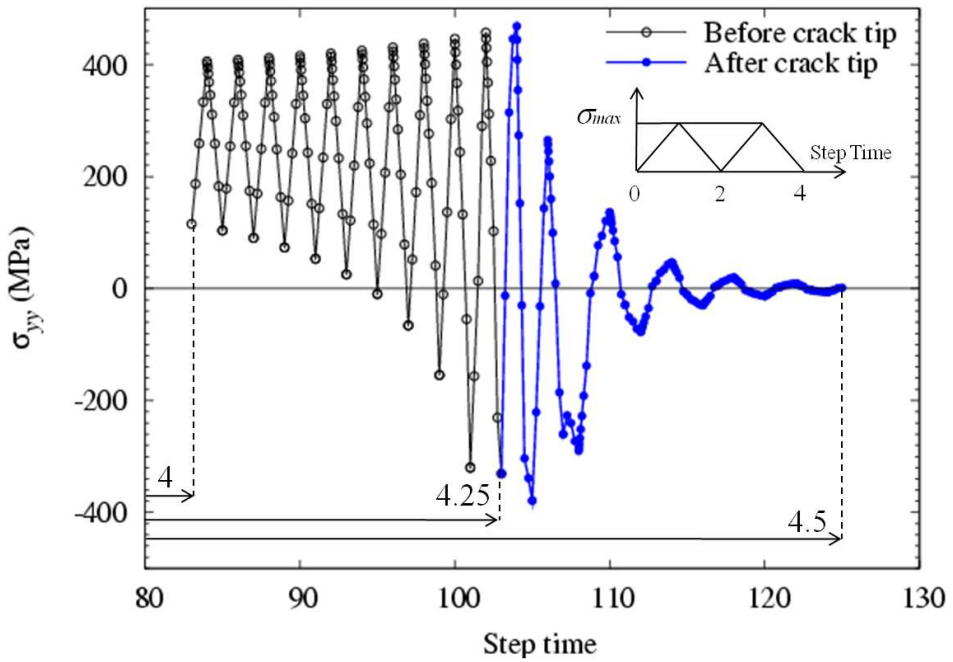

(b) History of the longitudinal stresses through a residual stress field at different crack lengths (unit mm).

Figure 4.14: Stress history.

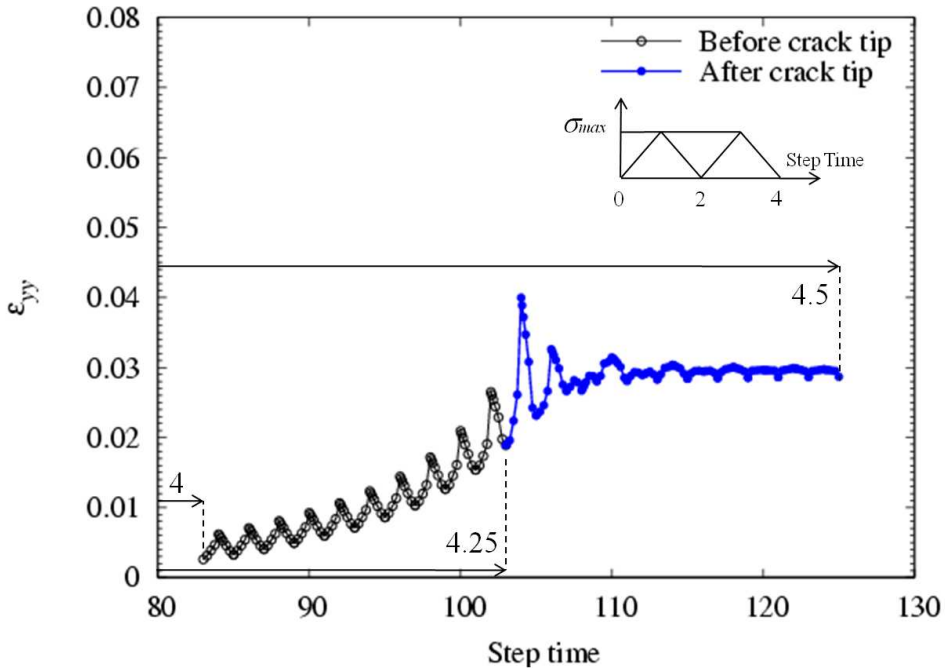

(a) History of the longitudinal strain without residual stress field at different crack lengths (unit mm).

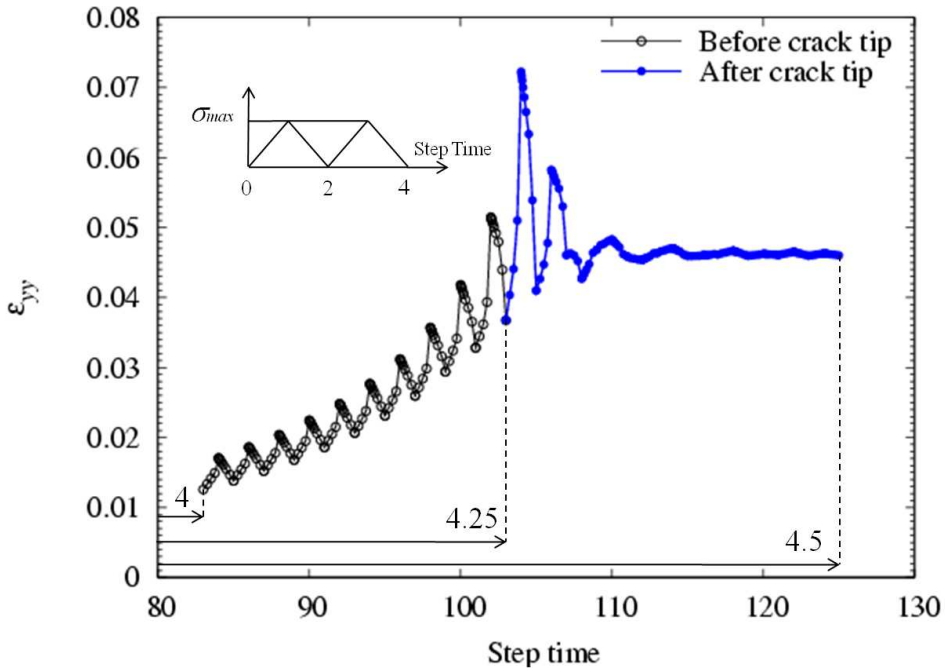

(b) History of the longitudinal strain through a residual stress field different crack lengths (unit mm).

Figure 4.15: Strain history.

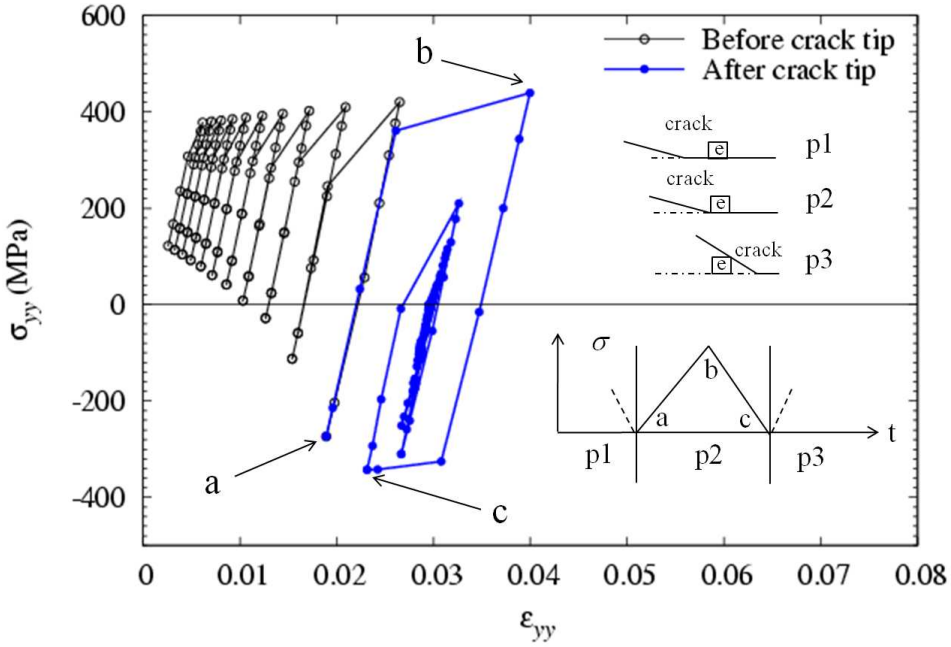

(a) History of the longitudinal stress and strain without residual stresses.

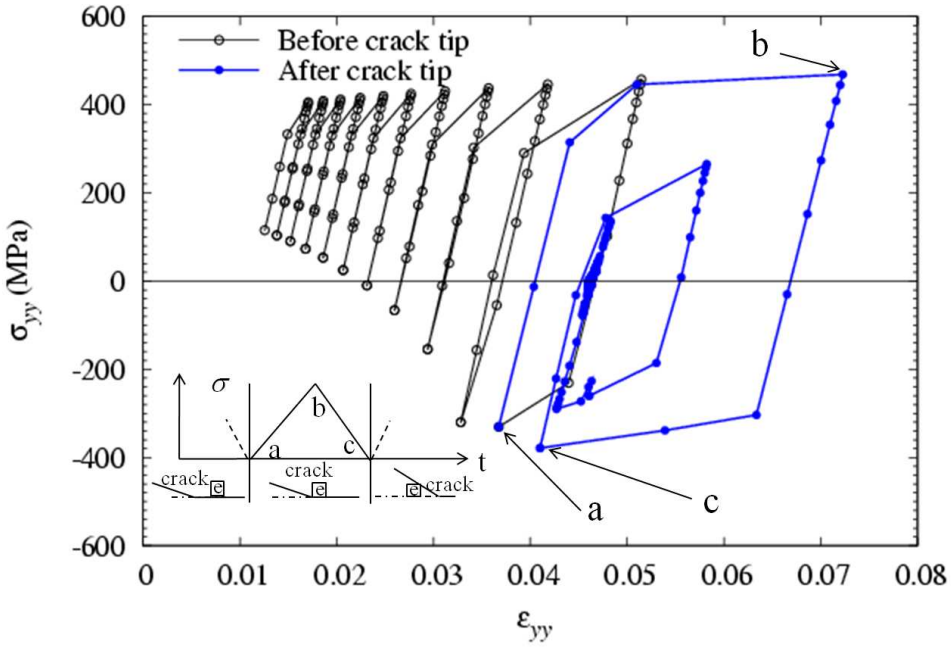

(b) History of the longitudinal stresses and strain through a residual stress field.

Figure 4.16: Stress strain history.

hardening plastic model discussed previously in chapter 2 and 3. When the crack goes through the reference element in position p3 the plastic strain remain but the stresses tent to go to zero except in minimum load condition where they are compressive as it was previously described.

4.3 Key parameters of plasticity induced crack closure

In the past the parameters that were chosen to study the plasticity induced crack closure without residual stresses were the plastic zone size, the longitudinal stresses at the crack tip and crack opening displacement which gives also a visual explanation of the plastic wake. Besides those parameters this section deems also the plastic wake in terms of plastic deformation hence the area where the strain have been considered plastic i.e. when they overcome the proof value of strain for that material. All those parameters, which interactions affects the final crack opening stress, have been presented in this section for both cases with and without residual stresses.

4.3.1 Plastic zone size

This section concerns the plastic zone size. Firstly two cases without RS are presented in order to compare the results from the FE analysis with the analytical formulation. Iso-stress lines have been plotted to visualize the plastic zone size and shape obtained by the FE analysis. Then the cases with RS are shown. Table 4.1 shows the different cases assumed for the study of the plastic zone size.

Table 4.1: Sample cases to investigate the plastic zone size: M(T) with 100 MPa and R=0.1.

Cases No	RS field	Material
1	Without	2024
2	Without	2198
3	VPPA RS (fig. 4.19(a))	2024
4	FSW RS (fig. 4.19(b))	2198

The evaluation of the plastic zone size is done by using the von Mises stresses because they take into account for the stresses in both directions. The definition

of the von Mises stress is:

$$\sigma_{vm} = \frac{1}{\sqrt{2}}\sqrt{(\sigma_1 - \sigma_2)^2 + (\sigma_2 - \sigma_3)^2 + (\sigma_3 - \sigma_1)^2} \tag{4.5}$$

Figure 4.17 shows case number 1 without RS for a material 2024-T351 with σ_{ys} = 324 MPa [157].

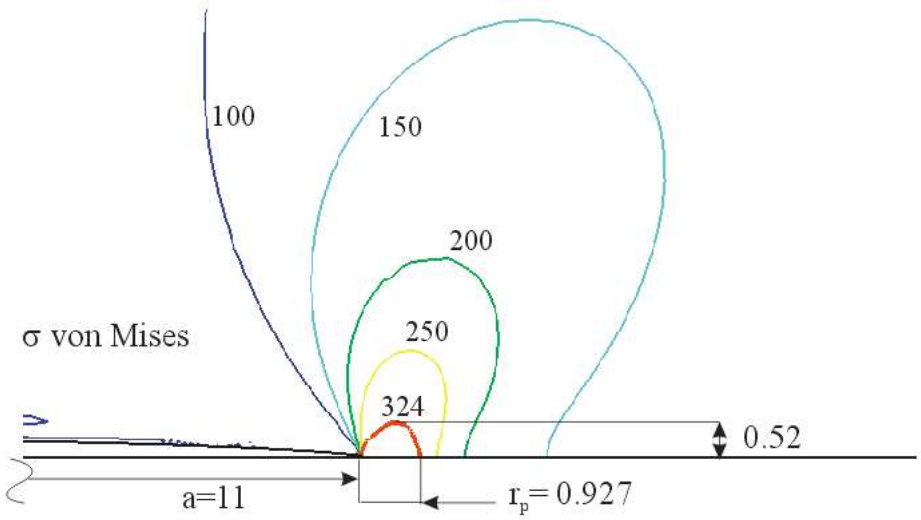

Figure 4.17: Iso-stress line for 2024 T-351 without RS.

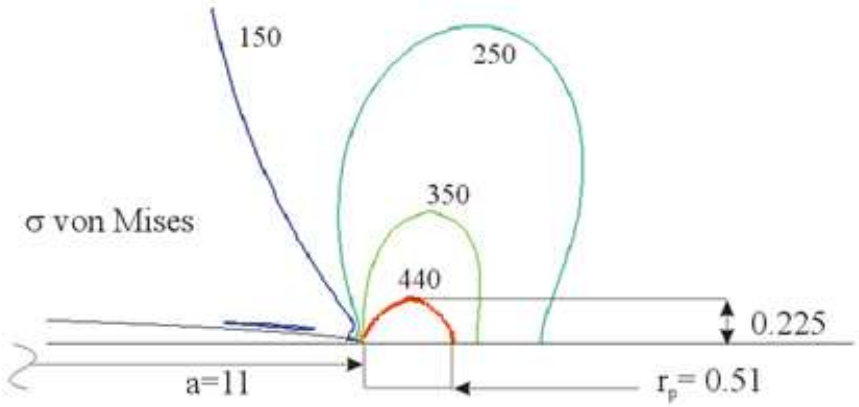

Figure 4.18: Iso-stress line for 2198 without RS.

The theoretical value for a crack length 11 mm for this case is r_p=1.02 mm which is close to the FE estimation. The percentage error by comparing with the theoretical value is 7%. Figure 4.18 show the case number 2, with the same load conditions but a different material: 2198 with σ_{ys}= 440 MPa [158]. The theoretical value for this case is r_p=0.56 mm which is the plastic zone size in

an elasto-plastic material. Since the σ_{ys} is higher the plastic zone size is smaller i.e. a higher load is necessary to reach plasticity condition (see figure 4.18). The percentage error is 8%. The plastic zone shape is not circular hence also the plastic zone height needs to be assessed. It is herein defined as the maximum distance from the crack propagation line to the iso-stress line of the yielding stress and it is indicated in figure 4.17 and 4.18 which show that both cases the height is 50% of r_p.

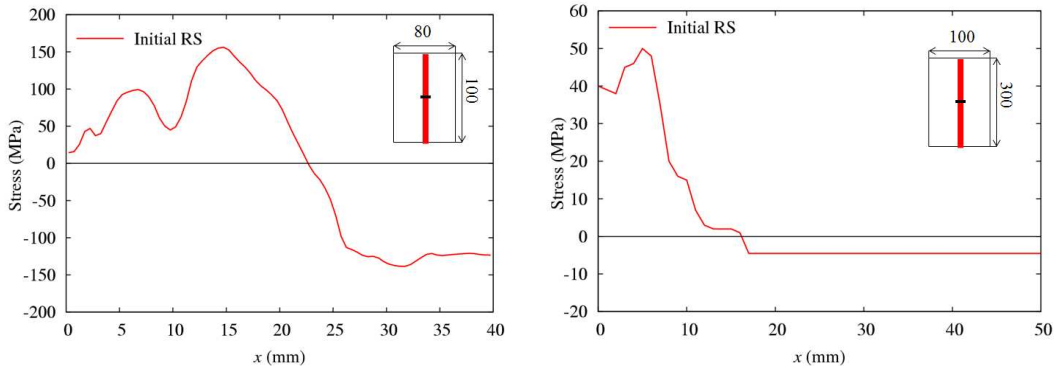

(a) Residual stress distribution for the 2024 T-351 material due the VPPA welding process.

(b) Residual stress distribution for the 2198 material due the FS welding process.

Figure 4.19: Initial RS distribution for different material and weld process.

The two aforementioned cases were also used to evaluate the plastic zone size with two residual stress fields (figure 4.19). A variable polarity plasma arc (VPPA) is the example that will be also explained in more details further this chapter and a FSW distribution obtain from measurement by the cut compliance method [159] and inputted in the FE model. The cases examined are number 3 and 4 referred to the table 4.1.

The plastic zone obtained with the FE is good compared with the theoretical value. Without RS there is a similar error of 7% and 8% for the first and second case respectively. The overall shape of the plastic zone is homothetic with respect to the change of σ_{ys}. The height of the plastic zone size increases about 100% as well as the r_p when the yielding stress increases of 35%. By applying a tensile residual stress field there is an increment of the plastic zone size and its height. In the case 3 the r_p increases by a factor of three while the height increases with a factor of 12. The residual stresses are in the order of 50 MPa near the crack tip while they are much higher just ahead at the crack tip: around 150 MPa. For this reason there is a relevant increment. Therefore the homothetic assumption from

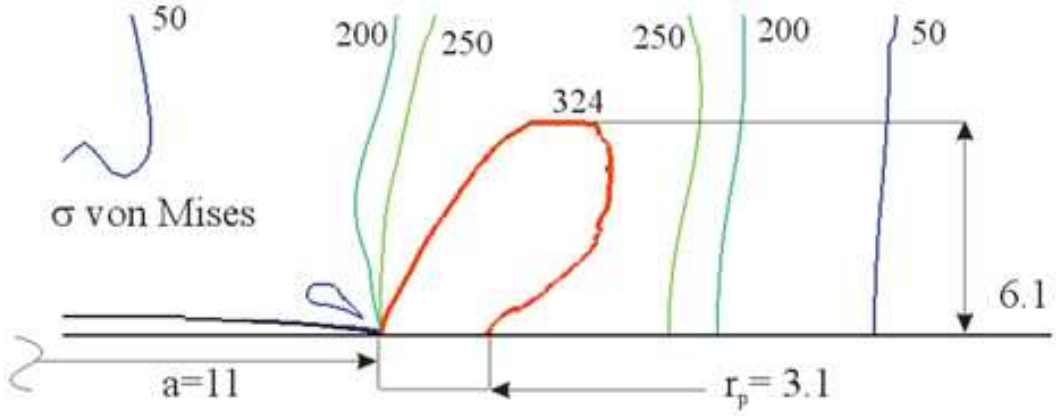

Figure 4.20: Iso-stress line for 2024 with RS.

the case without and with is not valid anymore because the weld residual stresses are mainly longitudinal for this reason the plastic zone size is more stretched in the y direction. Also in case 4, with a low weld residual stress field which is in the order of 10 MPa the plastic zone size changes its shape. The increment in plastic zone size r_p is 22% while the height is 28% bigger than the base material case.

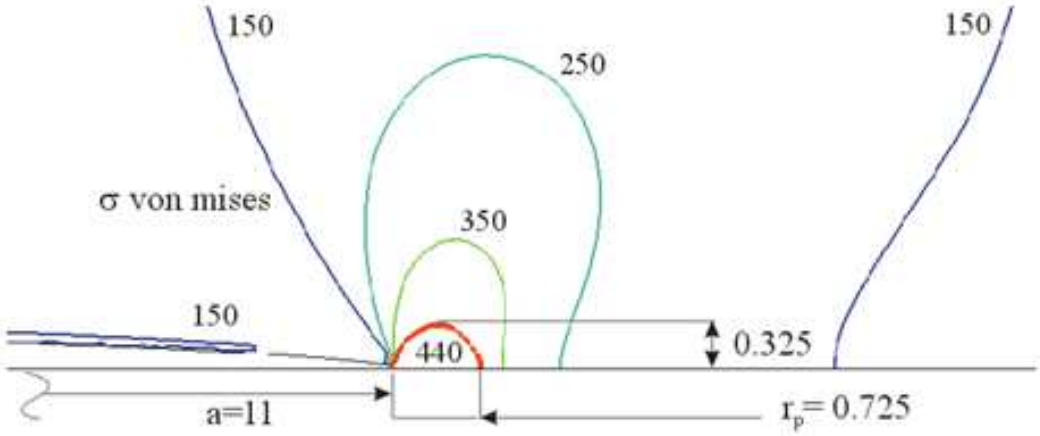

Figure 4.21: Iso-stress line for 2198 RS.

The change in shape and size due to welding residual stresses will influence the other plasticity induced parameters, such as the plastic wake, the stresses at the crack tip and also the profile of the free edge surface of the crack. All those will affect the opening stress level. Without RS the two plastic zone sizes have homothetic transformations for different σ_{ys}. This is not valid anymore in case of tensile residual stress field where the longitudinal stresses increase the height much more than the r_p. This will affect the formation of the plastic wake by

meaning of the plastic strain as it is discussed in the following section.

4.3.2 Plastic wake due to permanent plastic strain

Recognising the importance of the plastic zone for the formation of the strain this section assess how the tensile RS affects the wake left behind the crack tip, in terms of magnitude and shape.

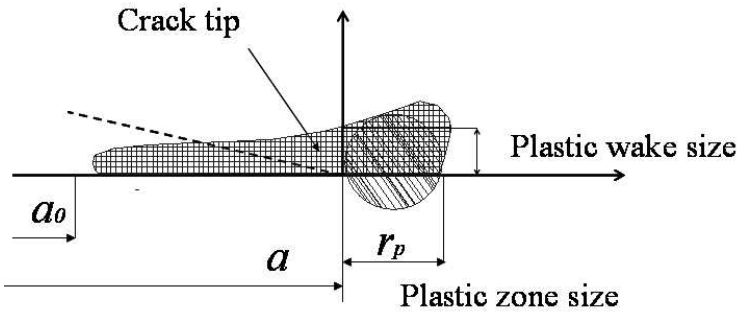

Figure 4.22: Plastic zone size and plastic wake definition.

The plastic wake is defined as the part behind the crack tip. For this reason the width of the plastic wake is defined as the distance from the symmetry line to the end of the plastic area at the crack tip. The definition of plastic zone size and plastic wake size is shown in figure 4.22. The evolution of the plastic wake, by means of the plastic strain ϵ_{yy} with the crack propagation is shown in figure 4.23 and 4.24. The grey part is the area where the strain ϵ_{yy} are higher than the proof strain 0.2%.

The comparison of the evolution of the plastic wake with the initial residual stress distribution shows that the area of plastic strain becomes larger when the crack approaches 11 mm of its length. At this point the residual stresses start to increase from 50 to 150 MPa (see figure 4.19(a)). The peak is reached at crack length 15 mm, at this point the plastic wake has the wider part. At a crack length of 20 mm the plastic wake becomes smaller than the previous crack length.

Residual stress field affects both the plastic wake and the plastic zone size in the same manner as shown in figure 4.25. The trend is the same i.e. when tensile residual stress increase proportionally with the initial RS field. Around 7 mm of the crack length the size of plastic wake and plastic zone size is the same and the

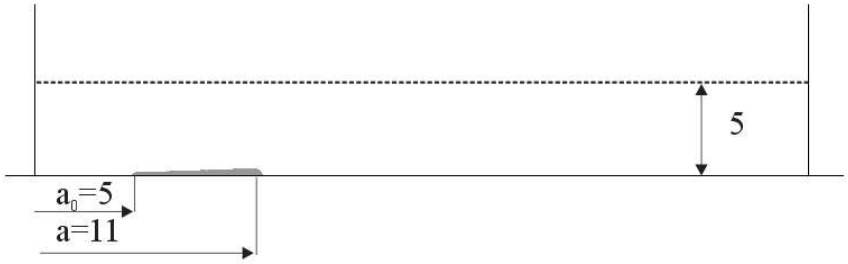

(a) Crack = 11 mm.

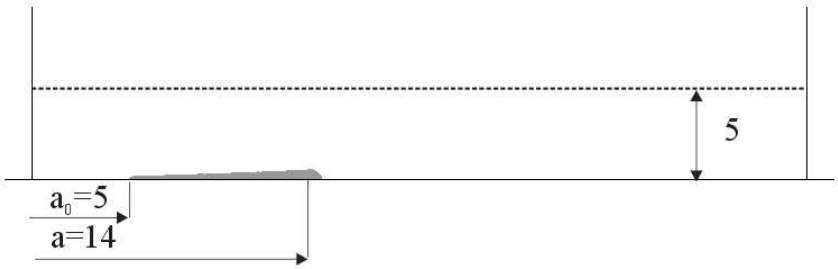

(b) Crack = 14 mm.

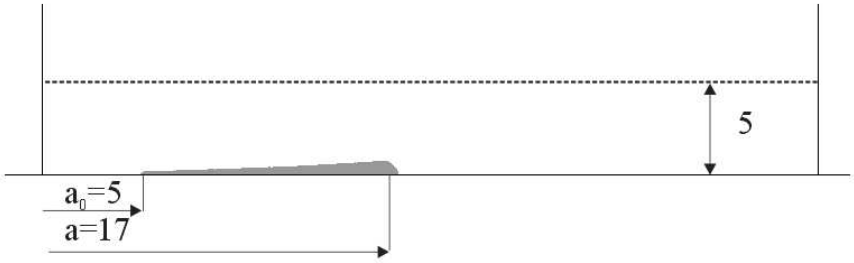

(c) Crack = 17 mm.

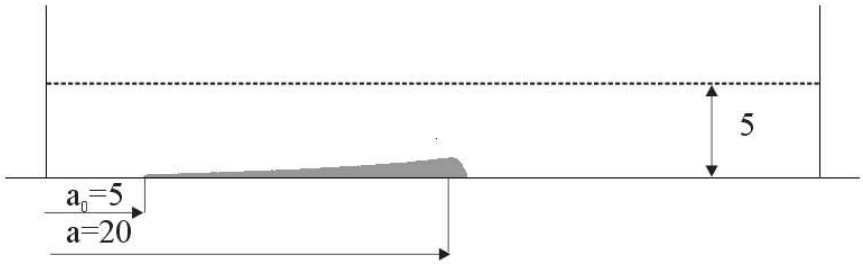

(d) Crack = 20 mm.

Figure 4.23: Plastic wake (dimension mm).

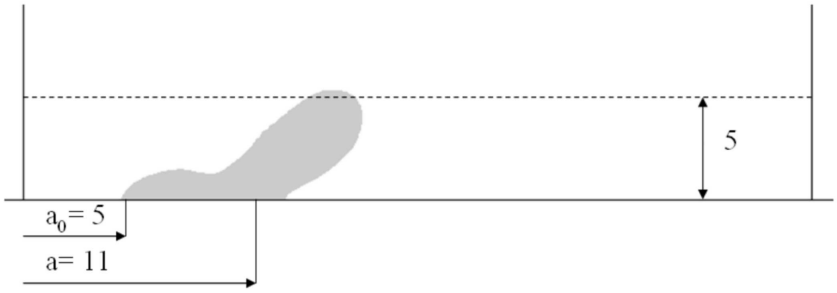

(a) Crack = 11 mm.

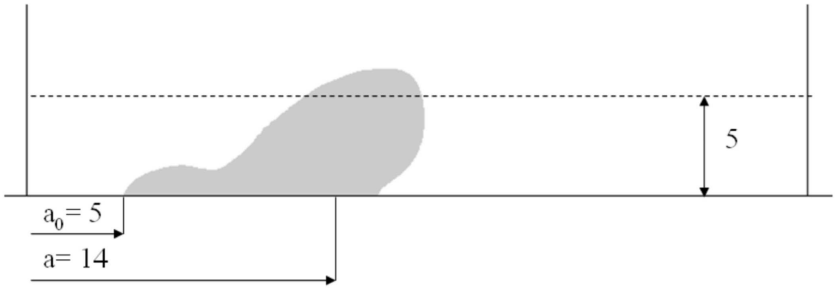

(b) Crack = 14 mm.

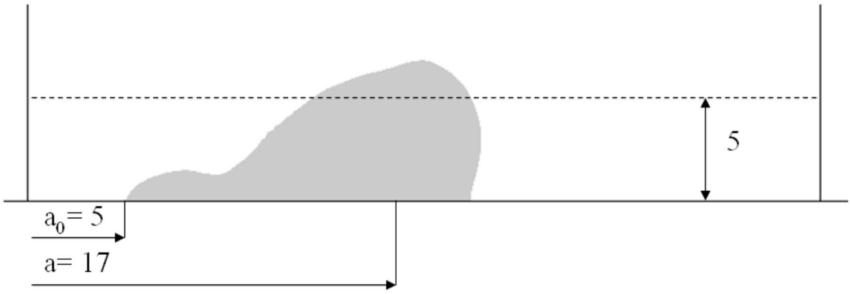

(c) Crack = 17 mm.

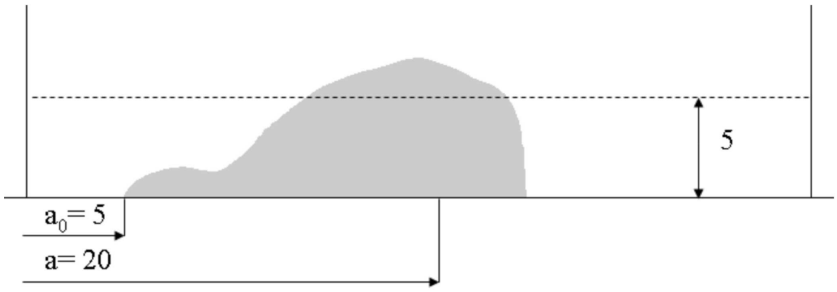

(d) Crack = 20 mm.

Figure 4.24: Plastic wake due to VPPA welding RS (dimension mm).

value is around 2 mm. However when the crack length is 14 mm the difference is higher. This is because the plastic zone size r_p is influenced by the stresses ahead the crack tip. In figure 4.24(a) the plastic wake at the crack tip is smaller compared to the part ahead to it. The profile of residual stresses has an high slope in that area hence plastic strain occur in a larger zone. For bigger crack length the plastic wake arises and it reaches a peak of 6 mm at a crack length of 17 mm. This part does not correspond to the maximum of residual stresses because the plastic zone size and the plastic wake size at the tip increases with the crack growing but decreases with the negative slope of RS profile. However the negative slope is not fast enough to overcome the increment of permanent strain area due to the growth of the crack i.e. a delay occurs. It is noteworthy that the plastic wake is bigger than the plastic zone size because of an opposite effect as that one described for a crack length of 14 mm.

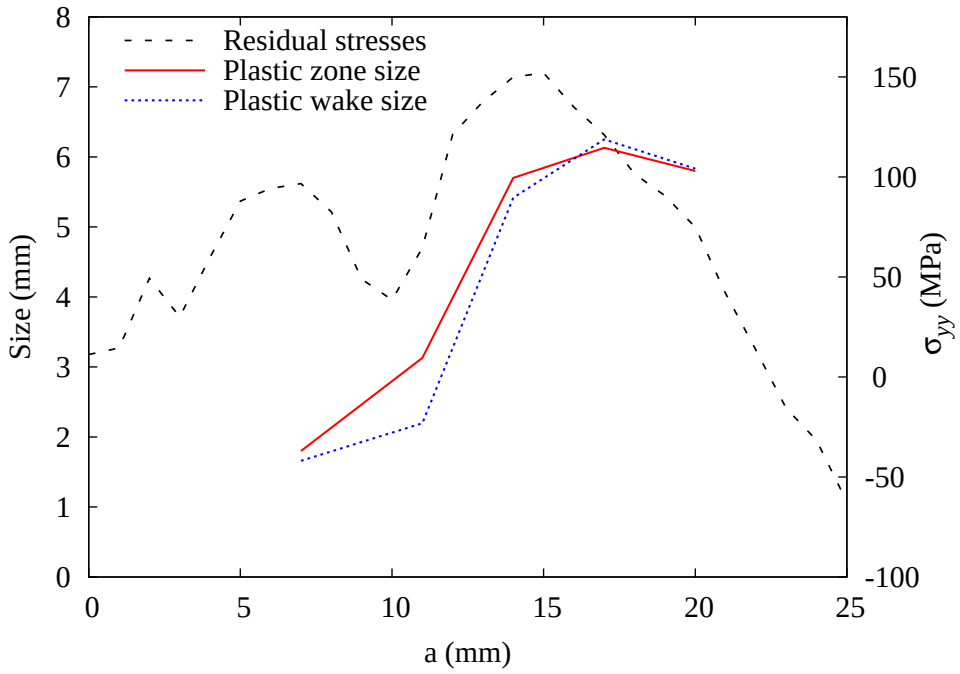

Figure 4.25: Plastic wake and plastic zone size in presence of residual stress field.

At crack 17 mm the stresses ahead the crack tip have become lower and the plastic zone size is earlier influenced by them. At crack 20 mm the size decreases because the decrement of the tensile residual stresses overcome the influence of a longer crack. The size of the plastic zone and the plastic wake is directly related to the initial residual stresses profile. They are also dependent on the material properties since strain and stress are related by the $\sigma - \epsilon$ material curve

as explained in section 4.2. The contribution of those two parameters is shown in section 4.4.2 where the crack propagates in a constant residual stress field.

4.3.3 Crack opening displacement

The plastic wake formation described in the previous section clearly influences the crack opening displacement profile as well as its closure and opening. This section presents the results of the COD at different percentage of the load for both cases with and without RS.

The crack opening displacement profile is clearly influenced by the plastic wake as it is shown in figure 4.26. From 5 mm distance from the centre of the weld a transient lump arise in proximity of the initial crack length. This is the starting point of the plastic wake which causes the crack surface to be partially close at load higher than minimum load. Tensile residual stresses produce a higher plastic wake as previously described, the profile is more deformed after the transient lump at 5 mm with tensile residual stress field.

When residual stresses occurs the COD increases this will influence also the longitudinal stresses at the crack tip. The crack is partially closed near the crack tip for crack length of 11 and 20 mm. The crack tip opening displacement which used to be the higher displacement in the case without RS may be lower in the case with RS. Figure 4.26(f) shows this trend which is caused by the distribution of the initial residual stresses which has lower values close to the centre of the plate. An early opening stress of the COD will modify the longitudinal stresses at the crack tip which will influence the opening stress. As expected figure 4.26 shows that the COD profile increases and also in minimum load condition the crack is mainly open. Only near the crack tip at low percentage of the maximum load the crack is partially closed. This will influences the stress distribution as it is shown below.

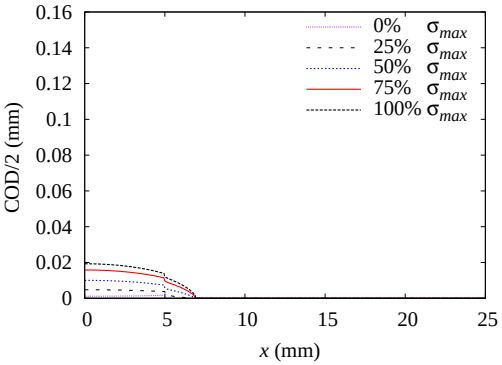

(a) COD without RS: crack length 7mm.

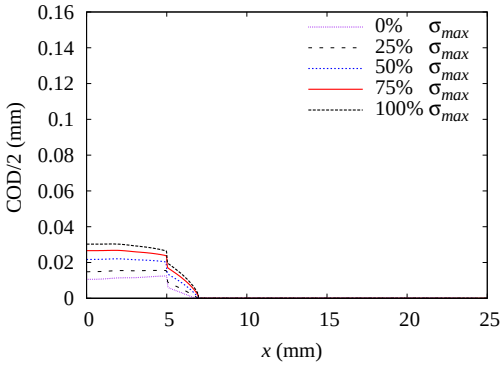

(b) COD with RS: crack length 7mm.

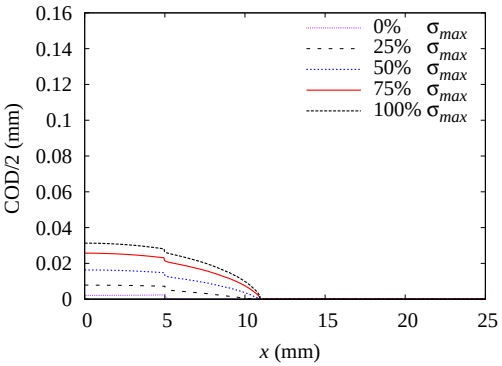

(c) COD without RS: crack length 11mm.

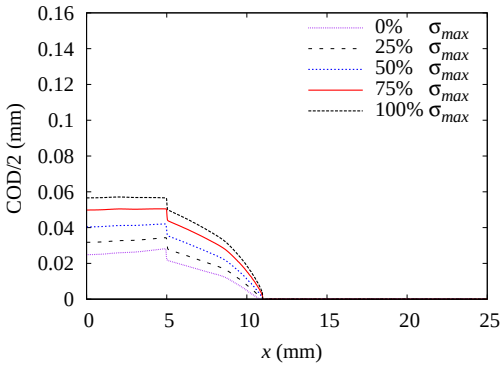

(d) COD with RS: crack length 11mm.

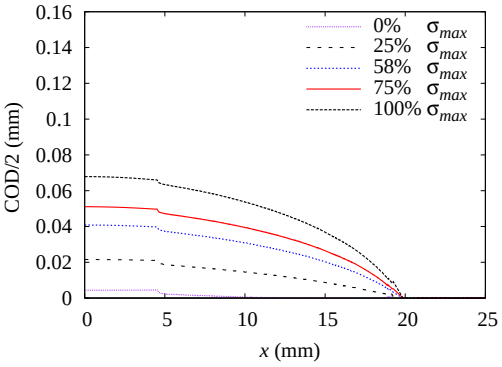

(e) COD without RS: crack length 20mm.

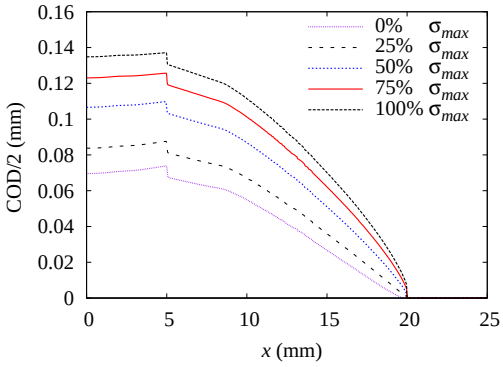

(f) COD with RS: crack length 20mm.

Figure 4.26: Crack opening displacement.

4.3.4 Crack tip stress distribution

The longitudinal stresses σ_{yy} are presented in figure 4.27 for the case with and without welding residual stresses at a crack length of 11 and 20 mm. Different load conditions are presented: unload condition, 25%, 50% and maximum load conditions. The distribution of stresses is related to the crack opening displacement previously described. Without residual stresses at unload condition negative compressive stresses arise because the crack is completely closed and the plastic wake causes the compression. During loading the zone of compressive stresses get closer to the crack tip and then only the zone ahead the crack tip is compressive. Since the stress method is adopted the compressive stresses ahead the crack tip are the most important to determine the opening stress. Note that behind the crack tip some tensile stresses arise which are due to numerical noise.

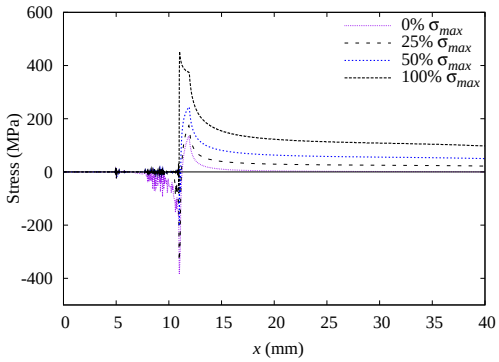

(a) Stresses at the crack tip without RS. Crack length =11 mm.

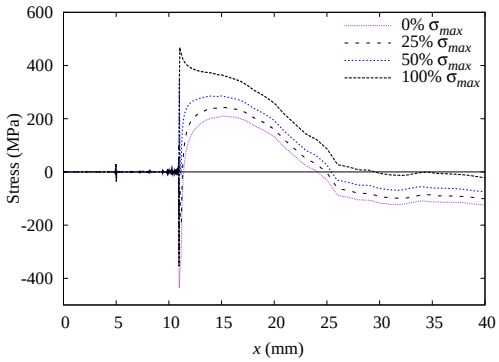

(b) Stresses at the crack tip with RS. Crack length =11 mm.

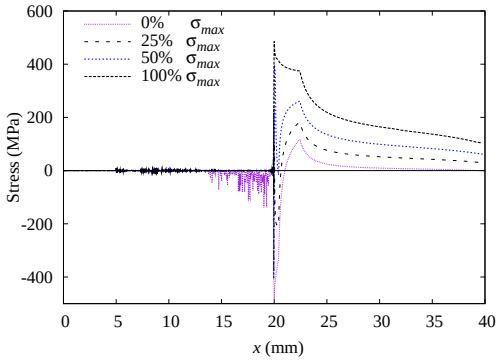

(c) Stresses at the crack tip without RS. Crack length =20 mm.

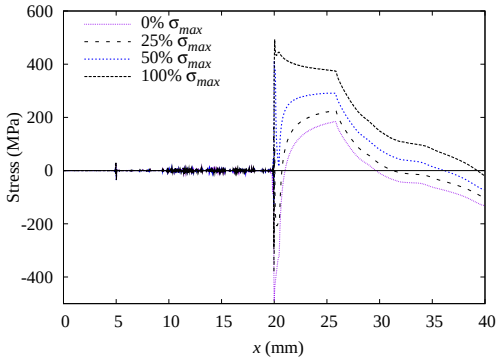

(d) Stresses at the crack tip with RS. Crack length =20 mm.

Figure 4.27: Stress at the crack tip.

4.4 Effect of residual stress on opening stress

4.4.1 Two opposite effects

Figure 4.28 show the effects of the crack closure in the classical case without the initial residual stress field.

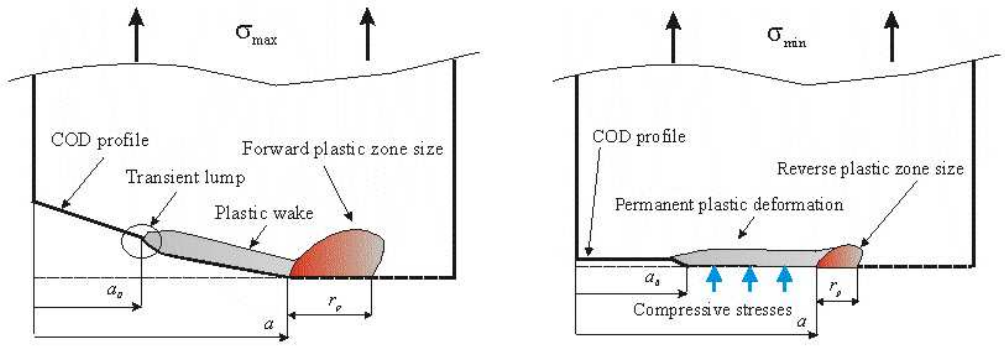

(a) Effects of plasticity on maximum applied stress.

(b) Effects of plasticity on minimum applied stress.

Figure 4.28: Plasticity induced crack closure.

The plastic wake is formed by the plastic deformation due to the plastic zone size during loading and unloading. This deformed profile of the crack opening displacement will produce compressive residual stresses under minimum load condition. It is important to remember this effect tends to fade with the increasing of the nominal stress R ratio because the minimum load can open the crack enough to diminish the effect of the compressive stresses due to the deformed COD profile. The crack opening stress is the main parameter. It is the applied stress which completely opens the crack and it can be established with the aforementioned methods discussed in chapter 3.

When initial weld residual stress occur, two opposite and separate effects can be distinguished. Figure 4.29 shows the two effects of a tensile residual stress field on crack closure. The first increases the plastic wake hence at a minimum load the compressive stresses which will arise will be higher compressive stresses because the COD profile is more deformed since higher strain have occurred. It has been established in section 4.3 that the evolution of the plastic zone size and plastic wake in presence of residual stresses has been found to increase for tensile residual stresses. This first effect increases the opening stress. Like overloading

this may affect the crack propagation because it increases the opening stress hence it diminishes the crack growth propagation by reducing the ΔK_{eff}. A bigger plastic zone size induces a bigger plastic wake which affects the opening stress by increasing the compressive stresses at the crack tip.

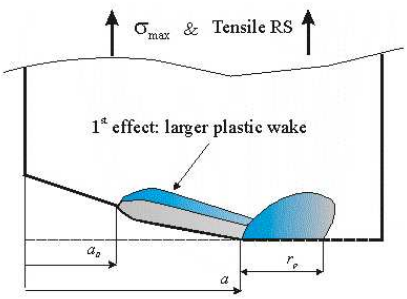

(a) First effect of tensile RS on maximum applied load.

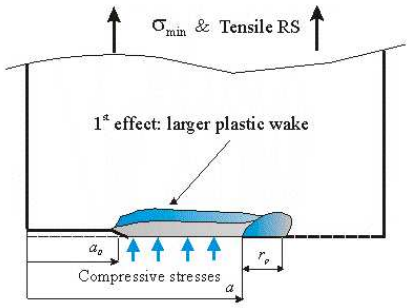

(b) First effect of tensile RS on minimum applied load.

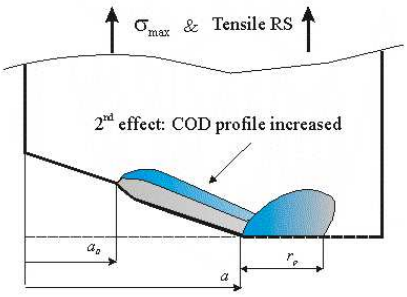

(c) Second effect of tensile RS on maximum applied load.

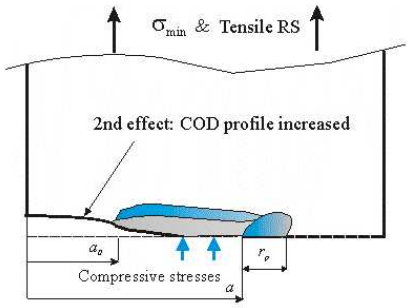

(d) Second effect of tensile RS on minimum applied load.

Figure 4.29: Two opposite effects of residual stresses on crack opening stress.

The second effect is not on the shape of the crack profile but on the magnitude. Tensile residual stresses that are above the crack line tent to open the crack hence they will reduce the compressive stresses and the value of the opening stress necessary to completely open the crack. This affects the opening stress profiles and consequently the stress ahead the crack tip. The opening stress necessary to transform the compressive stresses in tensile stresses will be lower i.e. a lower σ_{op}. The second effect decreases the opening stress.

The normilized opening stress is shown in figure 4.30 with and without RS. The solution calculated with the finite element agrees with the Newman equation in the case without RS. By accounting the weld residual stress field the opening stress decreases. The way at which decreases it is in according with the initial residual stress field. When the RS are around 100 MPa at 5 mm the value of

the opening stress is 0.3 while around 10 mm, when the RS decrease the opening stress value diminishes with a different slope. The lower value is for the higher peak of RS field, at 15 mm crack length with 150 MPa. The second effect discussed above is the dominant.

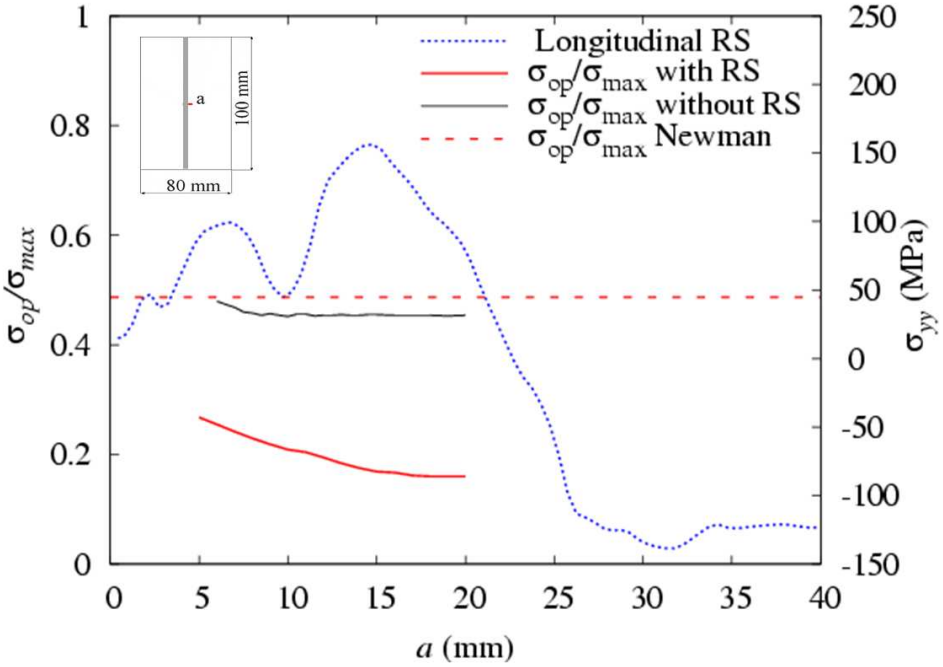

Figure 4.30: Opening stress level with and without RS.

4.4.2 Opening stress level in assumed constant residual stresses field

In order to establish the importance of the second effect on the crack closure and know how this will change the opening stress level, a study on different assumed constant balance RS fields has been performed. The configuration is shown in figure 4.31. Note that since half of the plate is assumed the moment is balanced. The crack propagates from 3 to 5.5 mm in two balanced tensile RS fields (+100/-100 MPa and +50/-50 MPa) and one compressive RS field (-25/+25 MPa). The applied maximum stress is 100 MPa and the R ratio is 0.

The profile of the displacement has a bigger transient lump because of high tensile RS and a smaller one for a compressive RS field (see figure 4.31). This confirms that for higher tensile RS the permanent plastic deformation is larger while

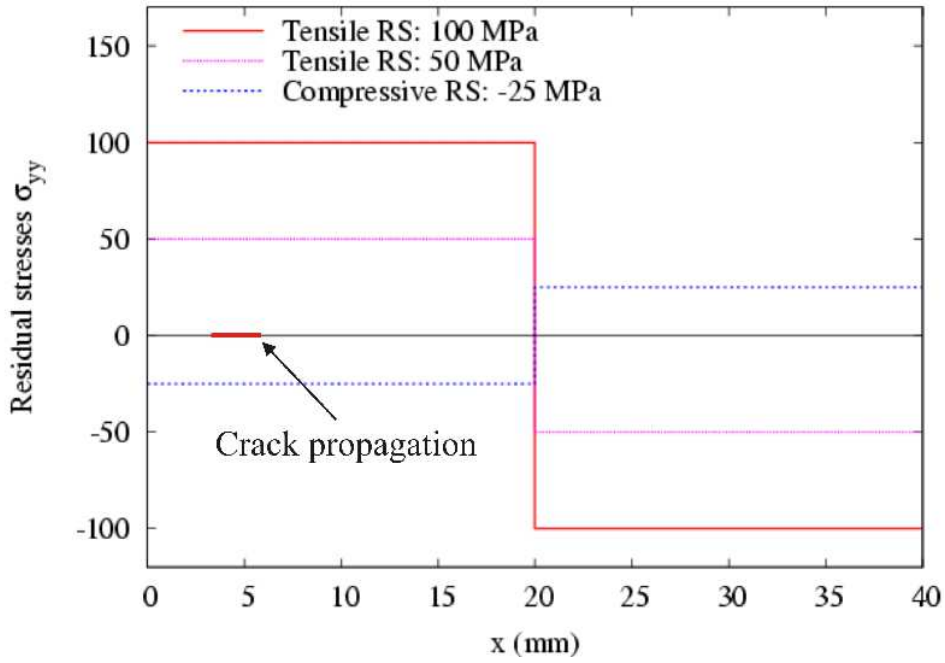

Figure 4.31: Distribution of constant balanced residual stress fields.

in compressive RS the deformation are lower than the RS free case. However the compressive stresses behind the crack tip are bigger because of the second effect of negative longitudinal RS (figure 4.32). The compressive RS field above the crack closes further the crack thus increases the negative stresses behind the crack tip. Figure 4.34 shows the different opening stress level for different assumed constant balanced RS field and it tells the importance of the stress field far from the crack tip which dominates the behaviour of the opening stress value. Figure 4.33 shows the stress distribution for the different residual stress fields in conditions of maximum loading with the respective COD. Note that behind the crack tip some numerical noise arise due the high stress gradient.

As it was shown previously the plastic zone size and the plastic wake at the tip have the same trend but when the crack grows within a tensile RS field they vary with a small difference of trend. When different RS fields are assumed the behaviour of the aforementioned variables is much more similar as the one shown in figure 4.35. In this case the plastic zone size and the plastic wake size at the tip have been evaluated for different constant residual stress fields with a crack length of 5 mm. The two parameters discussed are not changing linearly with the growing of the constant residual stress field. The table 4.2 shows the difference between the plastic zone size and the plastic wake size and the

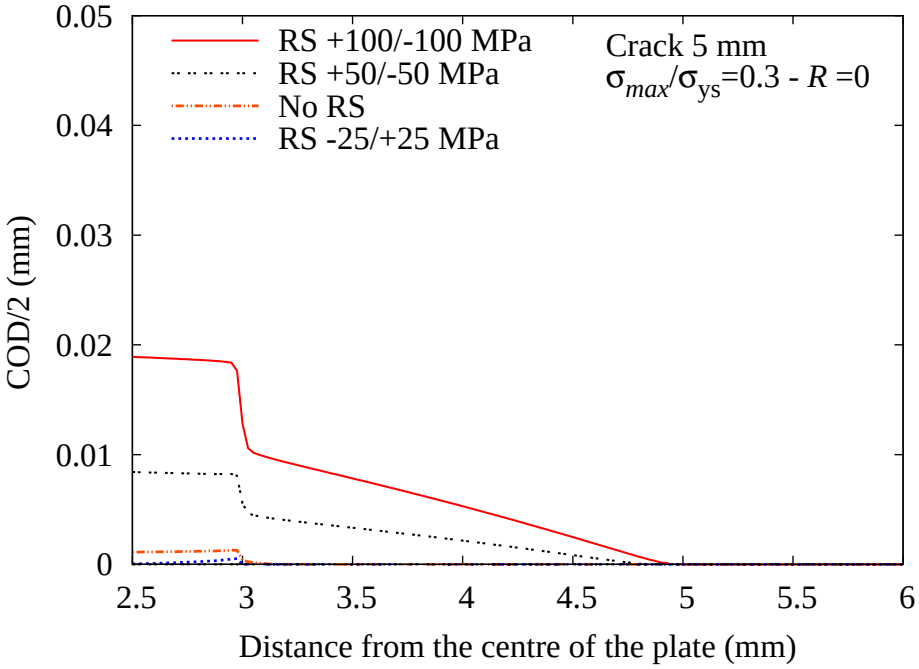

(a) Displacement at unload condition.

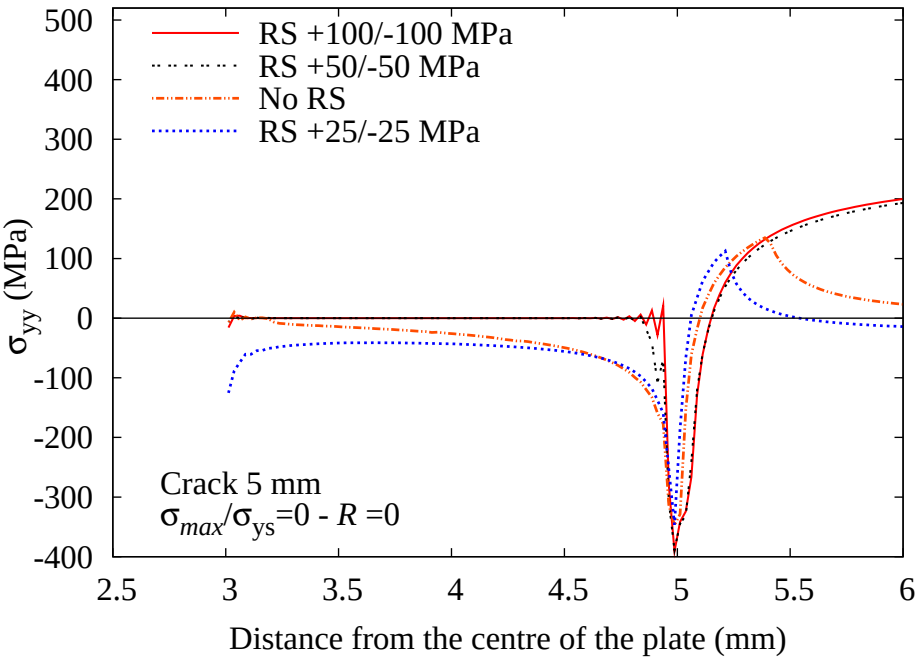

(b) Longitudinal stresses at unload condition.

Figure 4.32: Comparison of displacement and stresses for different constant balance RS field at unload condition.

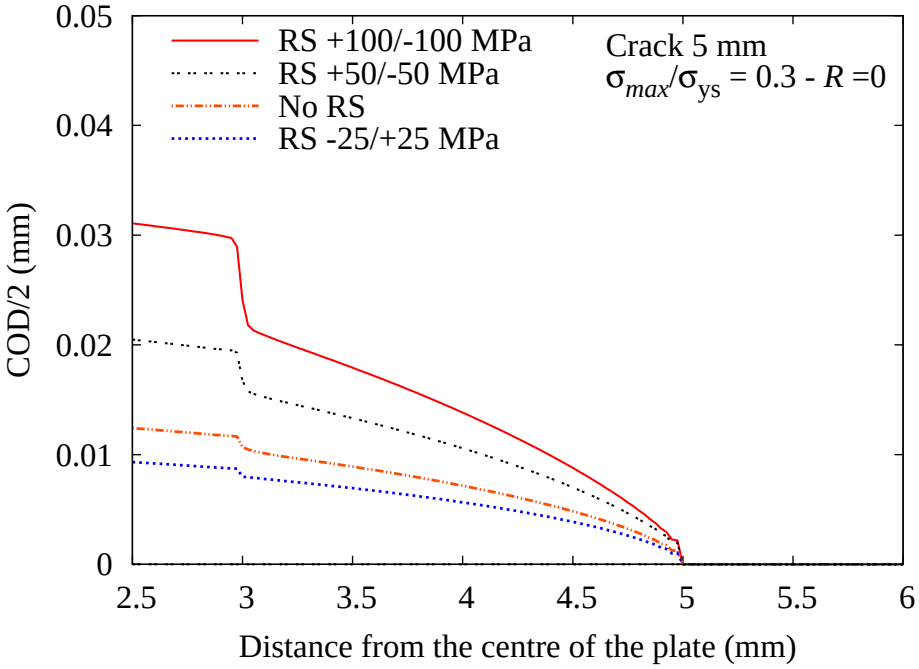

(a) Displacement at load condition.

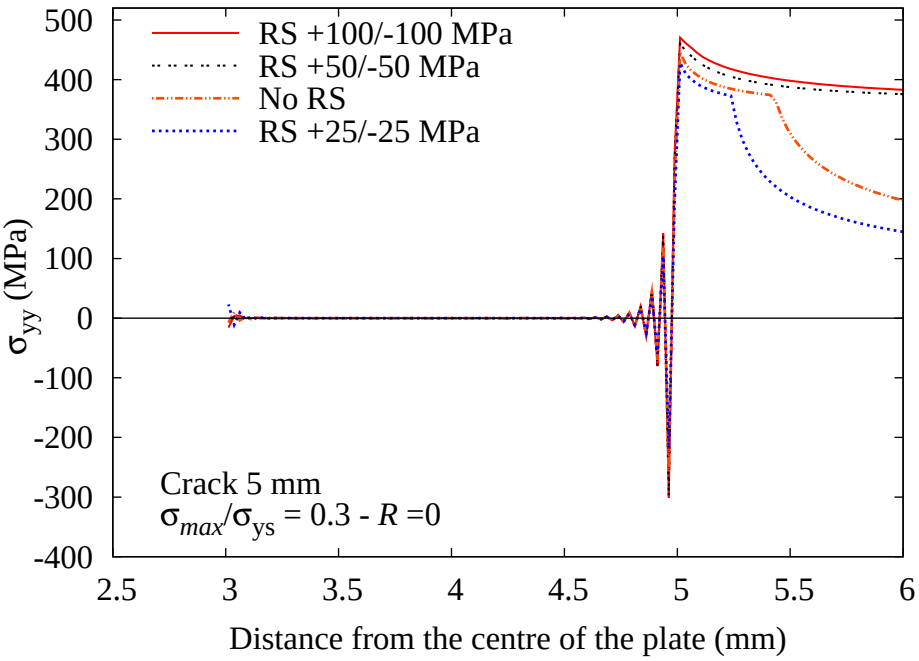

(b) Stresses at load condition.

Figure 4.33: Comparison of displacement and stresses for different constant balanced RS field at load condition.

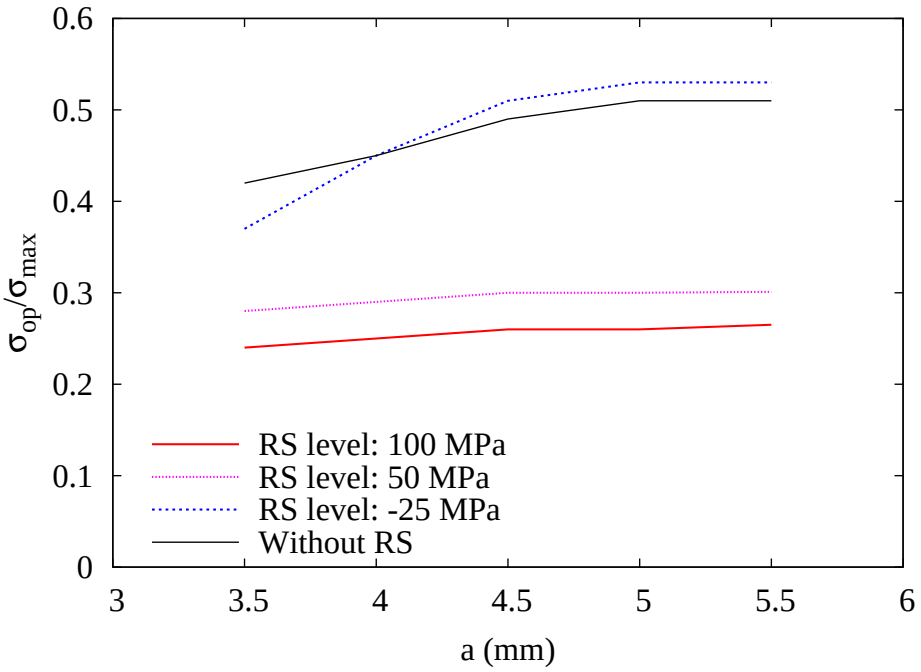

Figure 4.34: Opening stress level for different constant balanced RS field.

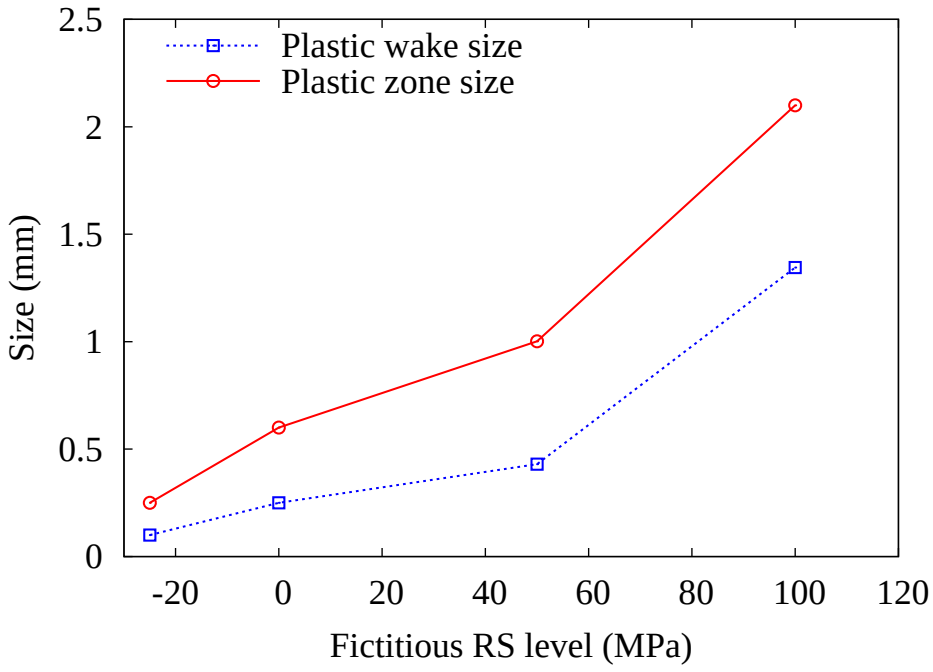

Figure 4.35: RS field effect on the plastic wake and plastic zone size.

difference decreases with increasing of residual stress field. When the difference is smaller the dimension of the plastic wake at the crack tip becomes closer to the large plastic zone size which is due to either high stresses both applied and residual or long crack length.

In this work plastic wake is considered to be the plastic strain ϵ_{yy} that defines the zone of the permanent plastic deformation. Table 4.2 shows that for higher tensile residual stresses the difference is smaller because the plastic wake increases. This is because the longitudinal residual stresses have a bigger influence on the longitudinal strain i.e. on the plastic wake. This is also the consequence of the non-homotetic transformation of the plastic zone with a residual stress field where the height of the plastic zone is more affected by the RS than the r_p.

Table 4.2: Percentage difference between forward plastic zone size and plastic wake.

RS field (MPa)	+100/-100	+50/-50	0	-25/+25
Difference	36%	57%	58%	60%

The trend of the increment of the forward plastic zone size is not proportional to initial RS field because of the material non-linearity assumptions.

4.5 Plasticity induced crack closure with compressive RS

This section explores the importance of the plasticity when the crack grows mainly in a compressive residual stress field. The evaluation of the opening stress value is mainly influenced by the second effect stated above which overcomes the first effect. For this reason the study of the stresses at the crack tip is less relevant hence the evaluation of σ_{op} is devoted to study the non-linear behaviour of the COD profile in order to understand RS influence on the crack growth driving parameter ΔK_{eff}. The test case assumed is an Eccentrically-Loaded Single Edge Crack Tension Specimen (ESE(T)) with a FSW measured distribution which is input in the FE and it is presented in figure 4.36. Further considerations on the measured value and the FE results will be given in chapter 5.

This section also gives an insight on the plastic zone size and strain for plane

strain conditions. This is because the study of the ESE(T) plate, like the C(T) is normally considered in plane strain condition because of the thickness of the specimen. The maximum applied load is 4300 N at a ratio R=0.1.

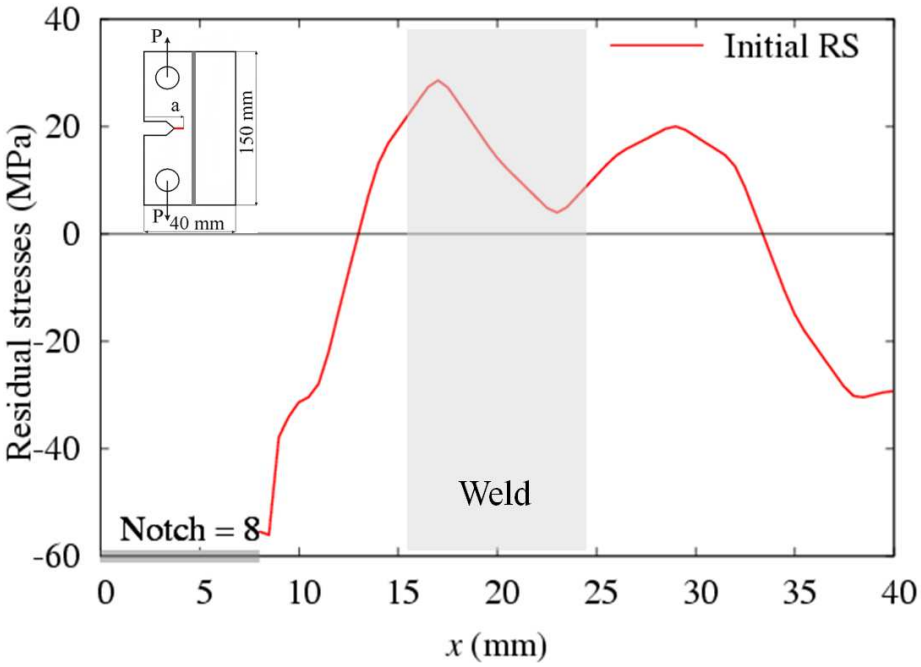

Figure 4.36: FSW ESE(T) distribution.

4.5.1 Crack closure model

The mesh used is shown in figure 4.37 where the smallest element is 0.0125 mm. The finest mesh needs to be all along the crack propagation line in order to obtain the opening stress at different crack length. For the ESE(T) or C(T) specimen it is common to assume the plane strain condition because of their thickness [40]. The elements used for this analysis are the plane strain elements PE4R from ABAQUS. From the ratio of the plastic zone size to the thickness, it is possible to define a criterion to distinguish the plane stress and the plane strain condition. According to Broek [32] it has been found experimentally that when the ratio is greater than 0.025, then plane stress condition can be assumed.

$$\frac{r_p}{t} < 0.025 \quad \text{(plane strain)} \tag{4.6}$$

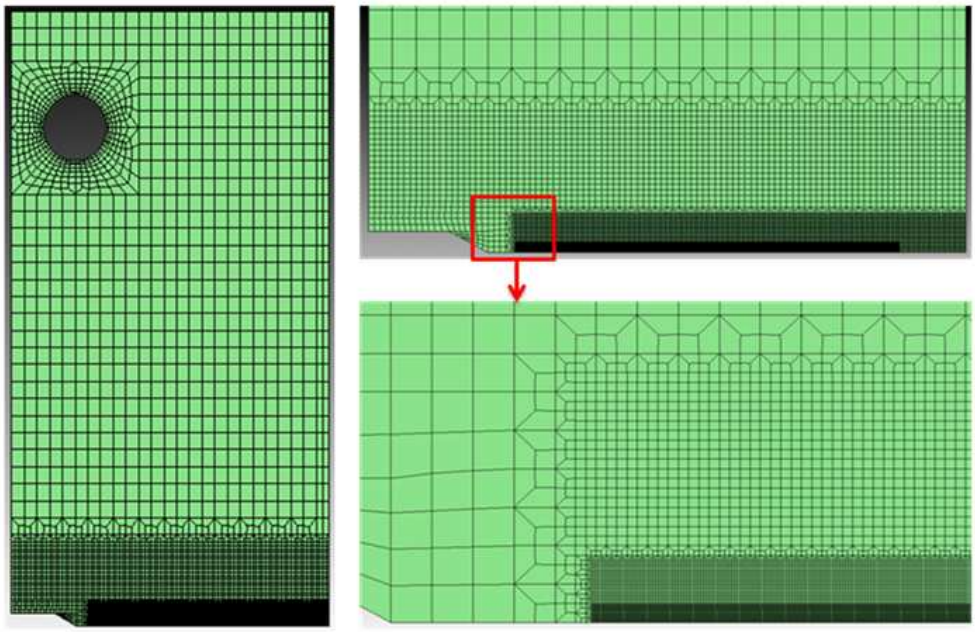

Figure 4.37: Mesh used for the elasto-plastic model.

The plastic zone size can be calculated by the following equations:

$$r_p = \frac{1}{3\pi}\left(\frac{\Delta K}{\sigma_{ys}}\right)^2 \quad \text{(for plane strain conditions)} \tag{4.7}$$

By using the previous equations, for mentioned load condition and geometry, the plastic zone size for a crack length of 16 mm is r_p =0.0415 mm for (plane stress condition) => $\frac{r_p}{t} = 0.00518 < 0.025$. The value of the ratio is lower than 0.025; for this reason plane strain elements have been used.

In order to verify the plastic zone size close to the crack tip, stress contour maps, by means of the iso-stress line via von Mises stress, show the shape of the plastic zone at a crack length 16 mm with and without residual stresses. Figures 4.38 and 4.39 show the plastic zone size for the case without and with residual stress respectively. Without residual stresses the plastic zone size is much lower than the case of plane stress conditions. There is also a similar error: the FE analysis undervalues the plastic zone size by 10% which is similar to that one found for plane stress element (i.e. 8% to 9 %). The compressive residual stresses decrease the plastic zone size as previously stated because of the first effect of RS. It was shown in section 4.1 that by changing the yielding stress the plastic zone size change with an homothety transformation but this does not hold anymore when

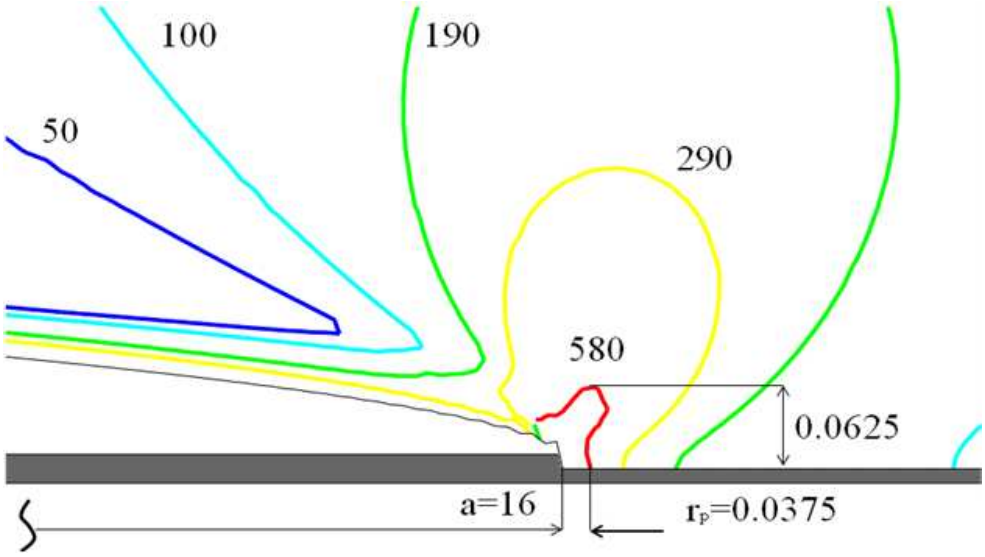

Figure 4.38: Iso-stress contour map at crack length 16 mm without RS (unit = MPa, mm).

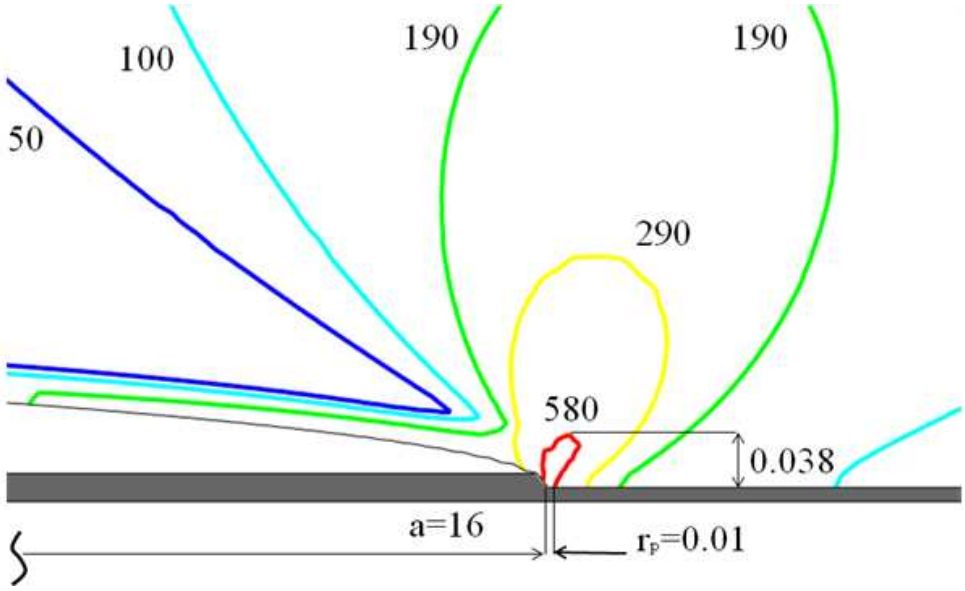

Figure 4.39: Iso-stress contour map at crack length 16 with RS (unit = MPa, mm).

initial residual stresses occur, both in plane stress and in plan strain conditions. Behind the crack tip there are non-zero von Mises stresses at the free edge, which indicates that plasticity occur and a plastic wake developed. Because of the first effect of RS the von Mises stresses are higher in the case of the parent plate.

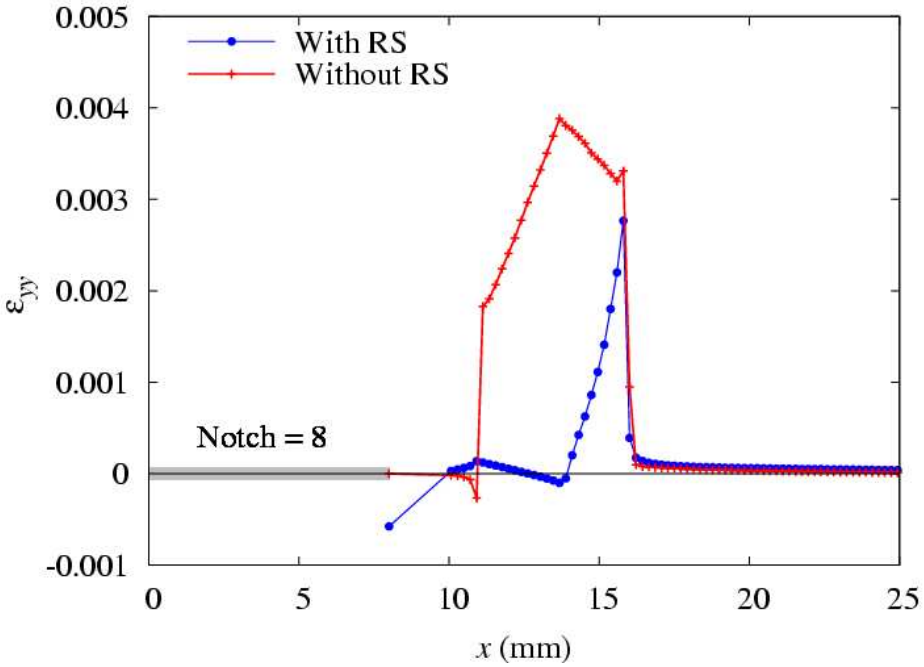

Figure 4.40: Comparison of the y-axis strains with and without residual stresses at crack length 16 mm at unload conditions.

In order to better assess the plastic wake developed in a compressive residual stresses with plane strain elements the y-axis strain components are calculated (see figure 4.40). Without RS after 14 mm the strains decrease because the plastic zone size is bigger and hence the strain gradient is shared with more elements i.e. the formation of the plastic wake tents to decrease. From other previous calculation of the strain shown in this chapter, it is possible to see a variation of the level of the permanent plastic deformation. The main responsible is the size of the mesh since the plastic zone is 0.03 mm when the elements is 0.0125 mm. The discontinuity ϵ_{yy} strain in the plastic wake was also found in section 4.1. With compressive welding residual stresses the plastic strain formation is negligible from 11 to 14 mm, but it is relevant after this point where the plastic wake start to develop. Also for plain strain elements the plastic wake develops but the compressive residual stresses decrease relevantly its formation.

4.5.2 Crack opening displacement and longitudinal stresses

The occurrence of residual stresses makes the problem nonlinear: compressive stresses act on the profile of the opened crack partially closing the crack itself. The crack opening displacement (COD) profiles will show the phenomenon. A first comparison of the COD of a parent plate with the welded plate shows that the compressive residual stresses decreases the COD as expected (see figure 4.41 and 4.42). The stress at the notch tip decreases of 50%, while at minimum load condition the crack is partially closed for the welded case. The typical parabolic shape of the COD without RS is deformed by the weld residual stresses. Since more compressive stresses arise close to the notch tip, the critical area where the opening stress will be evaluated is at that point, i.e. the last node that will likely detach.

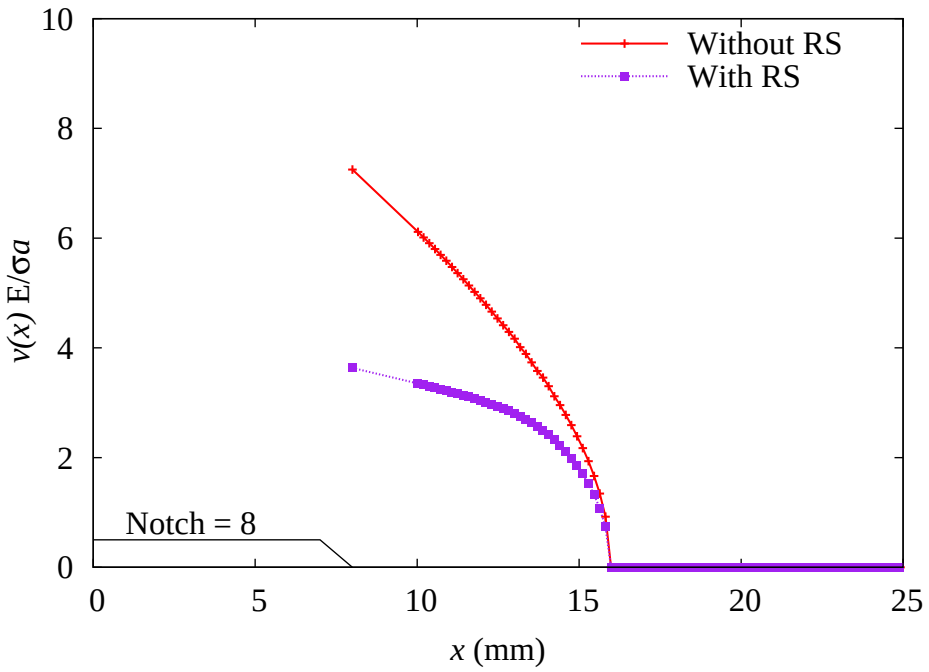

Figure 4.41: Comparison of the normalised COD with and without RS at maximum load.

The COD for different crack length shows that when the crack propagate the COD tent to increase at its maximum load but is still partially closed for longer crack length (see figure 4.43 and 4.44). For a crack length of 12 mm it is completely closed even if a minimum load of 430 N is applied. The aim of this analysis is to find what is the load that open completely the crack. The method herein used is by using the last node detached i.e. the node ahead the notch

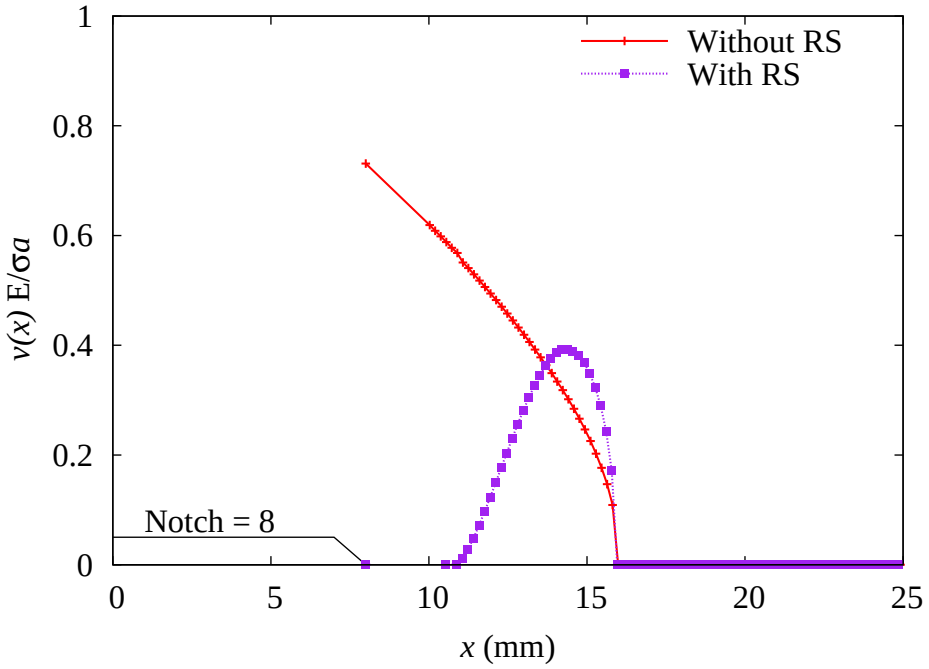

Figure 4.42: Comparison of the normalised COD with and without RS at minimum load.

tip. Figures 4.45 and 4.47 shows the different percentage of the load and the correspondent stresses are plotted in figure 4.46 and 4.48. The free surface of the crack shows zero longitudinal stresses while when the crack is closed compressive stresses arise. The longitudinal stresses are monitored for different applied load in order to find the actual opening stress value hence to find the effective stress intensity factor range ΔK_{eff}.

The FE analysis provides a discrete frame for each cycled load. The load is applied every 10% of the maximum load. In this way it is possible to obtain the opening stress value as the stress applied in order to have zero longitudinal stress at the last detached node close to the notch. The opening stress value obtained is given in figure 4.49. The cases with and without RS, both with elastic-plastic material, are compared. Without RS the opening stress value reaches stability only at 23 mm of crack length when the value is very close to the Newman equation. The plastic zone size is not large enough to induce the formation of the plastic wake and the reverse plastic zone size. In plane strain conditions the effect of the closure induced by plasticity at R=0.1 with 4300 N applied load, is not large enough to have an important formation of the plastic wake which induces the opening level to change. Only at 23 mm, when the crack is growing the plastic

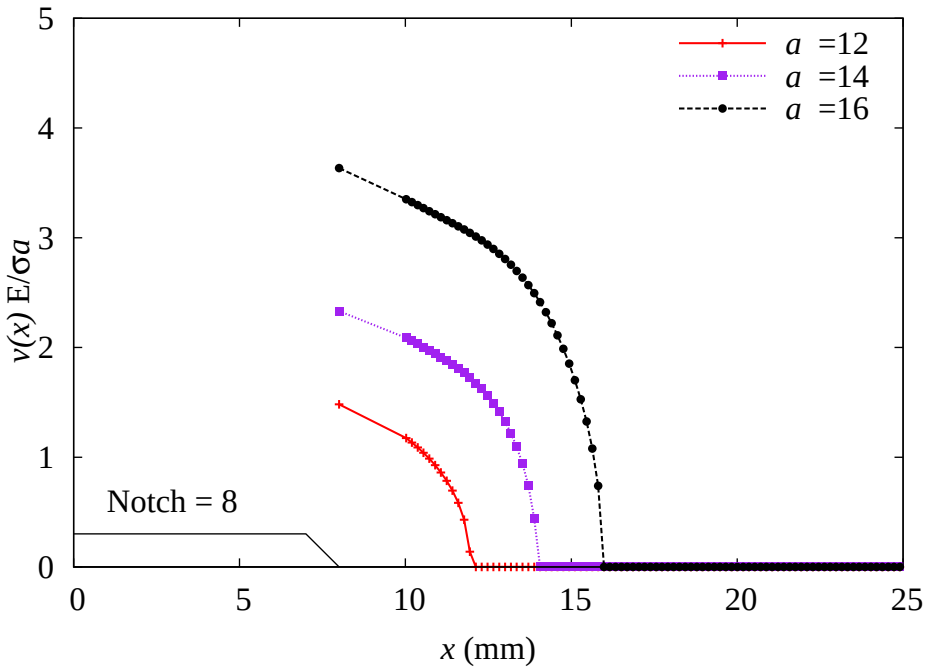

Figure 4.43: Normalised COD at maximum load at different crack length with RS.

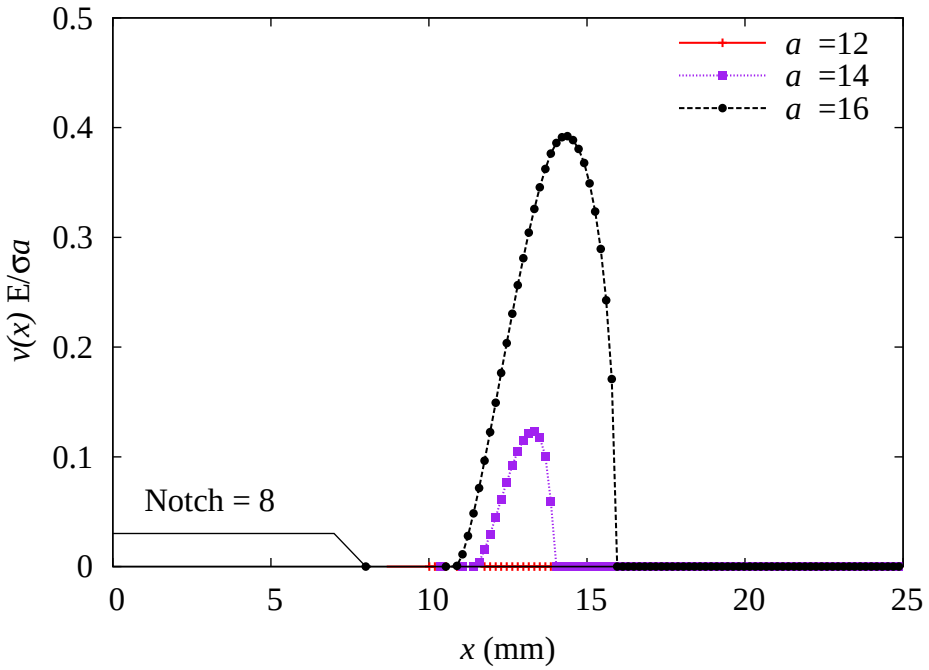

Figure 4.44: Normalised COD at minimum load at different crack length with RS.

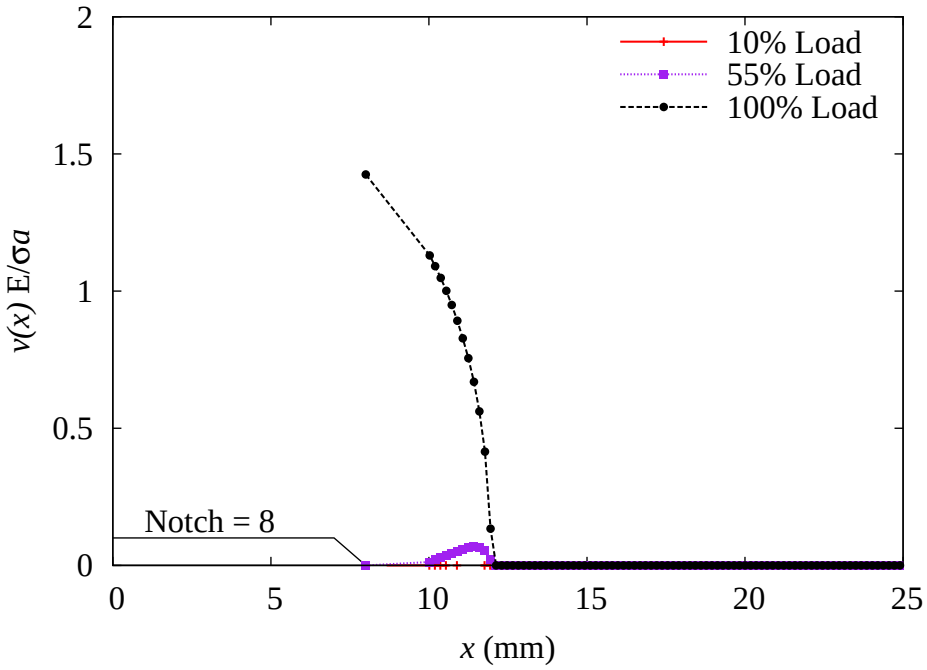

Figure 4.45: Normalised COD at different percentage of the load at crack length 12 mm.

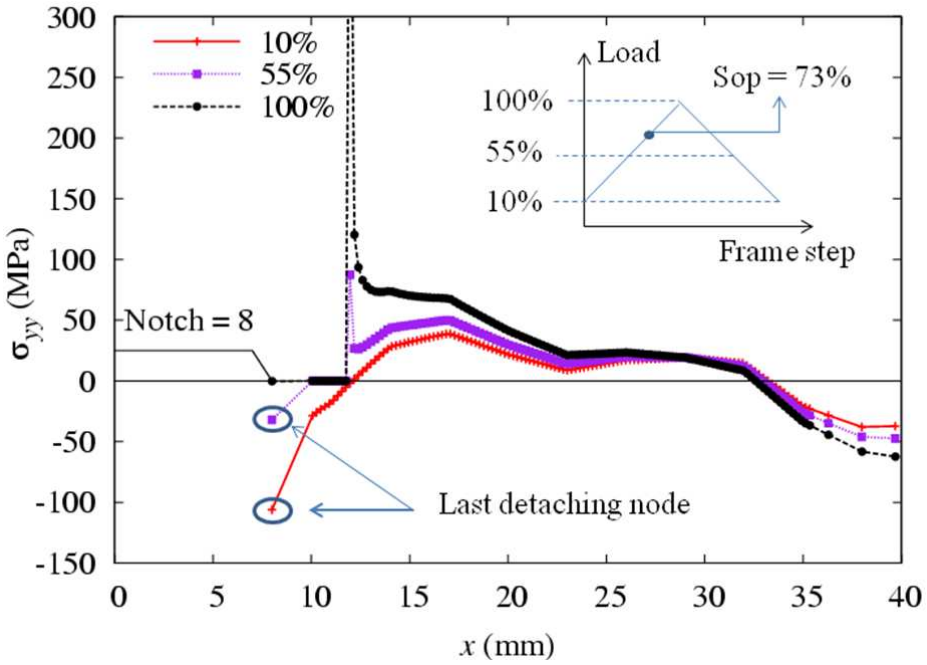

Figure 4.46: Different percentage of the longitudinal stresses at a crack length 12 mm.

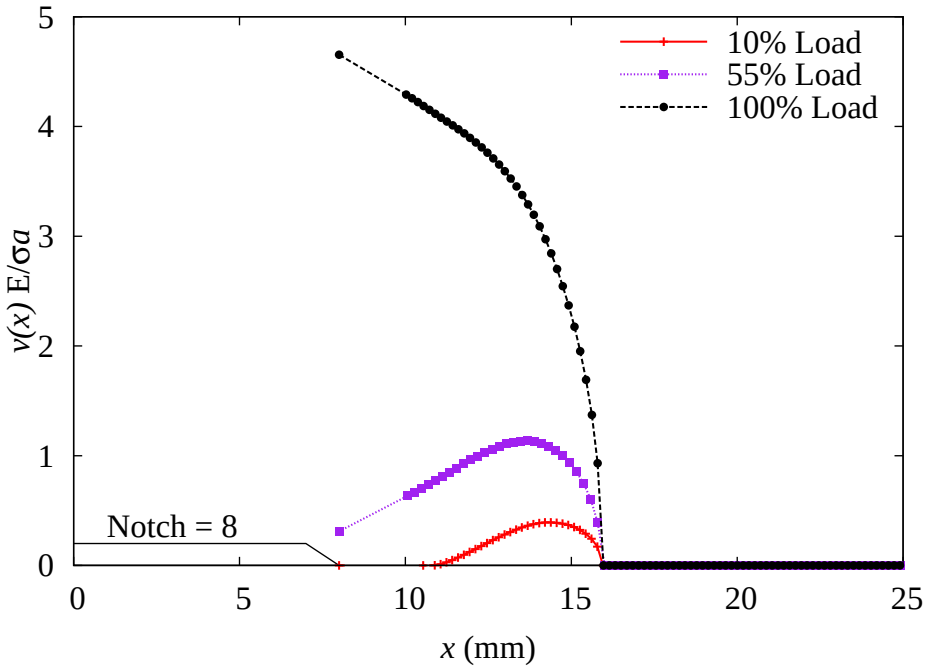

Figure 4.47: Different percentage of the normalised COD at a crack length 16 mm.

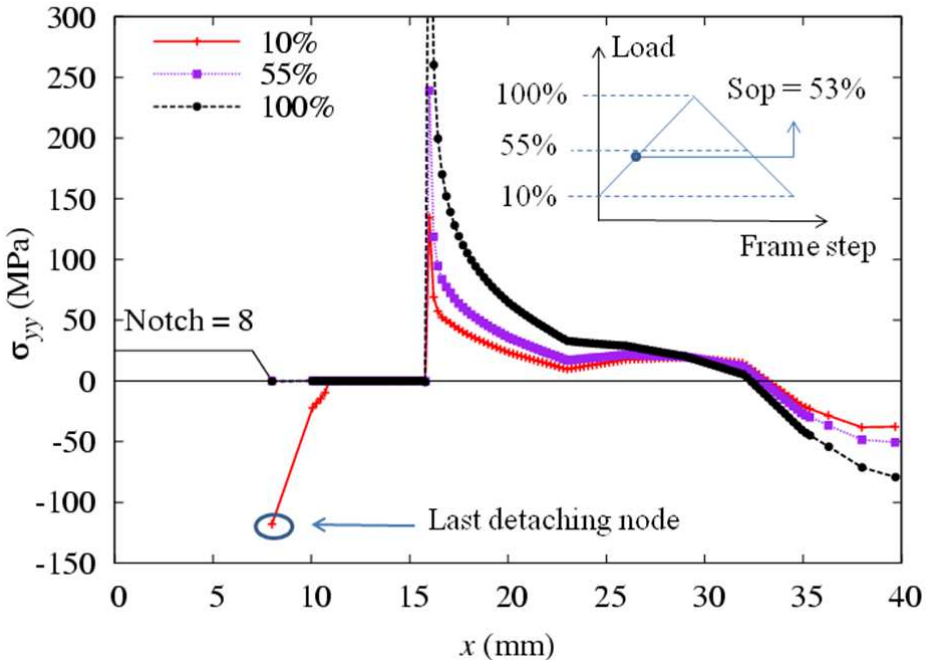

Figure 4.48: Different percentage of the longitudinal stresses at a crack length 16 mm.

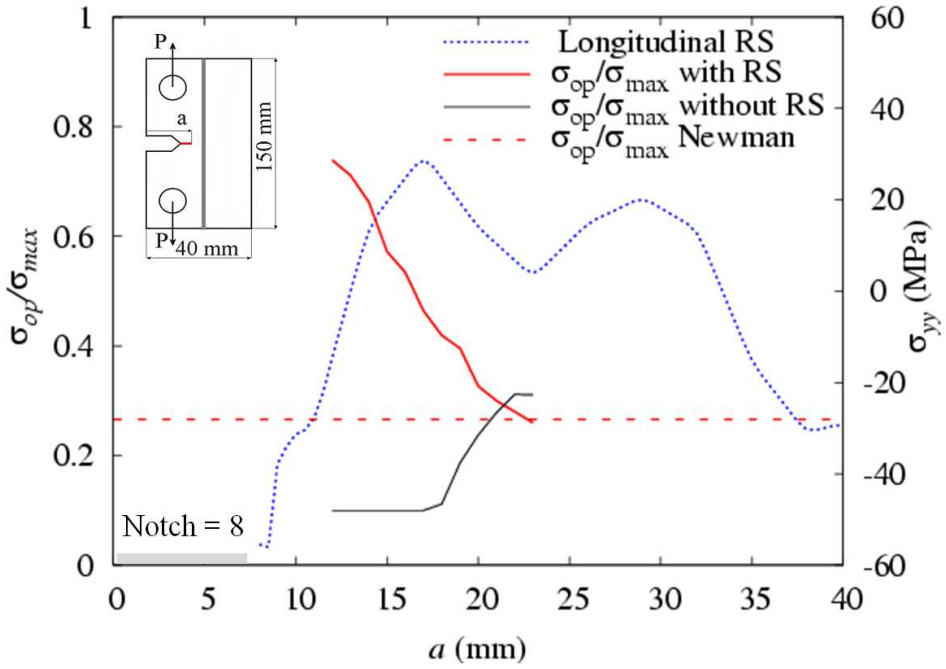

Figure 4.49: Opening stress with and without RS.

zone size becomes large enough, the value of the opening stress is changed by the occurrence of the plastic wake formation. At this point the first effect of the RS can be relevant, but the RS magnitude at this crack length is not high so the second effect of RS is dominant throughout the whole crack propagation. The case with RS which is obtained by considering the dominance of the second effect shows that the opening stress is very high when compressive stresses arise while when they decrease and become tensile the normalised σ_{op} decreases. Such behaviour influences the fatigue crack propagation via the driving force ΔK_{eff}. Those effects will be discussed in details in the next chapter.

4.6 Summary of the chapter

A crack closure model was successfully built and validated, for a case without RS, by comparing the outcome with analytical σ_{op} value. Similar results in terms of opening stress level were achieved and good results in crack opening displacement compared to the theory with error less than 2%.

The crack opening stress is history dependent because it depends on the previous residual stress field. For this reason a FEA for the full crack length path is

necessary. The evolution of the plastic material model is also provided showing the effect of the material plastic model. From the history of the stress and strain it was shown that elements ahead the crack tip have plastic deformation which contributes significatively to the formation of the plastic wake when the crack is longer. The study on the re-distribution of the initial weld residual stress establish that the re-distribution is mainly close to the crack propagation line while away from it the initial RS field is affected by minor changes. The re-distribution of plastic material model showed a better agreement of the measured data, with respect to the elastic material, in the area close to the crack tip.

This study achieved understanding on the mechanism of closure with RS field and it identifies the influence of residual stresses with assumed distributions of different signs and magnitudes. The classical parameters involved during the assessment of a plasticity induced crack closure analysis are compared for the cases with and without weld residual stresses. The plastic wake the plastic strain area develops following the trend of the residual stresses field. The plastic zone size influence the formation of the plastic wake in occurrence of a RS field. This changes the profile of the COD that will affect the stresses at the crack tip. Tensile residual stresses increase the crack opening displacement, the plastic wake but not the compressive stresses before the crack tip which are instead confined to a very small area close to the crack tip. Those effects will influence the opening stress level of residual stresses.

Two opposite effects have been found to drive the opening stress level through a tensile RS field. The first causes an increase in the σ_{op} because the increased plastic wake i.e. the plastic deformation increase the compressive stresses. The second is due to the stresses far from the crack tip that overcomes the previous effect and open the crack, thus it decreases the σ_{op}. This effect has been found to be the dominant. For this reason the opening stress level decreases in a tensile RS field. In a compressive RS field the second effect is still dominant but it will increase the σ_{op}. The second effect on the COD profile has a similar effect of increasing the nominal ratio i.e. decrease the crack opening stress. This dominance is also explained by the minor changes in the redistribution of the residual stresses away from the crack propagation. The σ_{op} decreases from a value which is close to 0.5 to 0.3 for the VPPA residual stress distribution. A quantification for cases with constant balanced residual stresses show the trend of the opening stress level which decreases when the RS are tensile while increases

when the RS are compressive.

The last section investigates the effects of the plasticity when the crack grows mainly in a compressive residual stress field. The crack tip plasticity was found to have a small relevance because of the load condition, 4300 N load at R=0.1, and because of the plane strain conditions. The opening stress level values is provided and it confirms that for compressive RS the σ_{op} values are larger while they decrease when the RS field becomes tensile.

Chapter 5

Predicting fatigue crack growth in weld residual stress fields

The aim of this chapter is to discuss the prediction methodology proposed in chapter 3 for two different test cases i.e. two different residual stress fields, in order to understand the effects of the weld RS on the fatigue crack propagation. Two methods have been used: the superposition and the crack closure approach. Chapter 4 presented the effects of plasticity with respect to the opening stress value σ_{op} that determines the fatigue crack grow driving force ΔK_{eff}. The latter is used in the crack closure approach that is assessed and compared with the superposition method for the different test cases. The objectives of this chapter are: to compare the two approaches; to assess the FCG laws, corrected with the R_{eff}, in terms of accuracy and versatility; to investigate the influence of the plasticity by meaning of the σ_{op}.

The first case, discussed in section 5.1, is a M(T) specimen where the crack grows from the weld i.e. the crack propagates mainly in a tensile residual stress field. The superposition method is compared with test results of constant amplitude load and constant stress intensity factor range. Also the residual stress field was found in the literature [27, 132, 146].

The second is an ESE(T) where the crack grows towards the weld i.e. the crack propagates mainly in a compressive residual stress field. The prediction results were compared with the experimental tests. Both fatigue crack growth data and measured residual stresses were provided by the project.

5.1 Crack growing from the weld

5.1.1 Problem statement: M(T) specimen

A classical configuration with a single weld in the centre is herein presented. Two load cases have been studied: constant amplitude load and constant stress intensity factor range.

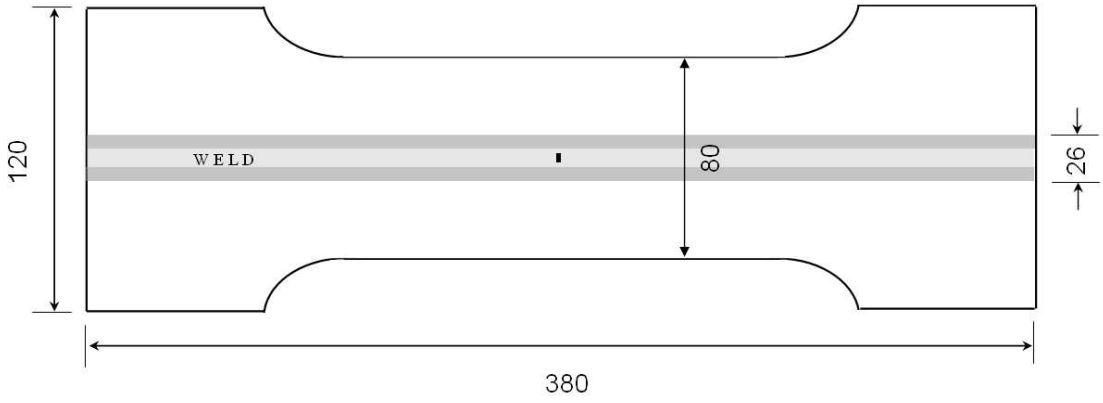

Figure 5.1: Sketch of the M(T) test sample.

Test sample in figure 5.1 was used in this study as presented elsewhere by the author [133]. It is a middle-crack tension, M(T), geometry made of aluminium alloy 2024-T351. The same test case with experimental data were from [27]. The sample contains a longitudinal weld by single pass autogenous variable polarity plasma arc (VPPA) welding process. Base material properties are $E = 73$ GPa, yield and ultimate tensile strengths 372 and 470 MPa, respectively.

In [24, 27], the neutron diffraction technique was used to measure the welding residual strains in the longitudinal, transverse and normal directions, which were subsequently converted to the corresponding residual stresses in each of the three directions. This initial residual stress filed is self-balanced and exists before any external mechanical loads being applied to the specimen and prior to the introduction of an initial crack. Many researchers have developed methods to input residual stresses into the FE models [27]. In this study two approaches were adopted, i.e. inputting equivalent initial displacements and inputting measured residual stresses. In the first method, initial displacements were determined from measured residual strains in both the longitudinal and transverse directions.

These displacements were then inputted into the FE model as an initial condition by a subroutine interfacing the ABAQUS code. From these initially applied displacements a distribution of residual stresses is imposed to the FE model. In the second method, measured residual stress distribution was inputted into the FE model using an ABAQUS subroutine named SIGINI. After inputting the stresses, ABAQUS command "UNBALANCED STRESSES" was called to balance the inputted stresses to satisfy the equilibrium condition. It is also necessary to relax the stresses under the equilibrium condition to make the stress-free condition at the free edges. Without external loads, the specimen is self-balanced under the initial residual stress filed.

Fig. 3.6 in chapter 3 shows the inputted residual stresses by both methods, which are in good agreement with the measured data published in [27]. Directly inputting residual stresses matches the experimental data better than inputting equivalent initial displacements. Since each node must be constrained for the displacement input method, this method cannot be used to model residual stress re-distribution during crack growth. The stress input method is a better approach because the condition of the virtual work principle is satisfied and the evolution of the residual stresses due to crack extension can be modelled.

5.1.2 Evaluation of the K_{res} and R_{eff}

Figure 5.2 shows the redistribution of residual stresses for different crack lengths and comparison with measured data in [27]. Since the FE analysis was linear elastic, there is a peak in the calculated stress distribution near the crack tip position that is much higher than the measured value due to the stress singularity effect. Such peak stress is dependent on the FE mesh size. In the crack tip zone, the comparison with the experimental data is poor. However, away from the crack tip region the calculated residual stress distribution due to crack extension agrees with the measured values. The discrepancy in the crack-tip stress values should not affect the fracture mechanics analysis conducted in this study, since the SIF was calculated indirectly from the strain energy release rate.

Figure 5.3 shows the K_{res} calculated by the VCCT. The K_{res} follows the trend of the initial residual stress distribution with a small delay. While the residual stresses reach their peak at 14 mm distance from the centre of the plate, the K_{res} reach its peak at 20 mm. Beyond this point K_{res} decreases as the residual

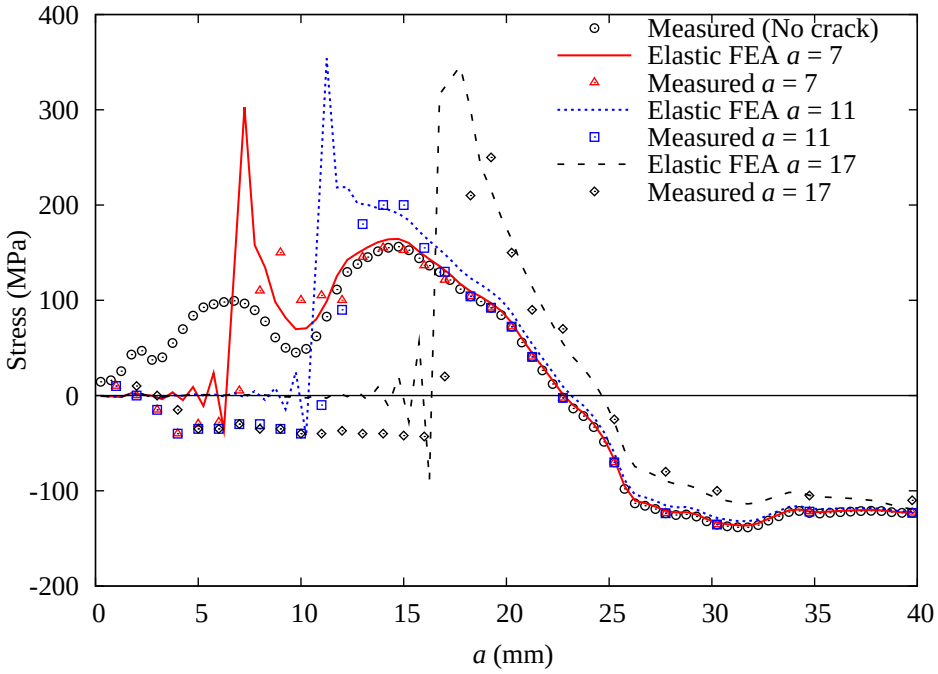

Figure 5.2: Redistribution of RS on the crack line.

stresses tend to become compressive. The delay is caused by the RS field above the crack propagation line which is still tensile and tent to open the crack causing such delay in the residual stress intensity factor.

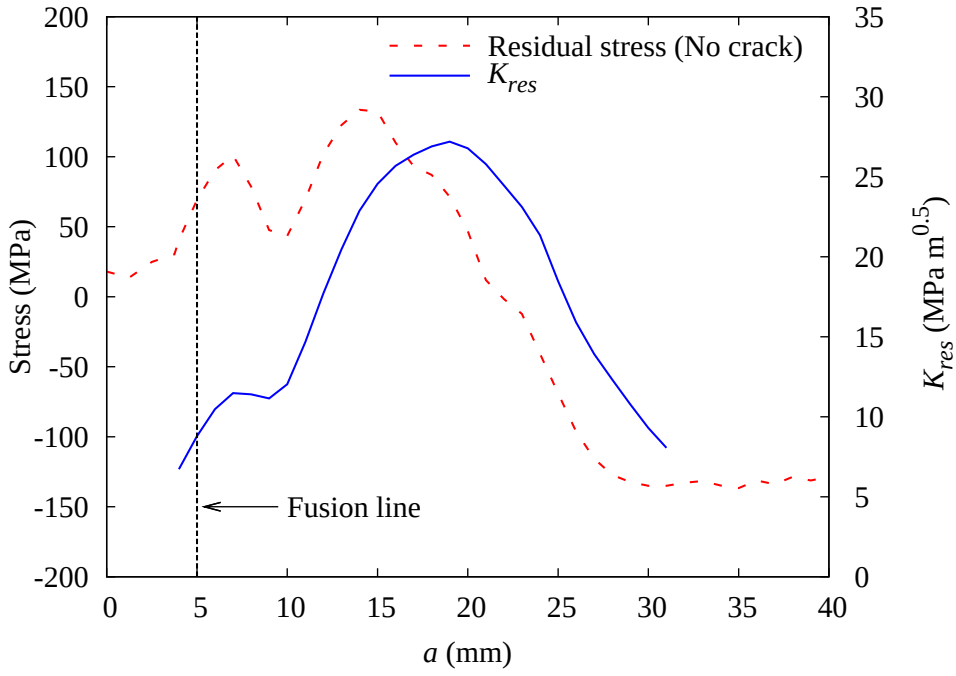

Figure 5.3: Calculated K_{res} for the VPPA residual stress distribution.

5.1.3 Constant amplitude load

The load case of this section is constant amplitude load, with a ratio R=0.1 and a maximum stress σ_{max}=51.5 MPa. Three different material laws have been implemented: Walker, NASGRO equations and Harter-T method. The values of the material constants used in this work are in table 3.1 in chapter 3. For further details on the Walker and NASGRO equations see the AFGROW manual [37].

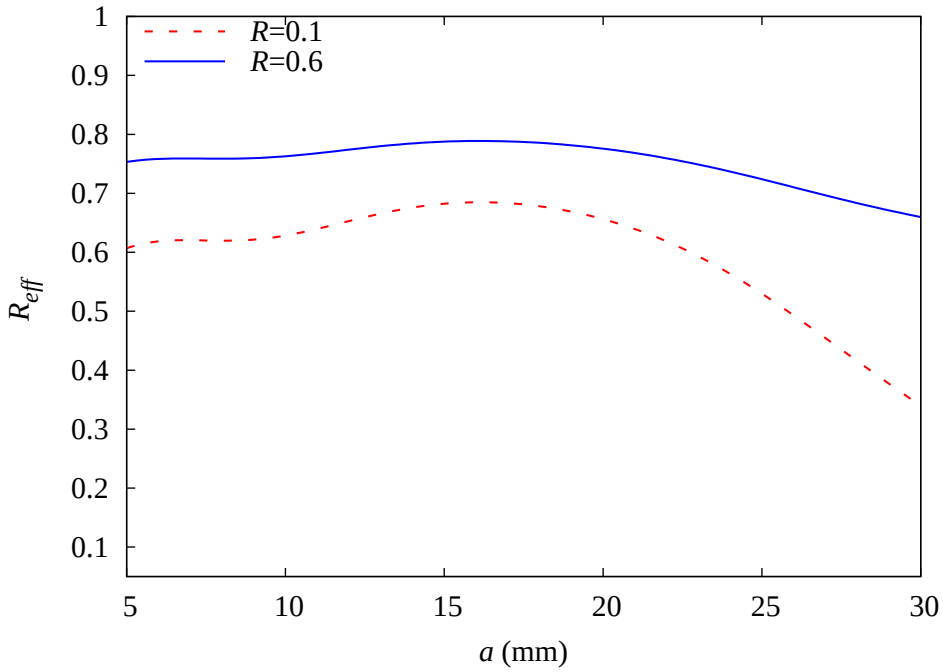

Figure 5.4: R_{eff} for the constant amplitude load.

Figure 5.4 shows the difference of the effective ratio for the two different nominal ratios of R=0.1 and 0.6. The first is more sensitive to the tensile residual stresses where the values go from the nominal 0.1 up to 0.6, which is an increment of 500%. The second case the increment is about 16% of the nominal case; the tensile residual stresses are less effective for higher ratios. In this work welding residual stress effect was accounted for by replacing the nominal R ratio with the effective ratio R_{eff}, which is a function of the K_{res} that can be determined by using WFM and FEM which can take into account the redistribution of the RS with the crack growth.

With this R_{eff} (which equation is explained in chapter 3), three well-known empirical laws were tested. Walker equation has an appealing advantage for

predicting FCG rates in residual stress fields. The limitation of the Walker equation is that it is too simplistic and it underestimates the final part of the FCG rates when the SIF approaches the material fracture toughness. Harter-T method is a good prediction law as described in chapter 3. All one needs to have is a set of measured da/dN data for two different R ratios for the base material. Although the crack closure effect on da/dN can be accounted for by the R ratio to a certain extent, further correlation of da/dN with another parameter should yield more accurate prediction as demonstrated in the results in the comparison with the experimental data. NASGRO equation also takes account of the final fast crack growth stage when K_{max} approaches K_{crit}.

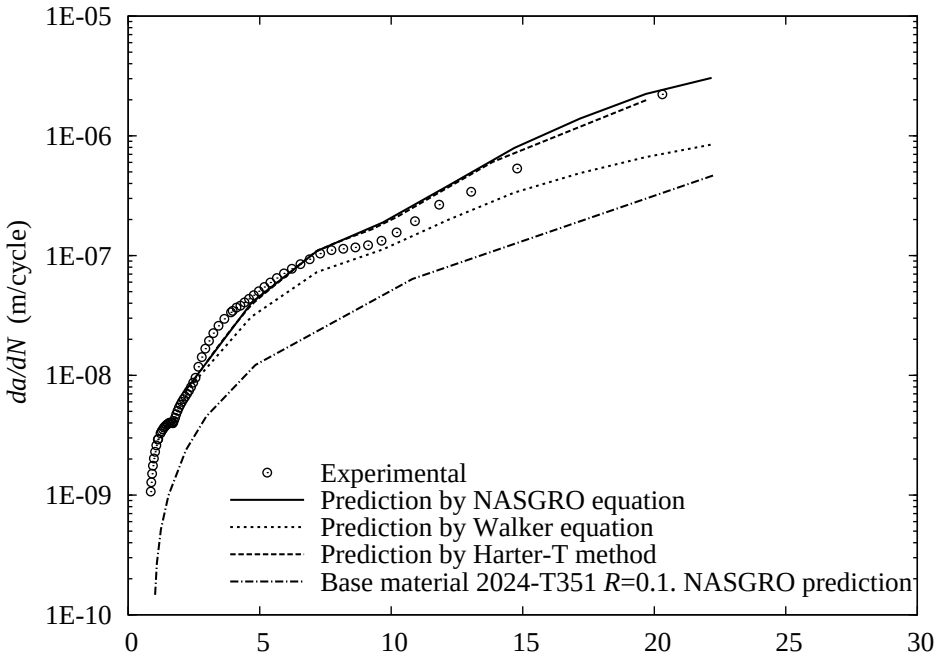

Figure 5.5: Comparison of predicted and measured FCG rates under constant amplitude load: nominal $R = 0.1$.

Fig. 5.5 shows the predicted FCG rates for $R = 0.1$ case with constant applied stress range of 46.35 MPa. For comparison the base material crack growth rate is also shown which was calculated by the NASGRO equation. For the welded joint, both NASGRO and Harter T-method give good predictions with typical error range of 5% between the predicted and measured. Walker equation underestimates the FCG rate considerably when half crack length a >17 mm with typical error range of 15-30%. Fig. 5.5 shows the $R = 0.6$ case with applied stress range of 42.6 MPa. For this test, the Harter-T method and NASGRO give good predictions. Walker equation gives good prediction when $a < 17$ mm. It

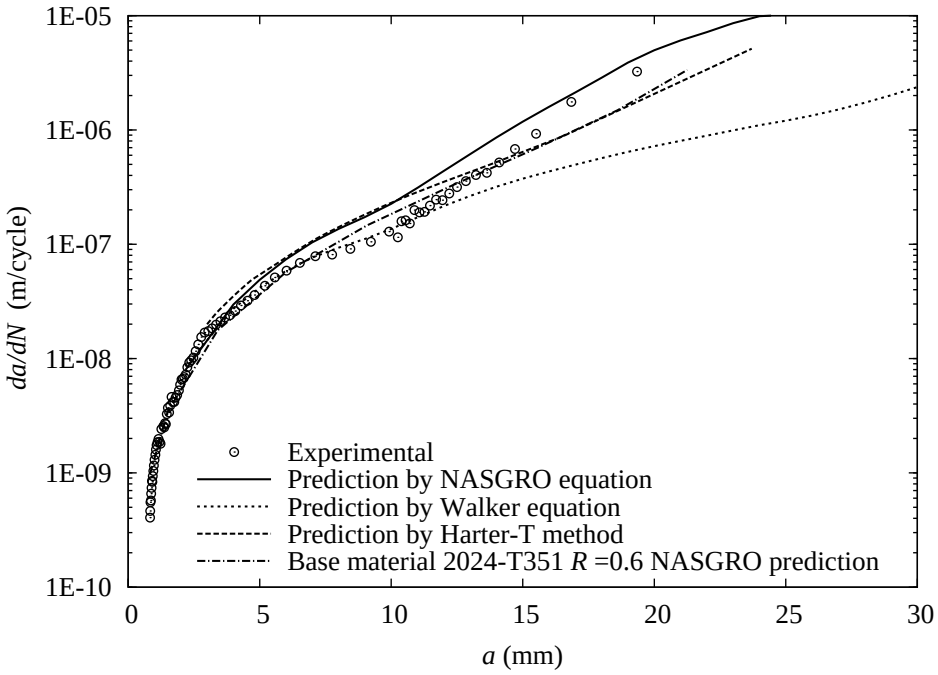

Figure 5.6: Comparison of predicted and measured FCG rates under constant amplitude load: nominal $R = 0.6$.

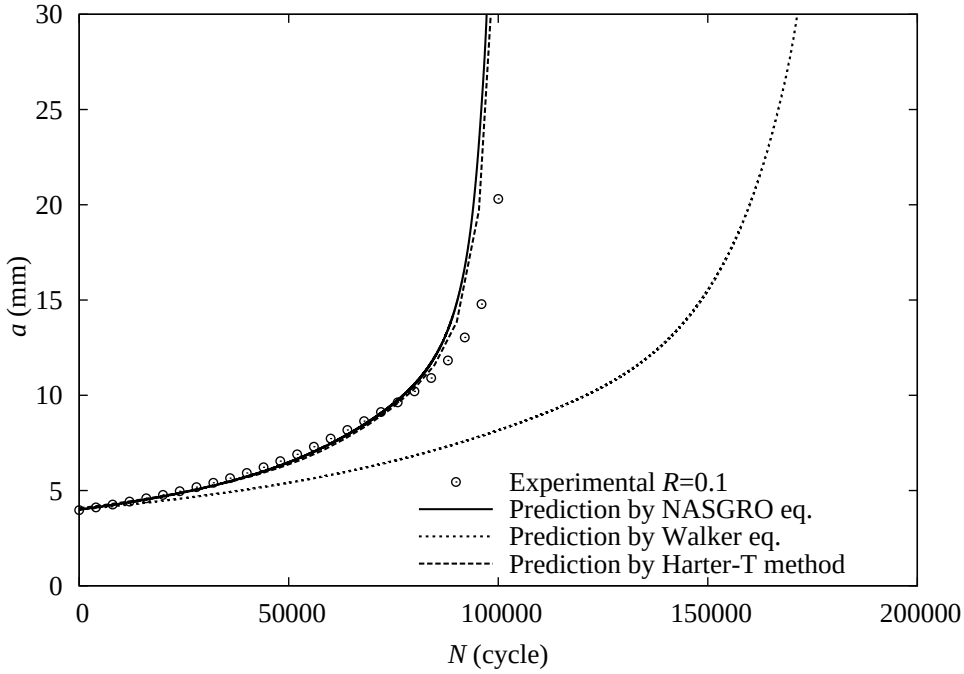

Figure 5.7: Comparison of predicted and measured FCG life under constant amplitude load: nominal $R = 0.1$ with VPPA RS field.

should be noted that in the measured crack growth rate curve there is a sudden change of the curve trend from a convex to concave within the crack length of 7.5 to 11.5 mm, whereas the predicted curves are generally in a convex shape. Note that the Walker equation, (similarly to the Paris equation) has a poor prediction towards the end of the curve because of its linearity in logarithmic scale, which do not consider the last part of a FCGR curve where the crack grow faster. The base material growth rate is also shown that is very close to the measured growth rates for the welded sample. NASGRO equation gives the best prediction of FCG rates for both R ratios due to the fact that it has more material "fitting" constants and also takes account of the fast crack growth regime when $K_{max,tot}$ approaches the fracture toughness K_{crit}. Fig. 5.6 shows that difference between the NASGRO and Walker predictions began to widen when $a > 17$ mm. For crack lengths 17-20 mm, $K_{max,tot}$ is in the range of 41-57 MPa$\sqrt{m}$. This is close to the fracture toughness of this alloy, which is about 65 MPa$\sqrt{m}$ (thickness 7 mm).

Figures 5.7 show the predictions of the life of the two nominal ratios. At nominal R=0.1 both NASGRO and Harter-T method are very accurate with an error less than 5% while the Walker equation over estimates the life more than 60% of the experimental tested data, which is mainly due to the large difference in the final part of the FCGR curve as it has been discussed above. The Walker equation predict a longer crack life, which agrees with the tests (a percentage error less than 10%), while the other two laws under estimate the experimental tests data with an error which is less than 30%.

5.1.4 Constant stress intensity factor range

For constant applied SIF range, constant rather than the load amplitude. The crack growth rate in a parent material case, will remain constant for different crack length, according to the Paris law. But in the case with RS crack growth rate will change along the distance from the welding. The nominal R ratio is 0.1. When SIF range is constant the following equation can be written:

$$\Delta K_{app} = const = \Delta\sigma\beta\sqrt{\pi a} = (\sigma_{max} - \sigma_{min})\beta\sqrt{\pi a} \tag{5.1}$$

The nominal R ratio has been kept constant:

$$\sigma_{min} = R\sigma_{max} \tag{5.2}$$

If the SIF range is constant the stress changes as the crack length is changing which means that the stress applied is a function of the crack length:

$$\sigma_{max}(a) = \frac{\Delta K}{(1-R)\beta(a)\sqrt{\pi a}} \tag{5.3}$$

Since:

$$K_{app,max} = \sigma_{max}\beta\sqrt{\pi a} \tag{5.4}$$

Combining eq. 5.3 and eq. 5.4 one obtains:

$$K_{app,max} = \frac{\Delta K}{(1-R)} \tag{5.5}$$

Approaching in the same way the K_{min} and the σ_{min} can be found:

$$\sigma_{min}(a) = \frac{R}{(1-R)}\frac{\Delta K}{\beta(a)\sqrt{\pi a}} \tag{5.6}$$

$$K_{app,min} = \frac{R}{(1-R)}\Delta K \tag{5.7}$$

As for the Walker equation the SIF range has been kept constant and the effective ratio has been taken into account:

$$\frac{da}{dN} = C[(\frac{1-f}{1-R_{eff}})\Delta K]^n \tag{5.8}$$

and so the Nasgro equation:

$$\frac{da}{dN} = C[(\frac{1-f}{1-R_{eff}})\Delta K]^n \frac{(1-\frac{\Delta K_{th}}{\Delta K})^p}{(1-\frac{K_{max}+K_{res}}{K_{crit}})^q} \tag{5.9}$$

The prediction for two cases has been shown in figure 5.8 which shows a good match between the predicted value and the experimental data. However for higher ΔK the error is bigger as shown in figure 5.9. Likely for higher ΔK the linear elastic analysis is limited because the load produce a bigger plastic zone

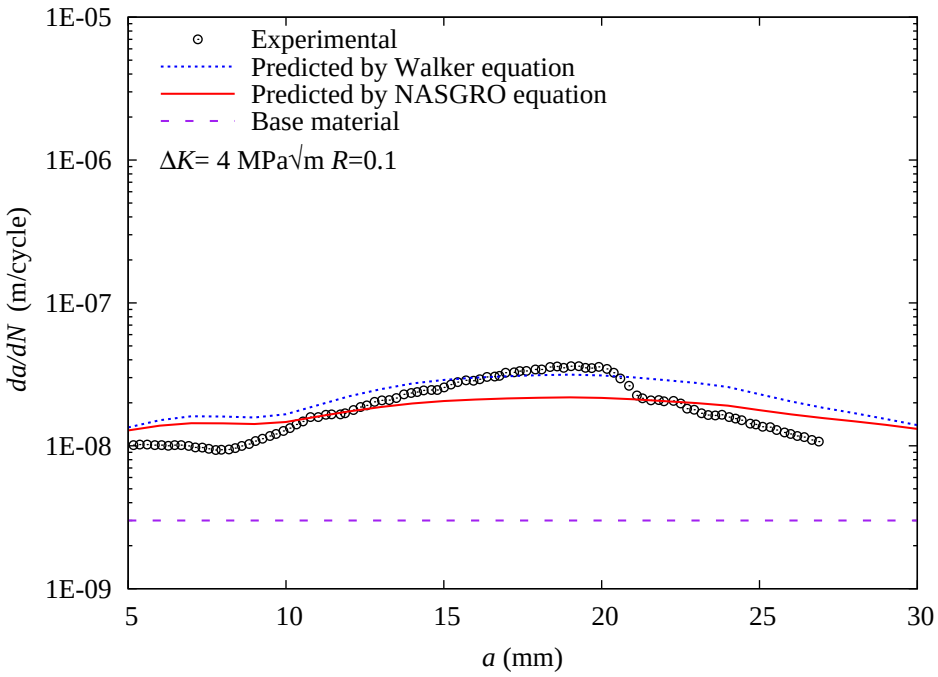

(a) $\Delta K = 4\ MPa\sqrt{m}$.

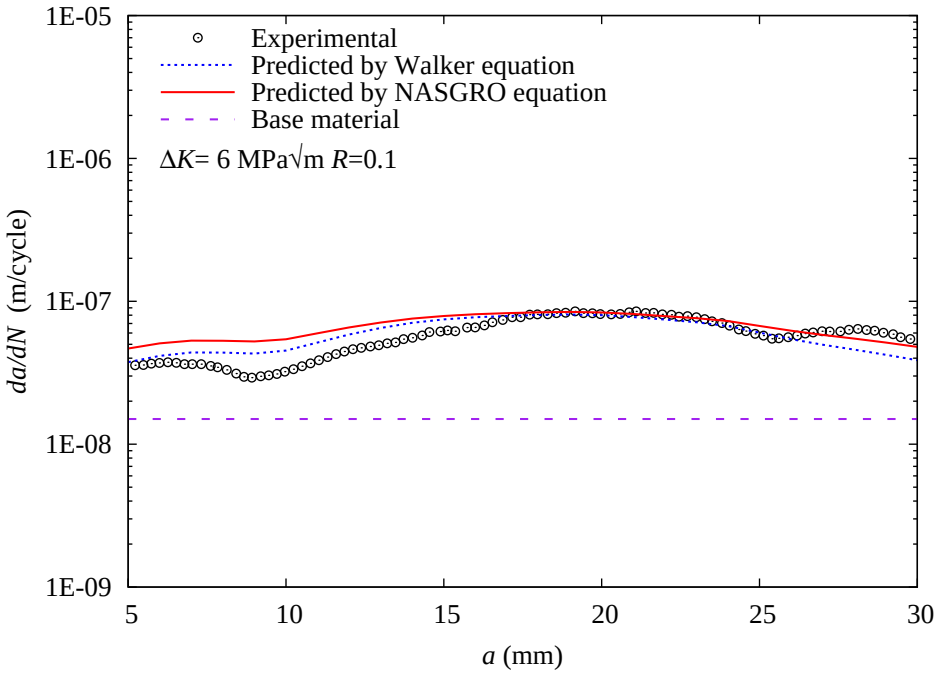

(b) $\Delta K = 6\ MPa\sqrt{m}$.

Figure 5.8: Comparison between prediction by Walker and Nasgro equation for ΔK=4,6 MPa$\sqrt{m}$ (Experimental data from [160]).

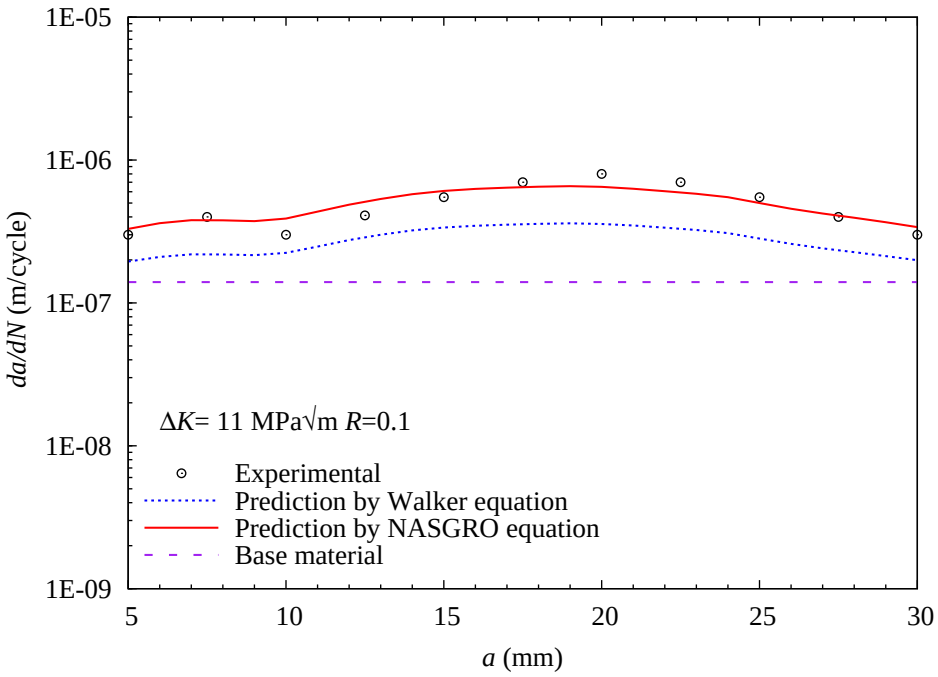

(a) $\Delta K = 11\ MPa\sqrt{m}$.

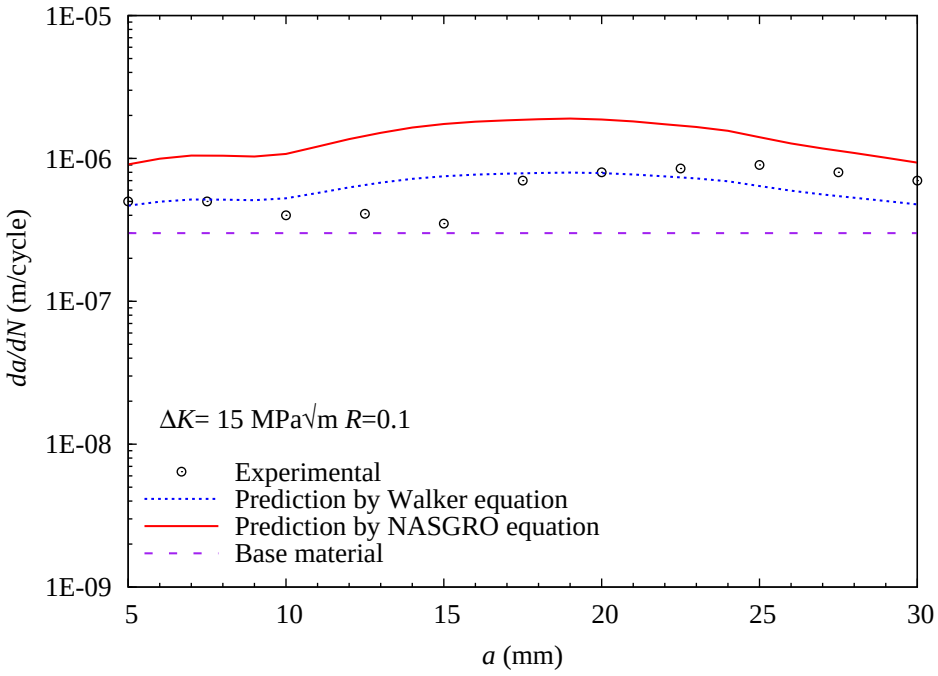

(b) $\Delta K = 15\ MPa\sqrt{m}$.

Figure 5.9: Comparison between prediction by Walker and Nasgro equation for ΔK=11,15 MPa$\sqrt{m}$ (Experimental data from [160]).

which can have benefits in terms of FCGR. Nevertheless those considerations are based on a single set of tests of constant ΔK.

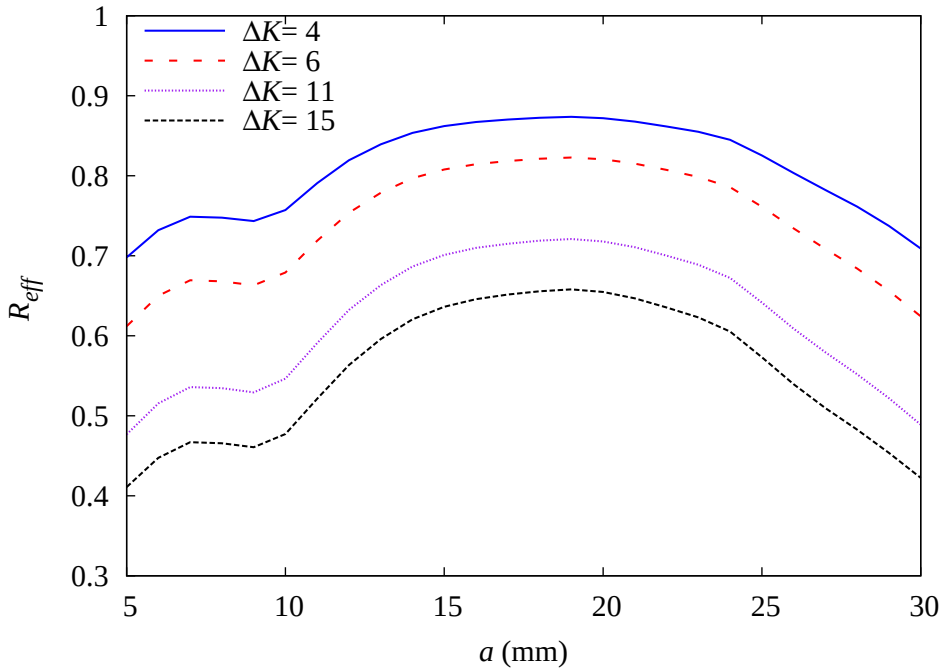

Figure 5.10: R_{eff} for the constant stress intensity factor range.

The base material FCG rate is constant under unchanged ΔK; hence the difference between the FCG rates of the welded and base metal is mainly due to the influence of welding residual stresses, which are accounted for by the R_{eff}. In this study, longitudinal welding residual stresses around the weld centre are high tensile stresses in the range of 100-150 MPa. Therefore K_{res} and R_{eff} are raised significantly. Fig. 5.10 shows the calculated R_{eff} values for the constant ΔK_{app} tests are much higher for the lower ΔK_{app} values. For ΔK_{app} = 4 and 6 MPa$\sqrt{m}$, R_{eff} = 0.6-0.86, hence there was almost no crack closure effect and the life prediction should be more accurate. Both the measured and predicted FCG rate trends follow the variation of K_{res}, which is lower at the fusion boundary (a = 5 mm) and at its peak at a = 17 mm. Walker and NASGRO predictions agree well with the tests of lower K_{app} (6 MPa$\sqrt{m}$). However, predictions are not consistent for the higher K_{app} (11 MPa$\sqrt{m}$), in which Walker equation gives better prediction for a < 15 mm. Changes in the microhardness and microstructures in the fusion and heat-affected zones will affect the mechanical properties in these zones and hence likely to affect the crack growth rates. This effect cannot be quantified by this present model and this may have affected prediction accuracy

in the crack length range of a = 7 - 15 mm.

5.2 Crack growing towards the weld

5.2.1 Problem statement: ESE(T) specimen

The geometry is an Eccentrically-Loaded Single Edge Crack Tension Specimen (ESE(T)) with a single longitudinal weld (see fig. 5.11).

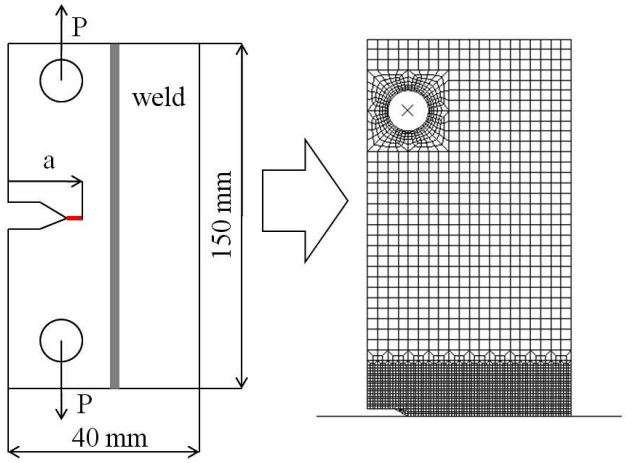

Figure 5.11: Geometry and mesh of the 1/2 FE model used for an elastic analysis.

The crack initially propagates in a compressive residual stress field starting from the notch and growing towards the weld. The objectives are to find the influence of compressive residual stresses on the crack propagation and to assess two different approaches for the FCG prediction. The material is an aluminium alloy of third generation 2195, thickness 8 mm, the maximum load applied is 4300 N and R=0.1. Dimensions and mesh are shown in figure 5.11. The welding process is the friciton stir welding (FSW). The experimental tests were conducted in the project and published in [158, 161].

Firstly the beta solution is compared with the solution from ASTM [162] without considering the welding residual stresses (see figure 5.12). The equation determines the stress intensity factor for this particular specimen is given in the

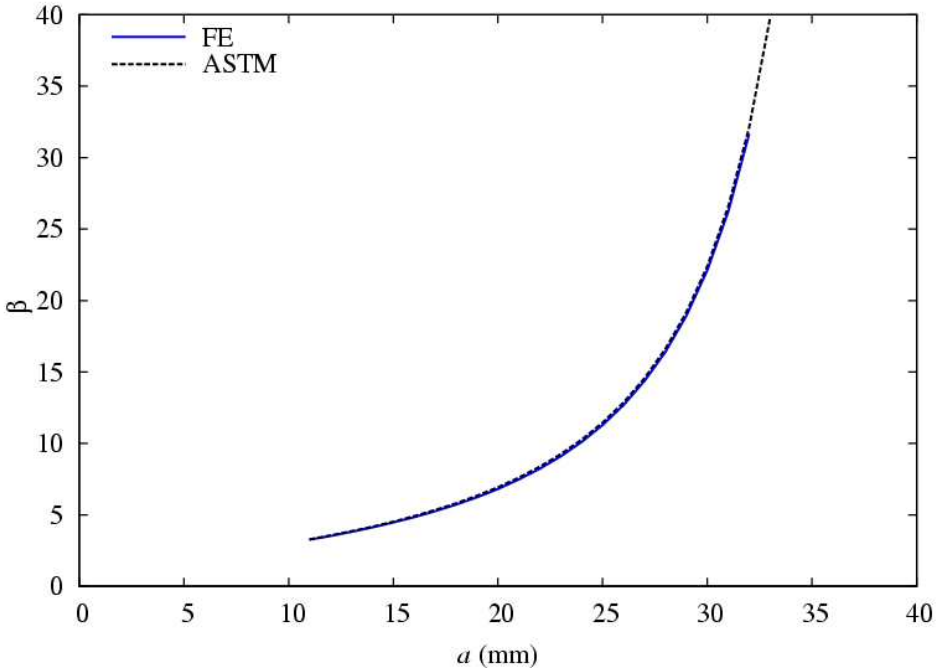

Figure 5.12: Beta solution for the ESE(T).

ASTM:

$$\Delta K = [\Delta P/(B\sqrt{W})]\beta \tag{5.10}$$

where W is the width of the specimen, P the applied load and B the thickness, while β is defined as:

$$\beta = \alpha^{1/2}[1.4 + \alpha][1 - \alpha]^{-3/2}G \tag{5.11}$$

where:

$$G = 3.97 - 10.88\alpha + 26.25\alpha^2 - 38.9\alpha^3 + 30.15\alpha^4 - 9.27\alpha^5 \tag{5.12}$$

$$\alpha = a/W \tag{5.13}$$

For $0 < \alpha < 1$ with a the crack length. The β solution obtained by the FEA conducted in this study is very close to the analytical solution (see figure 5.12).

The percentage error range varies from 0.5% to 1.5%.

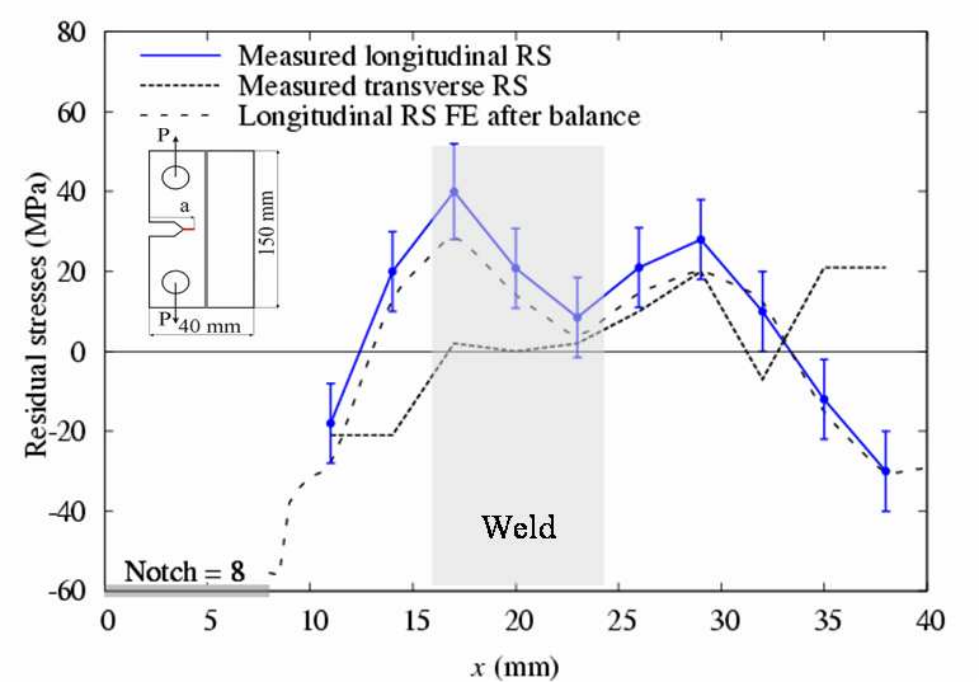

Figure 5.13: Measured residual stress field and FE input [courtesy GKSS].

Residual stresses shown in figured 5.13 were measured by project partner from the same specimen that has been tested. The residual stress measurements were carried out using high energy synchrotron beam line HARWII at DESY in Hamburg. A photon energy of 70 keV (wavelength: 0,177) was chosen using a SiGe monochromator. A Mar345 Image plate detector system and a Mar555 flat panel detector were used to measure the diffraction patterns (Debye-Scherrer rings) [163].

In order to calculate the residual stresses the residual strains need to be determined. These are calculated according to Braggs equation from the peak shifts of the Aluminium reflections. These are recommended, because of their isotropic characteristics providing access to the macro stresses. The measured diffraction peaks are fitted with a Pseudo-Voigt function [163]. Then the longitudinal and transversal strain ϵ_{yy} and ϵ_{xx} respectively are calculated and assuming plane stress conditions and isotropic material the classical equations of the continuum solid are applied to obtain the residual stresses:

$$\sigma_{yy}(x) = \frac{E}{1-\nu^2}(\epsilon_{yy}(x) + \nu\epsilon_{xx}(x)) \tag{5.14}$$

$$\sigma_{xx}(x) = \frac{E}{1-\nu^2}(\epsilon_{xx}(x) + \nu\epsilon_{yy}(x)) \tag{5.15}$$

where σ_{yy} and σ_{xx} are the longitudinal and transversal residual stresses respectively assessed on the symmetry line which is also the crack propagation line i.e. from the notch to the opposite free edge.

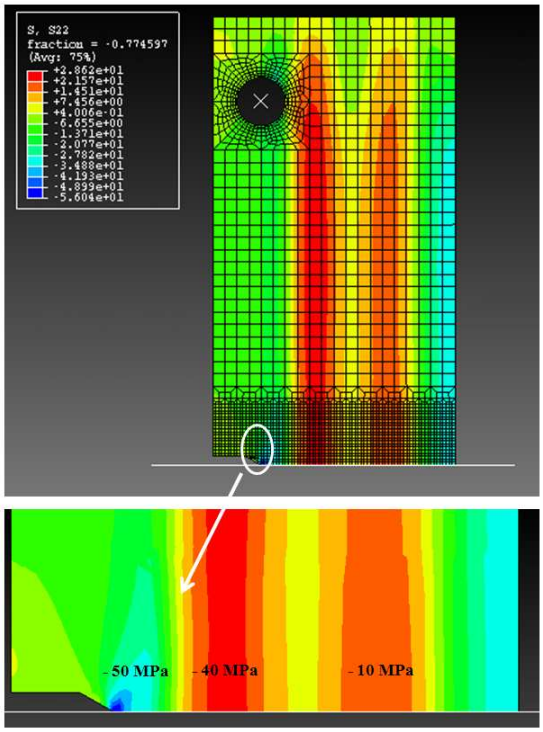

Figure 5.14: Longitudinal residual stresses in the FE model.

The actual measurement for the ESE(T) specimen are in figure 5.13 compared with the FE inputted residual stresses after the balance. Both transversal and longitudinal stresses are measured, showing a typical distribution for the friction stir welding. The double peak is due to the fact that the translational and rotational speed of the pin are summed in the advancing side which causes an higher temperature respect to the retreating side where the rotational speed is subtracted to the translational speed i.e. lower temperature. The outcome of this difference is that higher RS arise in the advancing side while lower RS arise in the retreating side.

The value of the measurement started at 11 mm and some values are missing between the notch root (8 mm) and the first measured value (11 mm). This is a sensitive area to calculate the opening stress σ_{op}. The stress field of half of

the plate was modelled by inputting the biaxial measured residual stress and balanced by ABAQUS (see fig. 5.14). Close to the notch compressive stresses arise in order to balance the stresses along the symmetry line where the stresses are more compressive in a smaller area. This will cause the crack to open later and to stay close at higher load than minimum, for this reason a crack closure approach is more suitable for the problem.

5.2.2 Evaluation of R_{eff} and ΔK_{eff}

The K_{res} was calculated in order to obtain the R_{eff} for different nominal R=0.1 and R=0.6 (see figure 5.15). Negative values of the K_{res} due to the compressive stresses bring also the R_{eff} to be negative for the case with the nominal R=0.1. When the nominal R=0.6 the R_{eff} is changed only for short crack length.

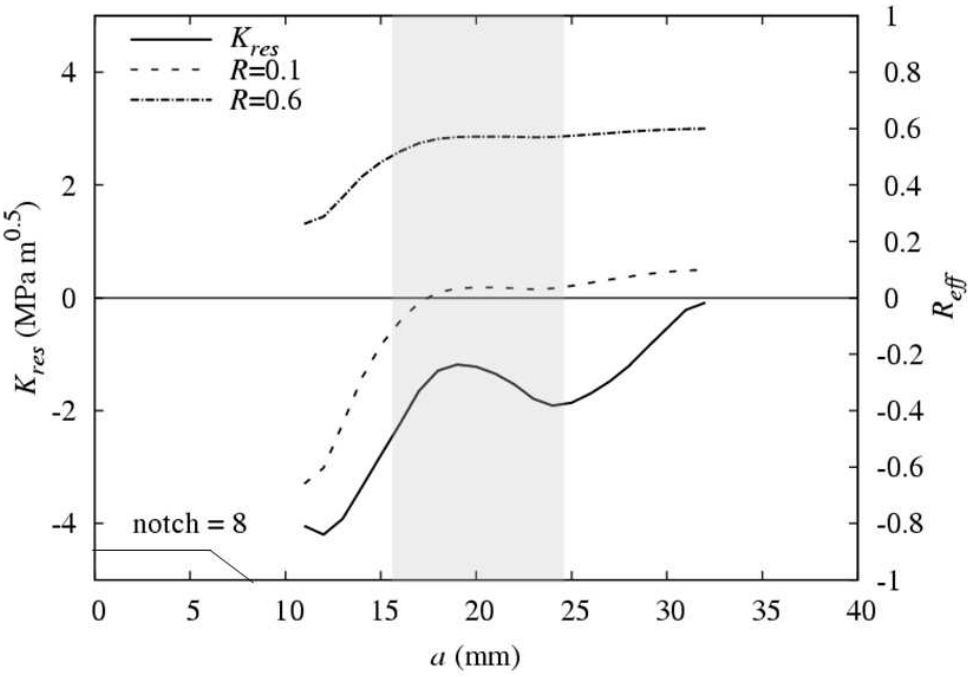

Figure 5.15: Effective ratio and K_{res} for the ESE(T) specimen.

In order to predict the effective stress intensity factor range hence the fatigue crack growth rate and the crack life two different methods have been compared. The first is based on the Newman equation [79] and the form the stress intensity factor calculation and the effective stress intensity factor. The second is based on the opening stress calculated with FE with the method explained above. The normalised load ratio parameter U can be determined in two different ways

depending on the which of the two mentioned methods above is used. The Newman equation based method calculates the U by using the R_{eff} while with FE R nominal is necessary together with the determination of the normalised opening stress σ_{op}/σ_{max}. Two opening factors are defined, one based on the stress and the second based on the stress intensity factor which are respectively: $f_{N,RS}$ and $f_{FE,RS}$. To obtain the ΔK_{eff} both methods are equivalent as it is demonstrated herein. The definition of U of the Newan based approach is:

$$U = \frac{(1 - f_{N,RS})}{(1 - R_{eff})} \tag{5.16}$$

where $f_{N,RS}$ is the Newman based opening factor for residual stress defined as:

$$f_{N,RS} = \frac{K_{op,RS}}{K_{\max,tot}} = A_0 + A_1 R_{eff} + A_2 R_{eff}^2 + A_3 R_{eff}^3 \quad \text{for} \quad R_{eff} > 0 \tag{5.17}$$

$$f_{N,RS} = \frac{K_{op,RS}}{K_{\max,tot}} = A_0 + A_1 R_{eff} \quad \text{for} \quad R_{eff} < 0 \tag{5.18}$$

for the finite element the U definition is:

$$U = \frac{(1 - f_{FE,RS})}{(1 - R)} \tag{5.19}$$

where:

$$f_{FE,RS} = \sigma_{op}/\sigma_{\max} \tag{5.20}$$

while $f_{FE,RS}$ is the opening factor calculated as it has been previously described. The opening factor for the two methods are shown in figures 5.16. The Newman based opening factor with and without RS is constant because the R_{eff} is mainly negative and the coefficient A_0 is constant while the A_1 which multiples the R_{eff} is lower (see chapter 3). Without RS the SIF based opening factor f correspond to the opening stress based on stress which in plane strain conditions is around 0.3 according to many previous results [40,79]. The opening stress with the finite

element becomes lower when the compressive RS field fades and tends to become tensile (further details were explained in chapter 4).

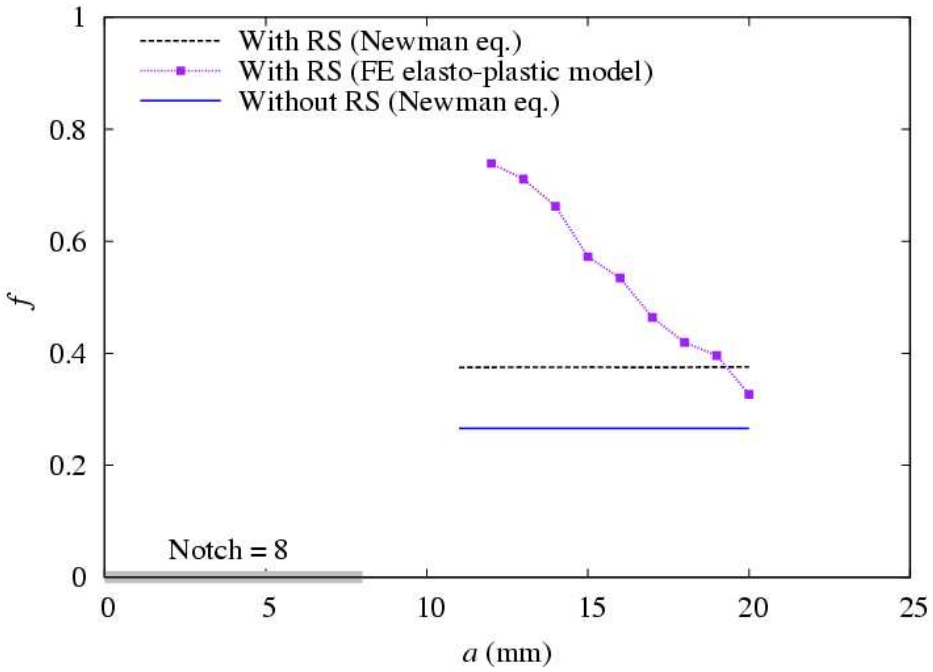

Figure 5.16: Comparison of the opening factor determined with the two methods.

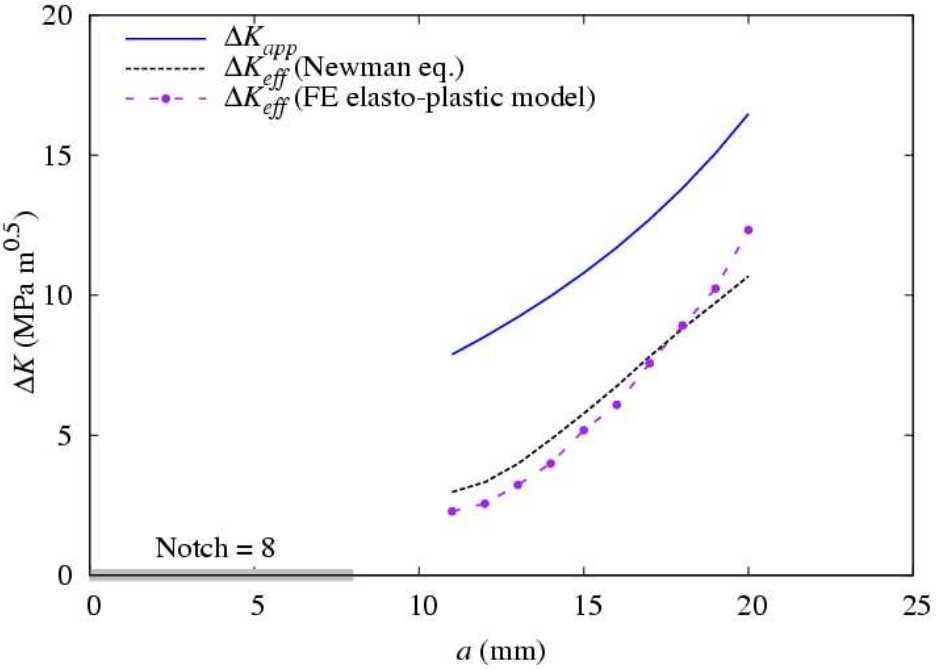

Figure 5.17: Effective stress intensity factor range.

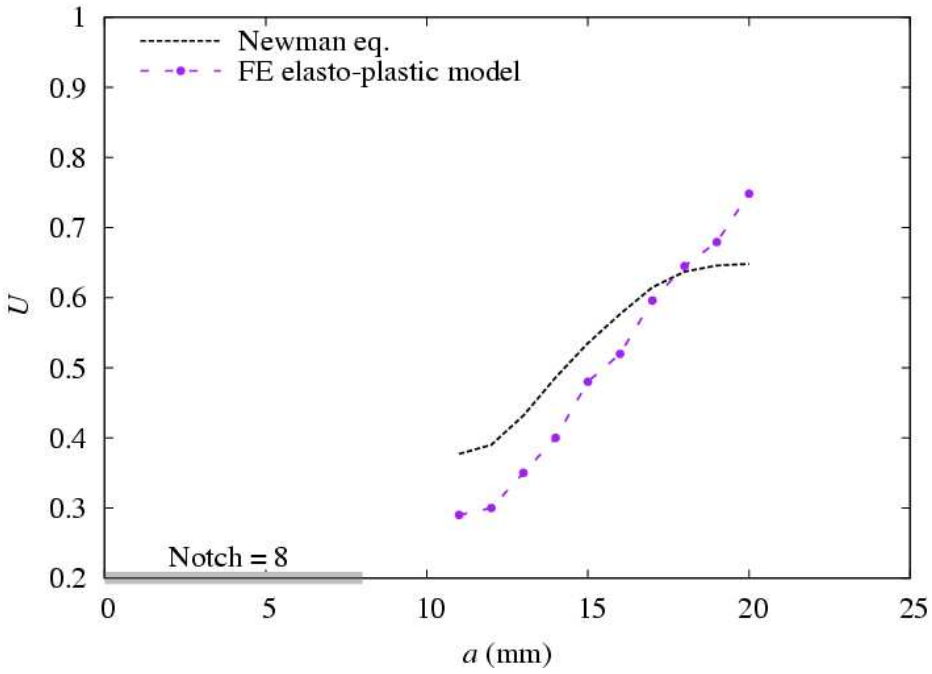

Figure 5.18: Normalised load ratio parameter.

The opening factor is very different for the two methods but the final U is close. This is because in one case is used the effective ratio and in the other the nominal stress ratio. The $f_{N,RS}$ is calculated by assuming the effective ratio, for this reason R_{eff} must be used to determine U. To demonstrate the validity of this assumption the following equation is expanded:

$$U = \frac{(1 - f_{N,RS})}{(1 - R_{eff})} = \frac{(1 - \frac{K_{op,RS}}{K_{\max,tot}})}{(1 - \frac{K_{\min,tot}}{K_{\max,tot}})} \tag{5.21}$$

$$U = \frac{K_{\max,tot} - K_{op,RS}}{K_{\max,tot} - K_{\min,tot}} \tag{5.22}$$

By knowing that:

$$K_{\max,tot} - K_{\min,tot} = K_{\max,app} + K_{res} - (K_{\min,app} + K_{res}) = K_{\max,app} - K_{\min,app} = \Delta K_{app} \tag{5.23}$$

$$K_{\max,tot} - K_{op,RS} = \Delta K_{eff} \tag{5.24}$$

One can write:

$$U = \frac{\Delta K_{eff}}{\Delta K_{app}} \tag{5.25}$$

A similar demonstration can be done for the case with the finite element in order to achieve the same conclusion:

$$U = \frac{(1 - f_{FE,RS})}{(1 - R)} = \frac{(1 - \frac{\sigma_{op,RS}}{\sigma_{\max,tot}})}{(1 - \frac{\sigma_{\min}}{\sigma_{\max}})} \tag{5.26}$$

$$U = \frac{\sigma_{\max,tot} - \sigma_{op,RS}}{\sigma_{\max,tot} - \sigma_{\min,tot}} \tag{5.27}$$

By multiplying the numerator and the denominator for the same quantity $\beta\sqrt{\pi a}$:

$$U = \frac{(\sigma_{\max,tot} - \sigma_{op,RS})}{(\sigma_{\max,tot} - \sigma_{\min,tot})} = \frac{(\sigma_{\max,tot} - \sigma_{op,RS})\beta\sqrt{\pi a}}{\Delta\sigma\beta\sqrt{\pi a}} = \frac{\Delta K_{eff}}{\Delta K_{app}} \tag{5.28}$$

This is the same result that is found before. The effective stress intensity factor range can be then calculated:

$$\Delta K_{eff} = U\Delta K_{app} \tag{5.29}$$

The normalised load ratio parameter is calculated and shown in figures 5.18 and 5.17. The effective stress intensity factor range for the residual compressive stresses are much lower than the applied stress intensity factor range which is the case without RS. The difference is consistent also in the fatigue crack growth rate prediction shown in the following figure 5.19.

5.2.3 Comparison of predictions with experimental results

A comparison with experimental results shows that the FE and the Newman based method are in a fairly good agreement with the experimental tests from 14 mm onwards but there are major differences in the initial part of the fatigue crack growth between 11 to 14 mm (see figure 5.19). Also the comparison of the crack closure approach with the superposition shows the erroneous assumption of the latter method when assuming compressive residual stress field.

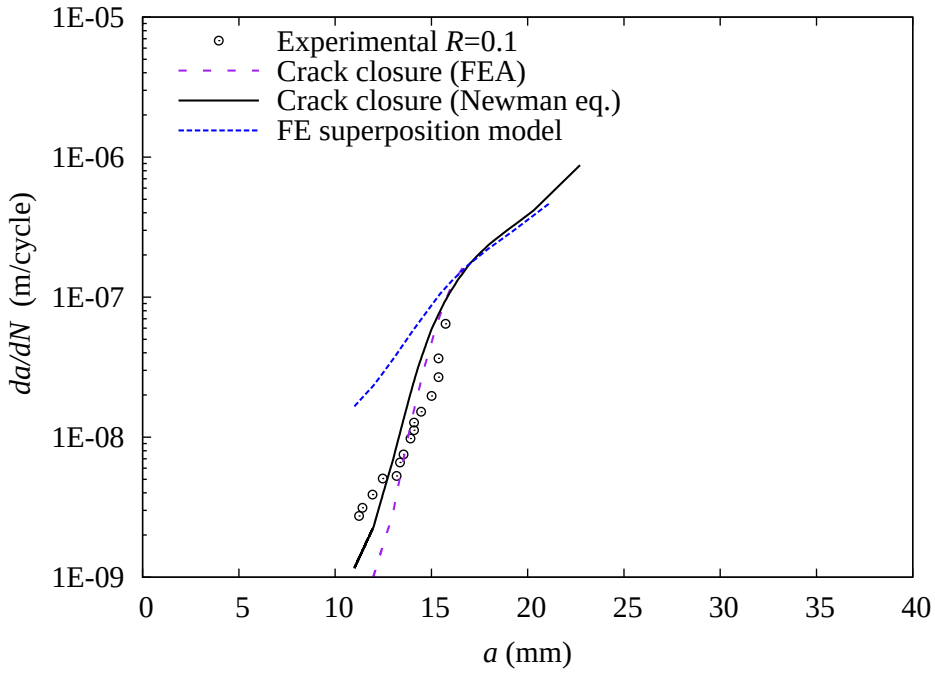

Figure 5.19: Two prediction methods for the crack closure approach with the superposition approach.

The fatigue crack life is shown in figure 5.20. The predicted life with the closure model is better than the Newman based approach. However the initial part of the prediction is the most critical because of the residual stresses induce a crack closure which is difficult to assess in term of opening stress. When using the Newman equation by meaning of R_{eff} the crack closure approach is closer in the initial part of the crack propagation, but it is overall too conservative. The initial part is the most difficult one which is very sensitive to the compressive residual stresses at the beginning. When the crack is shorter it needs more cycles to propagate, hence the error of the fatigue life increases and the compressive

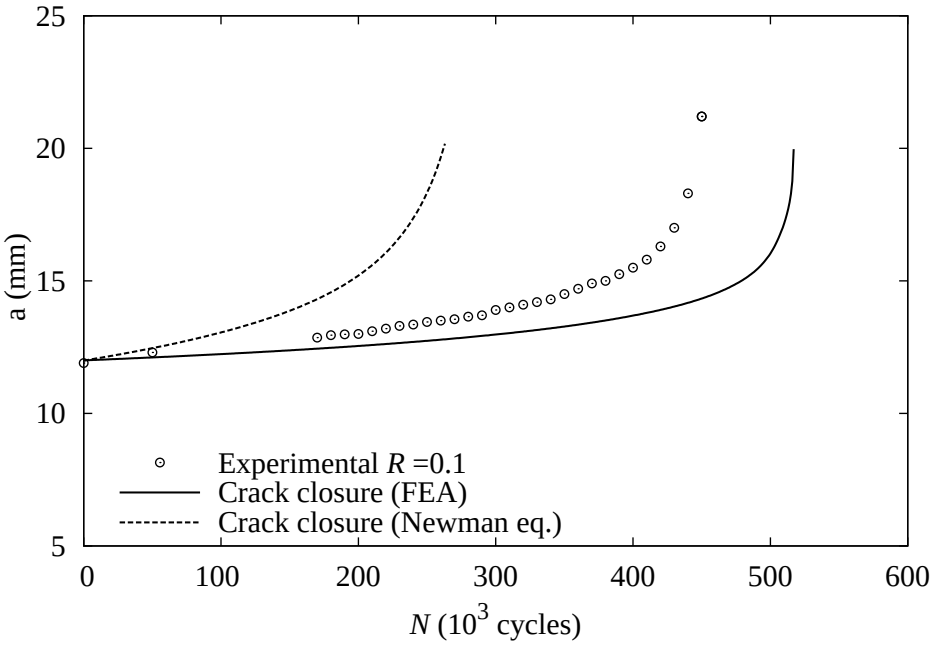

Figure 5.20: Fatigue crack life prediction.

residual stresses need to be very accurate in order to assess the opening stress level with more confidence and a better accuracy.

5.3 Discussion of the superposition and closure approach

The superposition and the crack closure concept have been used to predict the fatigue crack growth rate for two different residual stress fields: first the crack start to propagate from the weld and second the crack propagates towards the weld. Figure 5.21 shows a comparison of the two methods in the first case: the crack closure concept by using the elastic-plastic model previously described and the superposition method by using the Harter-T method. Both methods give a typical error range below 20%: the superposition has a typical percentage error of 15% to 18% in the second half of the crack propagation, while the crack closure approach has a lower accuracy in the initial part with but the overall percentage error is similar to the one of superposition.

Figure 5.22 shows that for low nominal R the superposition approach need to be

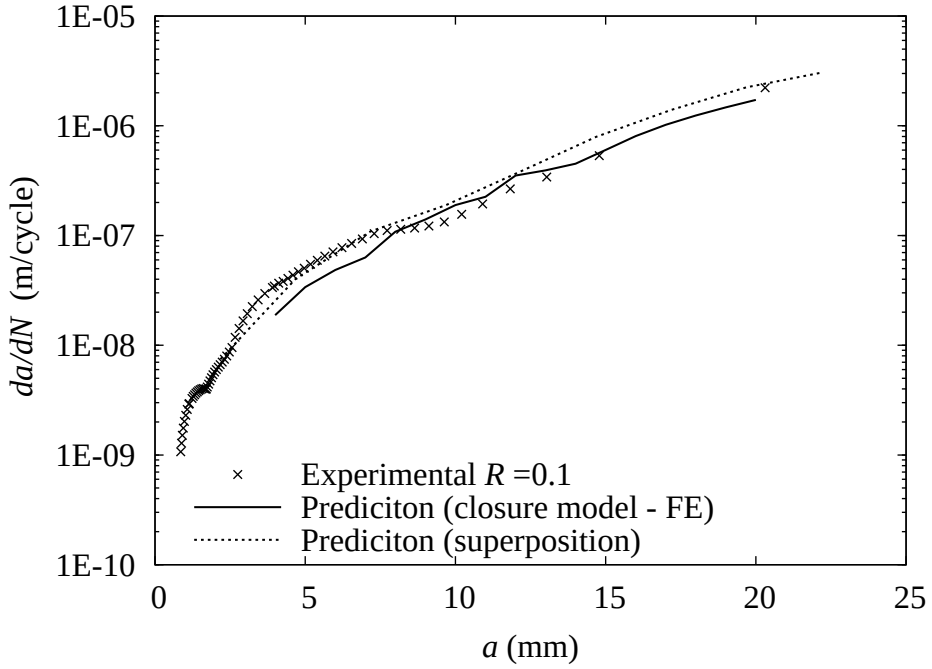

Figure 5.21: Comparison of the superposition method with the crack closure model for the M(T) specimen.

excluded in the prediction methodology. The relationship between the nominal stress intensity does not hold anymore because the minimum load is changed by the compressive weld residual stresses hence the effective stress intensity factor ΔK_{eff} needs to be addressed. The superposition is a reliable when the crack starts from the weld. Its main limitation is when the crack grows through a compressive residual stress field.

The two approaches have been compared with experimental tests, but some limitations needs to be clarified in order to provide further insight into the prediction methodology. Figure 5.23 shows the analysis procedure of the two approaches.

Three different fields have been covered in the FCG life prediction:

1. Stress analysis via finite element
2. Evaluation of fracture mechanics parameters
3. Fatigue crack growth prediction

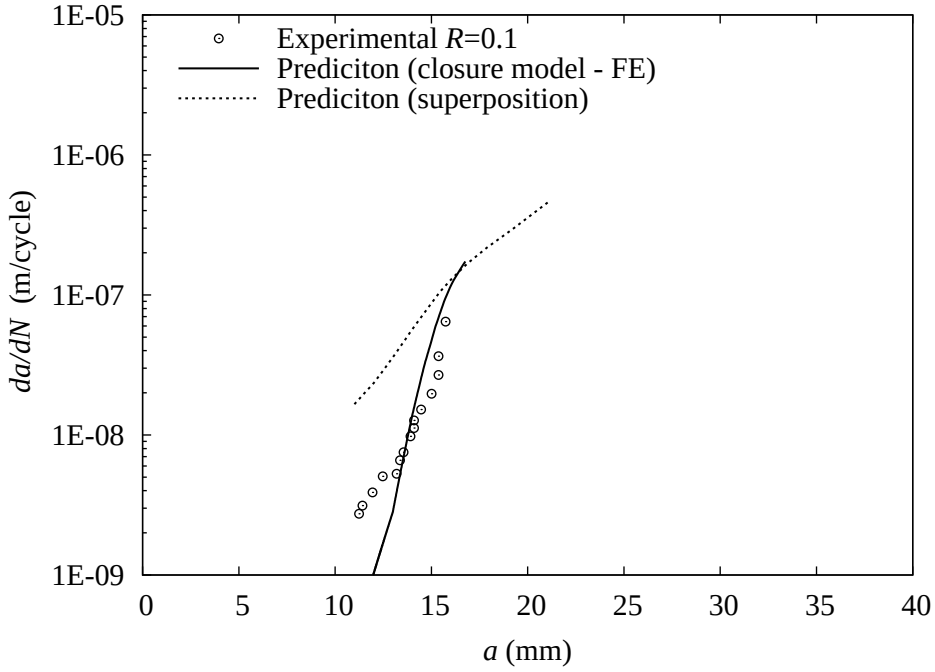

Figure 5.22: Comparison of the crack closure and superposition for the ESE(T) specimen.

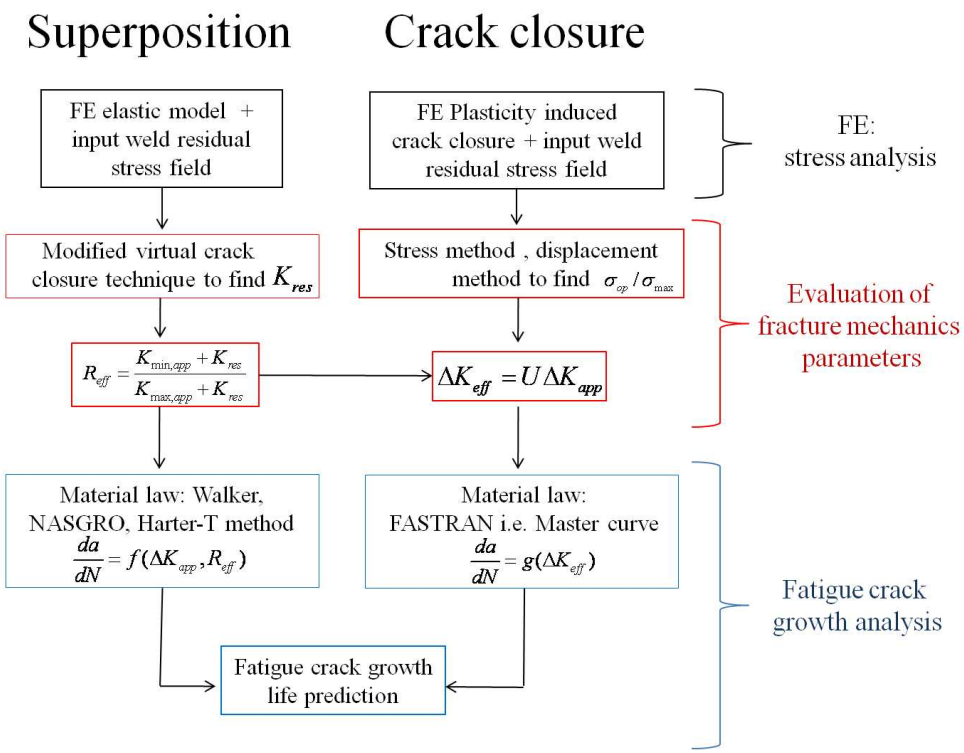

Figure 5.23: Analysis procedure of the two prediction methods.

The stress analysis can be done either by using an elastic analysis or by using a plasticity induced crack closure analysis by means of a quasi-static load analysis. The latter aims to find the normilized crack opening stress value σ_{op}/σ_{max} in order to find the ΔK_{eff}. The superposition is efficient because not computationally expensive for the crack propagation prediction and with a good level of accuracy, for this reason it has been used often in the past. However main limitations are that, when non-linearity of the crack opening displacement occur, the results are not reliable anymore. This is true when the crack grows into a compressive residual stress field, in this case the superposition principle is not valid anymore because the minimum load is changed by the weld residual stresses. For this reason the crack closure approach is more suitable. This method is more comprehensive but the value of the opening stress is not always easy to obtain. The plasticity induced crack closure FE analyses are computationally expensive, but they provide an insight into the crack closure mechanism and a better understanding of the behaviour of the crack propagation in presence of residual stresses by taking into account the plasticity effects. An alternative approach is by using the Newman analytical equation in order to calculate the ΔK_{eff}. This approach can be used for both compressive and tensile residual stress fields but it does not give any information on the crack behaviour, the crack closure parameters, the effects of the RS on the plasticity induced crack closure and viceversa.

In both methods the material law is very important. For aerospace aluminium alloys, the NASGRO, Harter-T Method and Walker equations can be easily obtained by the material databases (e.g. AFGROW [37]). However for new alloys or for welded plate, where the fatigue properties change, it is important to obtain the material crack growth properties by experimental tests.

5.4 Summary of the chapter

An analysis procedure is presented for predicting FCG rate in welded longitudinal butt joints with a crack starting either from the weld or towards the weld, by using two different approaches for both cases: the superposition and the crack closure approach.

The superposition was used together with different fatigue laws. Welding residual stress effect is accounted for by the effective crack tip stress ratio, which is used

in empirical crack growth laws. Comparisons are made with experimental tests of crack growth rates subjected to constant amplitude load and constant SIF range. For the constant amplitude load case, the Walker, Harter-T method and NASGRO equations all give acceptable predictions if the $K_{max,tot}$ is well below the material fracture toughness. NASGRO gives best prediction for the entire crack length range. For the constant SIF range cases, predictions are mainly affected by the effective R ratio that has a larger influence on lower applied SIF ranges. Although NASGRO equation gives the best prediction, the Harter-T method is more robust and versatile, because it can be used for new Aluminum alloys, by knowing the material at different R, which can be achieved with experimental tests.

In terms of calculation techniques, inputting initial residual stresses into a FEM and modelling residual stress redistribution with crack growth can be performed by the ABAQUS software package together with the FORTRAN subroutine SIGINI. Only the base material crack growth rate data and welding residual stresses are required in the analysis. The virtual crack closure technique is a reliable, robust and efficient method to calculate the stress intensity factor, and its validity it was demonstrated also for residual stress factor of weld residual stress K_{res}. The proposed method can be generally employed when crack initiates within a weld and initially in tensile residual stress field. This prediction method can be used for several welding processes, in which fatigue crack growth rates are mainly affected by welding induced thermal residual stresses and the influence of hardness and microstructure changes in the heat affected zones can be neglected. The effect of tensile RS on a crack starting from the weld is to increase the growth rate of the crack, especially for low nominal R. The RS stress profile also influences the final life of the crack: a high stress even with a narrow tensile band is more detrimental than a large tensile area with a low peak stress.

When the crack grows towards the weld it grows through a compressive residual stress field. In this case the superposition has a limitation hence a more suitable crack closure approach can be used. Both Newman equation and FEA have been used. The difficulty of the FE was to find the value of opening stress which has been found to be sensitive on the initial RS distribution and on the compressive stresses near the notch, close to the initial crack length. Both approaches underestimate the growth rate in the initial part of the crack growth.

In the finite element analysis plasticity effects have been taken into account under

plain strain conditions. The decrease of plastic zone size with respect to the plane stress conditions is confirmed, so the opening stress due to plasticity is lower and it occur only for longer crack length. Moreover the compressive stresses diminish the value of the σ_{op}. The results is that at 20 mm crack length the plasticity induced crack closure is relevant while before 20 the second effect, discussed in section 4.4.1, is dominant. The first effect is important only after 20 mm when the plastic wake developed.

The crack closure together with plasticity induced FE model is the more complete method to determine the fatigue life. It is versatile because it can be used for prediction and also to interpret the closure mechanism induced by plasticity. The final prediction is accurate for the crack growing from or towards the weld. A drawbacks is that is computationally expensive at the moment and it can be run only in a cluster grid computer. On the other hand the superposition approach is a reliable and efficient method which allows to predict the fatigue crack growth rate when the crack starts from the weld, but not when it grows in a compressive RS field i.e. when it goes towards the welding. The crack closure approach by using the Newman equation method is efficient and versatile and it can be used with a linear elastic analysis, avoiding the heavy computational effort, and it can be also used for both crack scenario: towards and from the weld. The drawbacks is that the interpretation of the closure mechanism i.e. the opening crack displacement behaviour, the plastic wake development or the redistribution or RS stresses can not be assessed.

Chapter 6

FSW fuselage longitudinal joints

This chapter contains the modelling and experimental test results of a friction stir welded panel with pad-up to be used for fuselage longitudinal joint. Section 6.2 explains the FE modelling technique which is used to assess the crack propagation. Several aspects have been taken into account in this section: secondary bending and initial residual stresses need to be combined and they have to be accounted to obtain the fatigue crack growth driving forces i.e. the effective stress intensity factor range ΔK_{eff}. The redistribution of a biaxial residual stress has been also taken into account and the importance of the transversal residual stresses on the fatigue crack propagation has been explained in terms of the effective stress ratio.

Experimental tests have been conducted, and measurements of the strain in order to assess the validity of the model, are discussed in section 6.3. The crack growth was monitored on both sides of the panel. A description of the specimens preparation and experimental test facilities is also provided in the same section.

The aim of this study is to assess how the crack propagates in a panel along the welding in the heat affected zone (HAZ). The objectives are to perform a stress analysis via FEM, to understand the influence of the pad-up and stringer in terms of secondary bending, to evaluate the residual stress field in terms of the effective stress ratio and to calculate the stress intensity factor solutions. A comparison of the prediction with experimental tests is presented in section 6.4.

6.1 Problem statement: fuselage panel with FSW joints and stringer features

Friction stir weld needs to be assessed for fuselage application in large civil aircraft. The concept proposed here contributes to evaluate the FSW in terms of damage tolerance design, hence in terms of fatigue crack growth. The component is an hybrid structure with FSW and classical rivets which joins the stringer with the panel. The weld mean to be an assembly joint of fuselage panel to be used in large civil aircraft.

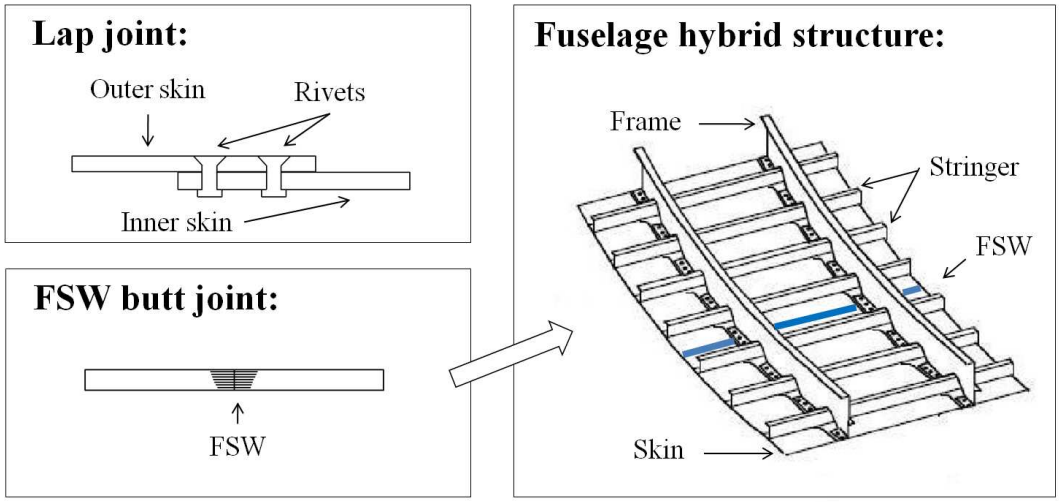

Figure 6.1: Application of friction stir welding in the fuselage structure.

Figure 6.1 shows the classical concept which is made by an overlap rivetted joint and a novel weld butt joint. The second concept decreases the weight of the structure because it avoids the rivets and without holes high stress concentrations does not occur anymore. Moreover the assembly FSW joint is faster than rivetting and the manufacture and maintenance costs are reduced [13, 164]. In order to compensate the reduced strength property in the weld, a pad-up with an increased thickness was machined which section is represented in figure 6.2. The circumferential stress σ_{yy} due to the pressurization are the main cause of crack propagation. The stresses can be calculated from the pressure difference by using the following equations:

$$\sigma_{xx} = \frac{\Delta p r}{2t} \tag{6.1}$$

$$\sigma_{yy} = \frac{\Delta p r}{t} \tag{6.2}$$

Where Δp is the difference between the pressure at sea level and at the cruising speed of the aircraft, r is the radius of the fuselage and t is the thickness of the fuselage. The σ_{yy} are the so called hoop stress which double the value of σ_{xx} that are the longitudinal stresses. By assuming standard air conditions and a large civil aircraft a maximum applied stress of 100 MPa is assumed. The nominal ratio is R=0.1 and the material is Al 2198 T-851 which properties are presented in table 6.1. The crack will propagates parallel to the weld because the circumferential stresses are investigated.

Table 6.1: Material properties of Aluminium 2198 [158].

	E (MPa)	$\sigma_{ys}(MPa)$	$\sigma_{UTS}(MPa)$	Elongation (%)
Al 2198	77000	436	491	14%

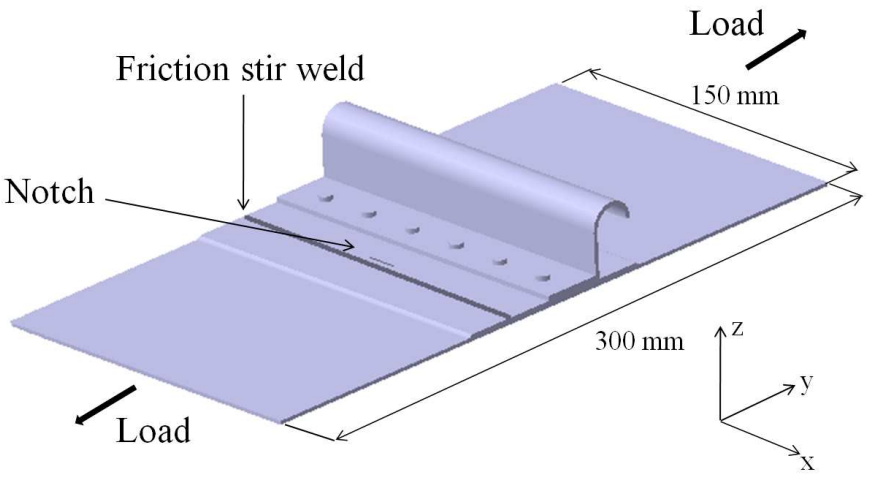

Figure 6.2: CAD drawing of the stringer panel test sample geometry.

The dimensions of the tested specimen, the friction stir weld position and the direction of the load are presented in figure 6.2 which is part of a fuselage longitudinal joint subjected to hoop stress. The notch is placed on the heat affected zone so that the crack will propagate parallel to the weld on the retreating side and its length is 18 mm with a conventional radius of 0.25 mm [162]. Further details of the stringer section can be found in the appendix B.

6.2 FE analysis

6.2.1 Modelling technique

A 2D model, which is shown in figure 6.3, was build in order to assess the stress field which could account of the secondary bending due to the pad-up increased thickness. Shell elements S4R with reduced integration have been implemented. Since energetic-based methods have been applied to find the stress intensity factor, a finer mesh was used near the pad-up region where the crack propagates. The smallest element size is 0.5 mm. Because of its symmetry only half of the panel was modelled.

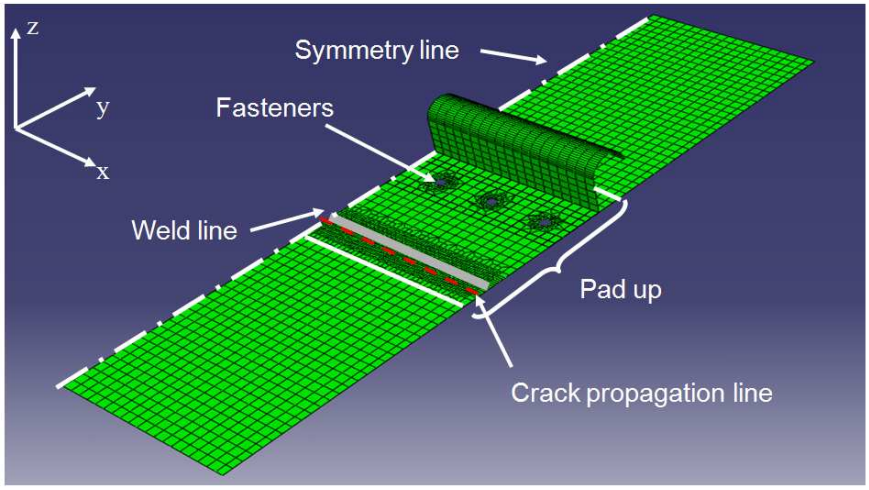

Figure 6.3: 2D FE model of the stringer panel.

The simplification made to build the FE model are summarized below:

- Pad-up: it was modelled by using an off-set, from the middle of the surface of the elements, which defines the distance, as a fraction of the shell thickness, between the mid surface to the reference surface of the elements where the nodes lies.
- Stringer: it was modelled by 2D shell elements, which normal axis changes with the orientation of the elements itself (see figure 6.3).
- Holes and Fasteners. The holes are coupled with a reference point with a rigid interaction, that means that rigid fasteners are assumed for this model. The error on the stress field on this assumption can be neglected

since the stress field close to the hole does not influence the stress field in the crack path.

- Interaction between stringer and panel. A contact between the stringer and the panel was implemented in order to avoid the overlapping material which would be physically not possible.
- Weld residual stress. A residual stress field was assumed with a typical FS weld distribution, input and balanced in the FE model by using the SIGINI subroutine.
- Crack propagation. In order to simulate the crack propagating in the pad-up area the nodes have been duplicates along a seed line which lies on the crack propagation path. At each step one node was duplicated in order to increase the crack length.

To verify the feasibility of the 2D model the stringer has to be modelled by including the fasteners and the holes. The 2D model is more efficient respect to a 3D model and can be also be more accurate.

To apply the load a clamping distance of 50 mm was applied which was simulated by coupling a reference point with the elements of the clamped area and then by loading the reference point. The stress intensity factor was then calculated at different crack lengths by using the modified crack closure technique including the bending effects as it is explained in section 6.2.4.

A further discussion on two different methods of model the stringer joint is discussed in appendix B. The behaviour of the stress field in the crack propagation is not influenced by those two approaches, for this reason the results of this chapter assumes the conditions stated in this section.

6.2.2 Stress analysis: secondary bending

Because of the stringer and the pad-up area in the panel, once an in-plane tensile load is applied to the specimen, a secondary bending occurs which effect can be quantified by the finite element analysis. The contour map in figure 6.4 shows the value of the displacement in the direction perpendicular to the panel plane. The maximum displacement is just more than 1 mm and it is in the pad-up

section. Such effect will modify the longitudinal stresses σ_{yy} by introducing a bending component that will change the stresses on the top and on the bottom skin surface of the panel. The stress and the strain have a different distribution depending on the top or the bottom surface (see figure 6.5). The average stress can be calculated by using:

$$\sigma_{mean} = \frac{\sigma_{top} + \sigma_{bot}}{2} \tag{6.3}$$

while the bending can be evaluated by using the bending stress:

$$\sigma_{bend} = \frac{\sigma_{top} - \sigma_{bot}}{2} \tag{6.4}$$

Where σ_{top} and σ_{bot} are respectively the longitudinal stresses on the top and bottom surfaces.

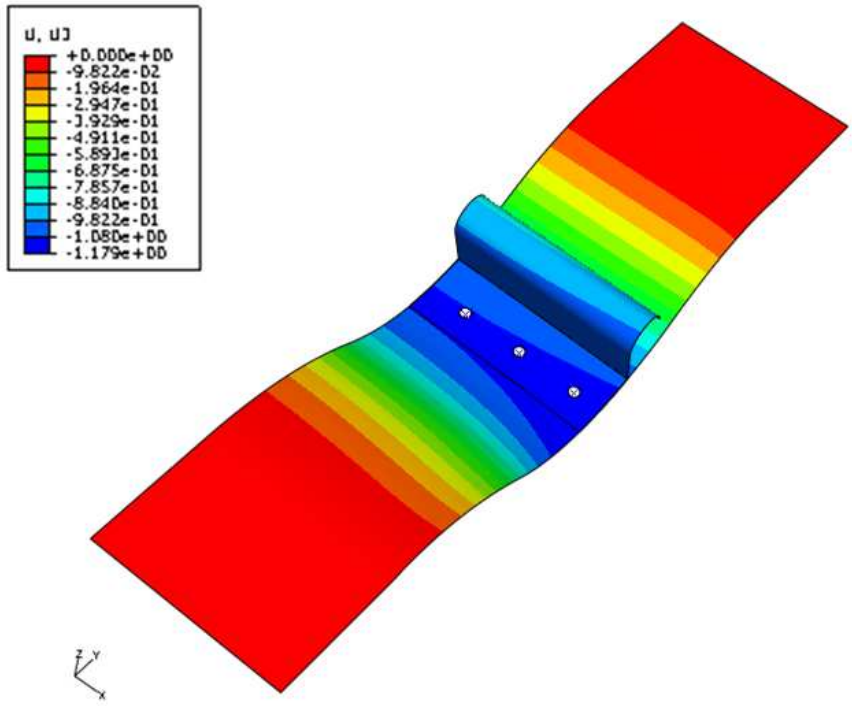

Figure 6.4: Contour map for the displacement (unit=mm).

Figure 6.4 shows the out-of-plane displacement at the symmetry line. The displacement has a second derivative negative i.e. the concavity is towards the bottom. This is the reason why in the following graphs the stresses and strains

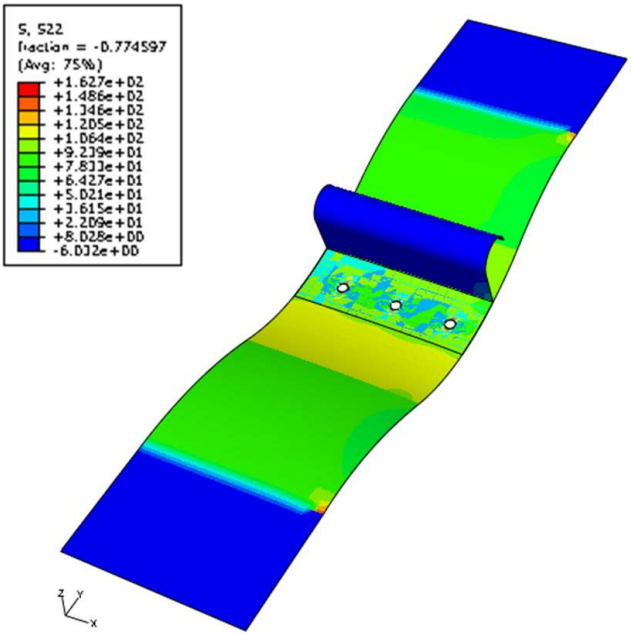

(a) Stress at the bottom surface.

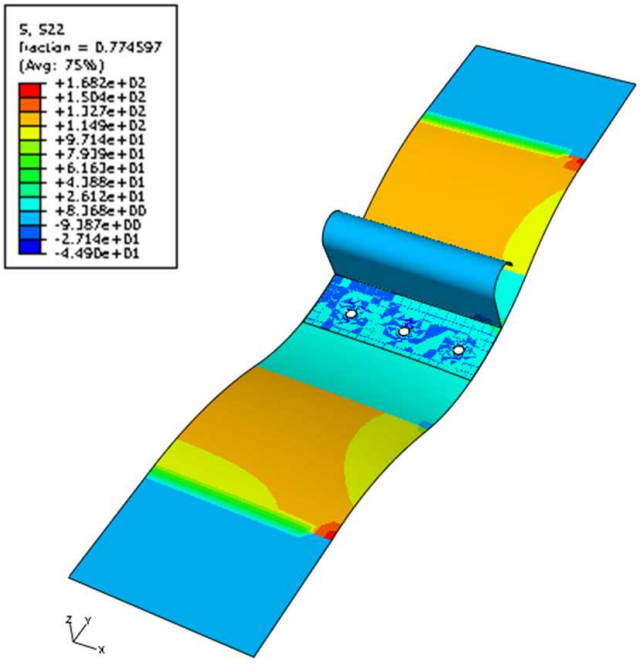

(b) Stress at the top surface .

Figure 6.5: Stress contour map in the stringer panel (unit=MPa).

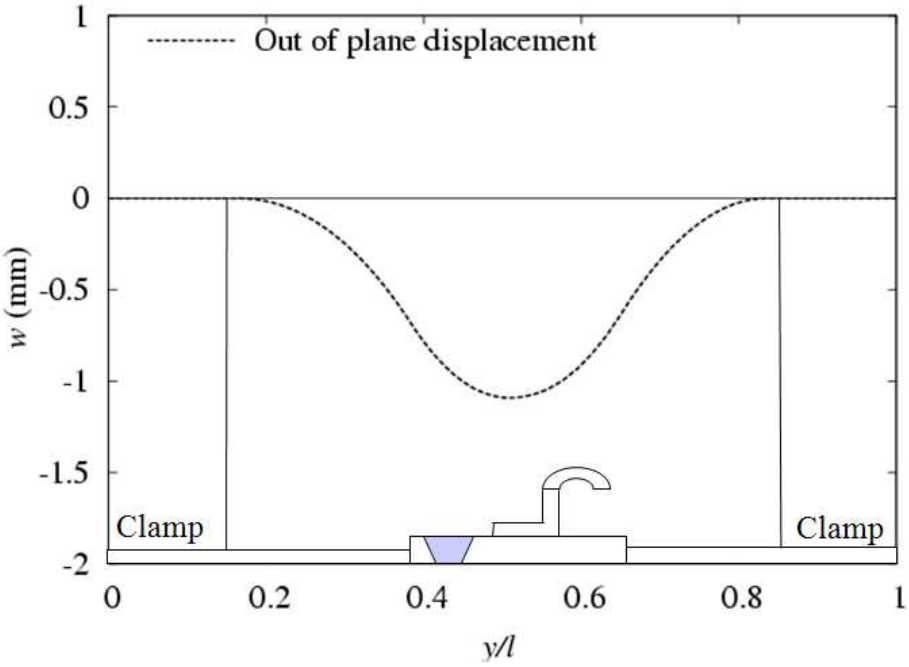

Figure 6.6: Out of plane displacement.

at the top face are higher than at the bottom surface. The out-of-plane displacement in the clamped panel has such concavity because it has to respect the derivability conditions.

Figure 6.7 show respectively the stress at the bottom and the top surface at the symmetry line. The concavity of the out of plane displacement explains those two graphs. Outside the pad-up area the stress and strain at the top are higher than those at the bottom because the concavity of the displacement is downwards while in the pad-up area the bottom stresses are higher because the concavity is upwards.

Figure 6.8 shows the component of the bending and the mean stress on the symmetry line. Higher bending stresses arise in the pad-up central area because more bending occur. The mean stress is 100 MPa in the panel while it is close to 60 MPa in the weld area where the crack will propagate as expected.

6.2.3 Weld residual stress effect

Welding has three influential factors on the fatigue crack propagation that are: residual stresses, change in microstructure, hardness changes therefore the ductile

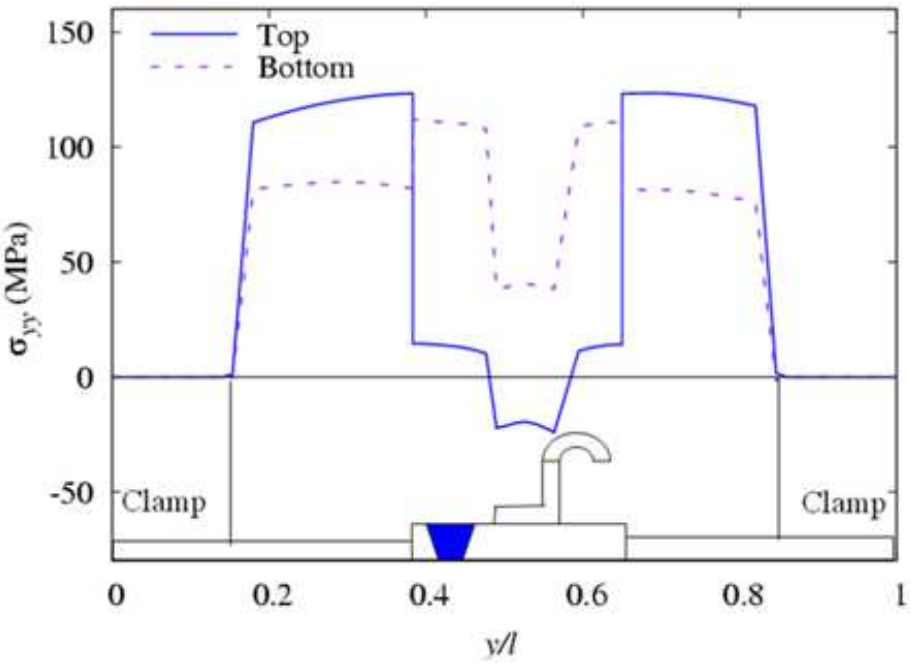

Figure 6.7: Longitudinal stress in clamped conditions.

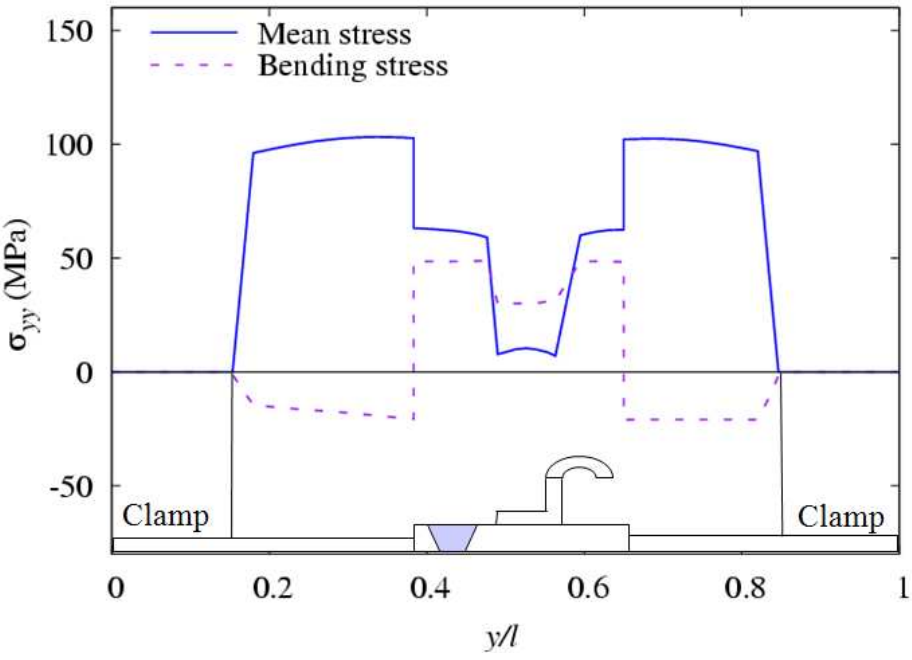

Figure 6.8: Mean and bending stress a the symmetry line.

properties, i.e. the yielding stress changes and it can influence the intrinsic material properties of the fatigue crack growth rate. When the crack grows into the nugget of the weld the microstructure has a big influence [158] but in this case the crack grows just outside the weld close to the heat affected zone (see figure 6.2). Generally the residual stresses have been found to have a big influence on the fatigue crack growth [22, 27, 133]. The aim of this section is to investigate the effect of the residual stress field on the stress analysis. When the weld is perpendicular to the loading direction the residual stresses transverse to the weld itself are more important on the fatigue crack propagation. The residual stresses longitudinal to the weld are normally higher but in this case they do not contribute to open the crack because they are perpendicular to the applied load hence no contribution to the opening mode I. Those are the stress parallel to the crack propagation line that have no effect on crack growth. Figure 6.9 shows a FSW residual stress field assumed from published RS field which were found in literature [20, 111, 113]. The transverse residual stresses are assumed to be around 20 MPa which is the worst case scenario as discussed in chapter 2.

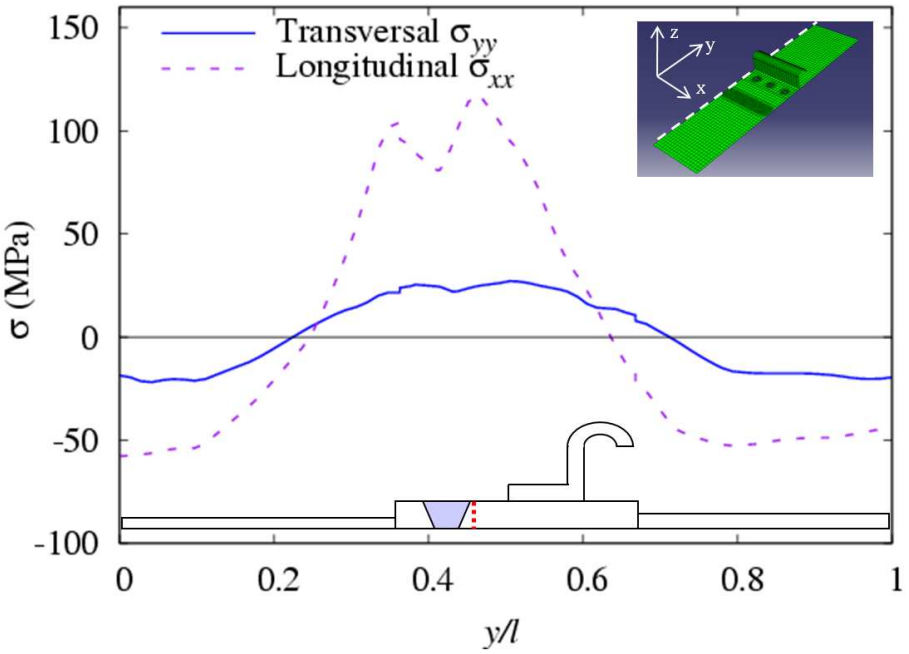

Figure 6.9: Inputted biaxial residual stress distribution.

This is the distribution and the magnitude that are inputted in the FE model to evaluate the effect of the welding. The two RS fields are balanced i.e. the integral of the stresses along the length y is zero. However they are not balanced respect

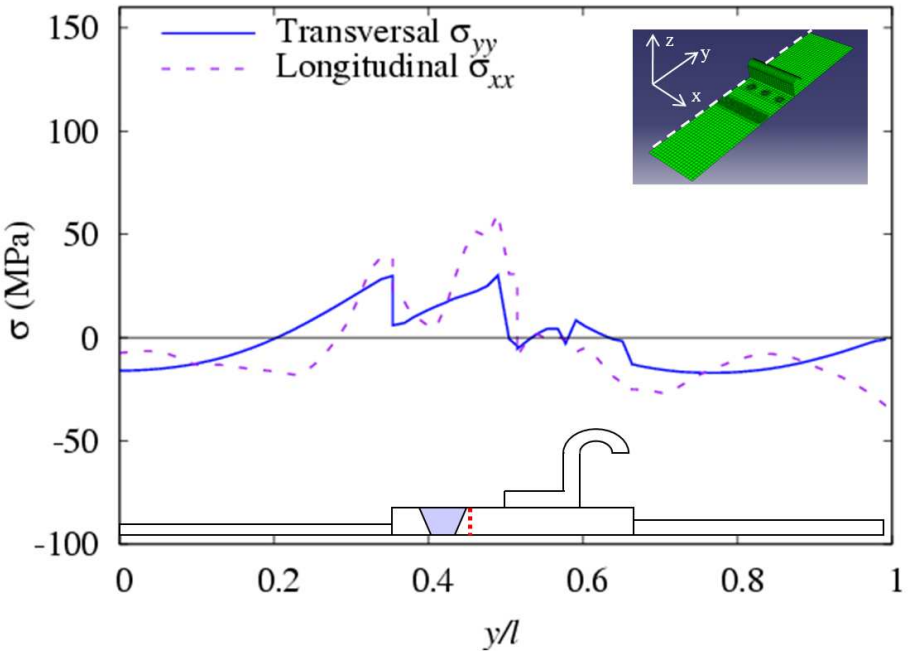

Figure 6.10: Biaxial residual stress distribution after balance on the symmetry line.

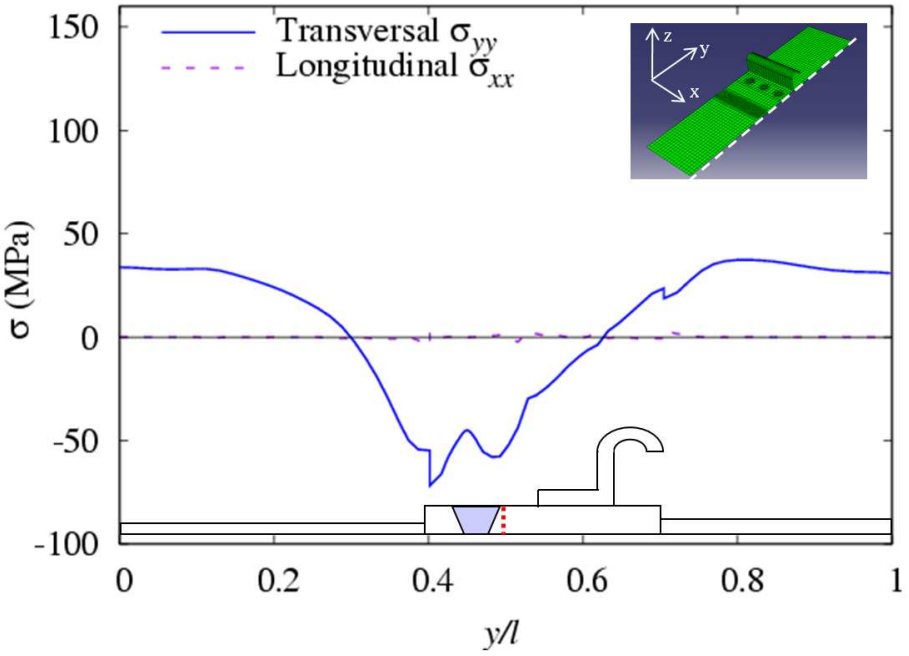

Figure 6.11: Biaxial residual stress distribution after balance on the free edge.

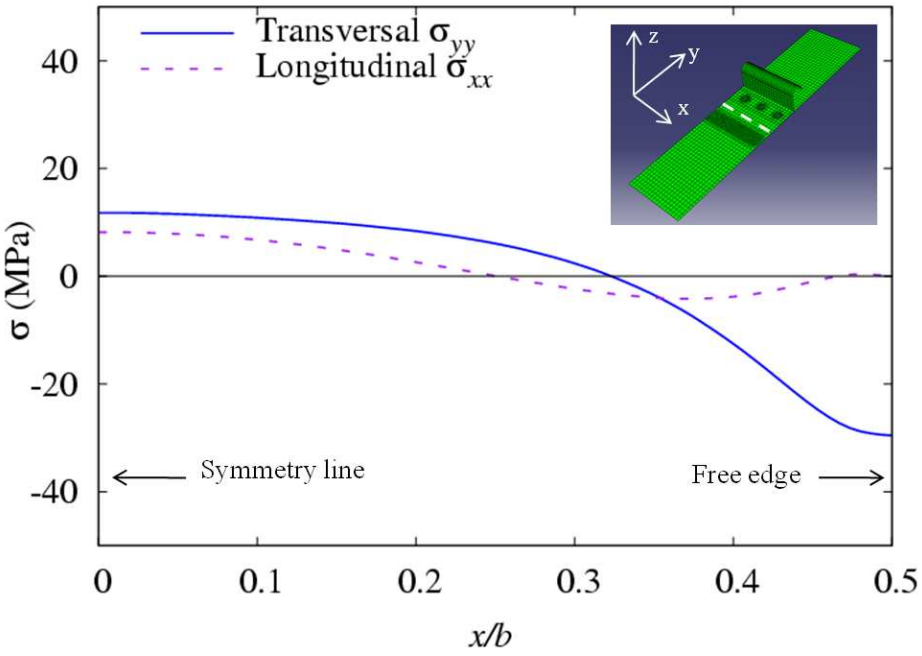

Figure 6.12: Biaxial stress distribution along the crack propagation line after balance.

to the geometry of the panel, for this reason they need to be settle considering the free edge, the change in thickness, and some eventually distortions that the RS field could cause. Figure 6.10 presents the biaxial residual stresses on the panel after the balance. Note that the redistribution of RS is not symmetrical because the specimen itself is not symmetric. It is interesting to notice how the stresses σ_{xx} become very low respect to the initial inputted RS. This is due to the geometry of the panel. The stresses σ_{xx} must be zero at the free edge because they are perpendicular to it hence in order to have a balanced residual stress field the σ_{xx} on the symmetry line need to be lower (see figure 6.11). Another reason is the change of the thickness in the pad-up. This high relaxation is mainly due to have the transversal direction longer than the longitudinal one. The ratio between the two characteristic lengths is strictly related to the relaxation of RS. The transversal stresses σ_{yy} after the balance behave in a different manner. They do not relax as much as the σ_{xx} because their direction is along the length which is double of the width. Moreover they are more affected to the change of the pad-up thickness. Figure 6.11 shows the biaxial RS field at the free edge of the panel. As expected the σ_{xx} are zero while the σ_{yy} changes in order to balance the stresses on the symmetry line. When the stresses are positive in the symmetry line they will be negative on the free edge. On the edge the negative

stresses values are around -50 MPa even if the tensile stresses are 20 MPa on the symmetry line. This is because the tensile stresses along the width will be tensile for a larger area than the compressive stresses.

Figure 6.12 shows the RS stresses plotted along the crack propagation line. From tensile stresses they both decrease and go negative in the last part close to the free edge. As expected the σ_{xx} stresses go to zero. The residual stresses have been balanced by using ABAQUS software as explained in section 3.

6.2.4 Stress intensity factor solutions

The MVCCT can be also used to calculate the stress intensity factor in presence of secondary bending due to the geometry of the panel which introduces a moment M_x and a rotation of the nodes around the x axis (figure 6.13). The original MVCCT takes the reaction forces and the nodes displacement which are on the symmetry line, hence it does not take into account the increase of stresses in the bottom surface due to the secondary bending. For this reason the contribution of the bending needs to be taken into account by adding the component of the moment M_x and the resulting rotation.

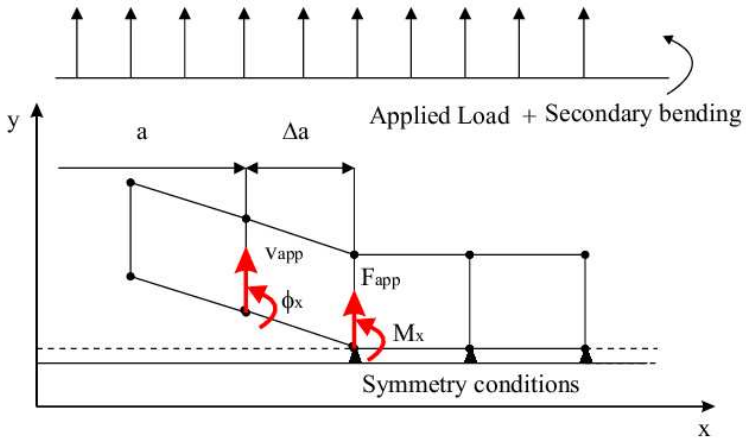

Figure 6.13: MVCCT with secondary bending effects.

According to the literature [165] the strain energy release rate due to an applied load which causes a secondary bending can be then calculated with:

$$G_{app,ben} = G_{app} + G_{ben} = -\frac{1}{\Delta at}(F_{app}v_{app} + M_x\phi_x) \tag{6.5}$$

Hence the SIF:

$$K_{app} = \sqrt{EG_{app,ben}} \quad \text{(plane stress)} \tag{6.6}$$

$$K_{app} = \sqrt{(\frac{E}{1-\nu^2})G_{app,ben}} \quad \text{(plane strain)} \tag{6.7}$$

Where the K_{app} is the SIF due to the applied stress which includes the influence of secondary bending. The stress intensity factor solution obtained for a maximum applied stress by using the MVCCT is shown in figure 6.14. The value obtained for the panel is very similar to the value of an equivalent M(T) specimen which maximum load is 60 MPa which is the stress value that occur in the pad-up area due to the increase of thickness. There is an increment of 10 - 20 % of the magnitude because of the secondary bending contribution.

The previous section shows that the transversal residual stress can have an influence on the fatigue crack propagation. This can be quantify in terms of stress intensity factor solution by calculating the K_{res} which is:

$$K_{res} = \sqrt{EG_{res}} \quad \text{(plane stress)} \tag{6.8}$$

$$K_{res} = \sqrt{(\frac{E}{1-\nu^2})G_{res}} \quad \text{(plane strain)} \tag{6.9}$$

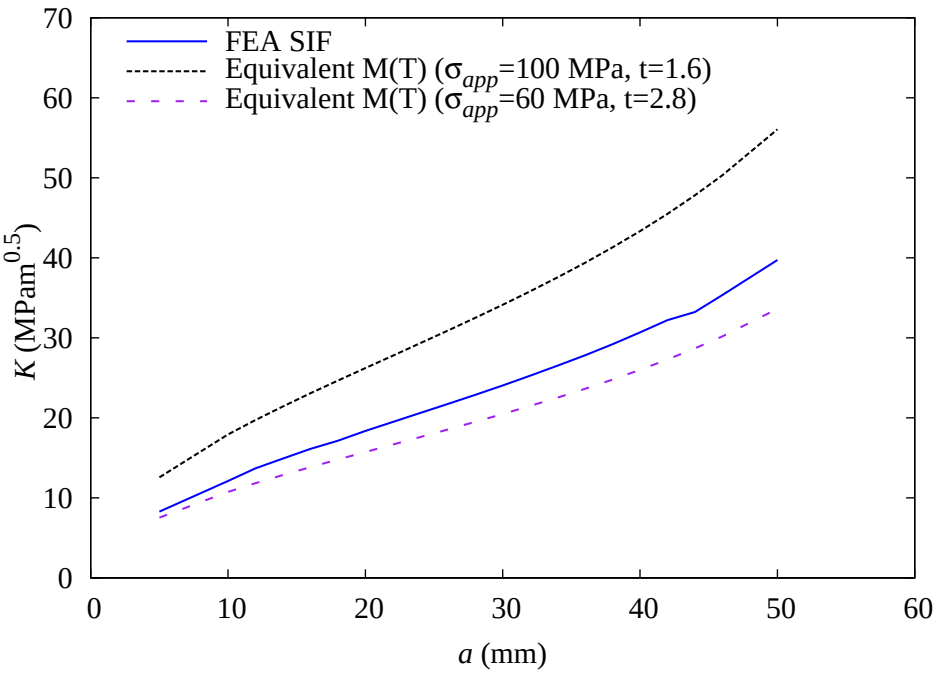

Figure 6.14: SIF calculated for the stringer panel and equivalent M(T) geometry.

Where G_{res} is calculated as previously explained in chapter 3. Both values of G_{res} and K_{res} for different crack lengths are shown in figure 6.15 which shows low values since the residual stresses were low.

In order to obtain the total stress intensity factor which includes the effects of the bending and the residual stresses the superposition is not valid anymore. There is a further component of coupling between the RS field with the applied tensional and bending load. For this reason it can also be written that:

$$K_{tot,max} \neq K_{res} + K_{app} \tag{6.10}$$

This is because with the superposition the coupling of the secondary bending with the residual stress will be not taken into account. Figure 6.16 shows the superpositions differences. $K_{max,tot}$ is calculated with one single analysis for both methods, so for the MVCCT:

$$K_{tot,max} = \sqrt{EG_{tot,max}} \tag{6.11}$$

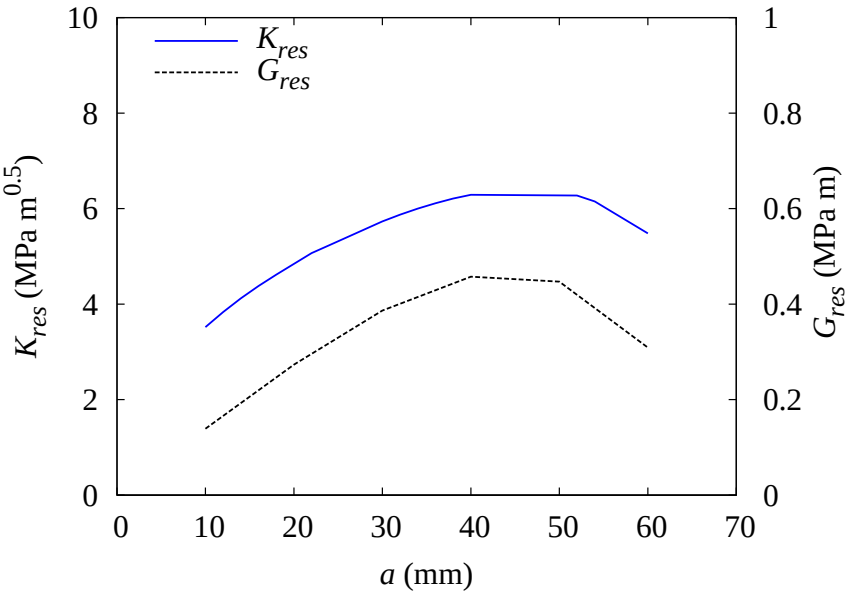

Figure 6.15: Strain energy release rate and K_{res}.

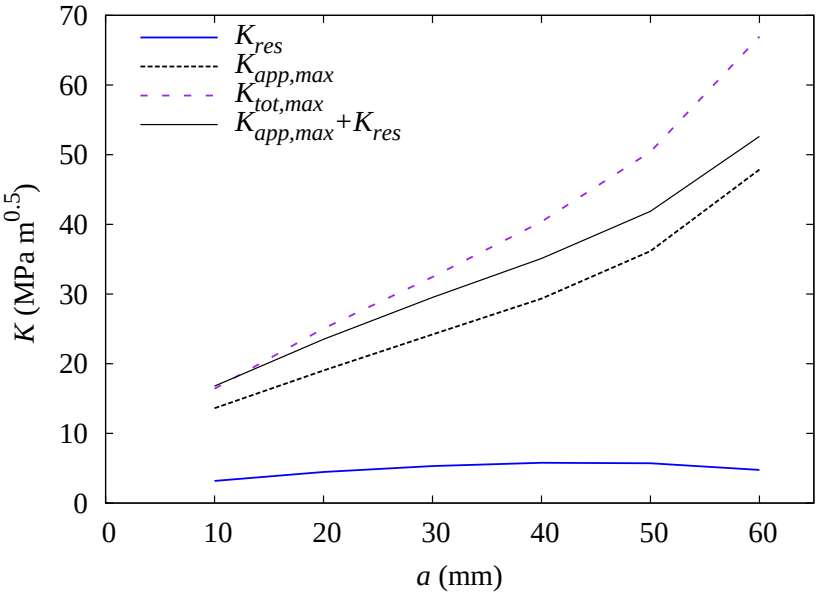

Figure 6.16: Superposition by using the MVCCT.

where G_{tot} considers both the secondary bending and the residual stress field:

$$G_{tot,max} = \frac{1}{\Delta a t}(F_{tot,max} v_{tot,max} + M_{x,tot} \phi_{x,tot}) \tag{6.12}$$

To find the effective stress intensity factor range the same equation:

$$\Delta K_{tot} = K_{max,tot} - K_{min,tot} \tag{6.13}$$

Which value is increased by the presence of initial residual stress field by more than 30% (see figure 6.17). Without secondary bending effect, $\Delta K_{tot} = \Delta K_{app}$.

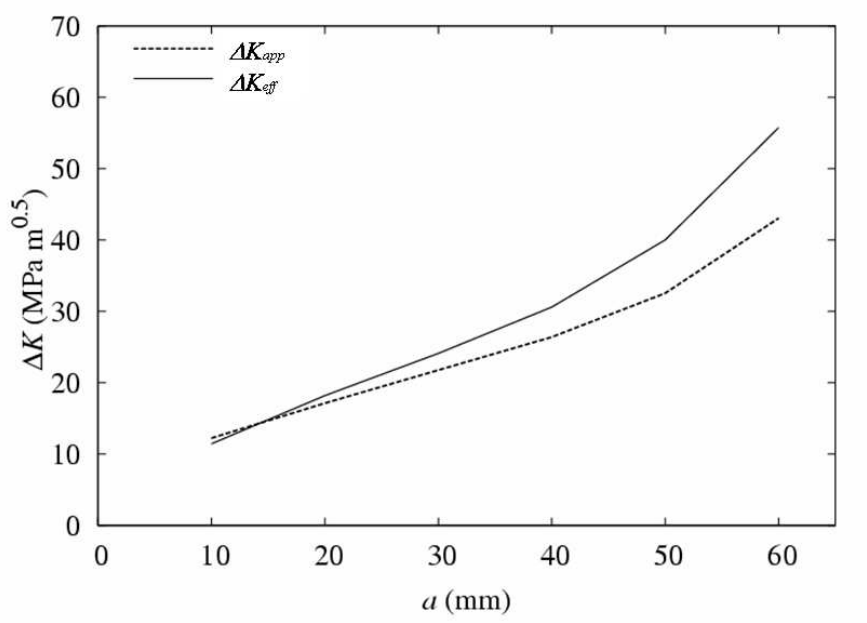

Figure 6.17: Stress intensity factor range.

Also the effective ratio R_{eff} influences the FCGR and it can be calculated as:

$$R_{eff} = \frac{K_{min,tot}}{K_{max,tot}} \tag{6.14}$$

The R_{eff} is changed respect to the nominal R up to 0.3 in the initial part when the RS are higher. The trend is similar to the distribution of the residual stresses along the crack propagation line.

6.3 Experimental tests

This section summarises the experimental tests conducted by the author. In order to assess the secondary bending due to the pad-up and stringer, and verify

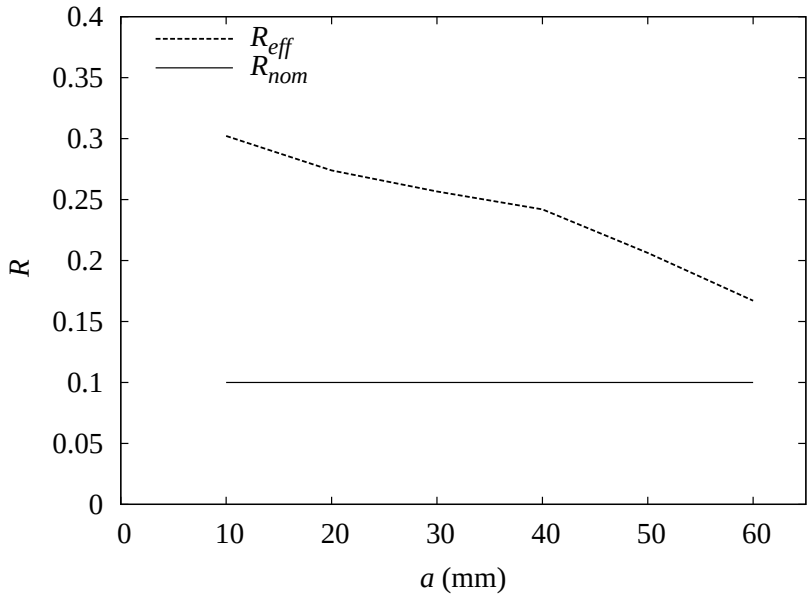

Figure 6.18: Effective R ratio.

the FE model, strains at selected location have been measured by using strain gauges. Measured fatigue crack growth life were compared with the prediction.

Figure 6.19: Fatigue test machine.

The INSTRON test machine used has a maximum load capability of 100kN as it is shown in figure 6.19. The panel was clamped at 50 mm at each end. The load is incrementally applied to a maximum of 100 MPa. A microscope was also used in order to observe the crack growing.

6.3.1 Test sample preparation and test process

A large sheet with two rivetted stringers was welded by AIRBUS (see figure 6.20) in order to assess the longitudinal FSW joint for fuselage panels. Since the scope is to study the crack propagating in a pad-up along the weld and the effects of the secondary bending induced by the pad-up itself and the stringer. Only one stringer has been considered and the following geometry was used. The coupons which geometry was previously described, is shown in figure 6.21. The notch is placed on the heat affected zone in the retreating side of the friction stir weld.

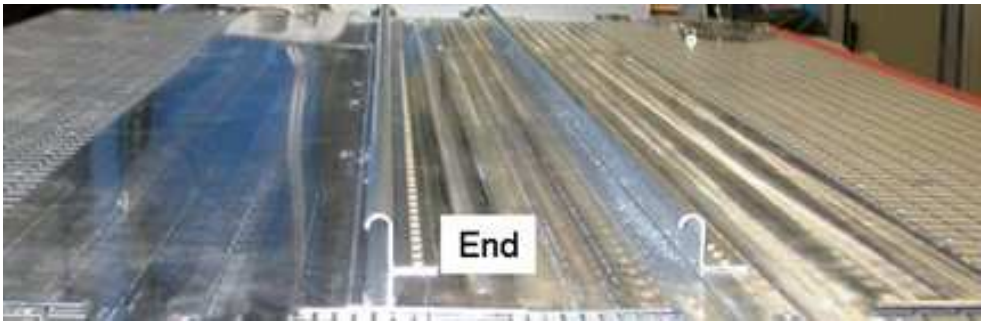

Figure 6.20: Large friction stir welded sheet with FSW direction.

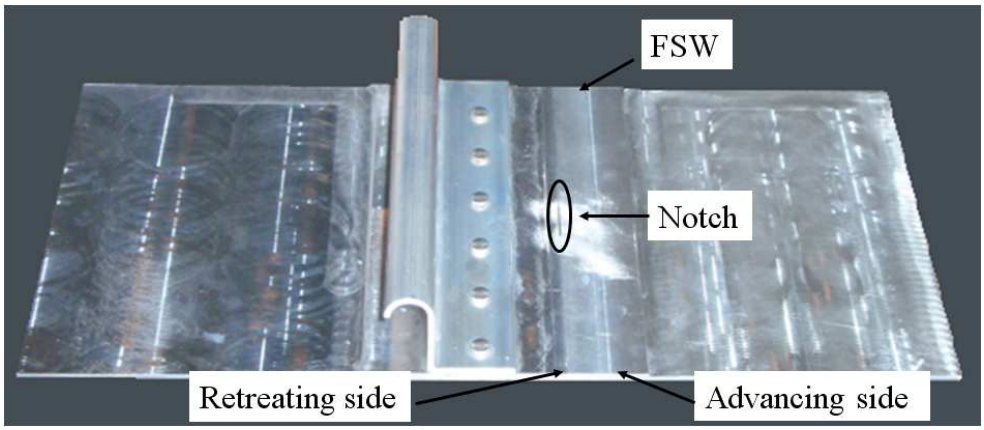

Figure 6.21: Photo of the test sample cut off from stringer panel.

Initial notched was made by electrical discharge machining (EDM), following the standard for the M(T) a radius of 0.25 mm with a length of 18 mm has

been made [162]. This is a common process to obtain material removal by using rapid electrical discharges or sparks that occur between two electrodes that are subjected to an electrical voltage. After the notch the specimen was polished in the area near the crack propagation in order to observe the crack propagation under cyclic load. Regular fine marks of 1 mm distance were scratched on the bottom surface using a Vernier height gauge (see figure 6.22).

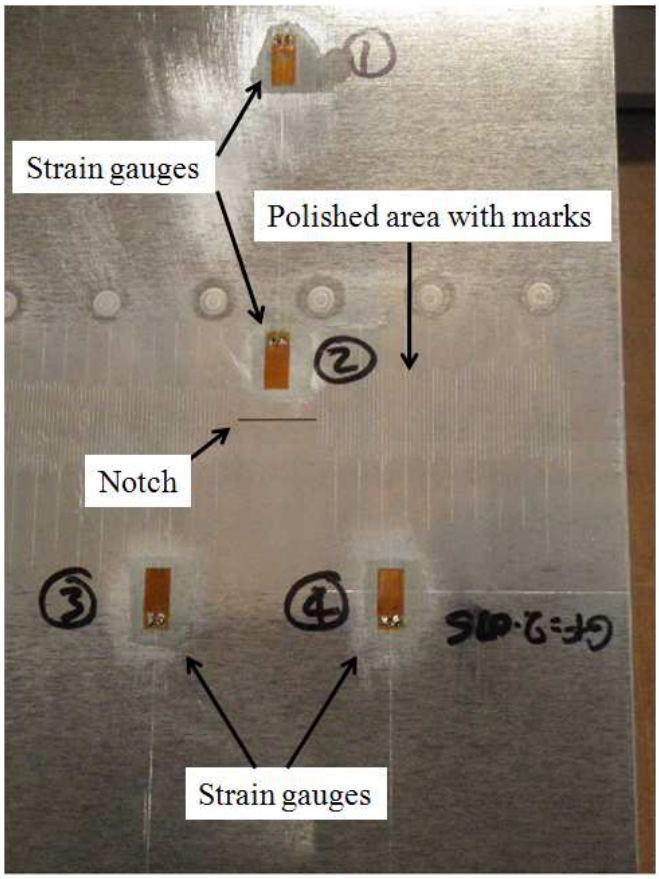

Figure 6.22: Preparation of the specimen.

Strain gauges were placed on both sides in order to understand the magnitude of the secondary bending. In order to do so they need to be bonded on the polished surface and then connected with a data amplifier by wiring them (see figure 6.23).

The strain gauge measurement principle is to measure the resistance of the circuit in the gauge. The gauge is connected to a Wheatstone bridge which measures the resistance of the circuit of the gauge. The connection of the Wheatstone bridge is standard, therefore it can be used to measure resistance by comparing

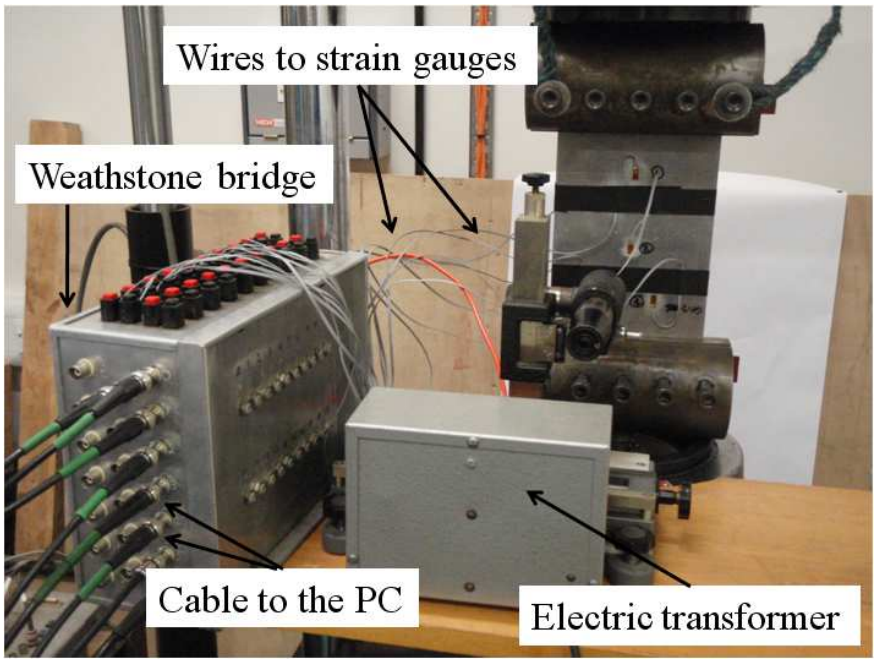

Figure 6.23: Strain gauges wire for measurement.

the unknown resistor against precision resistors of known value, hence:

$$GF = \frac{\Delta R/R_G}{\epsilon} \tag{6.15}$$

where GF is the gauge factor which is known and needs to be set before the measurement, R_G is the resistance of the undeformed gauge, ΔR is the resistance of the deformed gauge and ϵ is the strain. When the area within the strain gauge increases, the circuit area increases so the resistance is higher than its undeformed condition, i.e. the strain is tensile. In order to go from the voltage to the microstrain the following equation is used:

$$\frac{E_0}{E} = \frac{GF \cdot \epsilon \cdot 10^{-3}}{4} \tag{6.16}$$

Where E_0 is the difference in mV, E is the voltage and GF is the gauge factor. The values assumed are shown in table 6.2.

During the fatigue crack grow tests the crack was monitored by using a microscope and the marks previously done on the specimen. The pre-crack was at 1 mm length and it was at circa 3000 cycles (see figure 6.24). The crack was

Table 6.2: Parameters used in the strain gauges measurement.

Grid Resistance (Ohms)	120.0 ± 0.3 %
Voltage E (v)	5
Gauge factor	2.075

measured on both sides of the notch, right and left, and on the two surfaces which are the bottom surface and the top surface on the stringer side. Since secondary bending is involved, both top and bottom surfaces are observed for both experimental tests. The observation of the top surface was more difficult due to the compression, while the bottom surface was more easy to monitor hence more data are available.

6.3.2 Fatigue crack growth test results

Two test samples were tested at the same load conditions stated above. Figure 6.24 shows how the crack initiate and grow at the bottom of the specimen. It is measured with marks which interval is 1 mm. The crack was observed both on the right and the left side of the notch and on the top and the bottom surface of the specimen as defined in figure 6.25.

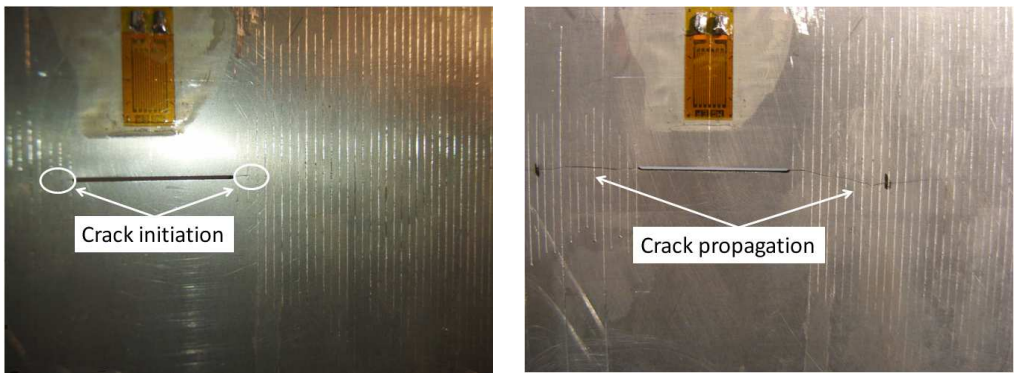

(a) Crack initiating from the notch. (b) Crack propagation.

Figure 6.24: Crack growth picture.

Figure 6.26 and 6.27 show the comparison of the top and bottom surface for the left and the right side of the notch respectively. They show a similar trend in the initial part of the crack growth: the top surface is lower. This was observed in both tests and it is explained by the higher tensile stresses which accelerate

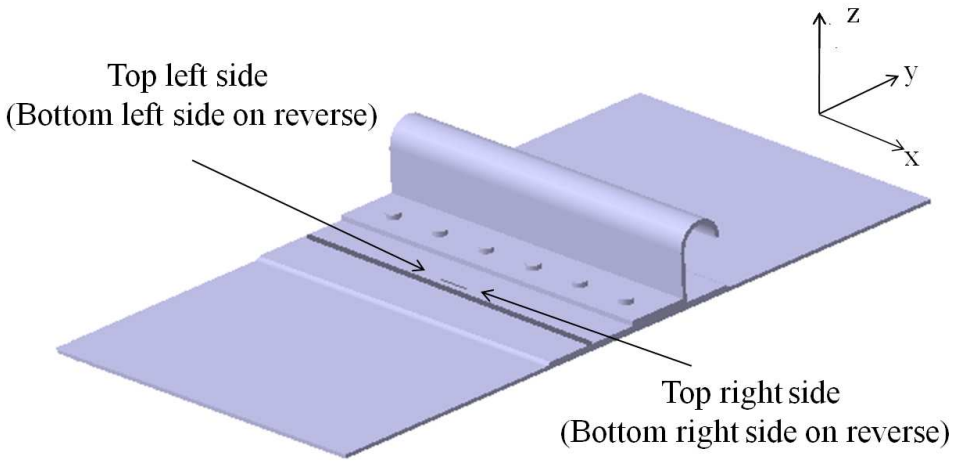

Figure 6.25: Definition of the crack propagation observation points.

the crack on one side with the respect to the other where lower tensile stresses occur, as it was observed by the FE analysis.

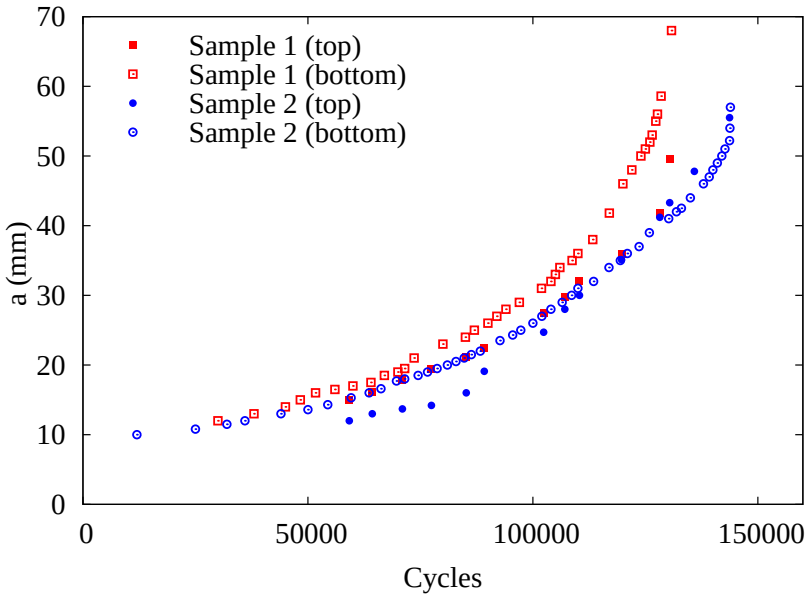

Figure 6.26: Comparison of the left side of the crack on top and bottom surface.

Figure 6.28 and 6.32 show the comparison of the left and right side of the notch in the for the first and the second test respectively. There is a good agreement in both test of the trend of the left and the right side. However this is not true for the rest of the crack propagation where for the left side of test two and the right side of test one the top surface was faster than the bottom. This is the

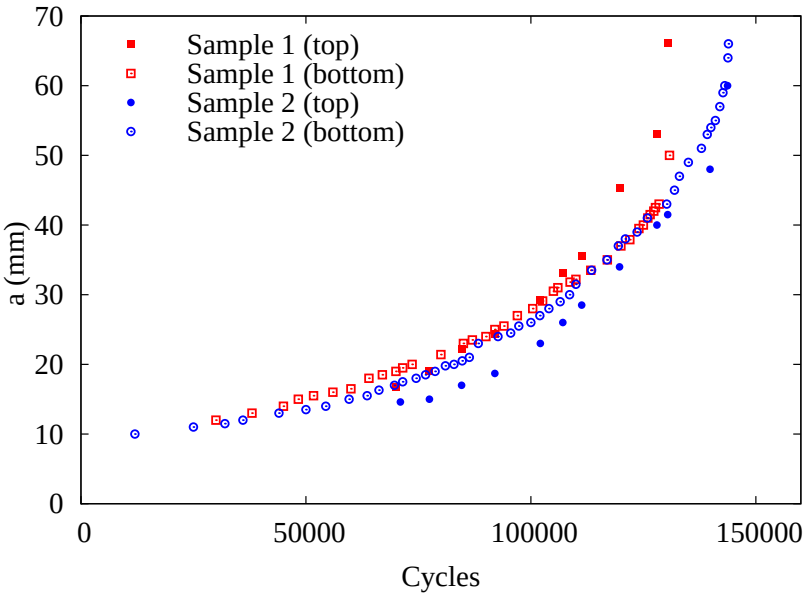

Figure 6.27: Comparison of the right side of the crack on the top and bottom surface.

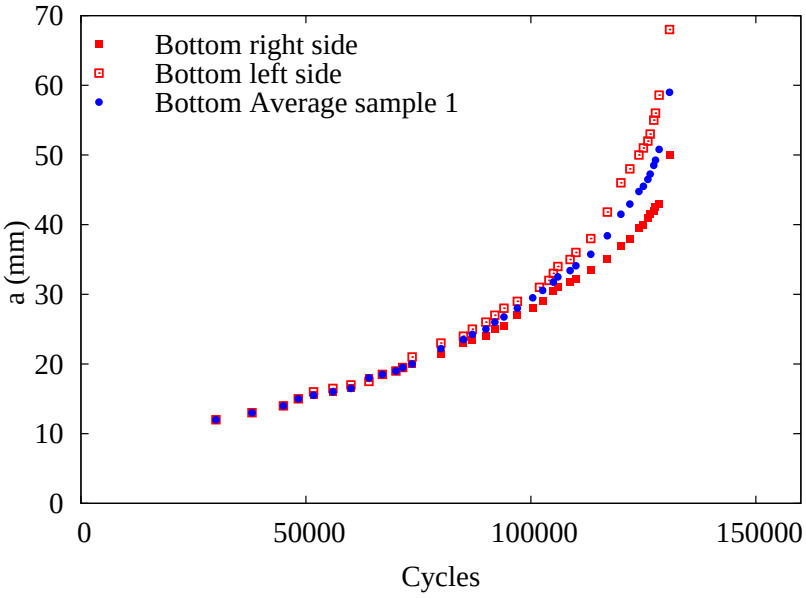

Figure 6.28: Comparison of the left and right side of the crack for sample 1, bottom surface.

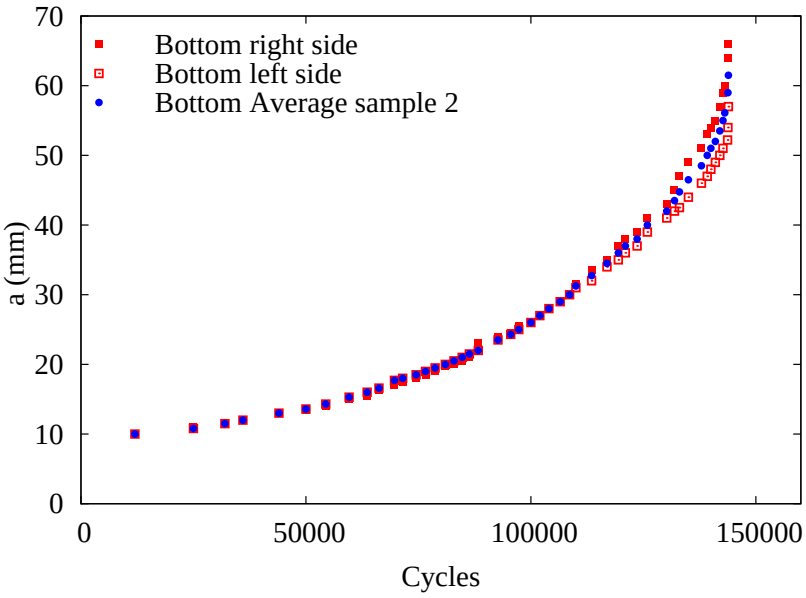

Figure 6.29: Comparison of the left and right side of the crack for sample 2, bottom surface.

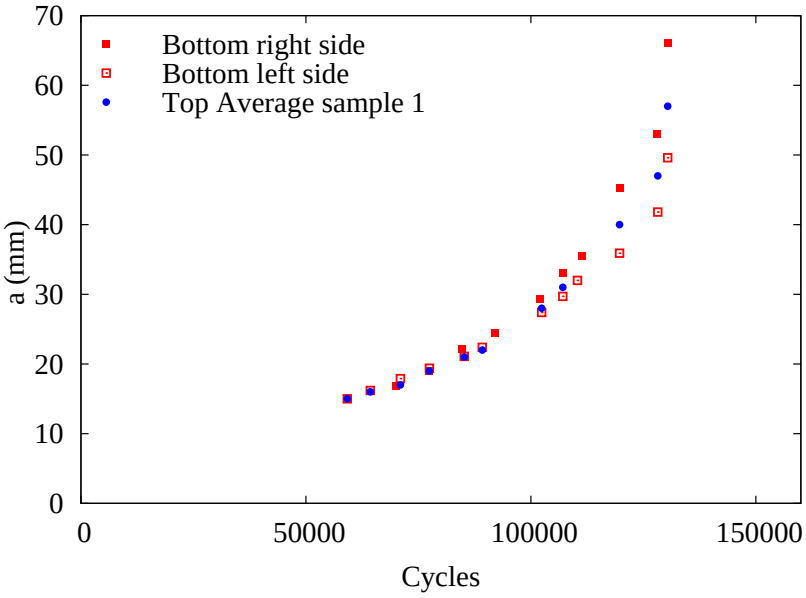

Figure 6.30: Comparison of the left and right side of the crack for sample 1, top surface.

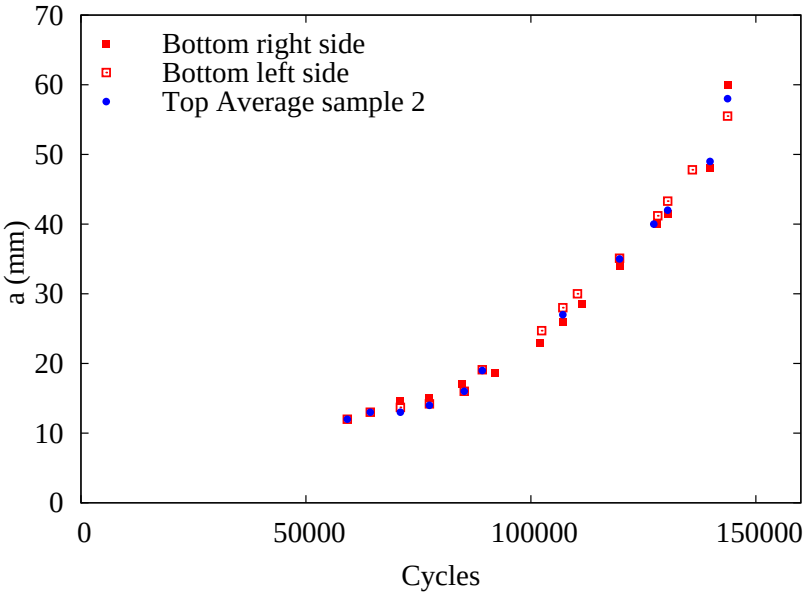

Figure 6.31: Comparison of the left and right side of the crack for sample 2, top surface.

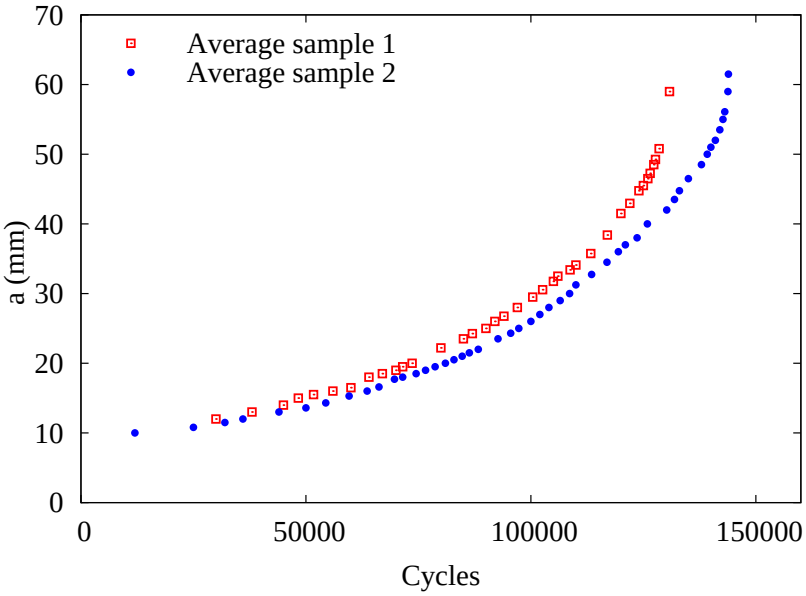

Figure 6.32: Comparison of the overall average of the two samples.

case in which some slightly deviation occur that change the plane of the crack propagation. The deviation in both cases is downwards towards the nugget area where the material is more ductile. The material properties in crack propagation area are not homogeneous and this may induce the crack to deviate one side only. Despite some changes of the crack propagation depending on the positions, both tests were consistent and their difference is 12% as it is shown in figure 6.32.

6.4 Comparison of modelling with experimental tests

6.4.1 Strains

In order to compare the strains in the model with the physical specimen eight strain gauges are placed on the positions shown in figure 6.33.

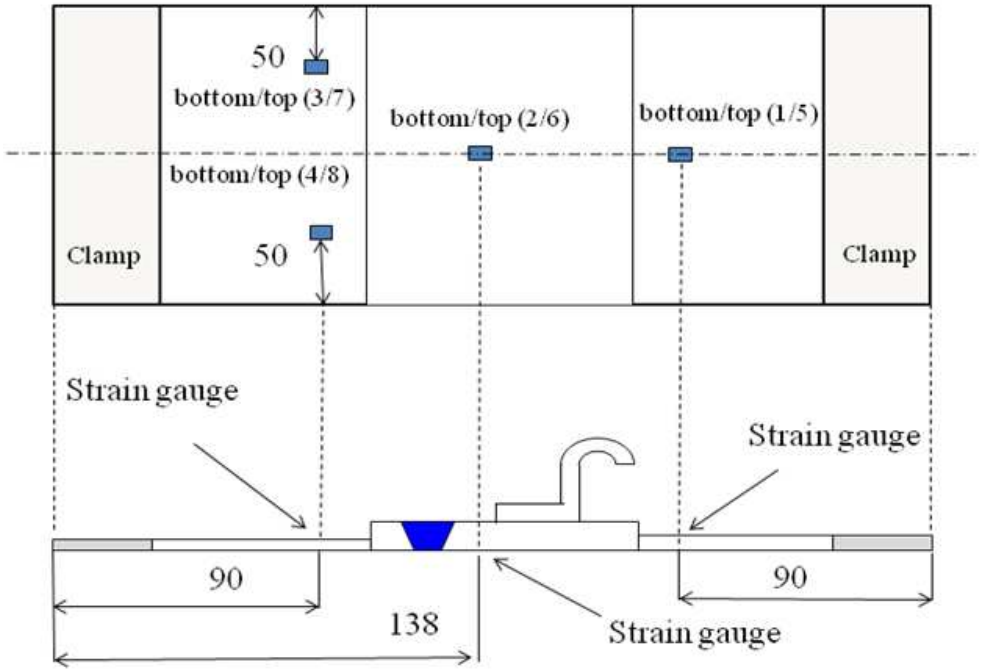

Figure 6.33: Strain gauges position (Dimension mm).

The comparison of the FE with the measured strain is very good for the gauges in positions 7 and 8 and there is also a reasonably good comparison for gauges number 1 and 5 where the calculated strain are 10-12% higher than the measured

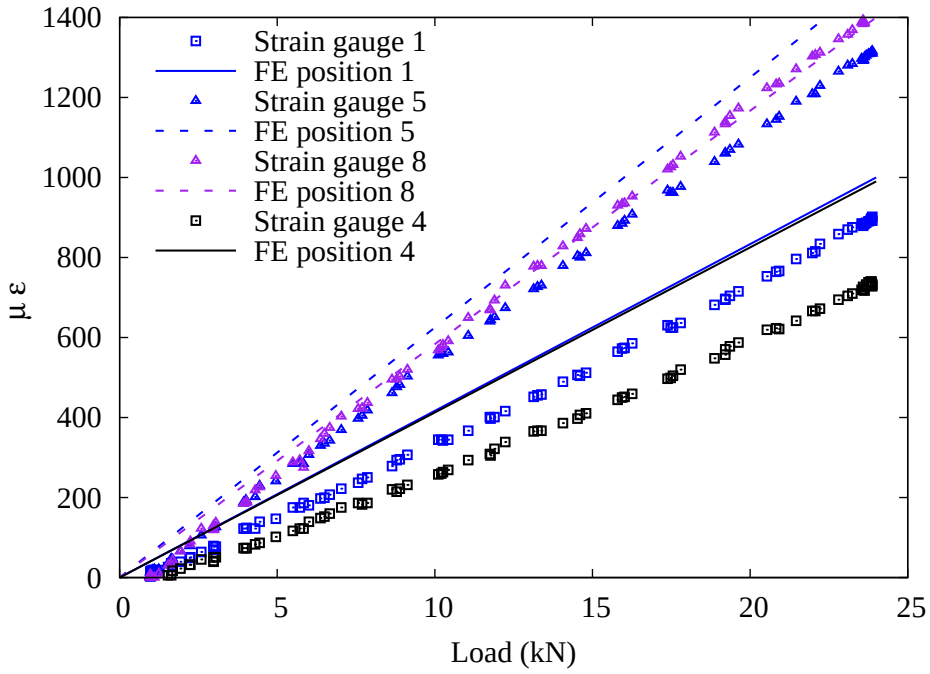

Figure 6.34: Calculated and measured strains.

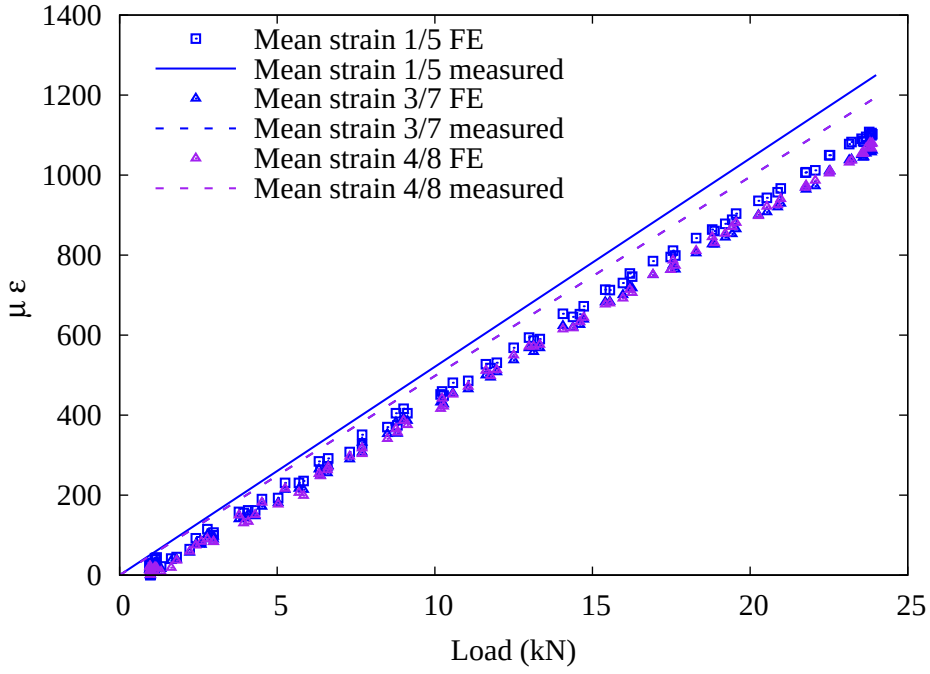

Figure 6.35: Calculated and measured mean strains.

one. The comparison is less accurate for positions 3 and 4 with and error higher than 30%. This can be explained by the actual thickness of the specimen and the nominal thickness of the specimen used in the FE model. During later measurements of the actual specimen the real thickness was found to be 1.7 and 2.74 mm for the panel and pad-up respectively. The calculated values used a nominal thickness which was 1.6 and 2.8 mm. Note the nominal thickness give the FE values of the general case hence can be applied also for other test cases. The measurement tests are valid only for this particular specimen. For this reason the measured strains are lower than the calculated one for the same applied stress of 100 MPa.

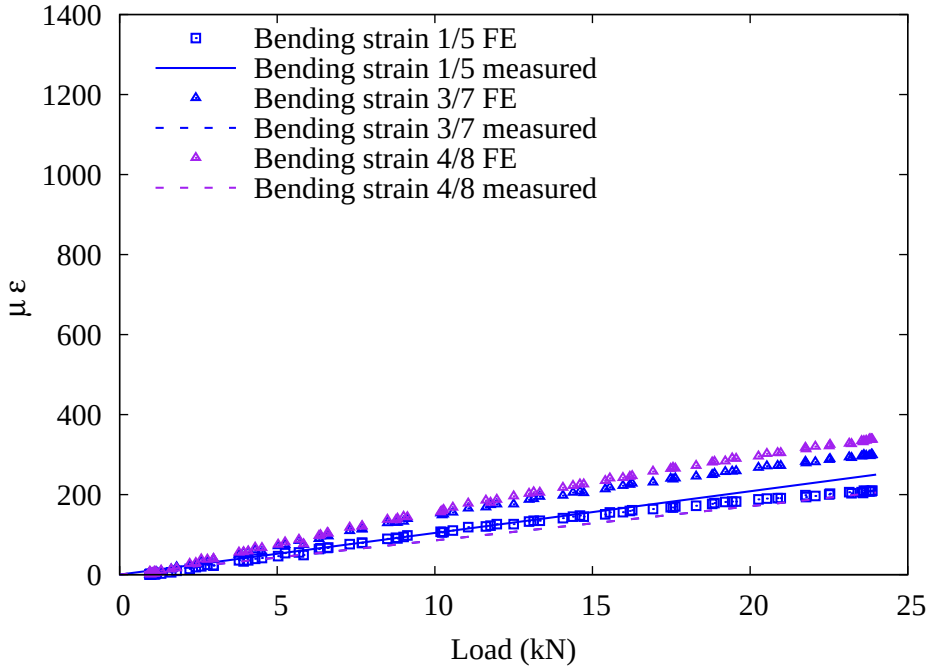

Figure 6.36: Calculated and measured bending strains .

The mean is shown in figure 6.35. The value of the measured are 7% lower than the calculated values. Because the real thickness is larger than the nominal the actual stress in the thin part of the panel is 6% lower. By assuming a elastic modulus of 77 GPa for the 2198 material, the mean stress corresponding to the 1250 $\mu\epsilon$ and 1150 $\mu\epsilon$ is 96 and 89 MPa respectively. The bending stresses are shown in figure 6.36 where the FE under estimate the measured values showing less bending. There is a good agreement again on the strain gauge 1 and 5 with an error less than 5%.

6.4.2 FCG lives

The prediction of the fatigue crack growth was made by employing two different material law curves i.e. the base material curve 2198 and the FSW material curve (weld metal WM). The first prediction uses the base material (BM) curve for different nominal R ratios, and the effective ratio was used to include the effect of the residual stresses. The WM da/dn material curve was taken from experimental [158] tests where an M(T) specimen made of the same material and with similar dimension to the panel (300X200 mm) was tested at a nominal ratio R=0.1. Moreover the crack is in the weld nugget centre and propagated parallel to the weld. Figure 6.37 compares the M(T) FS welded with the correspondent base material curve with R=0.1 which is the same R used for the stringer panel. This prediction has the SIF which considers the secondary bending by using the VCCT and the stress nominal ratio R=0.1 as input. The effective R is already in the FSW M(T) test curve. The method used is the Harter-T Method where there is a unique material curve at R=0.1.

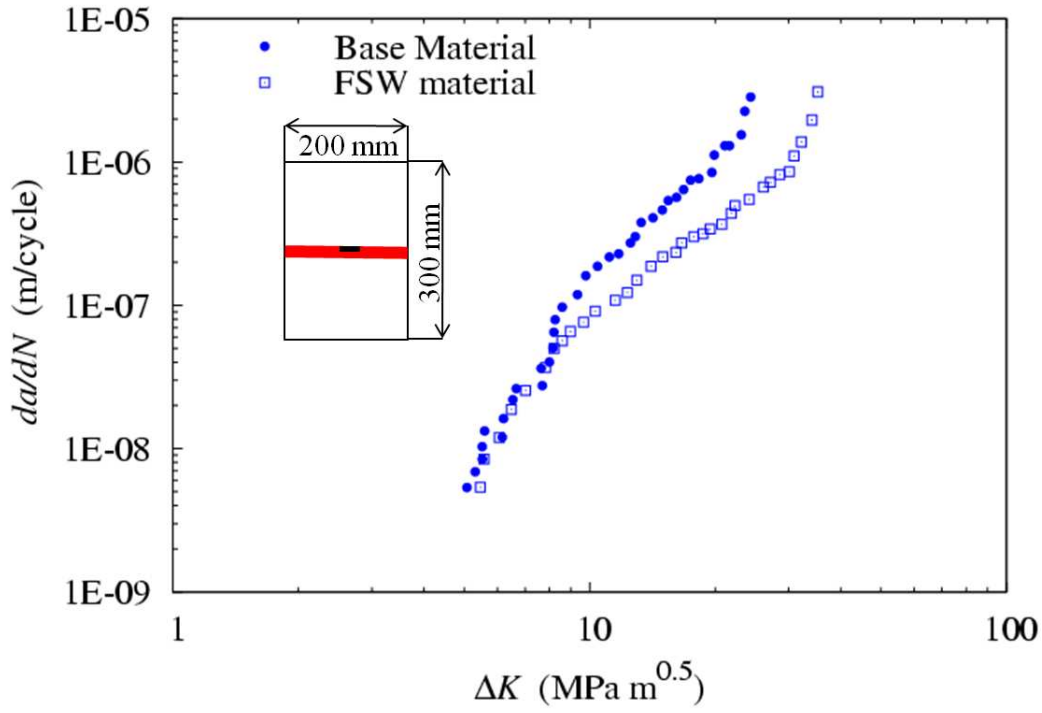

Figure 6.37: Material curve for 2198 FSW [158].

The comparison with the prediction shows that it is very important to choose the right material curve because the final prediction is very sensitive to it. It

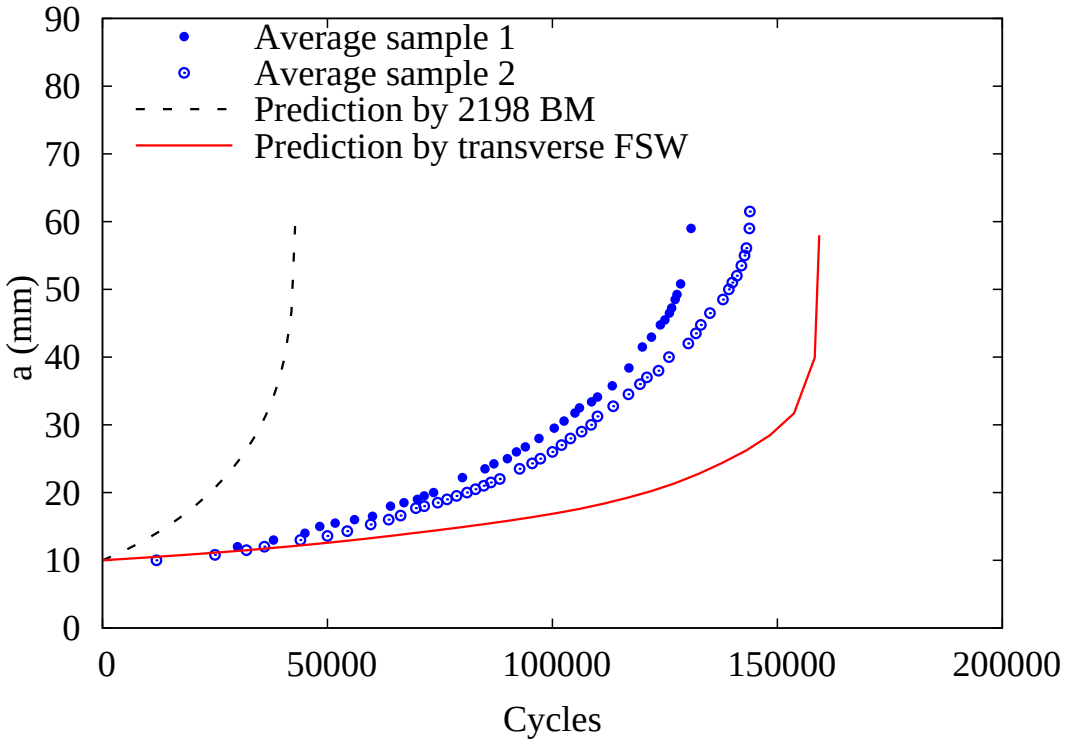

Figure 6.38: Comparison of the prediction with the experimental data.

is noteworthy the higher rate of the base material curve at R=0.1, which will further increase by considering the effects of R_{eff}. The FSW material law has already considered the residual stress contribution, hence this is the actual curve that needs to be considered to integrate the life. This explains the large difference of crack life shown in figure 6.38.

The error in the prediction by using the FSW plate is 21% which is less than the 30% scatter which normally occurs for fatigue [32, 49]. The material law herein used has only one curve at a R=0.1, but one needs more curves at different R in order to find the influence of the R_{eff} due to the residual stresses. However R_{eff} can be negligible if the residual stresses are low hence only the material curve can be used. Moreover the crack in this tests propagates along the weld in the heat affected zone in the retreating side, hence the fatigue properties are different from the fatigue properties in the nugget area. More investigation is necessary to understand the effects of the different fatigue properties at the different weld location, i.e. weld nugget area, heat affected zone, base material.

6.5 Summary of the chapter

A 2D FE model of a stringer panel with pad-up was build in order to assess the secondary bending and to observe the changes that this causes to the stress field. The results of the FE model were compared with the experimental measurement made by using strain gauges. Despite some error due to a difference between the nominal and actual thickness in the FE model and the physical specimen the comparison shows good agreement between the calculated and the measured strain values. The mean stress has an error which is lower than the 6% while the bending stress has errors which are from 5% up to 20% which are explained by a different thickness. The out of plane displacement shows a double curvature which is in accord with both FE and measured strain which are higher on the bottom and lower on the top when the curvature is upwards and viceversa when the curvature is downwards.

A typical biaxial residual stress field was assumed and input in the FE model. The effects of redistribution of longitudinal and transversal residual stresses have been evaluated in terms of K_{res} and R_{eff}. It was shown that also a low residual stress distribution increase the nominal ratio from R=0.1 up to 0.3 with a stress distribution of the order of 20 MPa. The stress intensity factor solution were also evaluated and non-linear effects of the secondary bending were accounted by adding in the MVCCT the bending component i.e. accounting of the moment and the rotation at the node at the crack tip. Then by knowing the K_{res}, the ΔK_{eff} was calculated by using the total stress intensity factor which were calculated from the SERR.

Experimental tests were performed and crack lengths were monitored at four different positions i.e. right and left at the bottom and the top surface. It was observed that the crack grew faster on the bottom of the surface except when the crack start to deviate into the nugget. The notch is placed in the heat affected zone and in both experiment tests the crack deviates into the nugget, a more ductile material. The importance of the crack propagation line position is pointed out in the comparison of the prediction with the experimental tests. There is a big difference in the life prediction depending on the material law used. The crack grows in the heat affected zone (HAZ) slower than the crack growing in the parent material.

Chapter 7

Conclusions

This is the conclusive chapter of the thesis. The summary of the research is presented in section 7.1 where the achievements of the objectives are addressed with conclusive remarks in section 7.2. Section 7.3 illustrates the novel findings of this research study. The limitations of the prediction methodologies and the approach of investigation have been discussed in section 7.4 in order to understand where the accuracy and the efficacy can be improved, and what are the future works that can be developed from this study, which are recommended in section 7.5.

7.1 Summary of the research

The research presented in this thesis addresses the effects of weld residual stresses on fatigue crack growth behaviour and life prediction methods. As the main influence the residual stresses have been discussed but also some considerations on the material laws that need to be used were done. The methodology developed to predict crack propagation, by accounting of the residual stress field due to the weld, was one of the first objectives which was achieved. It encloses stress analysis via FE, fracture mechanics by using superposition method and crack closure approach, and fatigue law which were modified in order to deem the initial residual stress field.

A literature review was done on different approaches to model the crack behaviour which grows through a compressive residual stress fields. It was found

a gap on the plasticity induced crack closure models without and with residual stress fields. Therefore a plastic model was build in order to evaluate the opening stress level induced by plasticity with a RS field. A first comparison without RS was done to validate the opening stress evaluation criteria with previous results found in literature. The model shows small error (in the order of 2%) in terms of crack opening displacement and in terms of opening stress values (less than 5%). The plasticity induced crack closure analysis was then investigated for a case with an initial weld residual stress field. A qualitative and a quantitative analysis of the main parameters such the COD, the plastic zone size and the plastic wake, were done. A relationship between plastic zone size, plastic wake, is quantified.

A better understanding of the mechanism of closure in presence of plasticity and residual stresses was given by identifying two opposite effects which influence the opening stress. It was explained that the second effect of RS, which increases the crack opening displacement, is dominant with respect to the first effects which creates a bigger plastic zone size, hence a bigger plastic wake. For this reason the opening stress value decreases when the crack propagates in a tensile residual stress field while it increases in a compressive residual stress field. The redistribution of residual stress when the crack propagates demonstrate that the redistribution of weld RS is mainly in the proximity of the crack line whilst 5 mm or more above it, their influence is still relevant and the changes from the initial distribution are minor. Such stresses mainly influence the crack opening stress value. A relationship between the opening stress and constant balanced RS fields is quantified as well as their influence in terms of stress, crack opening displacement, plastic zone size and plastic wake. The material law history and behaviour is also provided in terms of $\sigma - \epsilon$ curve and its effects on the two cases (with and without RS) are assessed and quantify for a particular chosen element. The plastic analysis of the ESE(T) shows that the crack closure for plane strain element is not relevant unless long crack propagation are deemed. In this case the second effect of the residual stresses field above the crack line propagation drives the crack opening value.

Several prediction methodologies for the crack propagation have been assessed. The FE method assures a balanced residual stress field from which the K_{res} was calculated via MVCCT. Prediction laws were compared by using either the superposition and the crack closure approach by meaning of the stress intensity factor

range ΔK_{eff}. It was found that the conventional superposition is not suitable for a crack propagating towards the weld, i.e. in a compressive RS, unless the Newman equation is used to calculate ΔK_{eff} via R_{eff}. Among the fatigue laws used within the superposition approach the most versatile and robust was the Harter-T method which could be used by simply knowing different material law curves at different nominal ratio R. The NASGRO equation was also showed to have a low percentage error (typically 12%) but it requires the knowledge of all the coefficients that can not be available for new materials. The comparison was made for different load condition and by using an M(T) specimen. Both constant amplitude load and constant stress intensity factor range were compared. When the crack grows into a compressive residual stress field the stress intensity factor range ΔK_{eff} is suggested because it better accounts for by the residual stress effects. The ΔK_{eff} can be then calculated by using either a plasticity induced crack closure model or by using the Newman equation with the R_{eff}. The drawbacks of using a plasticity induced crack closure is the computational effort, while the Newman equation is more efficient and equally accurate. It was found that plasticity has a marginal influence on the final fatigue crack growth rate. However a better understanding of their effects in welded structure is provided which is necessary to further investigate the behaviour of crack propagating under real load case scenario were overload may occur.

In the last chapter the investigation on a stringer panel which could be applicable to a fuselage was investigated. The structure was both tested and modelled. The stringer and the pad-up will affect the stress field in the crack propagation because of the secondary bending. Its influence was evaluated both by measuring the strain on the top and the bottom surface. The comparison between the two approaches was accurate even if some higher error occur for particular position, of the strain gauges, because of a difference between the nominal thickness and the real one. Experimental tests of crack propagation were run and the comparison with the prediction showed the importance of the choice of the material fatigue law. From experimental tests a deviation of the crack propagating from the thermal affected zone to the nugget was found. The latter demonstrate the importance of the fatigue material properties which can be matter for future work.

7.2 Conclusive remarks

In conclusion, the prediction methodologies of FCG, in welded residual stress field, are not affected by the material non-linearity under constant amplitude load conditions. The second effect of the residual stresses above the crack line overcomes a first effect that increases the plastic zone size. The following statements can be made:

- Tensile residual stresses create a first effect by producing a large plastic zone size, but no retardation of the FCG rate occur because the remaining stresses above the crack line increase the FCG.
- When the crack grows from the weld, the superposition approach via R_{eff} is a reliable and efficient approach as well as the crack closure approach which is accurate but computational expensive.
- When the crack grows towards the weld, crack closure approach via ΔK_{eff} can be used. ΔK_{eff} can be calculated with FE but also with Newman equation using R_{eff}, which save computational costs.
- When the crack grows parallel to the weld the thermal heat affected zone the material law is fundamental for FCG prediction while the RS are negligible because the transversal stresses have a low magnitude.

7.3 Contribution to the knowledge

Several novel findings and original approaches were found during this research work. The main aspects are herein listed:

- Assessment of the MVCCT in order to calculate the K_{res} and consequently the effects of the RS field on the crack propagation and assessment of the mutual work due to the synergy interaction of the purely mechanical force with the weld residual stress forces.
- Plasticity induced crack closure model with residual stresses: quantify the main parameters with and without RS, quantify the opening stress for

two RS field cases by taking into account the non-linear material effects, understanding of the effects of the residual stresses on the opening stresses induced by plasticity by identifying two opposite effects.

- Crack closure approach of a crack propagating into a compressive residual stress field: assessment of the Newman equation which account for the R_{eff}.
- Assessment of the fatigue crack growth life of a novel hybrid structure which combines the friction stir weld joints with classical rivetted stringers. The investigation was carried by both modelling and experimental testing.

7.4 Limitations

Limitations of the approaches are listed below:

- A large computational effort is needed for the plasticity induced crack closure analysis with residual stresses because a long crack propagation is needed to define the opening stress when the crack is propagating through the RS field.
- The superposition method can not be used to predict the crack growing through a compressive residual stress field. Therefore the caveats are applicable to two dimensional case.

7.5 Suggested work

Some possible future works that can be carried on starting from this research are suggested below:

- Extension of the plasticity induced crack closure with residual stress fields to other numerical methods such as extended finite element (XFEM) or boundary element methods (BEM) which could alleviate the computational effort involved in those analyses. Both of them are recent computational techniques that aim to alleviate the computational effort for singularity problems and increase the accuracy.

- Effect of the plasticity induced crack closure with residual stresses for variable amplitude load case i.e. overload, constant stress intensity factor range, random spectrum load.

- Discernment of the weld effects on the fatigue crack growth: microstructure, hardness properties and residual stresses. Understand the influence and the importance of all the three effects. Investigate the effect of the intrinsic fatigue properties of a welded plate by taking into account the crack propagation area: nugget, heat affected zone, thermo-mechanical affected zone, base material.

- Measurement of opening stress level in presence of compressive and tensile residual stress fields; application of more precise techniques, such synchroton or neutron diffraction, also to establish the differences in plane stress and plane strain for the plasticity induced crack closure and RS.

References

[1] P. Lequeu, F. Eberl, S. Jambu, T. Warner, A. Danielou and B. Bes. Latest Generation of Al-Li alloys Developed by Alcan Aerospace. In 19^{th} *Aeromat conference & exposition*, 23-26 June, 2008.

[2] B. Decreus, A. Deschamps and P. Donnadieu . Understanding the mechanical properties of 2198 Al-Li-Cu alloy in relation with the intra-granular and inter-granular precipitate microstructure . *Journal of Physic: conference series*, 240(1), 2010.

[3] Torsten Windhorst and Gordon Blount. Carbon-carbon composites: a summary of recent developments and applications. *Materials & Design*, 18(1):11 – 15, 1997.

[4] A.C. Orifici, I. Herszberg, and R.S. Thomson. Review of methodologies for composite material modelling incorporating failure. *Composite Structures*, 86(1-3):194 – 210, 2008.

[5] M.D. Isaac and O. Ishai. *Engineering mechanics of composite materials.* Oxford University Press, 2005.

[6] J.N. Reddy. *Mechanics of laminated composite plates and shells: theory and analysis.* CRC Press, 1997.

[7] M. C. Y. Niu. *Composite Airframe Structures.* Hong Kong Conmilit Press Ltd., 2005.

[8] H. J. Schmidt and B. Schmidt-Brandecker. Damage tolerance design and analysis of current and future aircraft structure. In *AIAA/ICAS International Air and Space Symposium and Exposition: the next* 100 *years*, Dayton, Ohio, July 2003. AIAA 2003-2784.

[9] M. Pacchione and J. Telgkamp. Challenges of the metallic fuselage. In 25^{th} *ICAS conference*, Hamburg, 2006.

[10] G. I. Nesterenko. Comparison of damage tolerance of integrally stiffened and rivetted structures. In *ICAS congress*, 2000.

[11] Xiang Zhang and Y. Li. Damage tolerance and fail safety of welded aircraft wing panels. *AIAA Journal*, 43(7), July 2005.

[12] W.M. Thomas. *Friction stir butt welding international patent application.* Number No. PCT/GB92. No. 9125978, 1991.

[13] R.G. Petitt, J.J. Wang and C. Toh. Validated feasibility study of integrally stiffened metallic fuselage panels for reducing manufacturing costs. *NASA/CR-2000-209342*, 2000.

[14] H. Matt. An emerging joining technology lets manufacturers rethink how products fit together. *Mechanical engineering*, March 2003. http://memagazine.asme.org/.

[15] COINS. Project proposal. Technical Report 30825, April 2006.

[16] M. Boz and A. Kurt. The influence of stirrer geometry on bonding and mechanical properties in friction stir welding process. *Materials & Design*, 25(4):343–347, June 2004.

[17] J. Pryzdatec. A ship classification view on friction stir welding. In *The 1st International Symposium on friction Stir Welding*, June 1999.

[18] E.O. Correa, S.C. Costa and J.N. Santos. Weldability of iron-based powder metal materials using pulsed plasma arc welding process. *Journal of Materials Processing Technology*, 198(1-3):323–329, March 2008.

[19] T. Saeid, A.A. Zadeh and B. Sazgari. Weldability and mechanical properties of dissimilar aluminum-copper lap joints made by friction stir welding. *Journal of Alloys and Compounds*, 490(1-2):652–655, February 2010.

[20] D.G. Richards, P.B. Prangnell, S.W. Williams and P.J. Withers. Global mechanical tensioning for the management of residual stresses in welds. *Materials Science and Engineering: A*, 489(1-2):351 – 362, 2008.

[21] G. Bussu. *Damage Tolerance of Welded Aluminium Aircraft Structures*. PhD thesis, Cranfield University, School of Industrial and Manufacturing Science, November 2000.

[22] G. Bussu and P. E. Irving. The role of residual stress and heat affected zone properties on fatigue crack propagation in friction stir welded 2024-T351 aluminium joints. *International Journal of Fatigue*, 25(1):77, 2003.

[23] R.C. McClung. A literature survey on the stability and significance of residual stresses during fatigue. *Fatigue Fract Engng Mater Struct*, 30:173–205, January 1997.

[24] L. Edwards, M. E. Fitzpatrick, P.E. Irving, I. Sinclair, X. Zhang, and D. Yapp. An integrated approach to the determination and consequencess of residual stress on the fatigue performance of welded aircraft structures. *Journal of ASTM International*, 3(2), February 2006.

[25] M.N. James, P.J. Webster, D.J. Hughes, Z. Chen, N. Ratel, S. Ting, G. Bruno and A. Steuwer. Correlating weld process conditions, residual strain and stress, microstructure and mechanical properties for high strength steel-the role of neutron diffraction strain scanning. *Materials Science and Engineering*, 427(1-2):16–26, July 2006.

[26] J. Lin, S. Ganaguly , L. Edwards and P.E. Irving. The effects of residual stress and HAZ on fatigue crack growth in MIG welded 2024 and 7150 aluminium. In *Fatigue*, 2003.

[27] C.D.M. Liljedahl, M.L. Tan, O. Zanellato, S. Ganguly, M.E. Fitzpatrick and L. Edwards. Evolution of residual stresses with fatigue loading and subsequent crack growth in a welded aluminium alloy middle tension specimen. *Engineering Fracture Mechanics*, 75(13):3881 – 3894, 2008.

[28] R.C. McClung and H. Sehitoglu. On the finite element analysis of fatigue crack closures. *Engineering Fracture Mechanics*, 33(2):253–272, 1983.

[29] J.C. Newman. A crack-closure model for predicting fagitue crack growth under aircraft spectrum loading. Technical Report Techincal memorandum 81941, NASA, January 1981.

[30] M. Beghini and L. Bertini. Effective stress intensity factor and contact stress for a partially closed griffith crack in bending. *Engineering Fracture Mechanics*, 54(5):667–678, July 1996.

[31] M. Beghini and L. Bertini. Fatigue crack propagation through residual stress fields with closure phenomena. *Engineering Fracture Mechanics*, 36(3):379–387, 1990.

[32] D. Broek. *Elementary engineering fracture mechanics*. Marinus Nijhoff Publishers, 4 edition, 1986.

[33] T. L. Anderson. *Fracture mechanics: fundamentals and applications*. CRC Press, 1995.

[34] M. Janssen, J. Zuidema and R. Wanhill. *Fracture mechanics*. Spon Press, 2004.

[35] J.R. Rice. Some remarks on elastic crack-tip stress fields. *International Journal of Solids and Structures*, 8:751–758, 1972.

[36] P.C. Paris and G.C. Sih. Stress analysis of cracks. *ASTM STP*, 381:30–81, 1965.

[37] J.A. Harter. *AFGROW users guide and technical manual*. Air Vehicles Directorate, AFRL-VA-WP-TR-2006-XXXX edition.

[38] W. Elber. The significance of fatigue crack closure. Technical Report STP-486, ASTM, 1971.

[39] E. Wolf. Fatigue crack closure under cyclic tension. *Engineering Fracture Mechanics*, 2(1):37–44, July 2007.

[40] K. Solanki, S.R. Daniewicz and J.C. Newman. Finite element analysis of plasticity-induced fatigue crack closure: an overview. *Engineering Fracture Mechanics*, 71(2):149–171, January 2004.

[41] K. Solanki, S.R. Daniewicz and J.C. Newman. Finite element modelling of plasticity-induced crack closure with emphasis on geometry and mesh refinement effects. *Engineering Fracture Mechanics*, 70(12):1475–1489, August 2003.

[42] J. Schijve. Some formulas for the crack opening stress level. *Engineering Fracture Mechanics*, 14(3):461–465, 1981.

[43] X. Niu and G. Glinka. On the limitations of the Petroski-Achenbach crack opening displacement approximation for the calculation of weight function. *Engineering Fracture Mechanics*, 26(5):701–706, 1987.

[44] A.H. Noroozi, G. Glinka and S. Lambert. A study of the stress ratio effects on fatigue crack growth using the unified two-parameter fatigue crack growth driving force. *International Journal of Fatigue*, 29(9-11):1616 – 1633, 2007.

[45] A.H. Noroozi, G. Glinka and S. Lambert. A two parameter driving force for fatigue crack growth analysis. *International Journal of Fatigue*, 27(10-12):1277–1296, 2005.

[46] S. Stoychev and D. Kujawski. Analysis of crack propagation using ΔK+ and Kmax. *International Journal of Fatigue*, 27(10-12):1425–1431, 2005.

[47] D. Kujawski. A fatigue crack driving force parameter with load ratio effects. *International Journal of Fatigue*, 23(Supplement 1):239–246, 2001.

[48] D. Kujawski. Correlation and prediction of fatigue crack growth for different R-ratios using Kmax and ΔK+ parameters. *Engineering Fracture Mechanics*, 71(12):1779–1790, 2004.

[49] S. Suresh. *Fatigue of Materials*. Cambridge University Press, 2006.

[50] D.P. Rooke and D.J. Cartwright. *Compendium of Stress Intensity Factors*. Her Majesty's Stationery Office, London, 1976.

[51] Y. Murakami. *Stress intensity factors handbook*. Pergamon, 1987.

[52] D.M. Tracey. Finite elements for determination of crack tip elastic stress intensity factor. *Engineering Fracture Mechanics*, 3:255–266, 1971.

[53] R.D. Henshell and K.G. Shaw. Crack tip elements are unnecessary. *International Journal of Numerical Methods in Engineering*, 9:495–509, 1975.

[54] E.F. Rybicki and M.F. Kanninen. A finite element calculation of stress intensity factors by a modified crack closure integral. *Engineering Fracture Mechanics*, 9:931–938, 1977.

[55] R. Krueger. The virtual crack closure technique: history, approach and applications. Report No. 2002-10 NASA/CR-2002-211628, ICASE, ICASE Mail Stop 132C NASA Langley Research Center Hampton, 2002.

[56] O.C. Zienkiewicz and R.L. Taylor. *The Finite Element Method.* McGraw-Hill, London, 1989.

[57] F. Dunne and N. Petrinic. *Introduction to Computational Plasticity.* Oxford University press, 2005.

[58] S.P. Timoshenko and J. N. Goodier. *Theory of elasticity.* McGraw-Hill Book Company, 1997.

[59] K. Solanki, S.R. Daniewicz and J.C. Newman. A new method for computing crack opening values from finite element analyses. *Engineering Fracture Mechanics*, 71(7-8):1165–1175, May 2004.

[60] N.A. Fleck and J.C. Newman. Analysis of crack closure under plane-strain conditions. mechanics of fatigue crack closure. *ASTM STP*, 982:253–272, 1983.

[61] R.C. McClung. On the finite element analysis of fatigue crack closure-1. numerical results. *Engineering fracture Mechanics*, 33(2):253–272, 1989.

[62] R.C. McClung. On the finite element analysis of fatigue crack closure-2. numerical results. *Engineering fracture Mechanics*, 33(2):272–293, 1989.

[63] R.C. McClung, B.H. Thacker and S. Roy. Finite element visualization of fatigue crack closure in plane-stress and plane-strain. *International Journal Fracture*, 50:27–49, 1991.

[64] S.J. Park and J.H. Song. Simulation of fatigue crack closure behaviour under variable-amplitude loading by a 2D finite element analysis based on the most appropriate mesh size concept. *ASTM STP*, 1343:337–348, 1999.

[65] Y.Z. Itoh, S. Suruga and H. Kashiwaya. Prediction of fatigue crack growth rate in welding residual stress field. *Engineering Fracture Mechanics*, 33(3):397–407, 1989.

[66] P. Lalor and H. Sehitoglu. Fatigue crack closure outside small scale yielding regime. *Mechanics of Fatigue Crack Closure*, ASTM STP 982:342–360, 1988.

[67] S.R. Daniewicz and J.M. Bloom. An assessment of geometry effects on plane stress fatigue crack closure using a modified strip-yield model. *International Journal of Fatigue*, 18(7):483–490, 1996.

[68] A. Gonzalez-Herrera and J. Zapatero. Influence of minimum element size to determine crack closure stress by the finite element method. *Engineering Fracture Mechanics*, 72:337–355, 2005.

[69] J. Wu and F. Ellyin. A study of fatigue crack closure by elastic-plastic finite element analysis for a constant-amplitude laoding. *Engineering Fracture Mechanics*, 33(2):253–272, 1989.

[70] H. Alizadeh, D.A. Hills, P.F.P. de Matos, D. Nowell, M.J. Pavier, R.J. Paynter, D.J. Smith and S. Simandjuntak. A comparison of two and three-dimensional analyses of fatigue crack closure. *International Journal of Fatigue*, 29(2):222–231, 2007.

[71] P.F.P. de Matos and D. Nowell. Numerical simulation of plasticity-induced fatigue crack closure with emphasis on the crack growth scheme: 2D and 3D analyses. *Engineering Fracture Mechanics*, 75(8):2087–2114, 2008.

[72] P.F.P. de Matos and D. Nowell. On the accurate assessment of crack opening and closing stresses in plasticity-induced fatigue crack closure problems. *Engineering Fracture Mechanics*, 74(10):1579–1601, 2007.

[73] P.F.P. de Matos and D. Nowell. The influence of the poissons ratio and corner point singularities in three-dimensional plasticity-induced fatigue crack closure: A numerical study. *Engineering Fracture Mechanics*, 74(10):1579–1601, 2007.

[74] J. Zapatero, B. Moreno and A. Gonzlez-Herrera. Fatigue crack closure determination by means of finite element analysis. *Engineering Fracture Mechanics*, 75(1):41–57, 2008.

[75] K.J. Kang, J. H. Song and Y. Y. Earmme. Fatigue crack growth and closure through a tensile residual stress field under compressive applied loading. *Fatigue of engineering Materials*, 12(5):363–376, 1989.

[76] J.C. Newman. FASTRAN-II- A fatigue crack growth structural analysis program. Technical report, NASA.

[77] P.F.P. de Matos and D. Nowell. Experimental and numerical investigation of thickness effects in plasticity-induced fatigue crack closure. *International Journal of Fatigue*, 31(11-12):1795 – 1804, 2009. Fatigue Damage of Structural Materials VII.

[78] S.R. Daniewicz and G.P. Potirniche. Modeling of fatigue crack growth threshold development for a microstructurally small crack. *Engineering Fracture Mechanics*, 72(9):1438 – 1453, 2005.

[79] J.C. Newman. An evaluation of the plasticity-induced-crack-closure concept and measurment methods. Technical Report TM-1998-208430, NASA, August 1998.

[80] H. Sehitoglu and W. Sun. *Engineering Fracture mechanics*, 33:371–388, 1989.

[81] A. Palazzotto and E. Bednarz. *ASTM STP*, 1020:530–547, 1989.

[82] P.F.P. de Matos and D. Nowell. Experimental and numerical investigation of thickness effects in plasticity-induced fatigue crack closure. *International Journal of Fatigue*, 31:1795–1804, 2009.

[83] D. Nowell, L.J. Fellows, D.A. Hills and Y. Xu. The effect of residual stress and strain on fatigue crack propagation: measurement and modelling. In *12th International Conference on Fracture (ICF12)*, 12-17 July, 2009.

[84] J.C. Newman. Analysis of out-of-plane bending in one-sided bonded repair. *ASTM*, STP 590:281–301, 1976.

[85] S.R. Daniewicz and S. Ismonov. Simulation and comparison of several crack closure assessment methodologies. *International Journal of Fatigue*, 32(2):428 – 433, 2010.

[86] J. Codrington and A. Kotousov. A crack closure model of fatigue crack growth in plates of finite thickness under small-scale yielding conditions. *Mechanics of Materials*, 41(2):165–173, February 2009.

[87] X. Zhang, A.S.L. Chan and G.A.O. Davies. Numerical simulation of fatigue crack growth under complex loading sequences. *Engineering Fracture Mechanics*, 42(2):305–321, May 1992.

[88] S. Pommier. Cyclic plasticity and variable amplitude fatigue. *International Journal of Fatigue*, 25(9-11):983 – 997, 2003.

[89] J.L. Chaboche. *Viscoplastic constitutive equations for the description of cyclic and anisotropic behaviour of metals.* Bull Acad Pol Sci, 1977.

[90] S. Pommier. Cyclic plasticity and variable amplitude fatigue. *International Journal of Fatigue*, 25(9-11):983 – 997, 2003.

[91] H.C. Choi and J. H. Song. Finite leement analysis of fatigue cracks in residual stress fields. *Fatigue and fracture of engineering materials and structures*, 18:105–117, 1995.

[92] J.C. Wang and Y.Z. Lu. Cyclic analysis of propagating short cracks at notches and short-crack growth behaviour. *Engineering Fracture Mechanics*, 34:831–840, 1989.

[93] R.C. McClung and D.L. Davidson. High resolution numerical and experimental studies of fatigue cracks. *Engineering Fracture Mechanics*, 39:113–130, 1991.

[94] C.Y. Hou and J.J Charng. The effect of the stress ratio during crack propagation and fatigue for 2024-T3 and 7075-T6 aluminium. *Engineering Fracture Mechanics*, 76(1):134–148.

[95] J.C. Newman. *ASTM STP*, 590:281–301, 1976.

[96] J.D. Dougherty, T.S. Srivatsan, J. Padovan. Fatigue crack propagation and closure behavior of modified 1070 steel: Experimental results. *Engineering Fracture Mechanics*, 56(2):167–187, January 1997.

[97] Karlsson & Sorensen Inc. Hibbit. *ABAQUS user/technical manual version 6.7*, 2007.

[98] A. Brot, Y. Peleg-Wolfin, I. Kressel and Z. Yosef. The damage-tolerance behaviour of integrally stiffened metallic structures. In *Israel Annual Conference on Aerospace Sciences*, 2008.

[99] C.D.M. Liljedahl, M.E. Fitzpatrick, L. Edwards. Evolution of residual stresses with fatigue crack growth in integral structures with crack retarders. *Materials Science and Engineering*, 523(6):152–159, June 2009.

[100] X. Zhang, M. Boscolo, D. Figueroa-Gordon, G. Allegri, P.E. Irving. Fail-safe design of integral metallic aircraft structures reinforced by bonded crack retarders. *Engineering Fracture Mechanics*, 76(2):114–133, 2009.

[101] B. Irving. Why aren't airplanes welded? *Welding Journal*, January 1997.

[102] I. Charit, R.S. Mishra and M.W. Mahoney. Multi-sheet structures in 7475 aluminum by friction stir welding in concert with post-weld superplastic forming. *Scripta Materialia*, 47(9):631–636, 2002.

[103] V. Soundararajan, S. Zekovic and R. Kovacevic. Thermo-mechanical model with adaptive boundary conditions for friction stir welding of Al 6061. *International Journal of Machine Tools and Manufacture*, 45(14):1577 – 1587, 2005.

[104] J. Su, T. W. Nelson, R. Mishra and M. Mahoney. Microstructural investigation of friction stir welded 7050-T651 aluminium. *Acta Materialia*, 51(3):713–729, 2003.

[105] J.A. Schneider and Jr Nunes. Thermo-mechanical processing in friction stir welding and processing II. *The Minerals, Metals & Material Society*, 51(3):43–51, 2003.

[106] M. Ericsson and R. Sandstro. Fatigue of friction stir welded AlMgSi-alloy 6082. *Materials Science Forum*, 331, 2000.

[107] P. Staron, M. Koak, S. Williams and A. Wescott. Residual stress in friction stir-welded Al sheets. *Journal of ASTM International*, 350:491–493, July 2004.

[108] R. John, K.V. Jata and K. Sadananda. Residual stress effects on near-threshold fatigue crack growth in friction stir welds in aerospace alloys. *International Journal of Fatigue*, 25(9-11):939–948, 2003.

[109] A. Chahardehi and F. P. Brennan. The effect of residual stresses arising from laser shock peening on fatigue crack growth. *Engineering Fracture Mechanics*, 77(11):2033–2039, 2010.

[110] P.J. Webster, L.D. Oosterkamp, P.A. Browne, D.J. Hughes, W.P. Kang, P.J. Withers, and G.B.M. Vaughan. Synchrotron X-ray residual strain scannin of a fiction stir weld. *Journal of strain analysis*, 36(1):61–70, 2001.

[111] S. Williams, P.A. Colgrove, H.R. Shercliff, P. Prangnell, J.D. Robson, P. Withers, D. Richards, A. Sullivan, N. Kamp, D. Lohwasser and M. Poad. Integrated modelling of the friction stir welding process. In *Proceedings of the 6th International Symposium on Friction Stir Welding*, 10-12 October 2006.

[112] Open University. Internal meeting and comunications. unpublished data, 2009.

[113] J. Altenkirch, A. Steuwer, M. Peel, D.G. Richards and P.J. Withers. The effect of tensioning and sectioning on residual stresses in aluminium AA7749 friction stir welds. *Materials Science and Engineering*, 488:16–24, 2008.

[114] L. Edwards P.J. Bouchard P.J. Withers, M. Turski and D.J. Buttle. Recent advances in residual stress measurement. *International Journal of Pressure Vessels and Piping*, 85(3):118 – 127, 2008.

[115] G. Ivetic, A. Lanciotti, and C. Polese. Eletric strain gauge measurement of residual stress in welded panels. *Journal Strain Analysis*, 44:117 – 126, September 2008.

[116] Standard test method for determining residual stresses by the hole drilling strin-gauge method. Technical Report ASTM E 837-01, West Conshohocker, Philadelphia, 2001.

[117] Y. Zhang, S. Ganguly, L. Edwards and M.E. Fitzpatrick. Cross-sectional mapping of residual stresses in a VPPA weld using the contour method. *Journal of strain analysis*, 52(17):5225–5232, 2004.

[118] Philip J. Withers. Mapping residual and internal stress in materials by neutron diffraction. *Comptes Rendus Physique*, 8(7-8):806 – 820, 2007.

[119] A. Steuwer, M.J. Peel, and P.J. Withers. Dissimilar friction stir welds in aa5083-aa6082: The effect of process parameters on residual stress. *Materials Science and Engineering: A*, 441(1-2):187 – 196, 2006.

[120] P.A. Colegrove and H.R. Shercliff. 3-Dimensional CFD modelling of flow round a threaded friction stir welding tool profile. *Journal of Materials Processing Technology*, 169(2):320–327, November 2005.

[121] M. Song and R. Kovacevic. Thermal modeling of friction stir welding in a moving coordinate system and its validation. *International Journal of Machine Tools and Manufacture*, 43(6):605–615, May 2003.

[122] C.M. Chen and R. Kovacevic. Finite element modeling of friction stir weldingthermal and thermomechanical analysis. *International Journal of Machine Tools and Manufacture*, 43(13):1319–1326, October 2003.

[123] F. Roger A. Bastier, M.H. Maitournam and K. Dang Van. Modelling of the residual state of friction stir welded plates. *Journal of Materials Processing Technology*, 200(1-3):25 – 37, 2008.

[124] K. Chang and C. Lee. Residual stresses and fracture mechanics analysis of a crack in welds of high strength steels. *Engineering Fracture Mechanics*, 74(6):980–994, April 2007.

[125] T. Teng, P. Chang and W. Tseng. Effect of welding sequences on residual stresses. *Computers & Structures*, 81(5):273–286, 2003.

[126] S.R. Rajesh, H.S. Bang, W.S. Chang, H.J. Kim, H.S. Bang, C.I. Oh, and J.S. Chu. Numerical determination of residual stress in friction stir weld using 3D-analytical model of stir zone. *Journal of Materials Processing Technology*, 187-188:224–226, December 2007.

[127] M. Beghini, L. Bertini and E. Vitale. Fatigue crack growth in residual stress fields experimental results and modelling. *Fatigue & Fracture of Engineering Material & Structures*, 17(12):1433–1444, 1994.

[128] G.A. Webster and A. N. Ezeilo. Residual stress distributions and their influence on fatigue lifetimes. *International Journal of Fatigue*, 23:375–383, 2001.

[129] G. Pouget and A.P. Reynolds. Residual stress and microstructure effects on fatigue crack growth in AA2025 friction stir welds. *International Journal of Fatigue*, (30):463–472, 2008.

[130] M.R. Hill. Modelling of residual stress effects using eigenstrain. In *Conference on fracture*, December 2001.

[131] A.M. Korsunsky, G.M. Regino and David Nowell. Variational eigenstrain analysis of residual stresses in a welded plate. *International Journal of Solids and Structures*, 44(13):4574 – 4591, 2007.

[132] J.M. Tan, M.E. Fitzpatrick and L. Edwards. Stress intensity factors for through-thickness cracks in a wide plate: Derivation and application to arbitrary weld residual stress fields. *Engineering Fracture Mechanics*, 74(13):2030–2054, November 2007.

[133] G. Servetti and X. Zhang. Predicting fatigue crack growth rate in a welded butt joint: The role of effective R ratio in accounting for residual stress effect. *Engineering Fracture Mechanics*, 76(11):1589–1602, July 2009.

[134] H.F. Bueckner. Observations on weight functions, engineering analysis with boundary elements. *The Minerals, Metals & Material Society*, 6(1):3–18, March 1989.

[135] W. Cheng and I. Finnie. Measurement of residual stress distributions near the toe of an attachment welded on a plate using the crack compliance method. *Engineering Fracture Mechanics*, 46(1):79–91, September 1993.

[136] L.P. Cook. Stress intensity factors handbook Volume 3 Y. Murakami (Editor-in-Chief) The Society of Materials Science. *International Journal of Fatigue*, 15(4):341–236, July 1993.

[137] T. Fett. Determination of residual stresses in components using the fracture mechanics weight function. *Engineering Fracture Mechanics*, 55(4):571–576, November 1996.

[138] T. Ghidini and C. Dalle Donne. Fatigue crack propagation assessment based on residual stresses obtained through cut-compliance technique. Technical Report 10.1111/j.1460-2695.2006.01059.x, EADS Deutschland GmbH, 2006.

[139] G. Glinka and G. Shen. Universal features of weight functions for cracks in mode I. *Engineering Fracture Mechanics*, 40(6):1135–1146, 1991.

[140] T. Fett. Limitations of the Petroski-Achenbach procedure demonstrated for a simple load case. *Engineering Fracture Mechanics*, 29(6):713–716, 1998.

[141] M. Beghini, L. Bertini and E. Vitale. Evaluation of the elastic stress distribution ahead of a crack by weight functions. *Engineering Fracture Mechanics*, 42(2):243–250, May 1992.

[142] H.F. Bueckner. A novel principle for the computation of stress intensity factor Z. *Angew. Math. Mech.*, 50:129–146, March 1989.

[143] X. Zhang R. Bao and N. A. Yahaya. Evaluating stress intensity factors due to weld residual stresses by the weight function and finite element methods. *Engineering Fracture Mechanics*, 77(13):2550 – 2566, 2010.

[144] A. Chahardehi and F.P. Brennan. A novel weight function for rms stress intensity factor determination in surface cracks. *Engineering Fracture Mechanics*, 2009.

[145] F. P. Brennan M.S. Abdul Manan. A novel weight function method to predict mode i stress intensity factors of multiple cracks. In *International Conference on Crack Paths (CP 2009)*, Vicenza, Italy, September 2009.

[146] O. Zanellato J. Lin M.L. Tan S. Ganguly P.E. Irving M.E. Fitzpatrick X. Zhang C.D.M. Liljedahl, J. Brouard and L. Edwards. Weld residual stress effects on fatigue crack growth behaviour of aluminium alloy 2024-T351. *International Journal of Fatigue*, 31(6):1081–1088, June 2009.

[147] G. Servetti, X. Zhang, Y-E Ma and P.E. Irving. Predicting fatigue crack growth rate in welded aluminium alloys: Effective stress ratio and crack closure corrections. In *12th International Conference on Fracture (ICF12)*, 12-17 July, 2009.

[148] T. Ghidini and C. Dalle Donne. Fatigue life predictions using fracture mechanics methods. *Engineering Fracture Mechanics*, 76(1):134–148, January 2009.

[149] K. Walker. The effect of the stress ratio during crack propagation and fatigue for 2024-T3 and 7075-T6 aluminium. *Engineering Fracture Mechanics*, 76(1):134–148.

[150] A.P. Parker. Residual stress effects in fatigue. In *ASTM STP*, volume 776, 1982.

[151] G. Glinka. Effect of residual stresses on fatigue crack growth in steel weldments under constant and variable amplitude loads. *ASTM Special Technical Publication*, (677):198–214, 1979.

[152] R. Galatolo and A. Lanciotti. Fatigue crack propagation in residual stress fields of welded plates. *International Journal of Fatigue*, 19(1):43–49, January 1997.

[153] C.D.M. Liljedahl, O. Zanellato, M.E. Fitzpatrick, J. Lin, and L. Edwards. The effect of weld residual stresses and their re-distribution with crack growth during fatigue under constant amplitude loading. *International Journal of Fatigue*, 32(4):735 – 743, 2010.

[154] Y.C. Fung. *Foundations of Solid Mechanics*. Prentice-Hall, 1965.

[155] J.C. Newman. A crack opening stress equation for fatigue crack growth. *International Journal of Fracture*, 24:131.

[156] J.C. Thompson F.K. Ibrahim and T.H. Topper. A study of the effect of mechanical variables on fatigue crack closure and propagation. *International Journal of Fatigue*, 8(3):135 – 142, 1986.

[157] *Metallic Materials and Elements for Aerospace Vehicle Structures*. MIL-HDBK-5H, 2005.

[158] P. Irving, Y. E Ma, X. Zhang, G. Servetti, S. Williams, G. Moore, J. dos Santos and M. Pacchione. Control of crack growth rates and crack trajectories for enhanced fail safety and damage tolerance in welded aircraft structures. In *ICAF Symposium*, 2008.

[159] L. Fratini, S. Pasta and A.P. Reynolds. Fatigue crack growth in 2024-T351 friction stir welded joints: Longitudinal residual stress and microstructural effects. *International Journal of Fatigue*, 31(3):495–500, March 2009.

[160] J. Brouard, J. Lin and P.E. Irving. Effects of residual stress and fatigue crack closure during fatigue crack growth in welded 2024 aluminium. *Materials Science and Engineering*, 427(1-2):16–26, July 2006.

[161] Y-E Ma, P.E. Irving, G. Servetti and X. Zhang. The effect of residual stress on fatigue crack propagation in friction stir welded 2198-T8 aluminium joints. In *12th International Conference on Fracture (ICF12)*, 12-17 July, 2009.

[162] Standard test method for measurement of fatigue crack growth rates. Technical Report ASTM E 647-00, Annual Book of ASTM Standards, 2001.

[163] GKSS. Internal meeting and comunications. unpublished data, 2009.

[164] COINS. Final report. Technical report, February 2010.

[165] C. H. Wang, L. R. F. Rose, R. Callinan. Analysis of out-of-plane bending in one-sided bonded repair. *International Journal of Solids and Structures*, 35(14):1653–1675, May 1998.

[166] A. Wade, M. Meith and R. Hill. Domain-independent values of the j-integral for cracks in three-dimensional residual stress bearing bodies. *Engineering Fracture Mechanics*, 69(12):1301–1314, August 2002.

[167] Y. Lei, N.P. O'Dowd and G.A. Webster. J estimation and defect assessment for combined residual stress and mechanical loading. *International Journal of Pressure Vessels and Piping*, 77(6):321–333, May 2000.

Appendix A

Dissemination of the results

The findings have been published/presented at the following forums.

1. G. Servetti, X. Zhang, Predicting fatigue crack growth rate in a welded butt joint: The role of effective R ratio in accounting for residual stress effect, Engineering Fracture Mechanics, Volume 76, Issue 11, July 2009, Pages 1589-1602.

2. G. Servetti, X. Zhang, Y-E Ma, P.E. Irving, "Predicting Fatigue Crack Growth Rate in Welded Aluminium Alloys: Effective Stress Ratio and Crack Closure Corrections", 12th International Conference on Fracture (ICF12), 12-17 July, 2009.

3. P. Irving, Y. E Ma, X. Zhang, G. Servetti, S. Williams, G. Moore, J. dos Santos, M. Pacchione "Control of crack growth rates and crack trajectories for enhanced fail safety and damage tolerance in welded aircraft structures", 25th ICAF Symposium, Rotterdam, 27-29 May, 2009.

4. Y-E Ma, P.E. Irving, G. Servetti, X. Zhang, "The effect of residual stress on fatigue crack propagation in friction stir welded 2198-T8 aluminium joints", 12th International Conference on Fracture (ICF12), 12-17 July, 2009.

Appendix B

Fuselage panel: technical drawings and modelling approaches

Figure B.1 shows the section dimension of the pad-up of the fuselage panel with FSW and rivetted stringer.

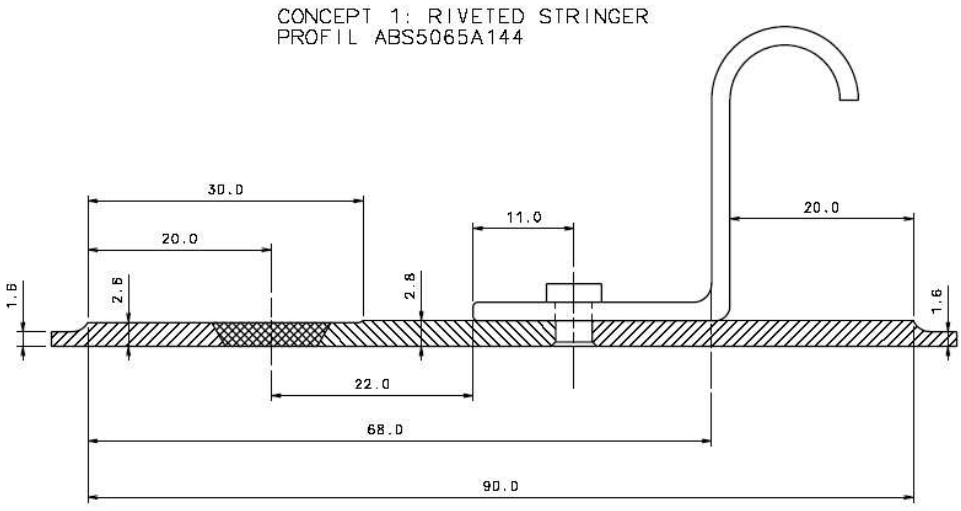

Figure B.1: Section of the hybrid concept: FSW and rivetted stringer [164].

The following study is an addendum to chapter 6, and it aims to investigate the J-integral method for calculate the stress intensity factor.

The J-integral has been found to have some problems dealing with residual stress field and some modifications have been proposed [166, 167] but they could be implemented in "house made" finite element code instead of the commercial FE code.

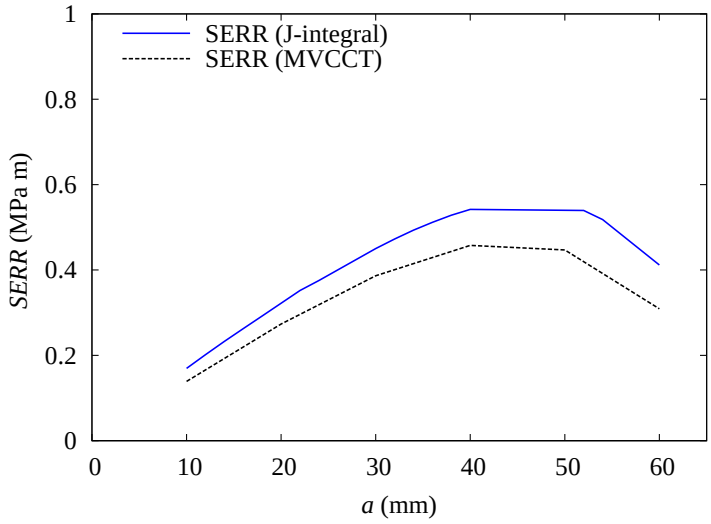

Figure B.2: Strain energy release rate from RS field.

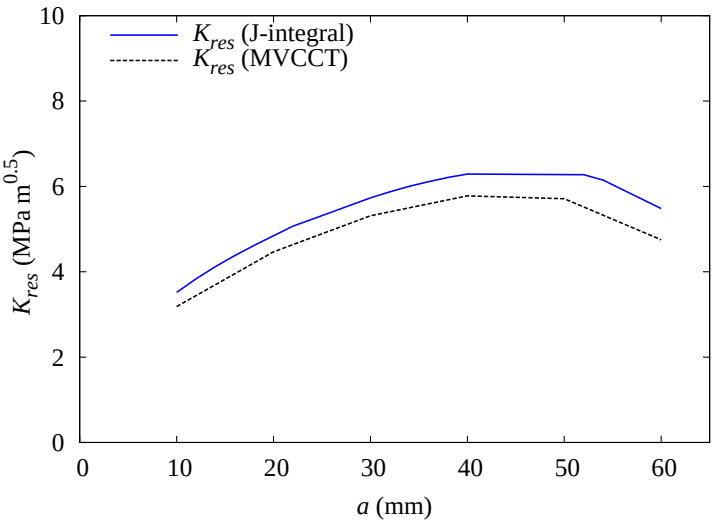

Figure B.3: Comparison of the residual SIF.

The definition of the J-integral is that is path independent hence any contour lines can be used to calculate the strain energy release rate. However with residual stresses this is not true anymore because the path will depend on where is calculated since the residual stresses change from one point to the other. Moreover the initial stress state is not taken into account according to ABAQUS FE

commercial code [97]. On the other hand some other authors used J-integral with RS by showing a good correlation of the crack growth prediction with the experimental tests [27] assuming a small error in the evaluation of K_{res}. The residual stresses that contribute to the SIF are in this case low so it is worth to see what is the error by using the J-integral together with the secondary bending. The evaluation and comparison of the two techniques is shown in figure B.2. There is a difference in the evaluation of the stress intensity factor and the strain energy release rate that is around 15%.

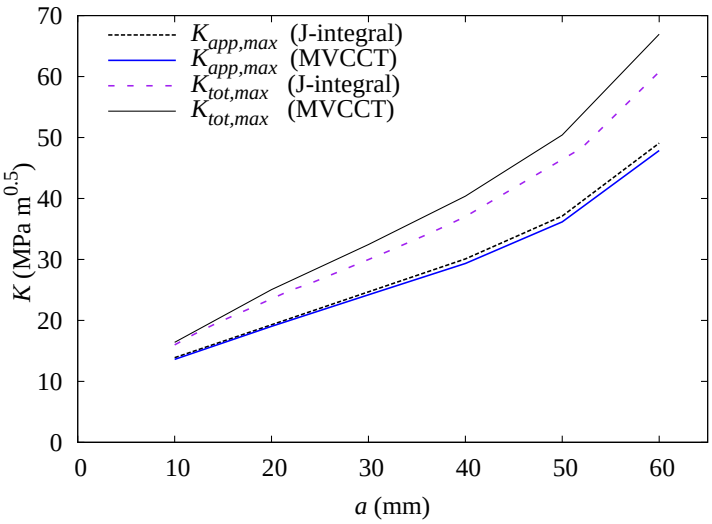

Figure B.4: Comparison of the total and applied SIF.

Figure B.4 shows how the residual stresses influence the two methods. Without RS hence by comparing K_{app} there is a difference of 2% hence J-integral and MVCCT consider the applied load and the secondary bending in the same way. However when including RS in the analysis the results are more different: at 10 mm crack length the K_{tot} are very similar but when the crack growths there an increment of 13% of the MVCCT respect to the J-integral. There is a further component of coupling between the RS field with the tensional and bending load which is not totally considered with the J-integral. The MVCCT can take into account of this coupling component.

This is because with the superposition the coupling of the secondary bending with the residual stress will be not taken into account. Figure B.5 and B.6 show the superpositions differences. $K_{max,tot}$ is calculated with one single analysis for both methods.

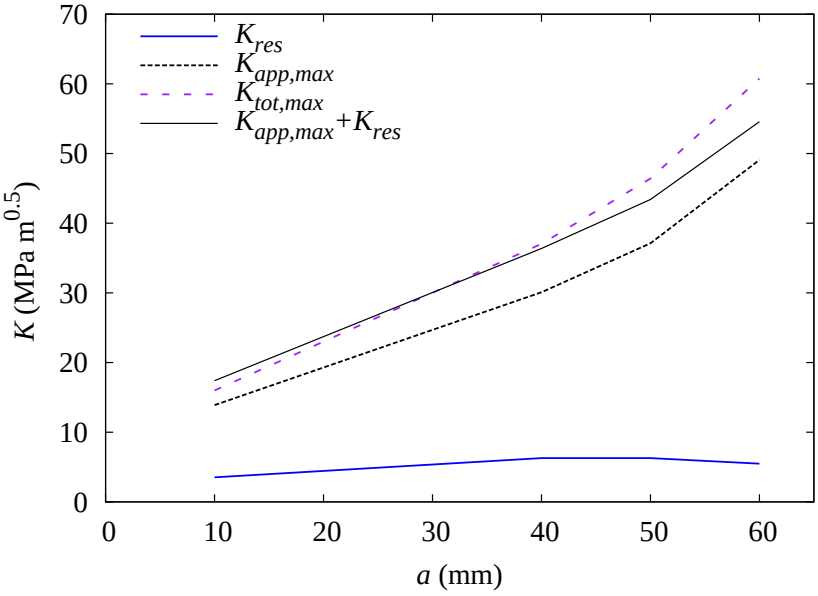

Figure B.5: Superposition by using the J-integral.

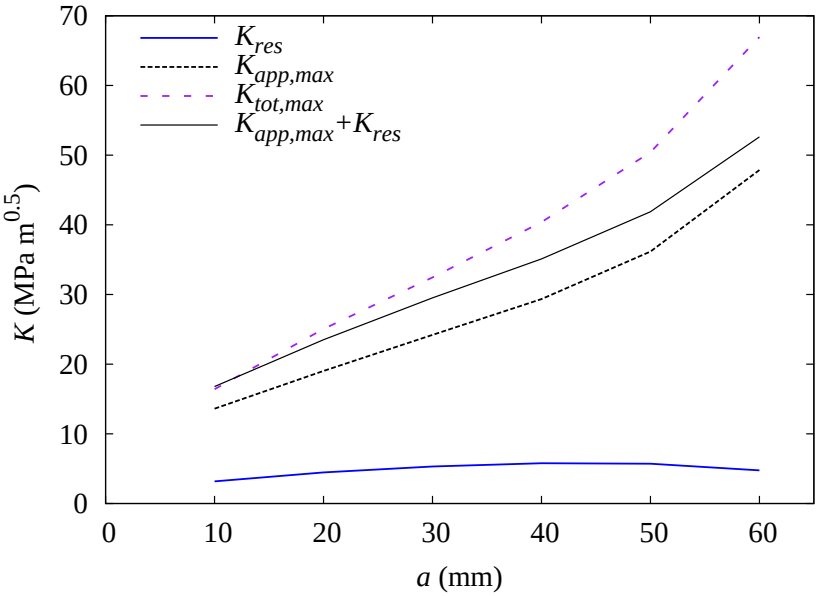

Figure B.6: Superposition by using the MVCCT.

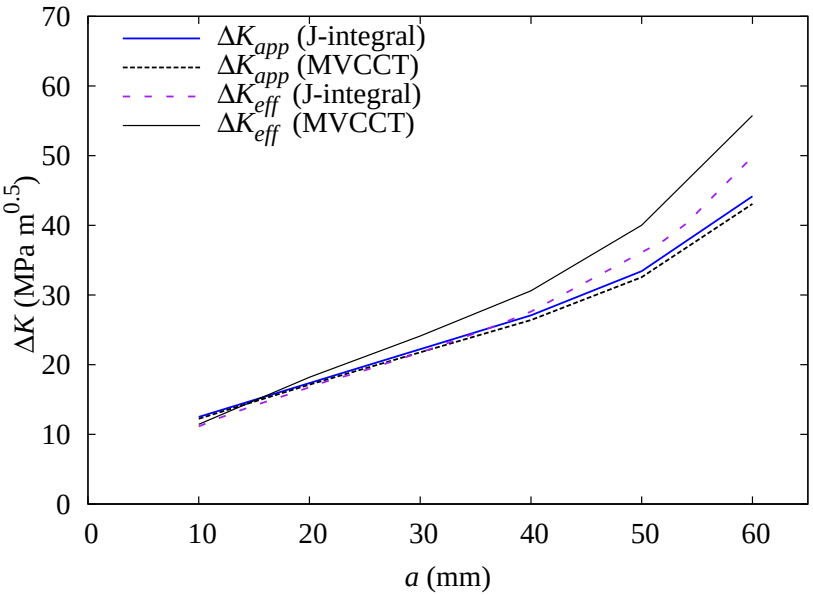

Figure B.7: Stress intensity factor range.

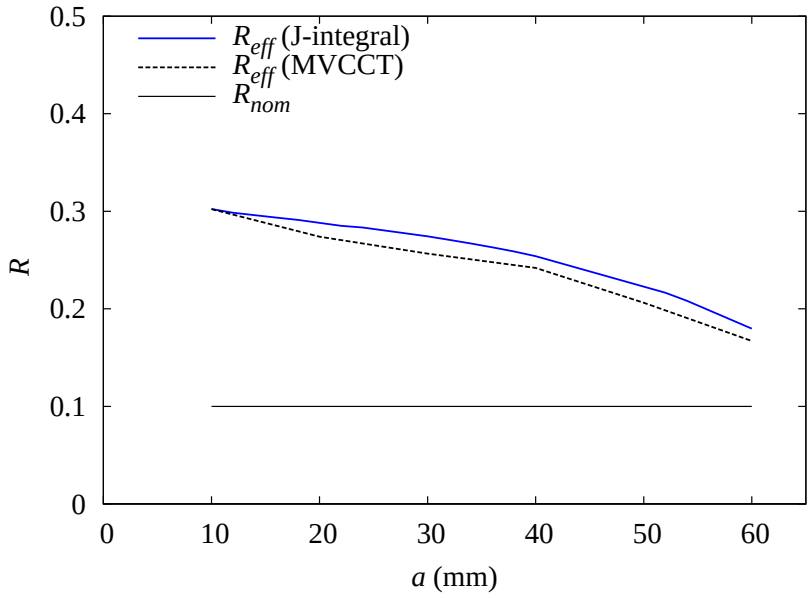

Figure B.8: Effective R ratio.

The results shown in figure B.7 confirm that without RS the two methods are similar but when introducing a RS field a difference of 10% occur. Also the R_{eff} is changed and this will also influence the fatigue crack growth rate. The trend is similar to the distribution of the residual stresses along the crack propagation line and the value calculated with the J-integral has no more than 5% of difference.